

# GROUND-PENETRATING RADAR FOR ARCHAEOLOGY

*Fourth Edition*

LAWRENCE B. CONYERS

# **Ground-Penetrating Radar for Archaeology**



# **Ground-Penetrating Radar for Archaeology**

Fourth Edition

*Lawrence B. Conyers*

ROWMAN & LITTLEFIELD  
*Lanham • Boulder • New York • London*

Published by Rowman & Littlefield  
An imprint of The Rowman & Littlefield Publishing Group, Inc.  
4501 Forbes Boulevard, Suite 200, Lanham, Maryland 20706  
[www.rowman.com](http://www.rowman.com)

86-90 Paul Street, London EC2A 4NE

Copyright © 2023 by The Rowman & Littlefield Publishing Group, Inc.

*All rights reserved.* No part of this book may be reproduced in any form or by any electronic or mechanical means, including information storage and retrieval systems, without written permission from the publisher, except by a reviewer who may quote passages in a review.

British Library Cataloguing in Publication Information Available

### **Library of Congress Cataloging-in-Publication Data**

Names: Conyers, Lawrence B., author.

Title: Ground-penetrating radar for archaeology / Lawrence B. Conyers.

Description: Fourth edition. | Lanham : Rowman & Littlefield, [2023] |

Includes bibliographical references and index.

Identifiers: LCCN 2023011736 (print) | LCCN 2023011737 (ebook) | ISBN

9781538179345 (cloth) | ISBN 9781538179352 (paperback) | ISBN

9781538179369 (epub)


Subjects: LCSH: Geophysics in archaeology. | Ground penetrating radar.

Classification: LCC CC79.G46 C663 2023 (print) | LCC CC79.G46 (ebook) |

DDC 930.1—dc23/eng/20230321

LC record available at <https://lccn.loc.gov/2023011736>

LC ebook record available at <https://lccn.loc.gov/2023011737>

 The paper used in this publication meets the minimum requirements of American National Standard for Information Sciences—Permanence of Paper for Printed Library Materials, ANSI/NISO Z39.48-1992.

# Contents

Figures, Tables, and Equations	vii
Acknowledgments	xiii
Preface	xv
Introductory Thoughts on This Edition	xv
<b>Chapter 1:</b> Some Basics of GPR	1
Geophysics Today and the Goals of This Book	4
Some Pet Peeves to Get Out of the Way	6
<b>Chapter 2:</b> Introduction to Ground-Penetrating Radar	11
History of GPR	16
<b>Chapter 3:</b> Radar Wave Generation and Propagation	25
Radar Antennas and Wavelengths	28
Ground Properties Affecting Radar Wave Transmission	30
Production of Reflections	33
Recording of Radar Waves	34
Acquisition Settings and Collection Procedures	38
GPR on Water	48
Antenna Frequency Constraints	50
Radar Wave Reflections	53
Dispersion and Attenuation of Radar Waves in the Ground	62
Basic Reflection Types	63
Resolution of Subsurface Features	66
<b>Chapter 4:</b> Ground-Penetrating Radar Equipment and Acquisition Software	85
Data Acquisition Software: Setup Parameters	88
<b>Chapter 5:</b> Velocity Analysis	99
Direct Velocity Measurements	102
CMP and WARR Tests	105

Transillumination Tests	108
Laboratory Measurements of RDP	111
Analysis of Point-Source Reflection Hyperbolas	113
<b>Chapter 6:</b> Post-Acquisition Data Processing	117
More on Initial Processing Steps	120
Amplitude Slice-Map Production	121
Isosurfaces and Videos	128
More Advanced Processing Steps	129
Migration	129
Frequency Filtering	133
Deconvolution	138
Hilbert Transform	142
Multiple-Offset Processing	142
Other Experimental Analyses	144
Data Processing Conclusions	145
<b>Chapter 7:</b> Interpretation of GPR Data	147
Synthetic GPR Models	149
Synthetic Modeling Applications	152
Horizon Picking	158
Amplitude Analysis in Slice-Maps	169
Subtle Feature Discovery with Amplitude Mapping	176
Production of Rendered Images	180
Very High-Frequency GPR	182
GPR and Magnetics Used Together	186
<b>Chapter 8:</b> Conclusions	193
Glossary of Common GPR Terms Used in This Book	197
References	205
Index	237
About the Author	243

# *Figures, Tables, and Equations*

Figure 1.1.	A reflection trace collected over a time-window of 36 nanoseconds.	2
Figure 1.2.	Example of a reflection profile where more than 600 traces are displayed together.	2
Figure 1.3.	Amplitude slice-maps from Petra, Jordan, in 25 cm depth-slices.	3
Figure 1.4.	Amplitude slice-maps of a crannog in Ireland showing subtle reflections features that display patterns that are important.	8
Figure 2.1.	Reflection profile from western Portugal displaying a buried living surface.	13
Figure 2.2.	Creation of a reflection trace.	14
Figure 2.3.	A GSSI SIR-4000 recording system with 400 MHz antennas.	15
Figure 3.1.	A propagating electromagnetic wave.	26
Figure 3.2.	The electromagnetic spectrum.	26
Figure 3.3.	An analysis of the depth where GPR waves attenuate.	29
Figure 3.4.	Reflection profile displaying a few point-source hyperbolas and metal.	32
Figure 3.5.	Collecting GPR reflection profiles in transects a meter apart.	35
Figure 3.6.	Collecting 400 MHz using a system supported in a backpack.	35
Figure 3.7.	Reflection profiles showing gaining.	40
Figure 3.8.	An antenna array system.	41
Figure 3.9.	An amplitude slice-map.	42
Figure 3.10.	Non-topographically adjusted reflection profiles.	44
Figure 3.11.	Air waves generated from curbs.	45
Figure 3.12.	Irregularity in the ground surface producing coupling changes.	46
Figure 3.13.	Reflection profile GPR in a lake.	48
Figure 3.14.	Laboratory tests to determine attenuation at different salinities.	49
Figure 3.15.	Frequencies generated from a 400 MHz antenna.	51
Figure 3.16.	A transmitting pulse.	51
Figure 3.17.	2 GHz, 16 MHz, and 900 MHz antennas.	52
Figure 3.18.	One-way radar wave velocities vs RDP.	54



Figure 3.19.	Model of radar wave reflection amplitudes on a flat surface.	58
Figure 3.20.	Differences in reflection amplitudes by the addition of water.	61
Figure 3.21.	Lateral variations in reflectivity and attenuation over only 4 meters.	62
Figure 3.22.	A planar reflection from the floor of a pit-house in eastern New Mexico.	63
Figure 3.23.	Many small reflection hyperbolas reflection from objects in a trash midden.	64
Figure 3.24.	Point-source reflection hyperbolas generated from individual buried objects.	65
Figure 3.25.	The radiation footprint of an antenna with a given center-frequency.	69
Figure 3.26.	Resolution of two interfaces using different frequency antennas.	71
Figure 3.27.	Model showing how the cone of illumination containing many propagating waves with refraction.	72
Figure 3.28.	Differing resolution of bedding planes dependent on coupling.	74
Figure 3.29.	Collecting GPR data in snow in Alaska.	75
Figure 3.30.	Comparison of two reflection profiles in snow and bare ground.	76
Figure 3.31.	Different types of background noise.	77
Figure 3.32.	Radar waves scattered and focused.	78
Figure 3.33.	Roman floor with focusing and scattering.	79
Figure 3.34.	Three frequency profiles over the same transect.	81
Figure 3.35.	Multiple reflections produced from the very reflective upper and lower surface.	83
Figure 3.36.	Metal reinforcing bars in the ground.	83
Figure 4.1.	The components of an antenna array system.	86
Figure 4.2.	An array system with seventeen antennas, nine transmitters, and eight receivers.	87
Figure 4.3.	A 500 MHz reflection profile with abundant background noises removed with frequency filtering.	97
Figure 5.1.	Very minor variations in the depth of a planar reflection surface due to change in the ground surface.	101
Figure 5.2.	Direct comparisons of reflections visible in a reflection profile to visible units in an outcrop.	103
Figure 5.3.	Collecting CMP data.	106
Figure 5.4.	Various ray pathways in a CMP test.	107
Figure 5.5.	Results of a CMP test.	107
Figure 5.6.	Collecting transillumination data.	109
Figure 5.7.	Results of a transillumination test.	110

Figure 5.8.	Laboratory tests of a soil sample showing some variations in RDP.	112
Figure 5.9.	Hyperbolas used to determine velocities in one profile.	114
Figure 6.1.	Basic processing steps on one profile.	118
Figure 6.2.	Two different displays of recorded reflections in a profile.	121
Figure 6.3.	Display of automatically created amplitude slice-maps.	122
Figure 6.4.	Construction of an amplitude slice-map from reflection profiles.	123
Figure 6.5.	Differences in maps using differing search radii in gridding and interpolation.	125
Figure 6.6.	Display of software that can generate multiple images on the same screen from topographically adjusted amplitude slice-maps.	126
Figure 6.7.	Comparison of resolution in amplitude slice-maps of a buried multi-room Roman building.	127
Figure 6.8.	An isosurface rendering of a buried Roman temple.	128
Figure 6.9.	Raw reflection profile displaying many reflection hyperbolas that are migrated.	130
Figure 6.10.	The difference in amplitude slice-maps between migrated and un-migrated profiles.	131
Figure 6.11.	The hyperbola axes used to test migration methods.	132
Figure 6.12.	Results of some migration software.	134
Figure 6.13.	Amplitude maps displaying processing procedures.	136
Figure 6.14.	Reflection profiles displaying reflections in each of the individual processing steps.	137
Figure 6.15.	Filtering of a 200 MHz reflection profile to display only the 50-100 MHz frequency reflections.	139
Figure 6.16.	Multiple reflections produced from a very reflective bedrock unit in a lake bottom.	140
Figure 6.17.	Deconvolution processing.	141
Figure 6.18.	Multiple-offset processing.	144
Figure 7.1.	Generation of a synthetic reflection profile.	150
Figure 7.2.	Synthetic reflection profile of a buried canal.	153
Figure 7.3.	Synthetic reflection model of a three-layer system.	154
Figure 7.4.	Example of planar reflections from a perfectly flat pipe varied in recorded depth.	155
Figure 7.5.	Synthetic reflection profile of a buried pit house with a floor.	156
Figure 7.6.	Synthetic model adjusted to mimic a reflection profile.	157
Figure 7.7.	Outcrop of the Jurassic bedrock.	159
Figure 7.8.	Reflection profile adjacent to where artifacts were found on the Jurassic bedrock surface.	160
Figure 7.9.	Automatic picking of the Jurassic reflection.	160
Figure 7.10.	Contour map of the Jurassic surface auto-picked.	162

Figure 7.11.	Top of a compacted organic-rich horizon.	163
Figure 7.12.	Reflection profile of the LU-6 horizon.	163
Figure 7.13.	Three-dimensional surface of the LU-6 picked horizon.	164
Figure 7.14.	Synthetic reflection profile of a buried Hohokam canal in southern Arizona	165
Figure 7.15.	Reflection profile that mimics the synthetic model.	165
Figure 7.16.	Amplitude slice-maps of the canal.	166
Figure 7.17.	Three-dimensional surface of the canal.	167
Figure 7.18.	Inside the Cueva Peluda at Atapuerca, Spain.	167
Figure 7.19.	Three-dimensional images produced of the cave.	168
Figure 7.20.	Reflection profile of the cave.	169
Figure 7.21.	Three-dimensional analysis of the cave.	170
Figure 7.22.	Creating amplitude slice-maps of a grid.	171
Figure 7.23.	The distinctive feature in the amplitude slice-maps.	172
Figure 7.24.	Possible errors that occur when horizontal slices cut across a surface of interest.	173
Figure 7.25.	Amplitudes from a buried living surface that crosses slices.	173
Figure 7.26.	Topographically corrected slices.	175
Figure 7.27.	Reflection profile showing very subtle reflection differences where a channel is composed of gravel.	177
Figure 7.28.	Amplitude slice-maps showing the subtle channel in a wetland area.	177
Figure 7.29.	Photo of a puddled adobe wall in southern Arizona.	178
Figure 7.30.	Reflection profile showing the adobe wall.	179
Figure 7.31.	Amplitude map of the area where the adobe walls were uncovered.	181
Figure 7.32.	Human footprints placed in mud to simulate the Laetoli prints in Tanzania.	183
Figure 7.33.	Reflections from the top of the clay surface where the footprints were made.	184
Figure 7.34.	Depth of the prints contour map.	185
Figure 7.35.	Data points used to produce the contour map processed by create a residual.	186
Figure 7.36.	GPR-amplitude maps corresponding to magnetic maps.	187
Figure 7.37.	Reflection profiles and corresponding magnetic values.	189
Figure 7.38.	Magnetic map and amplitude slice-map.	190
Figure 7.39.	Reflection profile compared to magnetic values.	191
Table 3.1.	Typical relative dielectric permittivities (RDPs) of common geological materials.	56
Table 3.2.	The center frequency wavelengths of differing radar antennas and the wavelength changes in material with differing relative dielectric permittivities (RDP).	66

Table 3.3.	Length (in meters) of radar waves in media of a given RDP and frequency.	68
Table 4.1.	Depth in meters to a reflector through a media of a given RDP.	90
Table 6.1.	Post acquisition processing objectives and methods.	119
Equation 3.1.	RDP, radar velocity relationship.	55
Equation 3.2.	The coefficient of reflectivity.	57



# Acknowledgments

Many thanks go to Jeffrey Lucius, now retired from the U.S. Geological Survey in Denver, Colorado, who worked me with GPR from the beginning. Also, many thanks to Dean Goodman, with whom I coauthored the first GPR book for archaeology, *Ground-penetrating Radar: An Introduction for Archaeologists*, who has been a friend and close colleague many decades. Many other collaborators have been a great help with GPR in the field, as well as advice for this 4th edition: Payson Sheets, Ken Kvamme, Mike Powers, Chet Walker, Arne Anderson-Stamnes, Immo Trinks, Alois Hinterleitner, Sam Connell, Paul Fish, Lauren Couey, Loren Davis, Mike Daniels, Lucia Bermejo, Sarah Lowry, Fabian Welc, Maeve Herrick, Emma St. Pierre, Andrew Bair, Huthaifa Qawasmeh, and Mohammed Al-Hameedawi.



# Preface

## INTRODUCTORY THOUGHTS ON THIS EDITION

It was with some amazement that I received a request from this book's publisher to consider writing a fourth edition on ground-penetrating radar (GPR) in July 2022. I was flattered and astonished when I looked up how few technical books of this sort make it past the first edition, let alone to a fourth edition. This started my recollection, going back to 1996, when I proposed to write the first edition of this work (with co-author and longtime friend and colleague Dean Goodman). Mitch Allen, the editor and owner of Altamira Press at that time, politely told me that he didn't think anyone would ever read a book on GPR for archaeology or for any other field, but he reluctantly consented to review a proposal from me. Dean and I pushed on writing the book, as I was a junior faculty member and knew I needed a book published to be considered for tenure. Dean followed my lead, as we both had no other immediate plans for other publications.

A few weeks later, Mitch called me on the phone (in the days before e-mail became the preferred method of communication) and told me he would recommend to his board (I think this "board" consisted of only him) that Altamira give us the "go-ahead" to write the book, but with the option of declining to publish until a complete draft was received and favorably reviewed. This was a no-risk proposition for Altamira, but I was still encouraged. Thankfully, he liked the final product, and it was well reviewed by others, with the first edition published in 1997.

This kind of reminiscing is off topic, but perhaps somewhat interesting when we consider how far the GPR method, not just for archaeology but for many other fields, has come since those early days in the late twentieth century. In the late 1980s, when I first started working with GPR, there was not even an inkling of a chance that a fourth edition would be warranted. I have been pleased over the years to hear from many people in fields other than archaeology who have read editions of this book and recommended their colleagues and students read it, as they said it is written in a way that non-technical users will understand.

Therefore, in 2022, I acceded to the request by the present publisher to write a fourth edition, but with a little trepidation. There are now thousands of people working with GPR all over the world, and a great deal has been written



about new and powerful applications, methods, and software during the last twenty-five years since the first edition. I also wondered if I could possibly incorporate all the advancements that have occurred with GPR in just the last ten years since the third edition was published.

When Dean Goodman and I put together that first edition, we were hard-pressed to find much other research on GPR to cite or borrow ideas from. That has now changed, and the GPR world consists of a large and vibrant community, so finding new and important published information to include in this edition was not difficult. I have therefore tried to find the most accessible literature from recent advances that I can understand, appreciate, or have experience with to include here.

When reviewing the references cited from the first edition, I realize how “old school” much of the methods and interpretations must seem today, which were new to us in those early years of GPR. It is also sad that many of the authors of those early works, which we relied on for background on methods and theory in the first edition, are now dead, or at least retired and inactive. In updating the references for this edition, I have decided to leave most of those earliest references in place as they represent an important history in the advances of GPR over three or more decades. Newer references used in this edition have been added to the early ones where applicable. Also, the basics of radar wave theory have not changed much in thirty years, so those early references are pertinent and for that reason alone will remain.

It is also interesting to reflect (pun intended) and realize that there was no good reason for me to consider writing the first edition of this work except that I was a junior professor in the academic world, where writing about a subject few cared about was tolerated (and even rewarded) by my colleagues. On that score, I am fortunate, as my academic career allowed me the time (and ultimately the reward) for writing with Dean the first book, which Mitch Allen thought nobody would read. I am glad he took a chance on us back then, or there would never have been a first edition, let alone this fourth.

With thoughts of that history still fresh in my mind, I am encouraged with the huge leaps in GPR data acquisition and processing that have occurred in thirty years, with many advancements occurring since the third edition of this book was published in 2013. The literature is full of both hardware and software advances, and GPR applications for a variety of disciplines, not just archaeology. I have cited some of that new literature for specific topics in disciplines that are somewhat remote from geology and archaeology, which is the focus of this book. They are just too numerous to mention all of them, but advances are always occurring in construction and infrastructure topics, and other farther-afield disciplines that include GPR on the planet Mars.

For this edition, I have added a variety of new method examples and results from some novel GPR collection systems and processing software that I could only have dreamed about in the early years. Thankfully I have many colleagues

who are the “second generation” of GPR practitioners. Many of whom have been able to help me with some of the newer, and often still experimental methods, which I have included here.

The backbone of this edition of the book is still GPR theory and basic data collection, processing and interpretation methods, and how an understanding of those can lead to success. I truly believe that only by understanding the fundamental methods and theory can one apply those to the data gathered both in traditional ways, but also with newer systems, to make robust and accurate interpretations. While software and hardware advances make up most newly published works, the interpretation of data used to allow those advances to contribute to all fields of research. This is still the most important component for all of us that care about results of a survey.

The GPR field has become so popular in the last decade that many newer practitioners are relying on software to perform all the “heavy lifting” in data analysis, which we used to do manually (Conyers 1995). Often these newer processing methods advance the user quickly (and with little effort) from raw reflection data to the production of images in three-dimensions. This is somewhat disturbing to me, as many of the processing steps leading to the 3-D visualizations have been incorporated in or ignored by that software. Users therefore have little knowledge of what has been done with their data, and perhaps don’t care too much as results are created with little effort on their part. There is nothing wrong with taking large reflection datasets and re-sampling hundreds of thousands of even millions of waves to produce images (such as amplitude slice-maps or other three-dimensional views), which are easy to interpret. But by relying only on those “immediate gratification” methods (Conyers 2015; Conyers et al. 2019) and bypassing an analysis of the raw data, much information is potentially lost or ignored. In this book I will therefore always return to what the data are telling us in their most basic forms (reflection profiles and often individual reflection traces), as this is where the basic information remains, even after it has been transformed into easy-to-interpret images.

I have several biases when it comes to GPR interpretation and analysis (Conyers 2012), the most stringent of which is to always use all the data at one’s disposal before arriving at interpretations. I began my life in GPR with little more than un-processed reflection profiles as a product from which to make interpretations. Coming as I did from the reflection seismic field (back when I had a “real” job before academics), these reflection profile images were not foreign to me. With GPR I only needed to get my thoughts focused on a different dimension from seismic acoustic waves where I was familiar, to the shorter wavelength electromagnetic waves. My previous background consisted of a reliance on reflected waves in their “rawest form,” so it was a natural transition for me to move to GPR reflections and just change my scale of analysis from deep in the earth’s crust to the near-surface medium. My bias in GPR analysis is therefore always to go back to the basic tools I grew up with, which

are individual waves, traces (which are series of waves or “waveforms”), which produce reflection profiles. Dean Goodman also started his career in seismic geophysics, so he brought that bias also to GPR.

My younger colleagues don’t know how good they have it, as the software we all use these days can move rapidly from an overwhelming abundance of reflections directly to easier to interpret and explain amplitude slice-maps and other three-dimensional displays. While we all love the results of visually dynamic three-dimensional images, I still believe that an understanding of how radar waves in the ground are distorted, reflected, refracted and attenuated is what leads to complete interpretations of those 3-D images. With that in mind, in this edition I have added many editorial and interpretive comments to the otherwise “dry” theory and methods that was used in earlier editions of this book.

I often tell my students, or others that will listen, that only an understanding of the basic principles of radar waves propagation and movement in the ground, can allow for a more complete understanding of what this complex geophysical method can tell us. I admit that in my previous writings I have not succeeded in this as I erroneously inferred that readers would see the benefits of understanding basic method and theory. After many conversations, and leading GPR workshops over the years, I now understand that to have been a false apprehension on my part. This edition I hope will go a little way to correcting my previous lack of explanations on the applicability of wave theory and try to show how these basic concepts can be useful in thinking through interpretations of datasets. Perhaps that might be appreciated by new readers, and even some older ones, who might consider brushing up on GPR theory a little bit and thinking about new ways to apply those basic concepts.

# 1

## *Some Basics of GPR*

Ground-penetrating radar is perhaps not only the most complex of the near-surface geophysical methods, but also the most powerful in that it provides a robust three-dimensional look at the ground. It involves the transmission of high-frequency radar pulses from a surface antenna into the ground and then records their reflection in both elapsed time of propagation and reflected wave strength (as measured in wave amplitude) of the returning waves to the surface (Figure 1.1). The elapsed time between when this energy is transmitted, reflected from buried materials or sediment and soil changes in the ground, can then be converted to depth. When many thousands of radar reflections are measured and recorded as antennas are moved along transects a two-dimensional picture of the ground can be produced (Figure 1.2) and many profiles within a grid can produce three-dimensional “pictures” of buried soil, sediment, and feature changes (Figure 1.3).

Mapping using GPR as well as other geophysical techniques has recently become so accurate that the possibility now exists to test any number of working hypotheses concerning a broad range of anthropological, geological, and environmental questions (Benech 2007; Conyers 2010; Conyers and Leckebusch 2010; Conyers et al. 2013). Some of these can be related to social organization and social change, when these cultural attributes can be directly related to the placement, orientation, size, geometry, or distribution of certain architectural and ancillary features on the landscape (Conyers 2022). Determining geological and environmental aspects of ancient buried landscapes such as soil changes and the nature of buried topographic features is also possible (Barone and Desibio 2015; Conyers 2008, 2016) and for forensic studies (Barone et al. 2015; Barone and Di Maggio 2019). Most important, GPR and other geophysical methods can gather a great deal of information about the near surface in a totally nondestructive way, allowing large areas with buried remains to be studied efficiently and accurately, while at the same time preserving and protecting them (Barone 2018; Garrison 2016; Gizzi and Leucci 2018; Witten 2017).

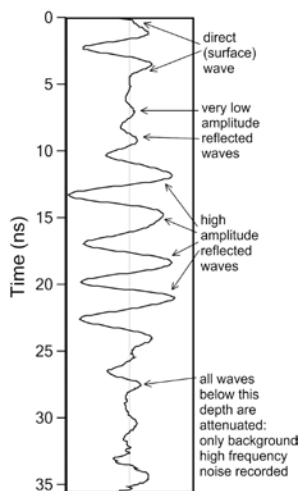


**Figure 1.1.** A reflection trace collected over a time-window of 36 nanoseconds showing the direct wave at the top with high and low amplitude reflection waves to about 27 nanoseconds. Below that are only background noise, which are waves from external sources that traveled to the receiving antenna in the air. No coherent reflected waves are displayed below 27. *Source: the author.*

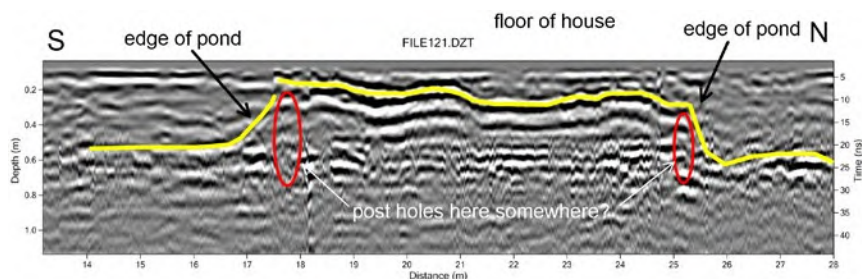
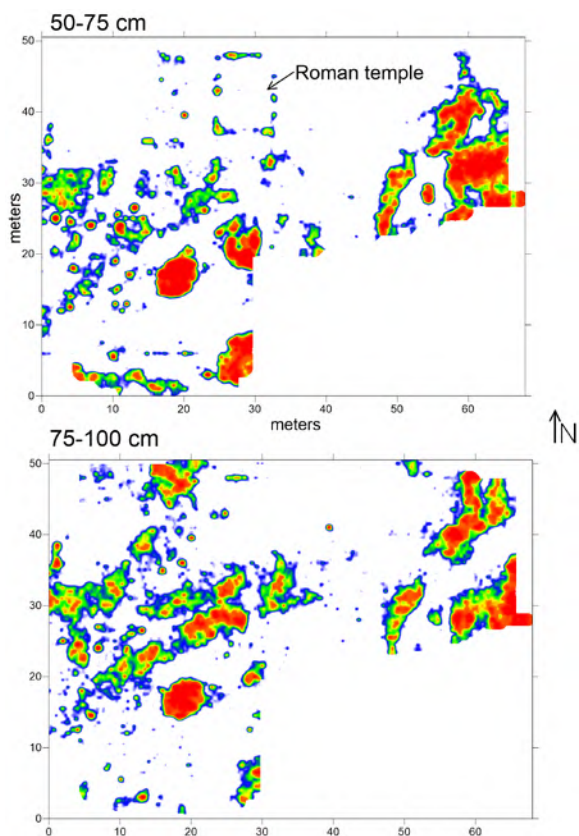


**Figure 1.2.** Example of a reflection profile where more than 600 traces are displayed together, which were collected along a transect 28 meters long. The yellow horizon shows a reflection recorded from a stratigraphic unit that was the base of a pond or lake, and which merges with a reflection generated from a raised platform and floor constructed in that pond. This is a crannog in western Ireland. *Source: the author.*

**Figure 1.3.** Amplitude slice-maps from Petra, Jordan, in 25 cm depth-slices showing a variety of potentially intersecting features, with one in particular on the north in the 50–75 cm slice. That distinct feature is a Roman temple, whose presence is readily apparent from basic pattern analysis of the high-amplitude reflections. *Source:* the author.



Cultural resource managers and others who evaluate areas slated for construction and development have rapidly grasped the power of geophysical methods to quickly, efficiently, and nondestructively discover and map sites for selective excavation or avoidance, producing greater economy of time and resources (Conyers 2011; Deiana et al. 2018; Johnson 2006; Lowry and Patch 2020; Nelson 2021; Miller et al. 2018; Stumpf et al. 2021; Wadsworth et al. 2021). This ability has allowed these methods to become very useful in the business of consulting archaeology as information from excavations can be projected to areas of a site that remain buried and often will remain so or avoided if possible during construction.

## **GEOPHYSICS TODAY AND THE GOALS OF THIS BOOK**

Today most GPR instruments are still manufactured for applications that are geo-technical, construction, and engineering related, as that is where the monetary profit resides. As a result, many of us, especially those of us in the archaeological community, are almost always forced to use “off-the-shelf” systems, whose manufacturers are motivated by these dominant customers. Only a small percentage of their profit comes from archaeological and geological customers. By necessity we have had to learn how to make these geophysical systems, often developed for other types of studies, work for our own needs. This can be both a blessing and a curse. While it is nice to have hardware and software that is well tested and supported by manufacturers, often the systems’ standard data collection and processing procedures must be modified for other than their intended needs.

Recently, because of individual necessity, many GPR users have had to use software programs specifically developed for other fields and apply them to our own applications. This can be a daunting task, as much of that software was written for “pipe finders,” engineers, and geo-technical specialists. In addition, in my field or archaeology, most of my students were trained in anthropology departments, which is common in North America (Conyers 2012). Those of us who teach in anthropology departments are quite aware that many of our students are drawn to archaeology for nonscientific reasons, such as their joy of finding or working with interesting artifacts. Their motivation for this field of study might also be their inability to get through advanced mathematics or science courses on their way to a college degree. Perhaps the romance of archaeology in general has motivated them to study archaeology. In the recent past, this has often meant that many anthropology students had a difficult time comprehending the physics or math that is necessary to understand geophysics, which may be one reason archaeological geophysics has grown relatively slowly compared to geophysics employed in other disciplines. This situation is now changing rapidly as a younger generation, raised with computers and not terrified by the prospect of analyzing digital data, has entered the field. It is encouraging that many of this new generation of students are ready both to learn and apply geophysical

techniques in their own research. Unfortunately, many are still not introduced to the subject in their typical undergraduate college classwork. This situation can only improve as geophysical methods become more common and are shown to be successful, and as a new generation of computer-savvy students move into leadership, management, and teaching positions.

This book is not intended to be a “how-to,” step-by-step manual to the GPR method. Other resources are available for that (Goodman and Piro 2013) as well as the often difficult-to-understand software manuals. The goal here is to introduce users to the GPR method both theoretically and methodologically, with examples of both successes and failures. And most important, to explain how the theory can be directly applied in data interpretation. Complicated formulas, electronic wiring diagrams, and especially step-by-step instructions on how to work each GPR device or software program are not included. There are simply too many systems available, and a corresponding abundance of processing and image-generating programs developed for each. To delve into the details of their own chosen GPR system or software package, readers will have to refer to cited reference material, equipment manuals, or other technical sources, which are continually being modified and advanced by each GPR system manufacturer and researcher.

Most published articles that include any component of near-surface geophysics always emphasize the successes, often with striking images of spectacular buried features, leading many to believe, often erroneously, that one-or-the-other method is successful. This tendency to focus only on geophysical successes, while relegating failures to the “memory hole,” is something all geophysicists are guilty of (Conyers 2012). Unfortunately, it leaves the impression on some that geophysical techniques can do most anything, or perhaps that some methods “worked well” while others did not. These impressions are unfortunate, especially when an attempted survey cannot do what is desired, leaving the geophysically uninitiated with the erroneous impression that a technique “doesn’t work,” giving all geophysics a bad name. I have therefore in this volume and elsewhere (Conyers 2012) included examples of failures and tried to explain why this was the case.

It is extremely important that geophysics be done in a deliberate manner, allowing for multiple working hypotheses to be tested and modified during data collection and processing before interpretations are made. Most important, when a survey is not successful in producing the results anticipated, the geophysical data and other information about the site should be reanalyzed and evaluated to determine why the final product did not produce the desired results. All factors that could conceivably have affected the quality of the final product each step of the way must be understood by all who are involved for any results to be useful. Unfortunately, this type of thoughtful and “reflective analysis” (overt pun) is rarely the case, as many users neither want to nor have the background to understand the complexities of both the geophysical methods



employed and the nature of the complexities that may have confronted. This is one of the many ongoing problems this edition of the book hopes, at least partially, to overcome.

## **SOME PET PEEVES TO GET OUT OF THE WAY**

We have arrived at a time in GPR where this complicated geophysical method has been embraced by many people in many different fields around the world. That is heartening. The software programs that allow for the processing and image production of huge databases of reflections, collected in a variety of fashions, is inspiring. The downside of this massive raw data collection, however, is that almost anyone can take raw data and produce interesting images from it. That “immediate gratification” data processing and analysis has led to many people to “almost automated” processing steps as a means to an end, with the product being 3-D images. Many GPR users begin their interpretation by searching for “patterns” in those images such as straight lines (Figure 1.3) ovals (perhaps storage pits or pit house edges?) square or rectangular features (building foundations?), and then drawing lines on images or annotating maps with possible patterns that becomes a final product. In Figure 1.3, the buried Roman temple on the north side of the 50- to 75-cm amplitude depth-slice is immediately visible and was therefore the focus of excavations that were done at this site at Petra, Jordan (Conyers et al. 2002). Later it was found that many other important features were also buried in this area, but because the pattern of the temple was so visible, those others were overlooked until later in the interpretation process.

I have often been disappointed with making interpretations based on only patterns in amplitude slice-maps. It is not often that a Roman temple is immediately visible, and often the patterns I “hope” represent something important turn out to be figments of my fertile imagination, a result of the gridding and mapping parameters, or some other phenomenon in the ground that I never fully understand. But we all keep doing this type of pattern searching anyway, as the “immediate gratification” thrill in finding exciting patterns is difficult to pass up.

As an example of this, a large grid from Ireland was collected over a small rise in a marshy area, with no surface expression of any buried architecture. The resulting amplitude slice-maps were “busy” with patterns, and I was unsure where to start (Figure 1.4). After some analysis I was visually drawn to an arcuate line of very small points, which seemed to outline something that was oval or partially rectangular with a rounded end. As I have often been disappointed by when I find these types of patterns that turn out to be nothing of interest, I was apprehensive of this “first pass” interpretation. After many hours of reflection profile analysis crossing this feature (Figure 1.2), it was apparent that there was a raised platform built in the marsh. In reflection profiles the raised area contained the remains of a house with a central hearth, and on one end the house could be seen to be bounded by a stone and wooden wall. The small “dots” found in my pattern search became an interesting pattern as they surround this raised

platform. With much analysis of both reflection profiles and amplitude slice-maps their origin became apparent. They are the subtle remains of posts that were placed in the marsh when a platform for the house was being built. In this case the patterns were quite important, but not recognized as such until much more data had been processed and analyzed. This feature was excavated and found to be a house, perhaps dating to the Neolithic age. It was built on an artificial island called in Ireland a crannog, which elsewhere were used for as both ceremonial and residential structures located in marshes or lakes (Fredengren 2016). The posts, which were never visible in the reflection profiles (Figure 1.2) and only visible as patterns in the amplitude slice-maps, were my first hint that this important feature was within the complex grid of reflection data. With this example it is apparent that the subtle patterns in the amplitude slice-maps were a good first indication that something important was buried here, but only later with detailed reflection profile analysis was this feature understood in three dimensions. This is a first demonstration of how the ubiquitous amplitude slice-maps are often a good place to start in data interpretation by locating patterns, but those conclusions need to be refined by studying the two-dimensional reflection profiles to understand what is in the ground.

The method of using only amplitude images to formulate all if not most of the conclusions in an interpretation is still common among many GPR practitioners. Using the crannog example, those amplitude slice-maps alone would have provided some interesting patterns but were only showing a part of the picture of what is buried here. In this example the posts were probably visible because radar waves propagating in this wet ground were focused in a very narrow cone and smaller features such as these were more likely to reflect greater numbers of waves (Gabler et al. 2021).

I see the reliance on only patterns all the time when I am asked to review papers for publication in journals and suspect it is just human nature to focus on what is most visible. My warning is that by doing so using only using amplitude slice-maps, there can be many other important items or features in a GPR grid that are important but take a little more time to find and understand. My comments to authors who present only this is type of a display (Figure 1.1) is almost always a version of “surely we can move beyond pattern recognition as a data interpretation method” or perhaps “how do the individual reflection profiles inform you as to the origins of these patterns?” In this book I will hopefully discuss ways that with a knowledge of GPR a more complete account of what is in the ground can be made.

Another continually disturbing trend, which never seems to go away, is that many researchers using GPR seem either reluctant or oblivious as to why they are conducting a survey other than to “find things.” Conclusions in submitted articles for publication that go beyond “look what I found” seem difficult to arrive at for unclear reasons. My goals early on with GPR was also to “find things” and much of my PhD research was basic work in trying to understand what GPR

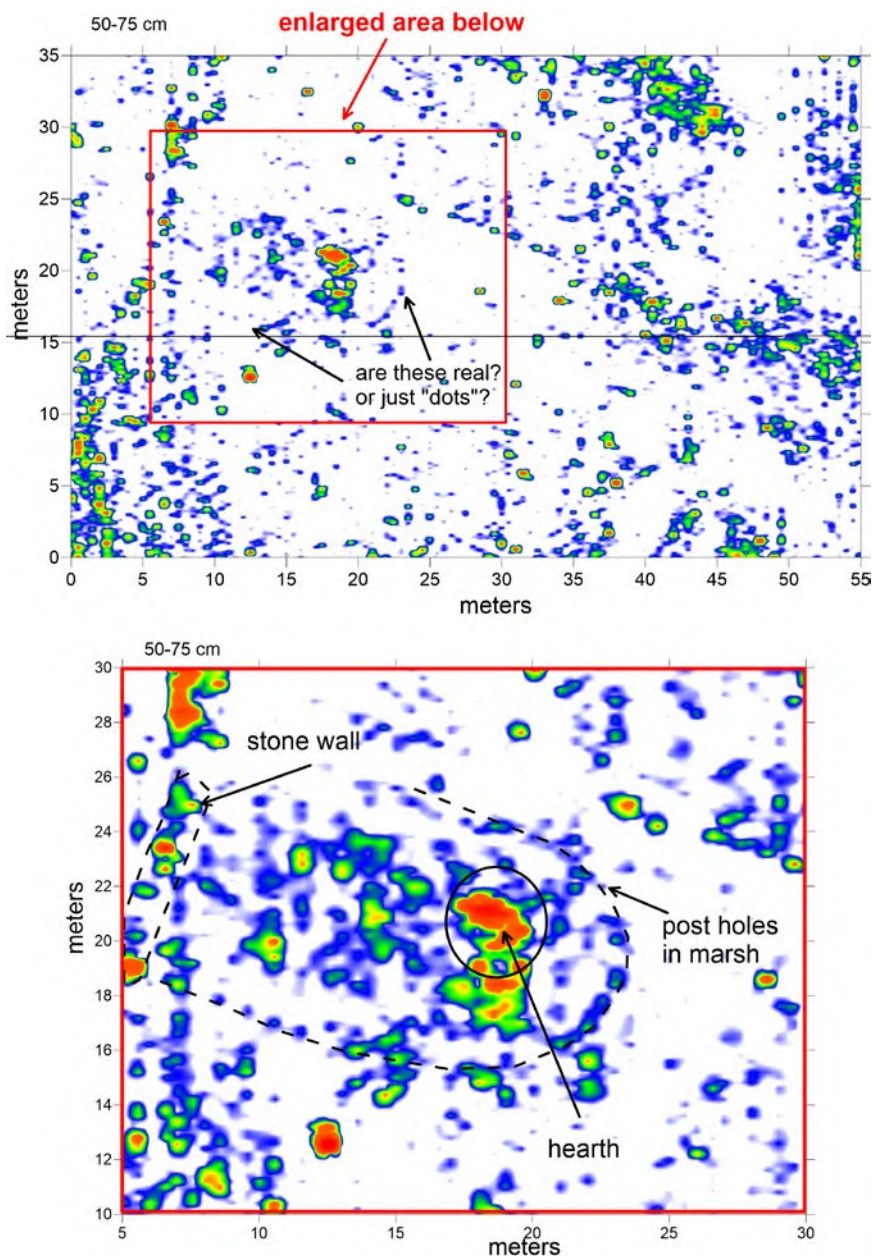


**Figure 1.4.** Amplitude slice-maps of a crannog in Ireland with subtle reflection amplitudes from post holes and interior features that are a hearth and a bounding stone wall. In this display, patterns are important for interpretation using the amplitude slice-maps. *Source:* the author.

could do for archaeology. I remember being asked in my PhD defense to discuss what the implications and conclusions were from my GPR work, and I was flummoxed to be asked this, as I was so involved in waveforms and data analysis, I had neglected to think about why I was doing this research. I quickly came up with some plausible reasons in the dissertation defense such as understanding past cultures (I was in an anthropology department) or history, which seemed to have escaped me in my writing. I forget exactly how I answered this probing question, which can be re-phrased as “So what?” After getting an academic job in a department of anthropology I was always concerned with justifying my research in that setting with conclusions beyond finding something that can be later dug up. I have written several papers on this subject trying to make the case that GPR can ask and answer questions about people and cultures (Conyers 2010; Conyers and Leckebusch 2010; Conyers 2022), none of which appear to have had much of an impact on the broader geophysical community. In most non-anthropological geophysical research around the world “finding things” remains the primary object of many GPR surveys.

Another “pet peeve” of mine is the reluctance by many who publish GPR works to conclude, other than to show what they found. This is a theme I have pondered for some time, and I can propose a few hypotheses, none of which I am totally happy with. One is that many GPR workers come to GPR with backgrounds in physics, geology, engineering and other “hard sciences” where asking what the broader applications of software or hardware development are, is beside the point. In those fields they never seem to be asked to conclude anything that might seem important to me, which are people of the past and their cultures.

It is much simpler to conduct a GPR survey, make some maps and images, write up what you did and then conclude something broad like “there are possible features of interest here” or something equally as vague. This can be a reasonable conclusion to make when there are very distinct features visible in patterns, as those can be the easiest to produce in amplitude slice-maps. If no patterns are found, then what? Perhaps just conclude that the effort was a failure? If patterns are found, concluding with a few distinct images in a short publication is a very good method to employ. Often the quantity of publications in peer-reviewed journals are how a faculty member and departments in a university are judged for promotion or financial awards, so I understand the motivation. I can see how someone using any geophysical method could churn-out many scientifically sound publications that conclude very little other than the authors did some good things and processed the data into nice images. Perhaps in the future this will change, as new users understand what they can do with robust and well interpreted GPR datasets. Explaining what conclusions mean about people, landscapes, cultural change or other important aspects of both environmental and archaeological disciplines can make a huge contribution to many fields.



# 2

## *Introduction to Ground-Penetrating Radar*

Ground-penetrating radar has a reputation as one of the more complex geophysical methods because it involves the collection of large amounts of reflection data from two-dimensional profiles collected in numerous transects within grid or arrays of multiple antennas that transmit and receive reflections at discrete points in space (Novo et al. 2013). At each distinct location there are usually tens or sometimes hundreds of reflections recorded, beginning at the ground surface to whatever depth is of interest, or to the depth at which all transmitted radar energy is attenuated. These unique series of reflections can be spaced by as little as a few centimeters, producing a very robust three-dimensional dataset of reflections, with each individual reflection and all with unique location in x, y, and z coordinates. When many reflections are processed into images that can be interpreted, there can be great utility for an understanding of buried materials within a three-dimensional space. The plethora of reflections can be overwhelming to any human brain to interpret, so the goal is always to determine which reflections (or series of reflections generated from reflections at one interface or feature) out of the millions that are recorded are important. If possible, the origins of reflections of interest can be determined by their distribution and intensity (as measured in wave amplitudes), and this can be used as direct evidence about what is in the ground and allows for interpretations as to the origins of features of interest.

The three-dimensional aspects of the collection of millions of reflections becomes even more complex as it takes certain ground conditions that allow the passage of radar waves and to others to generate reflections. Some understanding of the ground is therefore necessary. This can be difficult if a survey is being conducted in a new area where little is known about the geology, soils, or chemistry of the ground. But with enough background knowledge about how radar waves move and are reflected in the ground, accurate assumptions can still be made, which allow for good interpretations. This process can be very intimidating when first showing up at a site with little site-specific background

knowledge, but a few preliminary tests and calibrations can overcome those fears, which I will go over in some detail in this book.

Radar waves propagating in the ground are reflected back to the surface (and often scattered in many directions) when their velocity changes, usually along interfaces of differing materials. Those interfaces may be geological boundaries or when encountering archaeological features, moving into void spaces or often by individual objects. It is important to keep in mind that areas that produce no reflection of radar waves at all can be identified and are also important. Those non-reflective areas might be uniform geological layers or homogeneous soils or sediments that have no distinct boundaries and therefore produce no reflections (Conyers 2011). The human brain is selected to focus on distinct objects and as a result we often don't pay enough attention to uniform features, or anything that has little contrast. In GPR interpretation, it can therefore be important to pay attention to where no reflections or very low amplitude reflections were generated, as this is still indicating buried features that might be important.

It is no wonder that the plethora of reflections in three-dimensional space, with varying strength and distribution can become overwhelming to the novice (or even an experienced but pressed-for-time) GPR practitioner. Fortunately, we have various software programs that can take huge datasets of 3-D reflections, re-process the raw data, re-sample waves of interest and then generate images that can be interpretable. The goal is to determine how to get software to focus on the reflections that are useful to whatever the goals of the study might be, and to quickly make "sense" out of "nonsense." Some software has recently been developed, which claims to be "auto-processing," and this seems to suggest that this is a variation of "machine learning" or perhaps artificial intelligence procedures. Call me skeptical about this claim, as each location where GPR data are collected is unique and highly variable as to ground conditions. When goals of a survey are relegated to an automatically generated series of computer created images, the product is likely to be artistic and interesting. But are those results providing specific answers to specific questions? I am still a believer that only the human brain can ask and answer pertinent questions, and there needs to be an iterative process between our brains and the software to produce images that can be generated to specifically answer those questions. When images, however produced, are to be interpreted the human brain must then be employed to make interpretations that are important for whatever the questions might be.

Ground-penetrating radar data are collected by most users along closely spaced transects within a grid, with each transect producing a reflection profile generated from thousands of reflections received from various depths (Figure 2.1). Many closely spaced profiles then are used to produce the three-dimensional distribution of reflected waves. In the last ten years or so systems have become common that can simultaneously collect tens, or even hundreds,

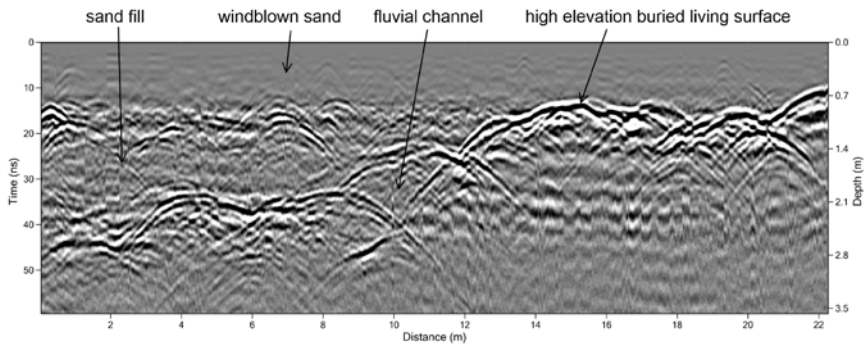


**Figure 2.1.** Reflection profile from western Portugal displaying a buried living surface on a raised area of high elevation on the right, with fluvial channels on the left. All is buried by aeolian sand. *Source:* the author.

of reflections in arrays from multiple closely-spaced antennas, producing narrowly spaced reflections within a three-dimensional “cube” (Gustavsen et al. 2020). These newer systems also use global positioning systems (GPS) with high accuracy and fast processing time to integrate spatial information with the reflections obtained within the ground so that all collected reflections can be adjusted for topographic changes and accurately placed into space (Conyers and Leckebusch 2010; Gaffney et al. 2012; Trinks et al. 2010). These systems are seeing an increase in popularity, but they continue to be quite expensive and processing of huge datasets can be difficult without advanced software.

Ground-penetrating radar, unlike many other near-surface geophysical methods, is an active method that transmits electromagnetic waves from surface antennas into the ground, and then measures the time elapsed between when the waves are sent and when they are received back at the surface (Conyers and Goodman 1997). Radar wave travel times are measured in nanoseconds, which are billionths of a second. As the antennas are moved along the ground surface (whether as individual antennas or in antenna arrays), individual series reflections are recorded at programmed intervals (often every two centimeters or greater distance) along transects, using a variety of collection techniques (Neal 2004). The “form” of the individual reflected waves (called a waveform) is wavelength and wave amplitudes. These waves travel back to the surface from a buried reflection surface, are received at an antenna, digitized, and displayed in a reflection trace (Figure 2.2). A trace is nothing more than a series of waves generated at various depths in the ground that have reflected back to one surface location. When many traces are stacked next to each other sequentially, a two-dimensional vertical profile is produced (Figure 2.1). With antenna array systems this collection procedure can save many hundreds of traces a second, and as the arrays are moved many thousands of traces can be collected and digitized over small areas of ground every second (Corradini et al. 2022).



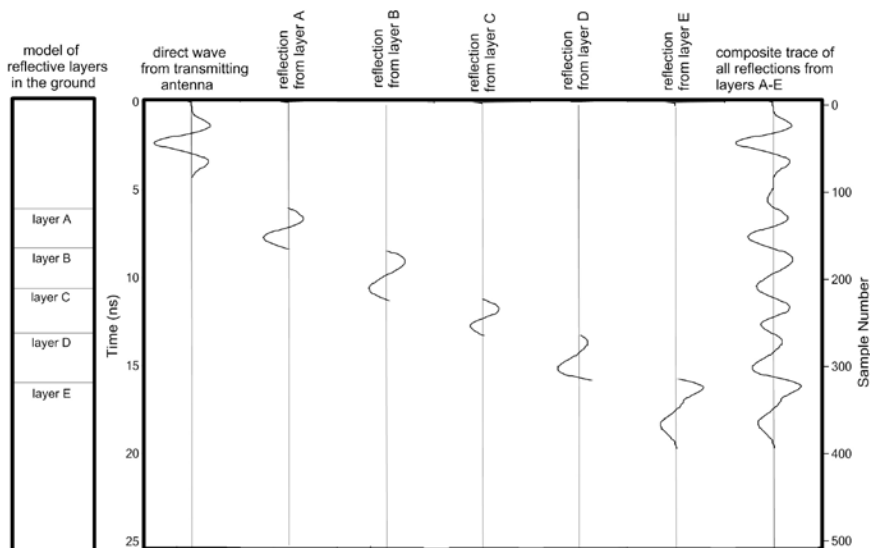


**Figure 2.2.** Creation of a reflection trace starting with the direct wave on the left, which begins at time-zero and with reflections produced from buried interfaces A through F. When all reflections are recorded at one location on the ground, a trace, which is a composite of all these individual reflections, is saved. *Source:* the author.

Depending on the amplitude of reflections in traces important aspects of the ground can be determined. If there is a layer in the ground that is distinctive enough (it varies enough in composition and water retention from the layers surrounding it), a high amplitude reflection will be generated (Figure 1.1). Along the same profile materials in the ground that do not generate reflections because of there are no distinctive buried surfaces, will allow radar waves to pass through it without generating any substantial reflections.

Reflected radar waves are often processed into two-dimensional profiles in “real time” and can be viewed on a computer screen during collection. The waveforms are recorded in elapsed time from their transmission to reception back at the surface (called two-way travel time). Once the velocity of the waves is calculated these wave travel times can be converted to approximate distance in the ground, giving each of the reflections within millions of traces collected in a grid a precise depth measurement. This three-dimensional result is not available with other near-surface geophysical methods. The amplitudes of the reflected waves are particularly important because their variations are directly related to changes in the physical and chemical properties of different materials in the ground.

Ground-penetrating radar surveys allow for a relatively wide aerial coverage in a short period of time, with excellent spatial resolution of buried materials and stratigraphy. Surveys can be conducted covering many hectares (especially

with multiple antenna array systems) that can be termed “landscape scale” studies (Gaballah et al. 2018; Gaballah 2019; Ranieri et al. 2014). Small very detailed grid areas are often advantageous, when features are small and difficult to see in large grids of data, and very high-resolution grids of perhaps 5×5 meters or even smaller are possible. Those smaller “mini-grids,” if collected with very high-resolution antennas where traces are spaced very close together, can yield amazingly accurate images of very small features. Typically, GPR is used to map materials at depths from a few tens of centimeters to 5 meters in depth. In optimum conditions, and using the appropriate antennas, these greater depths of resolution are possible, but not common (Conyers 2012).

Single channel (one transmitter and one paired receiver) GPR units are very portable and can be checked through on airplanes as baggage and transported in a backpack almost anywhere. Most systems are powered from a variety of high-amperage batteries. They can be integrated with global positioning system antennas that can record location and elevation data along with the radar reflections from the ground (Figure 2.3). The earliest model GPR systems recorded raw recorded reflection data on paper printouts that precluded post-acquisition processing (Conyers 1995). Thankfully those days are over. All modern systems very efficiently record digital reflection data that can be downloaded for later filtering, processing, and sophisticated data analysis. A few interesting systems can process data immediately after recording with blue tooth connections or other wireless transmitting to computers that generate “real time” results (Ozkaya et al. 2020). More commonly data are downloaded to a computer soon after acquisition for processing and interpretation, which can often begin while still in the field. Rapid analysis can be beneficial as buried features can be quickly identified and future data acquisition planned based on those rapidly generated results. In this way field operations can be an iterative



**Figure 2.3.** A GSSI SIR-4000 recording system with 400 MHz antennas on a survey cart with an attached RTK GPS antenna for location data. *Courtesy of GSSI Inc.*

process that incorporate collection, processing, analysis and interpretation, followed immediately by additional acquisition based on those results.

The success of GPR surveys is dependent on soil and sediment mineralogy, clay content, ground moisture, depth of burial, surface topography, and vegetation (Conyers 2012). It is not a geophysical method that can be immediately applied to all geographic or archaeological settings, although with thoughtful modifications in acquisition and data processing methodology, GPR can be adapted to a great variety of site conditions. In the past, it was assumed that GPR surveys would only be successful in areas where soils and underlying sediment are dry and often sandy ground was the preferred medium (Vickers and Dolphin 1975). I used to believe this dogma and was also successful in using GPR in this kind of environment. But I quickly learned that a variety of ground conditions are conducive to GPR surveys even those in wet areas with an abundance of clay (Conyers 2004; Conyers 2012; Doolittle et al. 2007). I made some egregious early mistakes by turning down research projects in warm tropical settings, because I believed that GPR dogma about dry, sandy ground. Over the years, I have collected very poor GPR data in dry sandy ground and produced wonderful results in wet clay areas (Conyers 2006, 2012).

Prior to conducting a GPR survey, it is important to take into consideration what types of equipment to use (especially antenna frequencies) so that proper collection methods can be employed, and data acquisition parameters adjusted to field conditions. These factors will vary considerably depending on the geographic and geologic setting of the surveys, surface obstacles, ground type and soil and sediment moisture composition, and the depth of the features and stratigraphy to be studied. Many, if not most of these variables will be unknown when initiating a survey, and even if they are generally known it can be difficult to take them all into consideration. Therefore, acquisition methods and equipment calibration parameters must often be adjusted and modified while in the field, especially after some preliminary data are collected and analyzed. At the beginning of a survey preliminary calibrations that appear to be adequate often are not optimum and must be changed during the initial phases of data collection. This can often be a somewhat nerve-racking experience, especially if bystanders are looking on expecting immediate results and asking the most common and annoying question: "Have you found anything yet?" When this occurs, all one can do is politely explain that a great deal of thought must go into preliminary analysis of field conditions before any results are available, and then get back to work. Often with some deliberation and modification optimum data collection procedures for each study area can be arrived at, but rarely before the first useful reflection profile is collected and studied.

## **HISTORY OF GPR**

The first large-scale application of radar (the acronym for RAdion Detection And Ranging) was during World War II when the British and later Americans

and Germans used crude but effective systems to detect airplanes (Buder 1996). The first attempt at what could be called ground-penetrating radar was made in Austria in the 1920s to determine the thickness of ice in a glacier (Stern 1929). The ground-penetrating aspects of radar technology were then largely forgotten until the 1940s and 1950s when U.S. Air Force radar technicians on board airplanes noticed that their radar pulses were penetrating glacial ice when flying over Greenland. Several mishaps occurred because airborne radar analysts were detecting the bedrock surface below the ice and interpreted it as the ground surface, neglecting to see the large thickness of ice above and leading planes to crash into the glacier surface. This realization that radar would readily penetrate ice ultimately led to numerous investigations into the ability of radar to detect several subsurface interfaces, including soils and the groundwater table. In 1967, a prototype GPR system was built by the National Aeronautics and Space Administration (NASA) and sent on a mission to the moon to determine surface conditions prior to landing a manned vehicle (Simmons et al. 1972).

The applicability of GPR to locate buried objects or cavities such as pipes, tunnels, and mine shafts (Fullagar and Livleybrooks 1994) was immediately recognized in the 1970s, and its widespread use as a geotechnical tool began. Methods were soon developed to define lithologic contacts (Baker 1991; Basson et al. 1994; Bristow and Jol 2003; Davis and Annan 1989; Jol and Smith 1992; van Heteren et al. 1994), faults (Deng et al. 1994), and bedding planes and joint systems in rocks (Bjelm 1980; Cook 1973, 1975; Dolphin et al. 1974; Moffatt and Puskar 1976). Soil scientists and hydrologists also began using GPR to investigate buried and surface soil units (Collins 1992; Doolittle 1982; Doolittle and Asmussen 1992; Doolittle and Collins 1995; Freeland et al. 1998; Johnson et al. 1980; Olson and Doolittle 1985; Shih and Doolittle 1984; Zajíčová and Chuman 2019) and the depth and nature of the groundwater table (Annan 2005; Beres and Haeni 1991; Doolittle and Asmussen 1992; van Overmeeren 1994, 1998). Other work has shown the utility of GPR for mapping specific packets of sediment for the definition of ancient depositional environments (Barone et al. 2011; Bridge et al. 1995; Bristow et al. 1996; Bristow and Jol 2003; Grasmueck et al. 2004; Jol et al. 1996; Jol 2009; McGeary et al. 1998; Sandweiss et al. 2010; van Overmeeren 1998). The applicability of using GPR techniques for locating unexploded ordinance and land mines has also been studied, with great promise (Bruschini et al. 1998; Daniels 2004). Civil and structural engineers have used GPR to map road pavement structures and have applied those data to the inspection of the interior of many different media (Al-Qadi and Lahouar 2005; Hugenschmidt et al. 1998; Hugenschmidt 2002). Forensic scientists and law enforcement agencies' desire to find buried bodies or other materials has expanded the use of GPR in a number of instances, locating graves and sometimes actual human remains of murder victims or other bodies in the ground (Conyers 2012: 129; Damiata et al 2012; Davenport 2001; Davis et al. 2000;

Ivashov et al. 1998; Nobes 1999; Schultz et al. 2006; Schultz and Martin 2011; Strongman 1992; Solla et al. 2012).

In the archaeological community GPR was first used to locate and help define buried archaeological features at Chaco Canyon, New Mexico (Vickers et al. 1976), to locate buried walls at depths of up to 1 meter. This initial survey collected only several experimental antenna traverses at four different sites and paper reflection profiles were generated and analyzed in the field. It was determined that a few of what were termed “anomalous radar reflections” represented the location of buried walls.

These rudimentary studies at Chaco Canyon were followed by several GPR applications in historical archaeology. Radar surveys were successfully used in the search for buried barn walls, stone walls, and underground storage cellars (Bevan and Kenyon 1975; Kenyon 1977). In these early studies what were described as “radar echoes” were recognized as being generated from the tops of buried walls, and depth estimates were made, using approximate velocity measurements based on local soil characteristics. Often the origins of reflections could be inferred by their shape and intensity, but little effort was made in understanding what about these buried features that had created the types of reflections that were visible.

Initial successes in historical archaeological applications were followed in the late 1970s at the Hala Sultan Tekke site in Cyprus (Fischer et al. 1980) and the Ceren site in El Salvador (Sheets et al. 1985), where I did my PhD research with GPR (Conyers 1995). Both early GPR surveys produced unprocessed reflection profiles in the form of paper records that were successful in delineating deeply buried walls, house platforms, and other buried archaeological features. It appears that these initial successes were likely a function of good ground conditions where electrically resistive matrix material that was relatively “transparent” to radar energy propagation, allowing for energy penetration and produced very distinct and relatively uncomplicated reflection records were recorded and immediately visible in simple displays, sometimes just paper print-outs of raw reflection profiles.

Most of the early GPR surveys for archaeology were “exploration” efforts whose goal was to locate graves, buried artifacts, and house walls, such as one of a sixteenth-century Basque whaling village in eastern Canada (Vaughan 1986). Here the ground was extremely challenging as it contained large cobbles and complicated stratigraphy that produced a variety of difficult to interpret reflection records. Nonetheless, this exploration survey found some large artifacts and archaeological features that were buried by up to two meters of beach deposits and peat, visible as distinct reflections in profiles. They were excavated and confirmed. This was good evidence for the utility of GPR even considering the difficult and complex ground conditions. That study was important because its results when published went beyond just locating anomalous reflections that might be something important in the ground. The researchers put some

thought into determining what was visible and what was not, and it was hypothesized that grave goods consisting of bone, did not contrast enough with the surrounding beach deposits to appear as distinct reflections. Some reflections were found to have been generated from buried walls that consisted of piles of beach cobbles used for walls and foundations. Those appear to have been difficult to discriminate from random rocks. I like this early published work as it spent some time attempting to understand what caused radar reflections, and what did not. It was the first publication that moved beyond the basics of pointing out “anomalous reflections” or “echoes” that may or may not have been generated from something of interest. This step is important, as the origins of reflections based on an understanding of both the ground and what radar energy does in the ground is the key to data interpretation.

An interesting set of GPR surveys were conducted in Japan in the mid-1980s to locate buried sixth-century houses, burial mounds, and what were termed “cultural layers” (Imai et al. 1987). As with previous work, all interpretations were made from analyzing reflection profiles only, as amplitude slice-maps had not yet been developed for GPR. These studies produced very high-quality reflection profiles and were successful in identifying ancient pit dwellings with clay floors, which were buried in some cases by as much as two meters of volcanic pumice and sandy soil. The interface of the house floors with the overlying pumice produced very distinctive reflections that were readily recognizable from viewing reflection profiles. In these studies, the volcanic matrix was mostly uniform in composition and composed of quartz-rich un-weathered ash, which readily allowed the passage of radar waves. The clay floors were constructed out of a distinctly different material, producing what was termed a “velocity contrast” at the interface of the floors and the overlying ash. This compositional contrast produced high amplitude reflections that were readily recognizable in reflection profiles. The reflection profiles were used as a guide to excavations that followed, confirming their interpretations. These excavations also revealed distinct stratigraphic horizons (that they termed “cultural layers”), which were buried soil horizons containing many stone artifacts discarded during different periods of occupation. This was an important study because it used reflection profiles as primary data from which to plan excavations. Those excavation results were then directly tied back to the GPR reflections to identify important geological horizons (anthropogenic soils) directly related to the ancient occupation.

Throughout the late 1980s and early 1990s, GPR continued to be used successfully in several archaeological contexts, but in most cases, these studies were what could be called “anomaly-hunting” exercises by those early adherents. Usually unprocessed or partially processed reflection profiles were viewed as paper records, or on a computer screen as they were acquired, and interesting reflections, which might possibly have had archaeological meaning, were excavated. Unfortunately, these surveys were poor at discriminating archae-

ological feature reflections from geological reflections and there were many reported “false positives” as well as “false negatives,” which were not identified and therefore remain unknown. Those studies often left anyone reviewing the results with the impression that GPR was a “hit-or-miss” method at best. It is important to remember that many of these early studies were making interpretations of only reflection profiles, none of which had been processed in ways we now consider standard procedure. They were largely analog-based images, which were all that was available before the advent of digital GPR systems.

About this time, I started to become involved with GPR for my PhD research. I was lucky to have some data to work with acquired at the Ceren Site in El Salvador (Sheets et al. 1985), which was collected before the invention of digital GPR. I was not involved in that initial work. It was planned by Gary Olhoeft (later at Colorado School of Mines) who had the foresight to attach a magnetic tape recorder to the GPR system, which “recorded” the data as minor voltage changes on an old-fashioned real-to-real tape. In collaboration with Jeff Lucius, we took that tape and converted the voltage changes in an early data digitizer, and ended up with one huge file of waves, with no definition of where each trace started and stopped (let alone each reflection profile), and therefore no way to take traces and make profiles out of them. Fortunately, Jeff Lucius is a programming genius, and he wrote some simple code to find the start and stop of each profile and determine where each trace began in the time-window. The recorded waves were properly organized, digitized, and reflection profiles produced. Once they were in digital format, we could process them by removing background noise and perform other very rudimentary data processing methods (Conyers 1995). The work for my PhD research relied only on those digital processed results but using only a manual analysis of the resulting reflection profiles, which were printed out on paper. As silly as it seems now, I colored reflections on the paper printouts with pencils and measured depth with a caliper. At that time, I had no access to software that would produce three-dimensional images of the ground, so those data points were put on a base map and hand contoured.

Many other workers in the late 1980s were also going to great lengths to “go to digital” with GPR, even though true digital systems were not yet on the market. Ken Kvamme in the early 1990s went to the length of scanning paper reflection profiles that had been printed on paper and using the images to assign digital values to shades of gray on the paper printouts. This was marginally useful, as the software to take digital GPR information and do anything sophisticated with it had not yet been produced.

Starting about 1990, Dean Goodman and his colleagues in Japan (Goodman and Nishimura 1993; Goodman 1994, 1996; Goodman et al. 1995, 1998) obtained one of the first digital GPR systems, which recorded data on small magnetic cassette tapes. He was the first to write computer code to take those digital GPR files and slice them horizontally to produce amplitude slice-maps,

which was influenced and guided partially by his PhD research in deep ocean seismic analysis. This initial code for what he later called “GPR-Slice” was written on an IBM 286 computer with two “floppy drives,” one with his rudimentary software program and the other with the data to be processed. Results were only visible on the computer screen and had to be “screen captured” to save the resulting images. While this process seems very elementary now, this was a great stride in GPR data processing as these studies opened many eyes to what GPR was capable of. The timing of Dean Goodman’s pioneering software development was fortuitously coincident with newly developed digital GPR systems (Goodman et al. 1995). It was about this time that I met Dean and we began to collaborate on the first edition of this book (Conyers and Goodman 1997). In this work, a wide range of ground conditions were discussed from both our work and computer models were constructed to help in the interpretation of reflection profiles. Back in those days all of us in GPR were still trying to figure out what radar waves did in the ground and how our generated images could inform us about the ground. That was a slow process and full of trial and error.

Very quickly people began to collect and process GPR reflection data using the digital advancements that were occurring in the 1990s (Neubauer et al. 1999). Amplitude slice-maps became the most common processing technique (then called time-slices), with reflection profile analysis taking a “back seat” perhaps because of the difficulty many had with interpreting the complex reflections in these images. It was quickly recognized that the amplitude slice-maps, in the right circumstances were often superior, especially with novices or those needing immediate results to present to novices. Profiles tended to be seen as confusing “wiggles” and there were often just too many of them in a grid to occupy interpretation time. By the early 2000s the application of two-dimensional computer simulation and three-dimensional processing techniques (Boniger and Tronicke 2010; Conyers et al. 2002; Conyers 2010; Conyers and Leckebusch 2010; Goodman et al. 1995, 1998, 2004; Goodman and Piro 2013) showed many that even GPR datasets that appeared to have no immediately interpretable reflections when viewed in confusing profiles can still yield valuable data when data are computer processed. These types of advancements have increased exponentially in the last 2 decades.

The advancements in GPR displays, mostly of amplitude slice-maps, demonstrated to many that GPR could map areas quickly and identify “anomalies” that often-represented features of interest (Butler et al. 1994; Sternberg and McGill 1995; Tyson 1994; Valdes and Kaplan 2000). Here I will quickly note that I am very much opposed to the use of the word “anomaly” with GPR as it is a vague “catch-all” term that often identifies the user as someone who really doesn’t know what has produced these “anomalous” reflections or perhaps someone who has not taken the time to think through their origins. I will try in this book to describe radar reflections and the images that are produced



from them in a way that will allow interpreters to say much more about buried features visible with GPR other than that they are “anomalous.”

When thinking about radar waves, and what produces them, every radar reflection that is generated in the ground is, by definition, “anomalous” (defined as something that deviates from the norm or mean). With radar waves the “mean” is no reflection at all, and therefore any reflection with any amplitude at all, is a deviation from that mean. Therefore, all radar data are composed of nothing but anomalies. Perhaps in amplitude slice-maps a high amplitude reflection that is continuous might be “anomaly” as it is different than whatever is not displayed in a profile. Those are likely to be surrounded by waves of lower amplitude, but they are also anomalous. Therefore, everything in a reflection profile is anomalous! To complicate this silly discussion even more, the areas of no reflection may be just as important as the high amplitude areas, or perhaps even medium-amplitude areas.

Here I will instead try to describe how an understanding of radar wave theory including propagation and reflection can identify specific buried features that are of interest using a variety of computer technology within software programs that are commonly available. Reflections will be defined by their geometry and reflection amplitude. Those waves can then be interpreted as being created from certain materials in the ground, and in that method, we can interpret what is in the ground in a much more robust way than just pointing out anomalies.

Besides the production of standard GPR images such as slice-maps and reflection profiles this book discusses how computer filtering and then enhancement of GPR reflection data can produce multiple images of the ground that are displaying certain specific properties of the buried features of interest (Boniger and Tronicke 2010; Conyers 2010, 2012; Conyers et al. 2002; Conyers and Leckebusch 2010; Goodman et al. 1998, 2004; Leckebusch and Peikert 2001; Leckebusch 2003; Leucci and Negri 2006). For instance, a very simple technique is to remove the lower-amplitude reflections (if it is determined they are not of interest) and then displaying only those that are high-amplitude (Conyers 2004). Once those images are made certain wave amplitudes of a defined magnitude might be displayed as “virtual reality” images of what lies below the surface. This could be done by “cutting through the block” of three-dimensional data (Conyers and Goodman 1997; Neubauer et al. 2002) or perhaps rendering in 3-D isosurfaces that are images of only the amplitudes desired, presenting the final product as rotating images or videos (Conyers et al. 2002; Goodman 1998; Goodman et al. 2004; Heinz and Aigner 2003; Leckebusch and Peikert, 2001; Piro et al. 2003). These are now all becoming standard practice.

Another advancement that has taken place in the last ten years is the use of multiple geophysical datasets from different methods to be merged and interpreted together (Ernenwein 2009; Piro and Goodman 2013; Kvamme 2005; Kvamme et al. 2019; Conyers 2015, 2018; Neubauer et al. 2002). This method

will be discussed briefly here but is beyond the scope of a book dedicated to GPR. Sometimes termed “data fusion,” it is a way to define certain attributes derived from certain datasets and compare and contrast them based on their spatial and other attributes. This has often been done by comparing, contrasting, and mathematically or visually “merging” data from one or more methods in a variety of map views. I find this to be much too complicated and with limited utility, as different geophysical methods are displaying different “readings” in very different ways when plotted spatially in maps. For instance, a trench, which is visible in GPR profiles will not readily appear in a slice-map, but it might be filled with organic matter and therefore yield a positive magnetic reading. Only when looking at a simple feature such as this in individual GPR reflection profiles, and then comparing the magnetic readings over that trench to the feature visible with GPR can an interpretation be made (Campana 2008; Conyers 2017; Filzweiser et al. 2017; Filzwieser et al. 2018). I am therefore always suspicious of data-fusion that attempts to “fuse” large databases together over a large area. This, in my opinion, is nothing more than trying to find correlation between “anomalies,” which is bound to lead to erroneous interpretations.



# 3

## *Radar Wave Generation and Propagation*

Radar waves that move in both the air and within the ground are a form of electromagnetic energy composed of co-joined oscillating electrical and magnetic fields (Figure 3.1). These waves are generated when an electric current oscillates in a conductive body, producing a subsidiary magnetic field (Kraus 1950; Rojansky 1979). Electromagnetic waves composed of both types of waves are generated and joined to propagate outward from the source, with the electrical portion of the waveform moving perpendicular to the magnetic (with an offset of the two waves' peaks and troughs, but this need not be discussed here). If either the magnetic or electrical component of the propagating wave is lost (attenuated, absorbed, conducted away or dissipated by spreading over a larger and larger area), the waves will cease to move and die. Propagation of radar waves occurs readily in air or any void space, and unless they encounter a medium that absorbs or reflects them, they will travel an infinite distance. Radar waves can penetrate up to a few meters or more in some ground conditions before they are attenuated, and the energy is lost.

Radar waves are a part of the electromagnetic spectrum that includes visual light, X-rays, ultraviolet and infrared radiation, TV, radio and cellular-phone transmissions, gamma rays, and many more (Figure 3.2). Each is defined by their wavelengths. This is important only in so far as a recognition that there are overlapping waves of many frequencies from sources other than GPR antennas. Many sources produce waves that are a similar wavelength to GPR antennas and therefore will interfere with radar waves that are recorded at a receiving antenna. This is particularly important in the higher frequency part of the radar spectrum, where waves from military transmissions, other radio sources and cell (mobile) phone transmissions. Military radar usually occupies the same range as some of the lower frequency GPR antennas (400 MHz and lower, while cell-phone waves overlap with the higher frequency GPR waves (800 MHz and higher). The frequency spectra inhabited by different applications are constantly changing as governments assign certain frequencies to various users (sometimes these are private companies that pay for the use

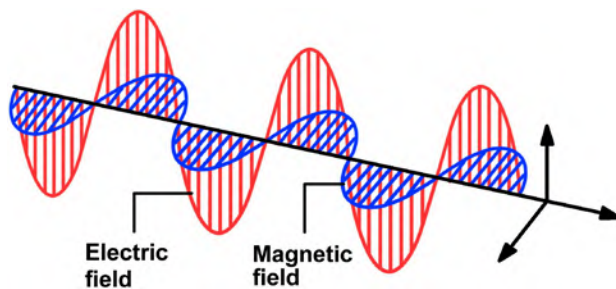


**Figure 3.1.** A propagating electromagnetic wave composed of conjoined, oscillating fields of electrical and magnetic energy. They oscillate perpendicular to one another as they propagate at the speed of light in air, and slower in the ground. *Source:* the author.

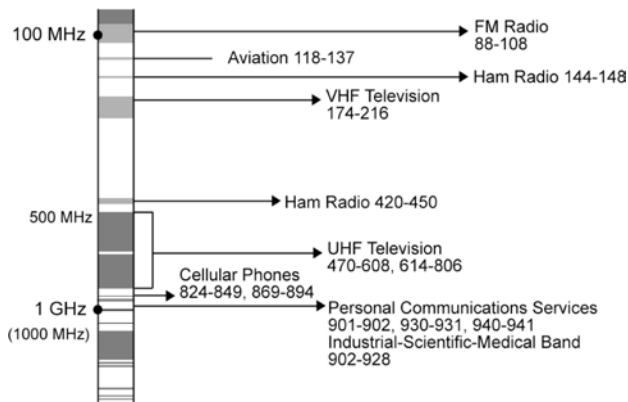


**Figure 3.2.** The electromagnetic spectrum that includes many sources of radar energy within the general boundaries of the radar-waves spectrum used in GPR. *Source:* the author.

of some frequencies). In Europe some frequency bands are jealously guarded, and permissions for GPR antennas of certain frequencies are necessary. Theoretically the International Telecommunication Union (ITU) is set up to monitor the allocation of frequencies and permissions for various devices, but those permissions tend to be quite “fluid” depending on what part of the world one is working (Chignell 2004). What is important is that during GPR data acquisition it is sometimes possible that GPR receiving antennas can be “blasted” with airborne electromagnetic waves from unknown origins, which can totally overwhelm GPR waves coming from within the ground. I have had this done to me commonly in Israel and in the USA near military facilities. There will be more on this subject and what to do about it discussed below.

Often in GPR we care a great deal about the propagation distance of waves in the ground. Usually there can be an approximate depth determined at which the transmitted waves attenuate, which occurs when the electrical or magnetic components of the radar waves are no longer oscillating. When one or the other components of an electromagnetic wave no longer oscillates, the propagating wave will cease to travel. The depth of wave attenuation is extremely important as we always need to know how deeply in the ground we can identify buried features we care about. This depth will differ depending on the composition of the ground.

Various explanations have been used to determine and explain depth of radar wave penetration in certain types of ground. Some early explanations pointed to, among others, the magnetic component of the propagating waves, which could affect transmission (Olhoeft and Capron 1994). In this idea magnetic losses (relaxation), which is a function of the magnetic permeability of materials, would affect that component of the propagating radar wave. Therefore, materials such as basalt lava, which is high in the mineral magnetite would potentially attenuate propagating radar waves within it (Carcione 1996). Actual analysis of GPR results in highly magnetic ground, however, has shown that the magnetic component of propagating radar waves is probably not a significant attenuating element (Conyers and Connell 2007; Shoemaker et al. 2020). There has been shown to be very good depth penetration of radar waves in un-weathered basalt that contains magnetic minerals. This is not the case when basalts or other materials that at one time were high in magnetic minerals are weathered to various clay minerals. Most clays, especially when they retain moisture, are highly electrically conductive, and it is this electrical conductivity that appears to be the major factor in the attenuation of radar waves in the ground (Alsharahi et al. 2016; Baker et al. 2007; Zhao et al. 2018).

In general, higher conductivity ground is a function of the types of clays that are present, and how moist those clays are. Clay minerals produced as a product of weathering (as opposed to clay “size fraction,” which only designates the size of very small rock fragments in a sedimentary unit) come in two general types 1:1 and 2:1 clay (Birkeland 1984). These designations are defined by the

ionic bonds in the clay and how their minerals adhere to each other in “plates.” The 1:1 clay, kaolinite being the most common, have a very low electrical conductivity (Bain and Smith 1994; Rhoades et al. 1974), so radar waves moving within materials that contain this clay mineral are not greatly attenuated. This is not the case for 2:1 clay, of which there are many types such as montmorillonite, smectite and bentonite. Those clays, when they retain water, are electrically conductive and highly attenuating to propagating radar waves.

Kaolinite is often the product of intense weathering common in humid tropical areas of the world where a good deal of water has moved through the ground (Walker et al. 1973). This clay mineral’s 1:1 structure impedes ion movement, and therefore has a low electrical conductivity, which results in little radar energy attenuation (Kriaa et al. 2014). In soils formed in more temperate areas of the world (Zajicova et al. 2019) 2:1 clay is more common and therefore are the primary limiting factor in radar energy propagation depth. In temperate areas that have a good deal of water movement, clays can also be translocated deeper in the ground (Birkeland 1984), which can be beneficial for GPR.

There are maps for each state in the United States (Doolittle et al. 2010) that estimate how well GPR will work based on published soil properties, which contain descriptions of clay types, as well as salt content of soils that were made for agricultural analysis. These can be good estimates of GPR effectiveness, but it is usually best to collect some test profiles prior to conducting larger-scale surveys as GPR effectiveness can differ greatly by location. There are some methods where multiple geophysical methods can be predictive indicators of GPR effectiveness (Van Dam 2016) including simple soil electrical conductivity meters.

It is usually easy to determine the depth of radar wave propagation, and therefore the depth at which the electrical conductivity of the ground has attenuated those waves. Some software programs have an automatic depth analysis that can calculate the depth at which “coherent” radar that are recorded at the surface antenna change to high-frequency wavelengths. The coherent waves are almost always those produced by reflection from interfaces in the ground. The less coherent and often high-frequency waves are recorded after there are no longer waves coming from that depth in the ground. When this happens, the only waves recorded are background noise, which is likely to be high frequency, short wavelength energy that has traveled in the air from some distant radio transmitter. (Figure 3.3).

## **RADAR ANTENNAS AND WAVELENGTHS**

In GPR, electromagnetic waves are generated at an antenna, the simplest of which is a copper wire or plate on which an oscillating electrical current is applied. The electrical current then produces a magnetic field subsidiary to it, and oscillating electromagnetic waves propagate outward. Many transmitting GPR antennas are shaped like “bowties” where electrical pulses are conducted

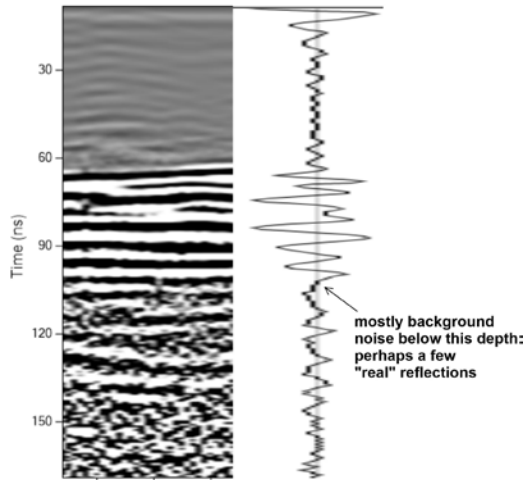


**Figure 3.3.** An analysis of the depth where GPR waves attenuate. It is visible both on the trace on the right and a small portion of a reflection profile on the left. While there may be a few coherent reflections below about 100 ns in this example, most of the propagating radar waves have been attenuated and only background noise from external sources is recorded. *Source: the author.*

to the middle or narrowest point of the copper plate and the electrical current radiates outward to far edges of the bowtie-shaped plate. At the margins of the plate are electrical resistors that arrest the electrical current. All this occurs at the speed of light. These radar antennas are termed dipoles.

Depending on the size of the copper plate, its shape and the way resistors are placed along its edges various frequencies of electromagnetic waves are created. The narrowest part of a bowtie generates the higher frequencies (shorter wavelengths) and the broader part the longer wavelengths. These are termed “broad band” antennas, which produce radar waves of many frequencies, with one “center frequency,” which is the mean of the broad band of frequencies produced.

To generate long wavelengths of a lower frequency, larger antennas are necessary. A general “rule of thumb” is that the total length of antenna needs to be one half the wavelength of the center frequency to be generated. For instance, an antenna that is constructed to transmit energy at 300 MHz (with a wavelength in air of about one meter) will need to be about 50 cm in length. It is much more complicated than this (Slolnik 1962) and recent antenna developments have produced a variety of sizes and shapes that can modulate



frequencies and are quite adaptive to different needs in modern GPR antennas. I will admit to being afraid to open my antennas' housings to take a look, because I am afraid I would not be able to put everything back together again.

Each wavelength of propagating energy will behave differently in various media, with longer wavelength waves often propagating deeper, but with less reflection from smaller objects or thinly bedded materials. Shorter wavelengths usually penetrate to shallower depths but reflecting much more readily from smaller buried discontinuities (Conyers 2012; Leckebusch 2003; Leucci et al. 2012; Neal 2004). There was a time when I tried to understand the complex equations that define this relationship of wavelength to depth penetration and asked a good friend who was well versed in radar theory. After he confused me for a while and gave me many articles on radar theory with many equations, I asked him to put this concept into terms that would allow others (and me) to understand. He made the analogy to taking a walk in the park. If a walker were to adjust stride deliberately move her feet shorter distances, she would tire much more quickly than with a longer stride. This is analogous to a higher frequency of wave oscillation "tiring out" quickly and becoming attenuated at a shallower depth. This is a much-too-simple explanation, but I think of it often when explaining this wavelength (frequency) property to propagation depth, where stride distance is a metaphor for wave oscillation frequency.

The frequency of propagating radar waves is measured in units of hertz, which is defined as cycles per second (Lax and Nelson 1976). Gamma rays, X-rays, and visual light have very high frequencies of wave oscillation that are many orders of magnitude higher than radar waves used in GPR, with extremely short wavelengths measured in fractions of millimeters. Radio waves, a subset of which are the common radar waves used for GPR, have much lower frequencies, with wavelengths of propagating energy that vary from a few centimeters to a few tens of meters in length. The radar energy used in most GPR applications has frequencies ranging between about 10 and 3,000 megahertz [2.6 gigahertz (GHz)] (Figure 3.2), with some very high resolution GPR antennas approaching 3 GHz.

## **GROUND PROPERTIES AFFECTING RADAR WAVE TRANSMISSION**

Soils, sediment, or rocks that are termed "dielectric" will permit the passage of a great deal of electromagnetic energy without dissipating it (von Hippel 1954). The more electrically conductive a material, the less dielectric it is, and the greater amount of energy will attenuate at a shallower depth.

Highly electrically conductive media include those that contain salt water and some that have certain types of electrically conductive clay, especially if that clay is wet. Besides clay, any soil or sediment that contains soluble salts or electrolytes in the groundwater will also create a medium with a high electrical conductivity. Agricultural fertilizer runoff that is partially saturated with soluble nitrogen and potassium can potentially increase the electrical conductivity of

a medium, as will moist calcium carbonate-impregnated soils in arid regions. Often desert soils, even if they appear to be extremely dry and therefore “should” readily allow radar transmission, contain hydrous salts in their interstices, which conduct electricity. In these types of soils, radar energy will often become attenuated at a shallow depth (Conyers 2012).

It used to be assumed that wet clay, no matter what type, would attenuate radar waves, and it was therefore unsuitable for GPR surveys (Conyers 2012; Leckebusch 2003). While this is often the case, good radar reflections have been recorded at a depth of more than two meters with a 400 MHz antenna in western Oregon, in ground composed almost entirely of saturated clay (Conyers 2012). This unusual success seemed mysterious at the time, and only after returning from the field and analyzing the soil and sediment samples collected at the site in a microscope was it discovered that the “clay” was not mineral clay. The ground was actually sediment composed of rock fragments that were of “clay size,” meaning they are smaller than 0.002 mm in diameter, which had not yet undergone diagenesis into mineral clays (Birkeland 1984). This wet clay therefore did not have the high electrical conductivity properties of the many 2:1 clay mineral. How one would readily determine in the field whether clay at a survey area was mineral clay or just sediment composed of clay-sized rock fragments, without detailed sedimentological and mineralogical analysis, is unknown.

Other minerals in the ground, especially those that can dissolve in water, will create free ions, which allow for greater electrical conductivity. Sulfates, carbonate minerals, iron, salts of all sorts, and any charged elemental species of mineral will create a highly conductive ground and readily attenuate radar energy at shallow depths (Van Dam et al. 2002). Under the very unfavorable conditions of wet (with slightly saline water), calcareous sediment or soils that contain certain clay-rich minerals, the maximum depth of GPR penetration in the ground can be much less than a meter.

Barring detailed soil chemistry studies at sites prior to data acquisition, the best method of determining an area’s conduciveness for GPR studies is to collect GPR data and visually determine depth of energy penetration in reflection profiles. Some researchers have attempted to use electromagnetic conductivity meters (EMs) and electrical resistance tools to measure near-surface ground conductivity, as those readings will generally determine whether GPR energy will successfully be transmitted to the depth desired (Bongiovanni et al. 2011; Calia et al. 2012; Leucci et al. 2012; Linford and Linford 2004; Yilmaz 2001). Care must be taken using this method, because these must be correctly calibrated to a known media first, or conductivity measurements can be invalid. To predict GPR efficacy in advance necessitates a trip to the site first for electrical conductivity tests. If GPR equipment were also available, it would probably be better to just take GPR equipment to the field also and collect a radar profile or

two at a prospective site to see how deeply radar waves will penetrate, which would yield more definitive results.

Research is still ongoing to devise an instrument that will quickly and accurately measure soil conductivity of samples, which can then be used to determine the efficacy of GPR in a survey area prior to going to the field. Some have attempted to use devices that were developed to determine the moisture content in grain shipped to storage elevators, which also use dielectric methods. Others have resorted to simple direct current devices that pass an electrical current from one electrode to another in the ground, measuring electrical resistivity, which is the inverse of conductivity. Both have had marginal success in predicting radar transmission because they are measuring either just one sample of near-surface ground, which may not be indicative of the ground as a whole, or perhaps obtaining a reading of an electrical current whose pathway in the ground cannot be readily determined. To date, there is no really good way to accurately measure electrical conductivity in the ground as it affects radar transmission, outside of some calibrated electrical devices and laboratory tests of samples obtained from various depths in the ground.

Radar energy will not penetrate metal. A metal object will reflect all the radar energy that encounters it. Metal objects are quite easy to see in GPR reflection profiles because they usually create multiple reflections stacked on top of one another directly below the first reflection (Figure 3.4). This is caused by radar energy reflecting off the metal object and traveling back to the ground

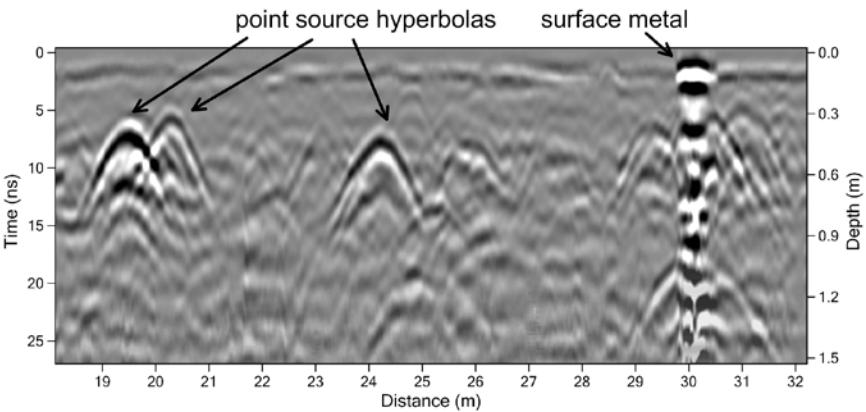


**Figure 3.4.** Reflection profile displaying a few point-source hyperbolas generated from individual objects in the ground and multiple high-amplitude reflections from surface metal. That piece of metal has become polarized, and the electromagnetic field oscillates within it, producing its own small radar antenna, which will continue to radiate radar waves to be recorded as long as the surface-transmitting antenna is directly over it. This produces a “barber pole” type of reflection, indicative of metal.  
*Source:* the author.

surface. The buried metal object then becomes its own small radar antenna as the waves oscillate within it and those waves are re-propagated back to the surface and recorded. Many waves recorded back at the surface are stacked on top of each other (the so-called barber pole reflections visible in profiles), which is a good indicator of metal. Other materials besides metal are also highly reflective, such as baked clay or some plastic objects, so multiple stacked reflections as shown in Figure 2.2 do not necessarily indicate solely metal objects. With non-metallic materials the objects do not become radiating objects like metal but reflect most of the waves that encounter them. Those waves are then re-reflected at the ground surface back into the ground and then re-reflected again to the surface from the object, many times repeatedly.

## **PRODUCTION OF REFLECTIONS**

Reflections produced in the ground occur at interfaces where physical or chemical changes cause the velocity of the propagating waves to change. When this occurs radar waves are reflected, and refracted and diffracted. If waves are then reflected to the surface and encounter the receiving antenna, they will be recorded. Energy will continue to move deeper beyond the first reflecting interface and travel deeper into the ground to encounter additional interfaces where additional waves are reflected to the surface to again be recorded (Figure 2.2). The remaining energy continues to propagate and be reflected, and refracted deeper and deeper in the ground until it finally dissipates. Energy moves into the ground in a conical pattern, and therefore its energy also dissipates due to spherical spreading over a larger area of ground with depth.

Buried discontinuities where reflections occur are usually created by changes in the electrical or magnetic properties of the rock, sediment or soil, variations in their water content, lithologic changes, or changes in bulk density at stratigraphic interfaces (Conyers 2012; Neal 2004; VanDam and Schlager 2000). Often, they are produced at interfaces between archaeological features and the surrounding matrix and along interfaces in sedimentary and soil units. Void spaces in the ground, which may be encountered in burials, tombs, tunnels, caches, or pipes, will also generate significant radar reflections because of a similar change in radar wave velocity (Solla et al. 2010). The amplitude of the reflected waves generated at a discontinuity is a function of the degree of velocity change that occurs at that interface (Conyers 2012).

While we mostly describe the interfaces where radar waves are reflected by their physical properties, for instance a bed boundary between sand and clay, the reflections are mostly created in near-surface soils and sediments by changes in the retained water between those units. Elsewhere I have detailed the theory behind this claim (Conyers 2012) with my realization coming from reflections that are received from totally water-saturated sediments in a lake. In that environment only porosity differences in various layers, where the voids are totally filled with water, creates the reflections. It is easy to see how in this

case it the water content only (as a function of porosity) that is producing a medium that is either “slower” or “faster” with respect to radar wave propagation (Conyers 2012; Neal 2004; Turesson 2006).

This simplified water-dependent explanation of what causes reflections may not occur everywhere, as there could be some extremely dry areas where it is only the difference between materials with differencing porosity filled with air that are creating the changes in velocity. That was apparent to me when viewing reflection profiles recently collected with the Mars rover (Hamran et al. 2022), which has a GPR antenna on it. Water on Mars was present billions of years ago in near-surface volcanic units, but at least near the surface it appears to have long ago dissipated. The published GPR reflection profiles from that interesting survey show dipping beds of what are likely volcanic units of varying porosity. This is a very good example of radar wave reflections produced only by changes in the porosity, which also create velocity differences. There are likely a few areas on earth where this may also be the case, but even in the driest of environments there is some water retained in clays or retained interstitially between sand or other materials, which will affect the velocity of propagating radar waves.

## **RECORDING OF RADAR WAVES**

To collect GPR reflections paired antennas, or multiple antennas in an array system, are moved along the ground in transects (Figure 3.5) usually within grids. It is often preferable to collect transects with defined Cartesian coordinates ( $x,y,z$ ). With very fast GPS location data recording it is possible to put reflected waves into spatial coordinates that is collected in a more random way. Specialized software is then necessary to process millions of radar reflections, each with its own GPS location in space, but this is possible (Gabrys and Ortyl 2020). In standard practice, one or more antennas generate propagating radar waves, and a second paired antenna (or multiple receiving antennas in an array) record the wavelets and record composite traces.

Radar antennas are usually housed in a fiberglass or plastic sled that is placed directly on the ground (Figure 3.6) or supported on wheels a few centimeters above the ground. A few systems have antennas that are supported some distance above the ground, but in this method much of the radar energy reflects off the ground surface, leaving little to couple with the ground and penetrate very deeply (Chandra and Tanzi 2019). Some recent attempts have been conducted where radar antennas are supported from drones or helicopters (Chanddra and Tanzi 2018; Merz et al. 2015; Wu et al. 2019) and while they may be capable of measuring near-surface soil differences, from what I have seen so far much of the reflected energy are high amplitude reflections generated at the ground-air interface. Airborne GPR has had more success when used on glaciers, as ice readily couples radar waves moving in air and transmits them to great depths (Grab et al. 2018).



**Figure 3.5.** Collecting GPR reflection profiles in transects a meter apart, with tracks showing the mostly parallel lines along which the antennas were moved, on a beach in Key West, Florida. *Source: the author.*



**Figure 3.6.** Collecting 400 MHz using a system supported in a backpack with an attached survey wheel for distance measurement, on an Inca floor in Ecuador. *Source: the author.*

Most commercial GPR systems have antennas that are mounted within about a half wavelength of the center frequency of the generated waves. This will allow the radar waves to couple with the ground (Blindow et al. 2007; Jol 2009; Koppenian 2009) and be transmitted downward. When two antennas are employed, which is the most common method of collection, one is used as a transmitter and the other as a receiving antenna, called bistatic collection mode. A single antenna can also be used as both a transmitter and receiver, called a monostatic system. In this type of data collection, which is usually employed with very large antennas (and also the antenna on the Mars rover where weight was a consideration), the same antenna is turned on to transmit a radar pulse and then immediately switched to receiving mode in order to detect and measure the returning reflected waves received from within the ground. Multichannel GPR systems are also common where multiple antennas produce waves in very rapid succession, while one or more adjacent antennas record the reflected waves (Conyers and Leckebusch 2010; Draganits et al. 2015; Novo et al. 2012; Novo et al. 2013, Trinks et al. 2010; Viberg et al. 2020). There are experimental antenna arrays being developed where tens or even hundreds of antennas in arrays can transmit in succession while all the other antennas within an array receive and record every wave that is reflected or refracted within the ground (Forte et al. 2021). This type of system has possibilities for the future, but the prototypes are very expensive and specialized software needs to be modified from seismic data processing where this method is commonly used in petroleum exploration (Forte and Pipan 2017; Linck et al. 2022).

Most GPR systems can generate and collect reflection traces at a very high rate and can be pulled behind vehicles on a roadway at high speeds, but this collection mode is usually not practical or desirable for most applications. In the past, data were collected using a sampling method where the first pulse from a transmitting antenna, which created a downward moving wave, was used only to collect the first sample of the returning wave from that pulse. In this recording method many digital samples in sequence are used to record the desired waveform. The second pulse generated was used to record the second digital sample and so on, until all the samples, which defined the recorded trace were used. This method is called “interval sampling” and each recorded reflection trace would need, for instance, 512 samples to define it, and therefore 512 consecutive pulses would need to be generated at the transmitting antenna. This is not difficult to achieve, as the earliest digital GPR systems were capable of generating 100,000 pulses or more per second, and there were usually plenty of pulses (and resulting transmitted waves) to define any trace, as long as antennas were not moved along the ground too fast. It was possible in this recording method that if too many samples were programmed to define each trace, or the trace spacing interval along transects was too short, the number of pulses generated could not keep up with what needed to be recorded.

Recently, the digitization process built into GPR systems is so rapid that there can be “real time” trace averaging at each unique location on the ground, to produce a much “cleaner” waveform defined by any number of digital samples. This is a trace “stacking” process where much of the background noise that is randomly collected can be removed by filtering out those waves that come from external sources before a composite digitally defined trace is saved. Termed “hyper stacking” by some manufacturers, the claim is that this that technology will enhance the depth penetration of radar waves. It is unclear to me how stacking waves that have already traveled into the earth to be recorded at the surface, will enhance their initial depth penetration. Perhaps what these claims mean to say is that this trace stacking method will remove unwanted recorded reflections that obscure the recorded waves from deeper in the ground. Those definition quibbles aside, this newly developed digitization process produces superior recorded waves, especially those reflected from deeper in the ground.

During the initial phases of GPR development some systems could only collect one trace at a time, and antennas needed to be “hopped along” the ground in steps, collecting each trace individually at each location hopped to. This collection method may still be appropriate in a few cases, perhaps where antennas are very difficult to move or where only individual traces are needed for a research goal. Most recent-vintage GPR systems are now moved continuously along transects collecting traces in sequence, with acquisition software programmed to collect them at defined distances. They can also be collected instead in programmed time intervals, with a certain number of traces recorded every second, which may be necessary where distance recording using a survey wheel attached to the antennas is not feasible.

Almost all GPR systems can collect data using an encoder wheel attached to the antennas that is calibrated for distance, or an RTK GPS systems that rapidly records geographic data to place traces into space (Figure 2.3). Sometimes both an attached wheel and GPS are used simultaneously, and in systems where arrays of antennas are moved along the ground multiple geographic data recording methods are used to place antennas (and their recorded traces) into space when antennas move along transects, turn corners and then go back along a new transect within a grid. I once used an extremely unwieldy distance measurement device attached to the antennas where string was spooled out from the antennas as they were moved, with the spool revolutions calibrated to measure distance. This was an idea quickly abandoned by the manufacturer as many of us using this method found that the ground became littered with used string, which blew around in the wind tangling us all up. In Guatemala local children who were watching us doing a survey using this string-spool device had great fun pulling on the string as it was spooling out of the reel in the antenna, making all distance measurements worthless.



No matter what the method used for placing reflected waves into space, the key to accurate spatial placement of radar waves is crucial for data analysis and interpretation. Only after this is accomplished can the recorded data be processed with confidence to produce precise maps of results. There can also be GPR surveys done indoors, underground or under dense tree cover where GPS satellites can't be used. In cases like this it is possible to use self-guided total stations to record antenna placement, or even GPS-like data collection procedures where "artificial satellites" can be placed nearby, and GPS-type data collected using triangulation methods. I have recently heard complaints from some users of these modified surveying techniques have sometimes experienced "time lags" between when location information is received from satellites or other means and when the reflections are recorded from the ground. When this error is identified, some have resorted to "time stamp" data put into both the recorded GPR traces and the GPS location data so that later recalibration of the two types of data are perfectly coincidental.

## **ACQUISITION SETTINGS AND COLLECTION PROCEDURES**

Antennas are usually connected to the GPR control unit by various cables (Figure 3.6). Some systems record reflection data digitally at the receiving antenna where it is digitized, and a data stream is sent through fiber optic cables back to the control module (Davis and Annan 1992; Neal 2004). Other systems send an analog signal from the antennas, through coaxial or other cables, to the control unit where the reflection waveforms are digitized and stored. A few systems have been developed that will wirelessly transmit recorded data from the antennas to a nearby control system, removing cables completely, which can avoid tangles (Srivastav et al. 2020; Trinks et al. 2020). All GPR manufacturers market systems that can be used by one person, with the GPR control unit, power sources, and antennas all placed on a wheeled cart or carried on a backpack for non-tethered transport within a grid (Figure 2.3).

For most standard GPR data collection, the elapsed time is measured between the radar pulse generation at the surface antenna, when the propagating waves move into the ground and the reflected waves are returned to the receiving antenna. In this way each wavelet has a unique time when it is recorded, which can be converted to depth. Recording is done within a "time-window" or the period of time a receiving antenna is "listening" for returning waves. This time period is always measured in two-way travel time (TWTT) and is programmed into the GPR acquisition software before any data are collected (Figure 1.1). This can be a tricky procedure as one must know, or try to understand, how deeply in the ground the waves need to propagate, which depends on what questions are being asked. It is also affected by the velocity of the propagating radar waves traveling in the ground. Neither of these crucial variables are usually available when starting a survey in a new area. I have made some terrible blunders by not paying attention to these two variables before programming

the time-window. Once I was hasty in recording data within a 30-nanosecond time-window. Later, after deliberating on why I had not “seen” what I expected to see in the reflection profiles, I recalculated the wave velocity and the recording depth needed. I quickly determined that the waves of interest were below the time-window programmed, and therefore not recorded. This was a terrible mistake and the only way to rectify it was to re-collect all the reflection data with a longer time-window (50 ns instead of 30 ns). I have since spent much time at the beginning of a survey collecting test lines, estimating velocity, and viewing test reflection profiles to determine depth penetration and resolution of the interfaces in the ground. That pre-acquisition analysis is time well spent.

All recorded waves received at the antenna are amplified, processed, and digitally recorded for immediate viewing on a computer screen and stored on some kind of digital medium for later post-acquisition processing and display. The data collected within a time-window includes the amplitude and wavelength of the reflected radar waves. The resolution of the amplitude of the waves is a function of the “dynamic range” of the recording system. In the early days of GPR all systems had 8-bit dynamic ranges. They quickly moved to 16-bit systems. Newer systems are higher than this, with each increase in dynamic range producing more digitally precise waveforms and therefore greater resolution.

Another acquisition setting are “gains,” sometimes referred to as “range gains,” which amplify the recorded waves received in the ground, so they can be viewed immediately on a computer screen. These gains can be adjusted before data are collected and a gain-curve applied to amplitudes (Figure 3.7), with those from deeper in the time-window needing greater gaining (due to progressive attenuation with depth in the ground). In the past some GPR systems applied the gains that were set during initial calibrations to all recorded waveforms. That turned out to be a bad idea, as many novice users were often setting gains in one area of a survey, saving them, and when the antennas were moved to other areas of a survey grid some recorded waves were gained too high, and their received amplitudes gained so high they were “off scale.” This is termed “wave-clipping” (Figure 1.1) and is to be avoided. Most new GPR models save the recorded waves as “raw” waves with no gains applied, to compensate for possible over-gaining mistakes. With this collection method gains must be reapplied during data processing and the production of images for interpretation. Another way around this problem has been incorporated into collection procedures by some GPR manufacturers that saves two complete datasets for each profile collected, one gained by those values set in the field, and one a raw reflection dataset.

Another important pre-collection setting is to filter out some of the recorded data to remove unwanted frequencies that are received. Those frequencies may have been generated from background radio wave transmissions of various frequencies or even “noise” within the GPR system. I have had little success with

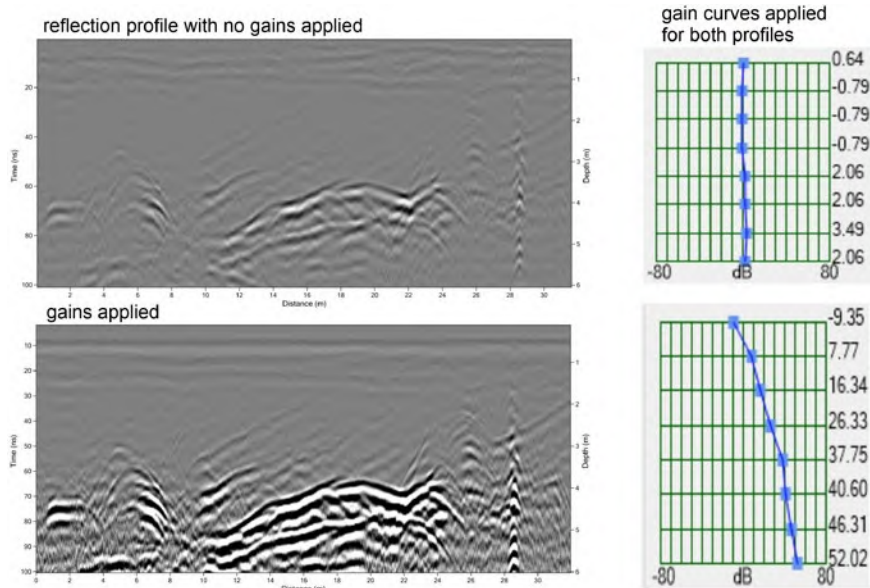


**Figure 3.7.** Illustration of a reflection profile where no gaining is used (upper profile), and so the reflections from deeper in the ground are barely visible. When arithmetic gains are applied the deeper reflection amplitudes are increased and become visible in the lower profile. *Source:* the author.

this procedure, as it is almost impossible to know the source or frequency of miscellaneous recorded radar waves. I have spent too much time with a variety of hand-held gadgets that purport to define radio wave frequencies in the air. While those appear to be fairly accurate for cell-phone transmissions, they are not very good at identifying radio waves from military sources or less traditional transmissions. I therefore usually set some broad acquisition filters that will allow the maximum amount of radar energy to be recorded during collection and perform filtering later during data processing and analysis to “clean-up” the recorded waveforms (Economou et al. 2015).

In most acquisition methods the antennas are moved across the ground at an average walking speed, recording received wave traces at a programmed separation distance. The shorter the distance between recorded traces, the greater the subsurface resolution. Most GPR systems can be pulled behind motorized vehicles, allowing more traces to be collected in a given amount of time. I often collect traces spaced every 3 and 5 cm, but if the transects are long (over 100 meters or so in length), I might program the system to collect traces with greater distance separation or else the resulting data files will become too large very quickly. While I have never collected data with antennas towed behind a very fast vehicle, it is possible, but important to calibrate the system so that no

data are lost due to non-recording that might happen if the digitization speed is not high enough. This could be caused by programming too short a distance between traces or perhaps too many samples used to define each trace. When acquisition parameters are not adjusted correctly, the digitization system could produce “data drop-off” and some waveforms will not be recorded. This has recently become less of a problem as newer systems can digitize much more quickly. The newer systems that are moved around the ground with all-terrain vehicles (ATVs) or small tractors allow for many hectares of data to be collected in a day (Figure 3.8) with reflections spaced at close intervals for very high resolution of the ground.

Most applications are done by acquisition of GPR data in a rectilinear grid over the area to be surveyed (Conyers 2013; Doolittle and Miller 1991), but this is not necessary with recent advances in GPS location (Goodman and Piro 2013; Trinks et al. 2010). Data processing software for GPR processing was initially developed using Cartesian coordinates that required points collected in  $x$ ,  $y$ ,  $z$  fashion where survey transects in a grid are acquired in either north-south or east-west orientations (or both, if desired). Newer GPS location systems can collect data in any orientation or even by the random meandering” method. In this way individual reflection traces can be given unique locations in space and reflection data processed by software that is not dependent on  $x$ ,  $y$ , and  $z$  coordinates within a rectangular grid (Figure 3.9). Specialized software is necessary for this type of collection and data processing.

Grids of data should be situated so that surface obstacles are avoided, and antennas therefore placed on the most even and horizontal ground possible. This almost never occurs. I can’t count the number of times that a collaborator has told me, “The ground is flat and clear there,” when we were planning a GPR project, and when I arrive, I find it cluttered with trees and large rocks, with the



**Figure 3.8.** An antenna array system moved by a farm tractor in Birka, Sweden. Here seventeen 400 MHz antennas are in the white box, collecting 16 traces spaced 8 cm apart in “swaths” that are about 140 cm wide. *Courtesy of Ewe and Immo Trinks.*

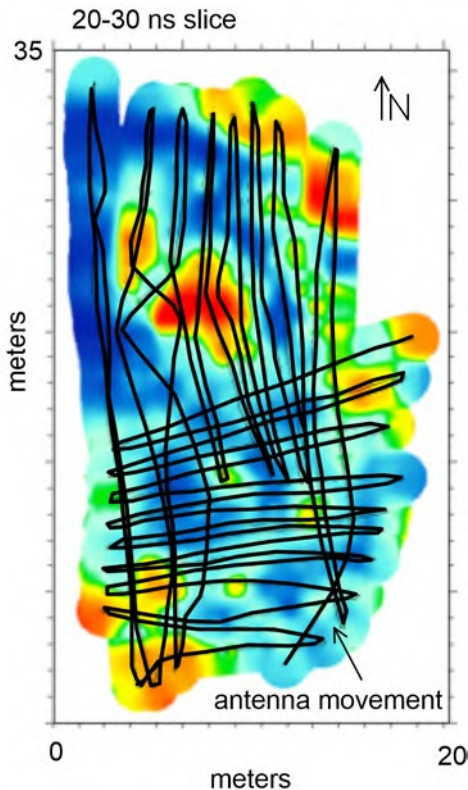


**Figure 3.9.** An amplitude slice-map generated from reflection traces collected in a non-Cartesian grid. The antennas were moved in a pattern that would cover the ground of interest. Traces were given individual locations using GPS, and an amplitude slice-map was constructed from the recorded traces. Source: the author.

ground sloping at precipitous angles (Conyers 2012). When this happens, it is necessary to improvise, as I did recently on the side of a hill in Costa Rica where it was difficult enough to walk unhindered, let alone collect evenly spaced profiles in grids. In that case, we could only collect a few smaller-than-optimal grids where we could move the antennas in a reasonable way, and all profiles had to be adjusted for topographic variations. This made the project an order of magnitude more complicated than I had anticipated.

No matter what the ground conditions, GPS locations of grid corners, at the very least, must be collected to place results into space. It can often be difficult to get collaborators to collect location data, so I always make my own rudimentary measurements “tying” my grid corners to landmarks using tape measures. Then even if GPS locations never arrive, I can use geo-rectified aerial photos or other maps place my results into space.

When surface obstructions are present, a grid pattern with antenna survey transects of different lengths can be easily constructed to avoid obstacles, often creating a complex grid pattern. All standard GPR-processing software can place reflection data collected in any grid pattern (as long as Cartesian

coordinates are used). This allows each reflection trace to have a unique location when amplitude slice-maps and other images are processed for analysis. Good note-taking that describes or tabulates variations in grid patterns, length of profiles, and the location of surface objects is crucial to process data later.

There are some collection procedures that vary from the standard rectilinear grids, which may be necessary to move around the ground efficiently or to adequately cover buried features that are unusual shapes. I have read of survey transects that radiate outward from one central area like spokes in a wheel, for instance, to define a moat around a central fort-like structure (Bevan 1977). I was forced into collecting a rhomboid grid in Central America within a sugarcane field on the side of a hill, as I could only move the antennas between planted sugarcane rows (Conyers 1995). One must be adaptable to site variations. Sinuous reflection profiles that are neither straight nor parallel to each other may be necessary when collecting GPR data on lakes in boats (Conyers 2012; Leckebusch 2003). This can be readily done with real-time GPS locations, but this then creates a very complicated grid of sinuous profiles due to the boat drifting in the wind or being piloted in various directions. Spatial software can later be used to place reflection traces into correct space during data processing (Figure 3.9). These non-rectilinear surveys necessitate additional data-processing time to spatially rectify all recorded reflections (Trinks et al. 2010), but they can be still just as useful as those acquired in standard rectangular grids.

When the ground surface is rough, uneven, or sloping, closely spaced topographic elevations along each survey transect must be obtained so that topographic corrections of subsurface reflections can be made during post-acquisition processing (Goodman and Piro 2013; Sun and Young 1995). If the ground is evenly sloping, it may only be necessary to survey the beginnings, ends, and a few elevations along each transect, or at each change in slope, and then interpolate elevations in between to save surveying time (Figure 3.10). When surface irregularities are numerous, elevation surveying must be done at more frequent intervals (perhaps every meter or less or at each change in slope), and data processing becomes more of a chore.

The location of any surface feature that could conceivably reflect radar energy should also be identified prior to or during data collection. Trees, overhead branches, houses, cars and even wire fences are good radar wave reflection surfaces and their locations must be accounted for as part of any data interpretation (Hong et al. 2018). Reflections from surface objects are often termed “air waves,” which are visible as they are mostly straight sloping reflections (Figure 3.11). They can also be produced by very reflective objects that are under the ground, but still near the surface (Stumpf et al. 2021).

I sometimes still chuckle about a public presentation where a colleague presented data that contained air waves, which had been sliced into horizontal depth-slices. This presentation claimed to show images of steps leading

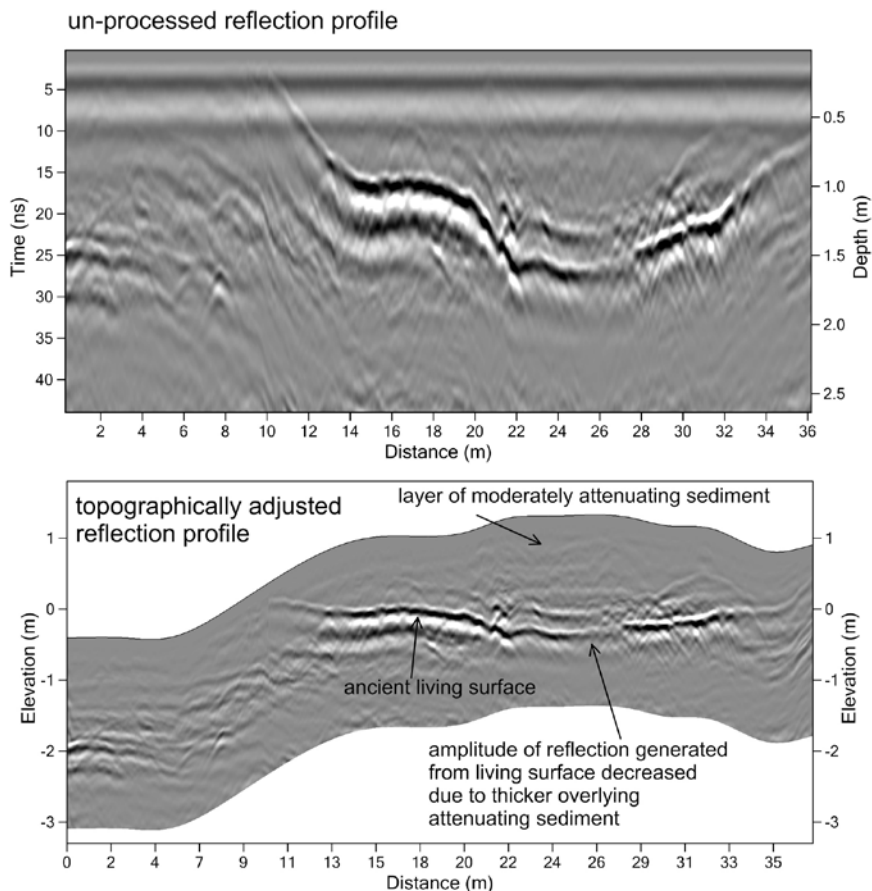


**Figure 3.10.** A non-topographically adjusted reflection profile on top, and that same profile adjusted for surveyed elevations on the bottom. The planar reflection of interest would be difficult to interpret without these elevation changes. This is a Pleistocene surface buried by wind-blown sand along the Portugal coast. *Source:* the author.

downward in progressively deeper depth slices at a Roman site. A photo of the site, which was part of the presentation, showed these “steps” in progressively deeper slices leading down from a substantial surface wall. This seemed a strange place to place a wall or the steps. I later asked to see a reflection profile from this grid, and it was obvious that what had been “sliced up” to produce the amplitude maps were air waves that had been generated from the wall as the antennas were moved away from that very reflective feature. The air waves were recorded from deeper and deeper in the time-window (as antennas were moved away from the wall), which were then sampled in each depth-slice. Air waves became steps leading downward! In this silly mistake, a simple identifi-

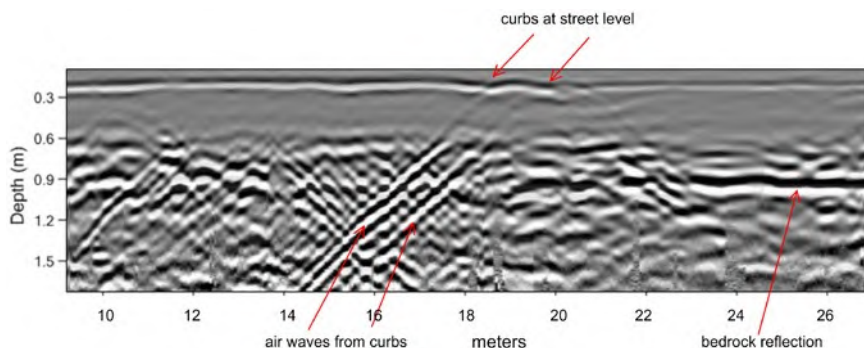


**Figure 3.11.** Air waves generated from curbs along a street in southern Portugal. They are easily identified as they are straight, as the waves that were recorded from the curbs traveled to the curbs and back to the antennas in air, all at the speed of light, with no variations in the velocity. *Source:* the author.

cation of the surface wall during data analysis would have explained the origin of these waves and avoided an embarrassing public display. I was polite enough not to bring up the air waves in public and kept this lesson to myself. It is a story I tell all my students about how important it is to make notes and take photos of the ground surface.

One of my students, who did not take this simple advice had a similar experience when she was using a wheelbarrow to move equipment around within a grid and mistakenly left it, tipped on its side in the middle of the grid. It made a perfect radar wave reflection surface for waves moving in the air between the wheelbarrow and the antennas, and its location could be seen in all her resulting images. There are complicated processing methods to remove these types of waves, but it is better to not collect them in the first place by either moving the wheelbarrow, or in the “steps” example locate a grid some distance away from the reflective surface so that the unavoidable air waves were below the recorded time-window.

Coupling is a concept to always keep in mind, as it is necessary to get radar waves to travel in the ground by allowing waves to couple with it, usually within about a half of a wavelength of the propagating waves in air. If they are higher than this above the ground much of the energy will reflect only from the ground surface, leaving little to penetrate deeper. Some materials are excellent at coupling radar waves, and others less so. These coupling variations produce variable reflection amplitudes in profiles that should be accounted for, but rarely can be. Coupling variations leading to wave amplitude changes can sometimes just be identified when visible as they are common and difficult to control for and avoid.

An important consideration when moving the antennas along the ground is to make sure that they are always the same distance above the ground or are



always directly touching it. Changes in antenna orientation with respect to the ground can potentially cause variations in the recorded reflections that can be confused with “real” material variations in the ground. Radar waves will also travel in the ground in varying directions as antennas are tipped, producing complexity that is not always discernable when processing data (Figure 3.12). These can be caused by variations in ground types, paving surfaces, vegetation, and bumps and obstacles.

I always consider it important to keep notes in a field book of all the profiles collected and their location and orientation in grids. This menial task cannot be understated because even the most sophisticated data collectors sometimes forget to correctly turn the system collection on and off for each profile collected in a grid, producing some profiles that might be too short, and others too long (or composites of many profiles in one). These errors can be a nightmare to sort out after returning from the field, so I always try to keep track of which profiles head in what direction within a grid, and if they should be even- or odd-numbered files, to make sure all is going well during collection. Setup parameters are usually saved in an abbreviated way as meta-data, but I prefer to have my own notes also. As reflection data are saved in individual files they are always numbered sequentially, and it can be easy to determine

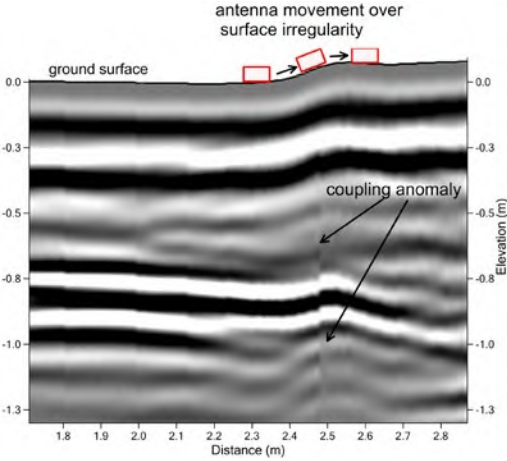


**Figure 3.12.** A minor irregularity in the ground surface has created an artifact termed a coupling anomaly in the reflection profile. This is created because the antenna was tipped moving over the surface feature, creating differences in when reflections were recorded by the receiving antenna and creating what looks like a geological fault.  
*Source:* the author.

what profile number should be where in space if someone is paying attention during collection.

Once I was hired to try to sort out GPR data that had been collected by a team who had no experience with GPR whatever. It was quickly apparent that these collectors had turned the system on to collect and off at random times, with some profiles being only a few meters long while others were huge (perhaps hundreds of meters long), which included many sequential transects within one file. When viewing those large files, it was apparent that data were still being collected as the antennas were moved around in the air between when one transect was finished and the next one started. While a “GPR detective” could have possibly figured this mess out, I had neither the time nor inclination to do so, and as a result these data were useless for all concerned. Much later I was sent a book written including results from this survey and the GPR results published were processed by a friend who apparently had more time on his hands than I did (or was paid a substantial amount of money). It was the most embarrassing mishmash of nonsense GPR, and I was glad it did not have my name associated with it.

Occasionally there is a need to immediately determine the location of important subsurface reflections using only profile analysis as data are being collected. This kind of “real time” interpretation is common for those in businesses finding buried pipes or other objects for engineering or construction applications (Alani et al. 2013; Bianchini et al. 2019; Lai et al. 2018; Rafezi et al. 2015; Venkateswarlu and Tewari 2016). Software is included in the newer GPR systems that can produce velocity determinations also in real-time, converting radar travel time to approximate depths. Those immediate results can include removal of background noise and perform other simple data processing procedures during collection. At the same time data are being recorded operators can view reflections on the screen that may be their “targets” and then, if desired, go backward and forward over buried reflection surfaces multiple times to make sure about their location, which is flagged or painted on the ground. In this type of procedure, there is no need to produce a grid map of the site, as customers only want the location of what can be seen immediately. It may not even be necessary with this method to set up a grid as reflection data are collected by moving in (what seems to me as a spectator) to be random ways. This is an easy way to conduct GPR data (and often quite fun, as one gets instant results), but it is full of pitfalls. There can be no “second attempt,” as data are not placed adequately into space, and therefore can’t be processed and analyzed later when returning from the field. I have used this procedure as an adjunct to more complete and exact surveys, but only when I have already figured out what is in the ground, and I have the attention of un-initiated viewers who just want to see what is in the ground. If I were to try to make these kinds of immediate interpretations before conducting a survey with multiple profiles in a grid, I would likely be wrong. The “pipe-finders” of the GPR world have much more experience in

the immediate interpretation methods than I, and I hear their expertise is well paid. The way I look at GPR analysis, this kind of “immediate gratification” GPR interpretation is “anomaly hunting in real time.”

### GPR ON WATER

Radar energy will easily pass through ice and fresh water into the underlying sediment, revealing features on and below a lake or river bottom (Annan and Davis 1977; Conyers 2012; Fuchs et al. 2004; Jol and Albrecht 2004; Leckebusch 2003). Radar antennas can also be easily floated across the water surface of a lake or river and directly on to the shore using inflatable boats or other small craft, all the while collecting data from the subsurface (Conyers 2012a: 75; Haeni et al. 2000). These water-collection techniques, however, will not work in salty or even slightly brackish water because the high electrical conductivity of the saline water will quickly dissipate the propagating electromagnetic energy as it enters the water column, leaving no energy to be transmitted to depth or reflected back to the surface.

I have sometimes collected GPR data on freshwater lakes, and even on lakes that appeared to be somewhat salty, at least from its general appearance (Figure 3.13). Results were always highly successful in freshwater bodies of water, but I was curious what the “cutoff” for radar energy propagation in fresh water might be. It has long been known and reported that fresh water is “good” and saline water is “bad” for GPR (Melleett 1995), so my graduate student Andrew Bair and I decided to do a very simple test in the lab to quantify these qualitative observations. We filled a large plastic container with a known volume of tap water and floated a 900 MHz antenna on the surface with a metal plate on its bottom. A salinity meter was used to measure the total dissolved solids as a proxy measurement of salinity. The tap water used (from Denver Colorado), turned out to have about 120 parts per million total dissolved solids (ppm TDS). Denver claims to have domestic water that varies between 75 to 120 mg/L (which is another calculation that defines this TDS salinity variable). Table salt was then measured in small volumes and dissolved

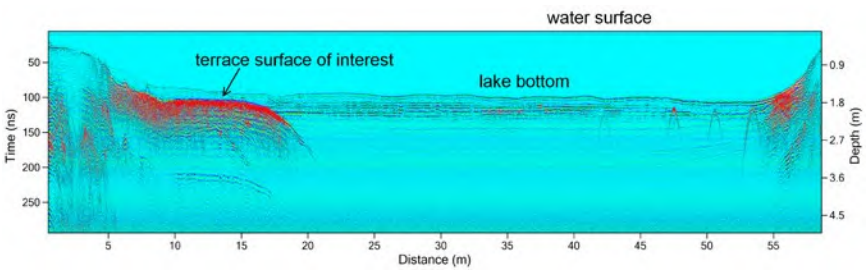


**Figure 3.13.** Reflection profile showing an underwater river terrace and lake bottom sediments in a reservoir in the Rocky Mountains, Colorado. *Source:* the author.

in the water by stirring and the TDS were calculated with each addition, and that calculation was confirmed with a salinity meter. A series of radar reflection traces were collected with the 900 MHz antenna and no gains applied at each step. Multiple traces were stacked into each composite trace recorded at each TDS reading. This was repeated 10 times for increasingly salty water, as table salt was added and mixed. The amplitude of the reflected wave produced from the metal plate at the bottom of the plastic water container was measured each time. A graph of salinity in ppm TDS was plotted against the recorded radar wave amplitudes generated from the metal place (Figure 3.14). This graph indicates that with TDS greater than about 750 ppm, radar waves were totally

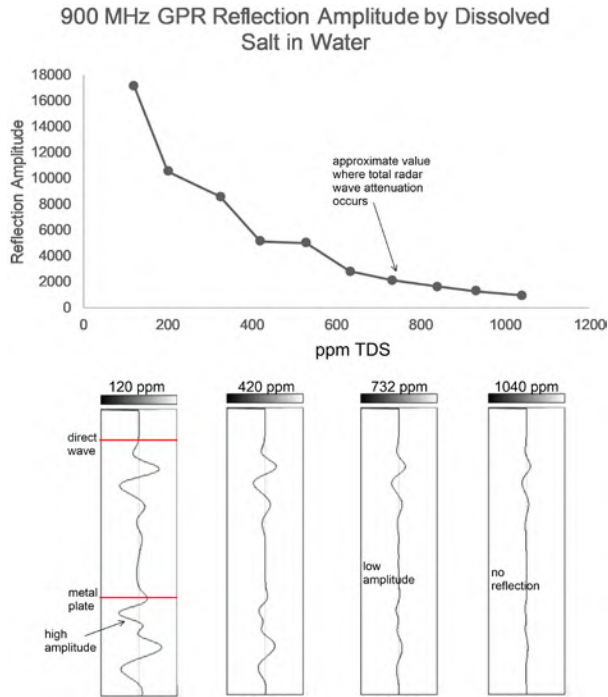


**Figure 3.14.** Display of reflection amplitudes in a laboratory test where 900 MHz waves were reflected from a copper plate in a container of fresh water. Salt was added to the water, and the parts-per-million total dissolved solids (TDS) were measured as a proxy measurement for salinity. The amplitude of the reflected wave decreases with increased salinity and is attenuated between about 700 and 750 ppm TDS. This indicates that good radar data are likely to result in salinities below about those figures. *Source:* the author.

attenuated in a water column 30 cm deep. Water is often defined as “fresh” if is below 1000 ppm TDS (1000 mg/L). These results indicated that GPR will be potentially successful in freshwater lakes with less than about 700 to 750 ppm TDS. Often these types of measurements can be found in published water-quality data or measured with a simple salinity meter to determine efficacy of GPR for a proposed survey in water. It is important to note that there is some frequency variability in these types of calculations (Bradford 2007), so these calculations on salinity constraints for GPR must be used as a general guideline. It was also found that even in fresh water there can be some changes in RDP within different levels of a lake, which is a function of temperature variations (Bradford et al. 2007).

## **ANTENNA FREQUENCY CONSTRAINTS**

One of the most important variables in GPR surveys is the selection of antennas with the correct operating frequency for the depth necessary and the resolution of the features of interest (Huggenberger et al. 1994; Smith and Jol 1995). Commercial GPR antennas used in most common applications range from 10 to 3,000 megahertz (3 GHz) center frequency (Annan and Cosway 1994; Fennner 1992; Jol and Bristow 2003; Malagodi et al. 1996; Neal 2004; Olson and Doolittle 1985). General-purpose GPR systems use wide-band dipole antennas that typically have a two-octave band width, meaning that the frequencies vary between one half and two times the center frequency. For example, a 400 MHz center-frequency antenna generates radar energy with wavelengths ranging from about 200 to 800 MHz. Many software programs can display a histogram of the reflected wave frequencies, which can be a guide to depth of energy penetration and resolution to determine what frequencies might be necessary to filter out or enhance during post-acquisition data processing (Figure 3.15). An analysis can be made of what frequencies are present in a profile, and the peaks of certain frequency bands can determine what frequency waves are best for resolving which features at what depth, and how these change along a profile. These data can be important for later filtering steps, if warranted.

Most refer to the 400 MHz center frequency antenna as “a 400 MHz,” but it is important to remember that this is a “broad band” antenna that transmits many frequencies of waves. No two antennas, even if they are labeled as having the same center frequency generate the same spectrum of energy. These variations can be caused by irregularities in the antenna’s bowtie-shaped copper plate and possibly variations in its electronic components.

A primary goal of all antenna manufacturers is to produce a distinct pulse of one sine-wave that can be transmitted into the ground (Figure 3.16). No antennas, however, produce perfectly “clean pulses,” and somewhat noisy transmitted pulses are always the norm. Post-acquisition data processing can often “clean up” the noisy reflections recorded by most antennas.

### 400 MHz antenna analysis of frequencies

**Figure 3.15.** Display of frequencies generated from and then reflected from the ground using a 400 MHz antenna. This type of analysis can help in determining what frequencies are being reflected from what buried features, and which frequencies can be filtered out to improve data quality by removing background noise. *Source:* the author.

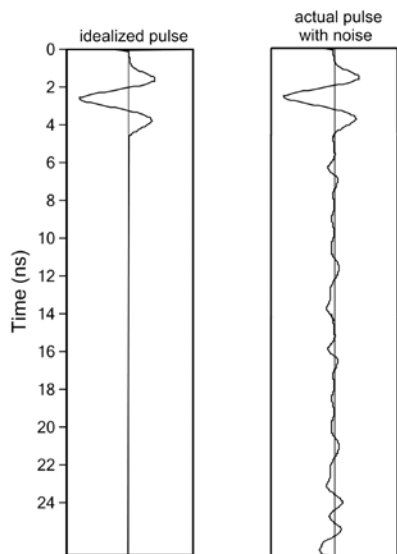
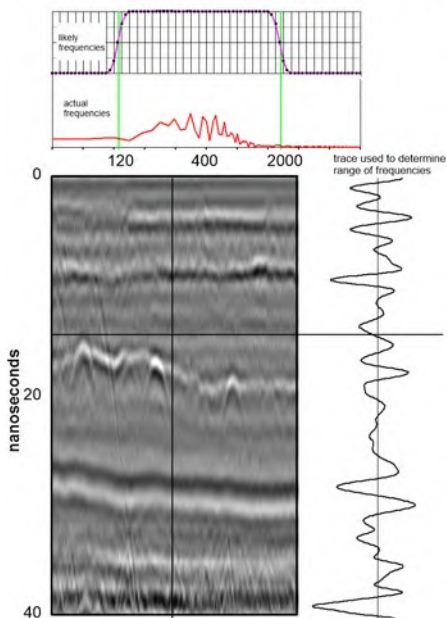


**Figure 3.16.** A perfect transmitting pulse on the left and one from an antenna, showing that all antennas generate some extraneous reflections throughout the time-window along with the initial transmitted wave. *Source:* the author.

Proper antenna center frequency selection can in most cases make the difference between success and failure of a GPR survey and must be planned for in advance. In general, the greater the depth of investigation, the lower the antenna frequency necessary (and the longer the wavelength transmitted) (Neal 2004; Smith and Jol 1995). Lower-frequency antennas are for the most part larger, heavier, and more difficult to transport than high-frequency antennas. In my first GPR survey a very antique 80 MHz antenna was used (it was new then), which was larger than an oil drum, cut in half lengthwise, and weighing between 125 and 150 pounds. It was supported just above the ground surface under an oxcart (Conyers 1995). Fortunately, the remaining antennas of this vintage have been recycled or are in museums. Newer low-frequency antennas can sometimes be moved by more than one person with the aid of tubular plastic supports (Figure 3.17). Whatever the transport mode these low-frequency antennas, such as a 16 MHz, can be unwieldy and often moved along transects using wheeled vehicles, sleds, or a graduate student. For good data acquisition over any surface other than a perfectly flat one, they can be programmed to collect individual traces in steps as they can be positioned correctly before data are collected and saved, and not continuously moved across the ground. In contrast, a 900 MHz antenna is smaller than a shoe box (Figure 3.17), weighs



**Figure 3.17.** Antennas of various frequencies from the 2 GHz “palm” antenna to the 16 MHz very low frequency antenna, with a more normal-sized 900 MHz antenna. Source: the author.

very little, and can be readily moved along transects. Some very high frequency antennas in the GHz range are very small, some the size of a child's toy (Figure 3.17), and they must be moved on one's hands and knees.

Most of the usual GPR antennas (higher than about 200 MHz) are shielded, which means they have components within the antenna housing that absorb radar waves that propagate naturally upward and to the sides. This shielding is supposed to allow energy propagation only downward into the ground. The hope is that shielded antennas will not produce air waves (Figure 3.11) that are reflected off nearby surface features, objects, or people pulling the antennas (Conyers 1995; Lanz et al. 1994). With long experience, I have found this is not actually the case, as radar waves often propagate in unexpected directions no matter what shielding is built into the antennas.

Propagating radar waves will always reflect first from the ground surface immediately after they are generated and then move horizontally along the ground and then upward into the air. Waves are also likely to move along the ground-air interface and then move in many unexpected directions. Caution must be exercised when interpreting GPR results in case there are "stray" waves in a dataset that can be confused with reflections from the ground (as in the "steps" story above). These stray waves can usually be identified with some effort, but only if an interpreter is aware of this phenomenon and is paying attention during data analysis as are they discovered. They are most common with unshielded low frequency antennas but can be found in datasets acquired with any antenna frequency (Leckebusch 2003; Nuzzo 2005).

## **RADAR WAVE REFLECTIONS**

Identifying radar reflections of interest (usually those of high amplitude that can be readily seen in profiles) begins with understanding how reflected waves are produced. Any time radar energy crosses a contact between two materials in the ground with different physical or chemical properties, the velocity of the passing waves will change, and some energy will be reflected toward the surface. The degree of velocity change at an interface is directly correlative to the amplitude of the resulting reflected wave (Neal 2004). All sedimentary layers and other buried materials in the ground have certain properties that affect the velocity of electromagnetic energy propagation and therefore the strength of the reflected waves (Van Dam et al. 2002). Most often the degree of reflection (as measured in recorded wave amplitudes) that occurs at buried interfaces is a function of the variations in retained or distributed water, which can be directly related to the physical properties of the buried units (Calia et al. 2012; Conyers 2012; Conyers 2004). Other measurable properties of materials in the ground that affect radar propagation and reflection are electrical conductivity (often related to the amount of retained water and clay content and type) and, to a lesser extent, magnetic permeability (Olhoeft 1981; Reynolds 2011; Van Dam



and Schlager 2000). If these are known (which is rarely the case for most sites, as detailed laboratory analyses must be conducted on soil and sediment samples or electrical tools must be taken to the field to perform these tests), the amount of reflection at buried interfaces and the depth of energy penetration can potentially be determined.

The proxy measurement of the velocity of radar waves through a material is termed relative dielectric permittivity (RDP), also called by some the dielectric constant. This complex measurement takes the electrical and magnetic properties of buried materials into account and is a measure of the ability of a material to store a charge from an applied electromagnetic field and then transmit that energy (von Hippel 1954; Wensink 1993). For most GPR applications, this RDP value is used as a proxy measurement for velocity and can be determined empirically from measurements in the field and through analysis of hyperbolic-shaped reflections in reflection profiles. In many areas of the world GPR users do not use RDP as a value to denote velocity, but instead the actual velocity of radar waves is used, often as nanoseconds per unit of distance (meters or centimeters). This can be a little confusing as some authors sometimes use two-way travel time (TWTT) velocity and others one-way velocity, and sometimes neglect to identify which measurement of velocity they are referring to. For this reason, I prefer RDP, and if necessary, I can convert to velocity for certain applications. This simple conversion will be discussed more below and can be seen visually (Figure 3.18). Elsewhere in this book, I will discuss velocity using values of RDP only.

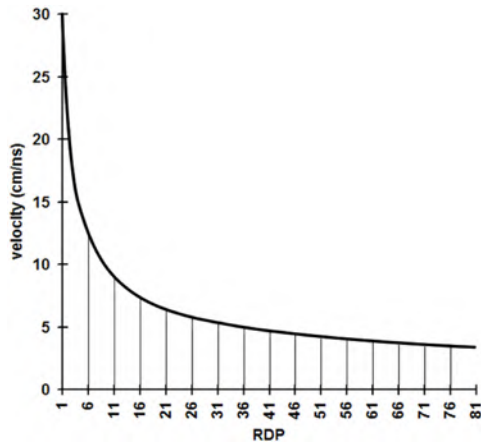


**Figure 3.18.** Graphic display of the comparison of one-way radar wave velocities to calculated relative dielectric permittivity values (RDP). *Source:* the author.

It often can be important to calculate RDP from velocity specifically, and Equation 1 can be used. This is a simple equation for RDP, where if the velocity can be calculated for a medium in the ground RDP can be determined. It can be useful if a velocity test is made in the field by viewing an object on the computer screen, and if its depth is known so RDP can be calculated. I have used this equation rarely, usually when I need an RDP value quickly for other analyses and have not had time to test for velocity in other ways.

$$K = \left( \frac{C}{V} \right)^2$$

Equation 3.1. Relative dielectric permittivity (K)  
and radar velocity (V) relationship.  
C=speed of light (0.0299 cm/ms).

The higher the RDP of a material, the slower radar waves will move through that medium (Figure 3.18). Radar waves moving in air or the vacuum of space travel at the speed of light, with a defined RDP of 1. In the earth's atmosphere this value is approximately 1.0003, a little higher than 1 because of the addition of water vapor (Dobrin 1976). The highest RDP of any medium on earth where radar waves typically propagate is fresh water, which has an RDP of 80. Salt water has a defined RDP of 81, but as radar waves will not propagate within it due to its high electrical conductivity, they are attenuated, and this RDP value is not used for any calculation that I know of.

The RDP of frozen fresh water (ice) is about 3. Ice is an excellent medium for radar waves to couple with and for their propagation, and in glaciers, waves can move downward many hundreds of meters, which is possible even when using a 400 MHz antenna (Arcone 1996; Arcone and Kreutz 2009). A bed of water-saturated peat, which is composed almost wholly of organic material and fresh water, has a relatively high RDP in the range of 30 or even higher depending on the amount of water it contains. Radar waves moving through this type of material are only moderately attenuated as there is little electrical conductivity in organic materials and fresh water. Propagating waves will penetrate deeply but at a relatively slow speed. The same is true with other soil units that do not contain electrically conductive clays and are water saturated (Clarke et al. 1999; Conyers 2012; Utsi 2004; Worsfold et al. 1986).

Most soils and sediments found in much of the world have RDP values that range between 3 and about 40 (Table 3.1). In a totally dry state, most naturally occurring materials in the ground have an RDP that varies very little, usually between about 3 and 4 (Conyers 2012). There is almost nowhere on earth where this occurs, outside the laboratory, as most typical ground materials continue to retain some water interstitially even when the ground appears to be desiccated. When just a small amount of water is added to the ground, the

**Table 3.1. Typical relative dielectric permittivities (RDPs) of common geological materials**

<i>Material</i>	<i>RDP</i>
Air	1
Dry sand	3-5
Dry silt	3-30
Ice and snow	3-4
Asphalt	3-5
Volcanic ash/pumice	4-7
Limestone	4-8
Granite	4-6
Permafrost	4-5
Coal	4-5
Shale	5-15
Clay	5-40
Concrete	6
Saturated silt	10-40
Dry sandy coastal land	10
Average organic-rich surface soil	12
Marsh or forested land	12
Organic rich agricultural land	15
Saturated sand	20-30
Fresh water	80
Sea water	81-88

Modified from Davis and Annan (1989) and Geophysical Survey Systems, Inc. (1987).

RDP will increase, sometimes dramatically (Conyers 2004). Take, for instance, dry quartz sand (with an RDP of 3; Table 3.1) that is totally saturated with fresh water (with an RDP of 80). The overall RDP of this material can be estimated by taking the water-filled sand porosity of 30 percent (or .30) and multiplying it by the RDP of water, which is 80. This is then added to the RDP of the solid sand alone (3), which makes up the other 70 percent of the total volume (calculated  $.70 \times 3$ ). Adding the two values gives an estimate of the RDP of the total volume of saturated sand at 26:  $([0.30 \times 80] [0.70 \times 3])$ . I often try to make calculations like this in my head when the RDP of the ground is not immediately available by looking at the ground and exposures nearby. This is rarely accurate as almost all materials in the ground contain a variety of constituents in various amounts such as clay and organic matter that can interact chemically or physically with the pore water, producing a complex blend of materials, each of

which have different RDP values. But initial estimates are better than nothing when calibrating for data collection, and velocity can be refined later.

To generate radar reflections, the change in RDP between two bounding materials must occur over a short distance. This usually occurs along bed boundaries or interfaces between very different types of rock or sediment. When the RDP changes gradually with depth there are only very weak if any reflections generated (Van Dam and Schlager 2000). The amplitude of reflections generated at an interface between two materials with known RDPs can be calculated using Equation 2 (Neal 2004; Sellmann et al. 1983; Walden and Hosken 1985; Van Dam et al. 2002) deriving a value termed the reflectivity coefficient. I have never found this to be a very useful equation, and I have very rarely seen it used in the literature. There are so many variables including physical and chemical parameters of buried units that we are usually confronted with estimating an average RDP at various depths in the ground, and perhaps spatially over a grid of data that these values are difficult to arrive at. Even more important is that if these variables were known how they might change spatially and with depth to be useful in most complex ground has never been apparent to me. I have added the equation anyway, in the hope someone can show me how it was used in a useful manner for interpretation. It has been used in a general way in some computer models that help in interpretation where this equation can estimate the amplitude of reflected waves in simulations.

$$R = (\sqrt{K_1} - \sqrt{K_2}) / (\sqrt{K_1} + \sqrt{K_2})$$

Equation 3.2. The coefficient of reflectivity (R) at an interface between two materials that have differing relative dielectric permittivities (K1 and K2).

I spent some time years ago trying to quantify reflectivity of radar waves, as well as their propagation depth and attenuation in a way that would allow for accurate prediction of how various ground conditions' suitability might be for GPR (Conyers 2004). In this endeavor I collected many soil sediment and rock samples, crumbled them to clay-sized fractions, dried them out in an oven, and then measured their RDP values using a network analyzer. Systems of this sort are used for a variety of purposes, often to measure water content in harvested grain crops. To my amazement, almost all the samples I collected, when totally lacking water, had RDP values of between 3 and 4 (Conyers 2012). These values are somewhat frequency dependent. In this Quixotic endeavor I spent way too much time dropping distilled water on the various samples and measuring them again with differing water saturations. It shouldn't have been any surprise to me that the addition of water increased the RDP in each sample dramatically. There were almost no differences in the RDP values of all samples of various materials when the same amount of water was added. The obvious

conclusion is that the major (perhaps only?) variable that affects RDP in most near-surface ground is water. With a water RDP of 80, it is intuitively apparent that water retention is the obvious factor in producing the variations in RDP that occur in the ground.

I have generalized a little bit here, as there are a few materials that do not fit these general conclusions for RDP such as metal objects, void spaces, very hard rocks or stones with little porosity, and modern objects such as plastic and asphalt. In addition, many minerals and other exotic materials in the ground, not normally found in most near-surface archaeological and geological contexts, also have very different properties that can potentially produce differential properties that affect the transmission and reflection of radar energy (Olhoeft 1981).

For the sake of this argument about radar, velocities (as measured by RDP values) range from very dry sand (RDP=3) and fresh water (RDP=80), making up two end points of a radar wave velocity continuum. All other normally occurring materials in the ground will therefore range between these, with only void spaces (RDP=1) residing outside these two end members. All other near-surface materials will then vary depending only on the relative proportions of water retained in them.

To illustrate the concept of reflected wave amplitude and water content, a simple model was constructed (Figure 3.19). In this model a sand layer overlies a clay unit, with a sharp interface between them. Using relative dielectric permittivity (RDP) values for these materials, a set of calculations can allow for a

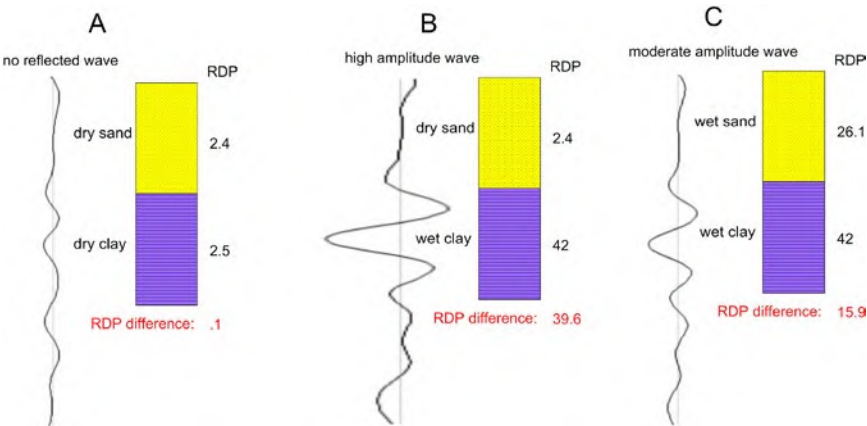


**Figure 3.19.** Model of radar wave reflection amplitudes when waves encounter an interface between materials of differing RDP. The greater the change in velocity (as measured by RDP), the higher the amplitude of the reflected wave. This simple model demonstrates how in this example the differences in RDP are purely a function of the water content differences between the two units. *Source:* the author.

basic understanding of how water differences relate to reflection generation and amplitude.

The first model calculates the amplitude of a reflected radar wave generated at the interface when both sediment types are totally dry (Figure 3.19 A). Some additional simple calculations are then necessary for this scenario:

- If the sand is totally dry and has a porosity of 30 percent (about as high a porosity value possible for a typical uncompacted sand), then 30 percent of the sand has an RDP of 1 (when all pore spaces are filled with air) and 70 percent of the unit (the sand itself) has a RDP of 3. The calculation to determine RDP of this dry sand is therefore:  $(.3 \times 1) + (.7 \times 3) = 2.4$ .
- A totally dry clay layer has a porosity of 50 percent (typical for an uncompacted clay): The RDP of the clay particles in that layer are modeled as having an RDP of 4 and the void space has an RDP of 1. The total clay layer RDP is therefore  $(.5 \times 4) + (.5 \times 1) = 2.5$ .

This model shows there is essentially no difference in the RDP (and therefore no velocity change) when radar waves cross between the two units when they are totally dry, and almost no reflection amplitude is recorded at the interface in this model (Figure 3.19: A).

Using the same materials water is added to the system. If the clay were totally water saturated but the sand remained completely dry (unlikely in the real world) the following calculation determines the RDP of the clay:

- Fifty percent of the clay's pore spaces are filled with fresh water (RDP=80), and the other 50 percent of the unit is clay has an RDP of 4:  $(.5 \times 80) + (.5 \times 4) = 42$ .

Using these RDP values the model is again used to generate a predictive reflected wave at the interface between the saturated clay on the bottom and the dry sand above (Figure 3.19 B). The difference in RDP is 39.1, which corresponds to a very high velocity change in the propagating waves that move across the interface, and a high amplitude reflected wave is generated.

Finally, both units are modeled as totally water saturated. The saturated sand RDP can be calculated this way:

- Sand porosity is 30 percent, filled with water (RDP = 80), and the remainder of the sand has an RDP of 3:  $(.3 \times 80) + (.7 \times 3) = 26.1$ .

The model shows a moderate amplitude reflection produced at the sand-clay interface when both are saturated with water, as the RDP difference between the two is 15.9 (Figure 3.19: C).

The purpose of these calculations and models is to demonstrate that differences in RDP (and therefore velocity contrast and the resulting amplitudes generated) are only a function of the amount of water retained in the pore spaces of each unit. The units when totally dry are so similar with respect to the velocity that radar moves between them with no wave reflection. What is generating the reflected wave (and varying its amplitude) is the amount of water that is held by each unit in its pore space. So, while all GPR practitioners continue to discuss reflections we can see in GPR images as representing boundaries between units that we try to define by their constituents, it is important to keep in mind that it is only the ability of those materials to retain and distribute water that is producing the various reflections.

This is important also because there can often be reflections visible in profiles that do not correspond to geological boundaries in the ground that may be visible to us in exposures. When these differences do not match what we can see, it is likely water variations must be considered as the important variable. There can even be changes in radar wave velocity that are a function of extremely difficult to discern variables such as compaction, the permeability of units (that inhibits water drainage or allows rapid groundwater movement) or chemical or organic variations. None of these may be “visible” to us in exposure and may be possible to understand only with some detailed work on the sediment constituents, but these are usually not available to us without a good deal of effort.

Staying on the “water theme,” elsewhere I have shown several examples of how water differences are far and away the controlling factor in GPR (Conyers 2012). I have collected grids of data one year and processed those data into images where a variety of important buried features were visible (Figure 3.20). In a summer that had been very dry, the pit-house floor was visible in the amplitude slice-map. The next summer, which was very rainy, the data were collected again over the same grid (Figure 3.20). The resulting data were again processed, and the resulting amplitude slice-maps at the same depth in the ground show only differentially retained pockets of water. The buried features visible using the first season’s results were effectively invisible. At other sites the opposite was true, and it took a torrential rainstorm to produce enough ground water that pooled on or was absorbed by various materials in the ground to allow those materials to be visible. This was even the case at one site along the Atlantic Ocean coast where both rain and tidal changes varied both amount of fresh water in the ground and the depth to salt water, affecting results over just a few hours (Conyers 2012). These anecdotes are even more reason to pay a good deal of attention to water, the weather, and even the tides.

Another survey in coastal Peru, with presumably dry sandy soil (it had not rained in that area for decades), also had a very high electrical conductivity, and therefore radar energy was also attenuated at a very shallow depth (Conyers

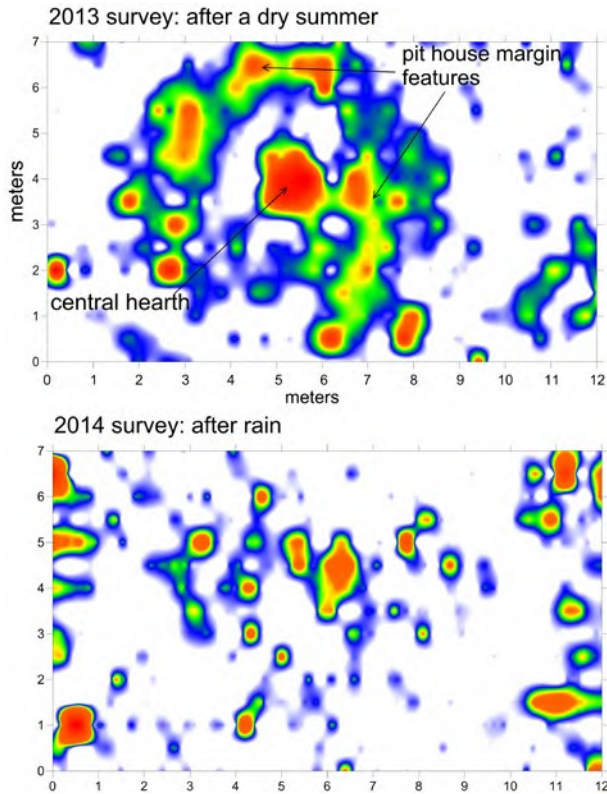


**Figure 3.20.** Differences in reflection amplitudes by the addition of water to the ground due to water variations. The upper map is constructed from 400 MHz data collected during a very dry summer in northern New Mexico. The lower map is the same grid collected the next year after a rainy summer. In that map, only pockets of water are visible.  
Source: the author.

2012). In this case, electrically conductive salts were bound with clay in the sand, making the medium highly electrically conductive and therefore non-dielectric. This example illustrates how the old GPR adage—that dry, sandy soils are “good” for radar penetration while wet clay is “bad”—can be very misleading, as there are many other more important factors controlling radar propagation (Conyers 2004; Conyers 2012; Gerber et al. 2004). The most important is water, and a close second is the electrical conductivity of the ground, both of which are difficult to predict in advance of conducting a GPR survey.



### DISPERSION AND ATTENUATION OF RADAR WAVES IN THE GROUND

Another factor that affects the depth of radar wave penetration and the amplitude of reflected radar waves is wave dispersion. As waves move through the ground, less is available for reflection due to attenuation and spreading. When what remains of the original transmitted energy is finally reflected toward the surface from within the ground, the remaining energy will suffer additional attenuation within the materials through which it passes before finally reaching the receiving antenna. As a result, radar energy is always progressively weakened as it propagates deeper in the ground. These variations can also occur very quickly laterally, depending on the types of materials that are present and their composition (Figure 3.21). However, there is always a maximum depth of radar wave penetration and therefore potential reflection, which is different for every site, no matter what antenna frequency is used, or post-acquisition processing techniques are employed (Conyers 2012).

The depth of radar energy penetration and subsurface resolution is highly variable. There is a common misconception that if a high-frequency antenna (say, a 400 MHz) is only capable of transmitting energy to 50 centimeters in the ground, then a lower-frequency antenna will transmit deeper (Leucci et al. 2012). If a 200 MHz antenna was also tried, and its maximum depth of penetration was about the same as the 400 MHz, then that ground is almost surely highly electrically conductive, and no antenna, no matter what frequency or how powerful, would be able to transmit to a greater depth.

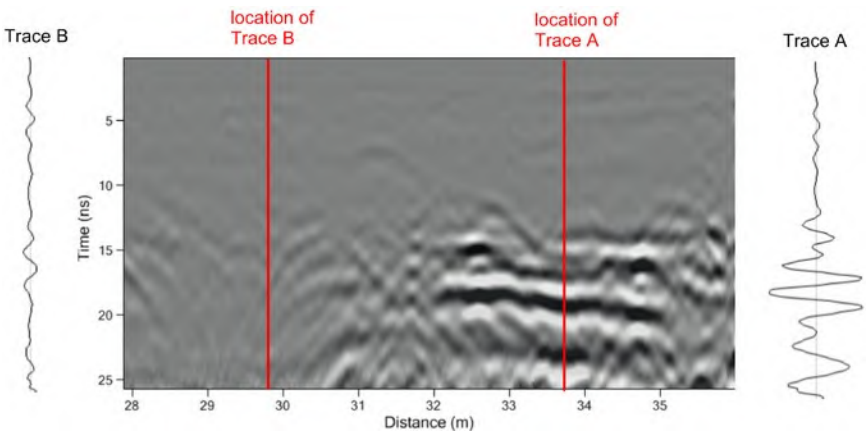


**Figure 3.21.** Lateral variations in reflectivity and attenuation over a distance of only four meters. *Source:* the author.

**BASIC REFLECTION TYPES**

A series of reflection traces collected along a linear transect that are produced from a buried layer will generate a horizontal or sub-horizontal reflection band in profiles (either dark or light in gray scale reflection profiles) that is referred to simply as a planar reflection (Figure 3.22). These types of distinct reflections are usually generated from a subsurface boundary such as a stratigraphic horizon or some other physical discontinuity such as the water table, a buried soil horizon, or any other generally horizontal feature of interest. In Figure 3.22, the distinct planar reflection was produced from a buried floor. A second general type of reflection is termed a point-source reflection generated from one distinct aurally restricted feature or buried object (Figure 3.22). Single objects of this sort can be individual rocks, metal objects, pipes that are crossed at a right angle, the tops of buried walls, and a great variety of other smaller objects. They are visible in two-dimensional profiles as hyperbolic-shaped reflections, even though they were generated from a “point,” or aurally restricted feature in the ground. A large number or density of hyperbolas in a reflection profile can often make interpretation difficult as many closely spaced small hyperbolic reflections have axes that interfere with each other and produce a very complex and “busy” profile (Figure 3.23).

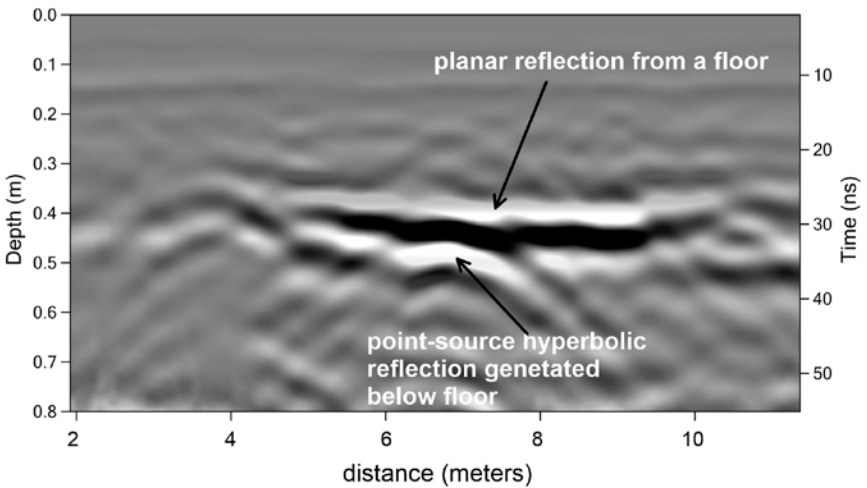


**Figure 3.22.** A planar reflection generated from the floor of a pit-house in eastern New Mexico, with a sub-floor object producing a point-source reflection hyperbola.  
*Source:* the author.

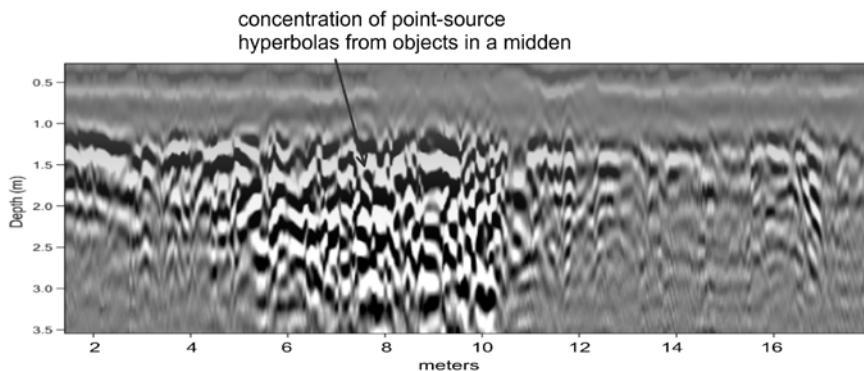


**Figure 3.23.** Many small reflection hyperbolas reflection from objects in a trash midden in southern California using a 400 MHz antenna. Each hyperbola interferes with others, producing a complex array of reflections. *Source:* the author.

Point-source reflection hyperbolas, sometimes termed diffractions, are generated because most GPR antennas produce a transmitted radar beam that propagates downward from the surface in a conical pattern, radiating outward as energy travels to depth (Figure 3.24). Radar waves will therefore be reflected from buried features that are not located directly below the transmitting antenna but are still within the “beam” of the propagating waves. Oblique radar wave travel paths to and from the ground surface are longer (as measured in two-way radar travel time), but the reflections generated from objects not located directly below the antennas will still be recorded by the system as if they were directly below and appear deeper in the ground. As the antenna moves closer to a buried point source, the receiving antenna will continue to record reflections from the buried point source, prior to arriving directly on top of it, it will continue to “see” the point-source and record it in its correct location only when directly on top of it. The same phenomena occur after the antenna moves away from the object, resulting in a reflection hyperbola where only its apex denotes the actual location of the buried point-source. The hyperbola’s axes are a record of the oblique wave paths. In some cases, only half of a hyperbola might be recorded, if just the corner or edge of a buried feature is causing the discrete reflection, such as the edge of a buried house floor or platform of some sort. In another fashion, one axis can be recorded if the buried object generating the reflection is oriented in the ground in such a way that only one part of the feature reflects energy to the surface, and when the antenna moves away from the object, the reflected waves move away from the surface antenna and are not recorded.

The presence of reflection hyperbolas is considered by some to be a distraction during data interpretation because they are not denoting the “real”

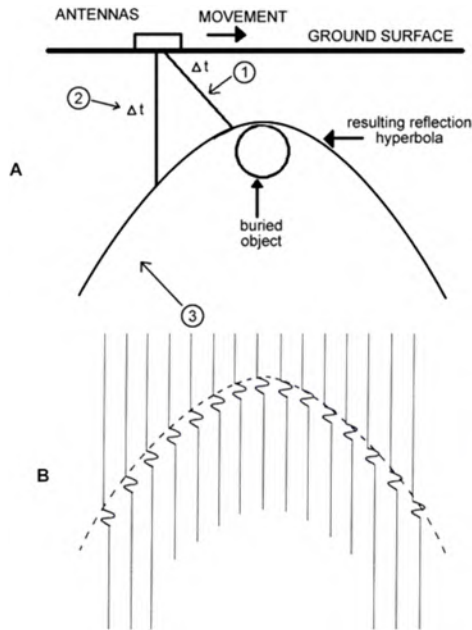


**Figure 3.24.** Point-source reflection hyperbolas are generated from individual buried objects as transmitted waves from a surface antenna propagate outward and are reflected, to return to the surface antenna in a non-vertical pathway (1). They are recorded as if they were generated directly below (2). As the antennas move toward this object, the distance in the non-vertical paths decreases, and only when the antennas are directly on top of the object are waves recorded correctly. The same occurs as the antennas move away from the buried object, creating a reflection hyperbola in profile (3). *Source: the author.*

location of buried features but are the product of the geometry of radar wave travel paths in the ground. Their presence, however, can aid in interpretation because hyperbolas are easily identified in reflection profiles and denote a specific size and possible geometry of individual objects in the ground. Most important, their utility in determining velocity cannot be overemphasized as their shape is a product of the average velocity of the radar wave travel paths to and from the surface to the buried objects. If it later becomes necessary to remove reflection hyperbolas from profiles, software programs discussed below can “collapse” the hyperbola axes to their apex using data migration procedures. This is often appropriate when performing more complex spatial analysis and mapping buried features in three dimensions where many hyperbola “arms” can create false reflection features that tend to blur the location of some objects in amplitude slice-maps and three-dimensional images.

RESOLUTION OF SUBSURFACE FEATURES

Subsurface resolution is greatly dependent on the wavelength of propagating radar waves and the geometry of the buried materials in the ground of interest. Lower-frequency antennas (those of 10 to 200 MHz) generate long-wavelength radar energy that can penetrate up to 50 meters or more in certain ground conditions but can resolve only very large subsurface features. In pure ice, antennas of this frequency have been known to transmit radar energy many kilometers, and they are commonly used to determine the thickness of glacial ice or the orientation of sub-ice bedrock surfaces (Arcone and Kreutz 2009; Bogorodsky et al. 1985; Delaney et al. 2004). In contrast, the penetration depth of a 900 MHz antenna waves in most ground is about 1 meter, and often less, but its generated reflections can resolve features down to a few centimeters in diameter. A tradeoff therefore exists with this inverse relationship between depth of penetration and subsurface resolution. Table 3.2 shows the dominant wavelength for different center-frequency antennas, and how those wavelengths change as waves move through materials of differing RDP.

The ability to resolve buried features is largely a function of the wavelength of energy reaching them at the depth they are buried. A “rule of thumb” is that the minimum object size that can be resolved is about 40 to 50 percent

**Table 3.2. The center frequency wavelengths of differing radar antennas and the wavelength changes in material with differing relative dielectric permittivities (RDP)**

<i>Antenna Center Frequency (MHz)</i>	<i>Wavelength of Center Frequency in air (meters)</i>	<i>Center Frequency wavelength in a medium with RDP=5 (meters)</i>	<i>Center Frequency wavelength in a medium with RDP=15 (meters)</i>	<i>Center Frequency wavelength in a medium with RDP=25 (meters)</i>
1000	0.30	0.13	0.08	0.06
900	0.33	0.15	0.09	0.07
500	0.60	0.27	0.15	0.12
300	1.00	0.45	0.26	0.20
120	2.50	1.12	0.65	0.50
100	3.00	1.34	0.77	0.60
80	3.75	1.68	0.97	0.75
40	7.50	3.35	1.94	1.50
32	9.38	4.19	2.42	1.88
20	15.00	6.71	3.87	3.00
10	30.00	13.42	7.75	6.00

of the downloaded wavelength reaching them in the ground (Jol and Bristow 2003; Orlando 2007; Yilmaz 2001). Downloading of radar energy always occurs as energy passes in the ground (Jol and Bristow 2003) and it decreases in frequency, increasing the propagating wavelength of the radar waves. For instance, a 400 MHz center-frequency antenna will generate energy with a wavelength of 75 centimeters in air (Table 3.2). When that energy downloads as it moves into the ground, its dominant frequency decreases to about 300 MHz, which is a wavelength of about 100 centimeters. However, as soon as the propagating waves moving deeper in the ground after downloading, the waves almost always encounter material of higher RDP, which occurs as the water saturation increases with depth. In this process the wavelengths will rapidly shorten (Table 3.3). It is almost impossible to predict what the downloaded wavelengths of any radar energy transmitted from an antenna would be as they travel through complex ground, and it is usually sufficient to be aware that wavelengths are estimates in Table 3.3.

An estimation of propagating wavelengths is important because an object much smaller than about 40 to 50 percent of the wavelength of radar waves intersecting them would likely not be resolvable in reflection profiles. For instance, with a 400 MHz antenna waves would be transmitted with a wavelength of .335 meters in material with an RDP of 5 (Table 3.3). Using the rule of thumb of 40 percent to calculate resolvability  $[(.335\text{m} * .4) = .134\text{m}]$  any object smaller than about .134 m (13.4 cm) in diameter would probably not be resolvable.

Unfortunately, it is often not known in advance what the target depth of features of interest is, their dimensions, or often the ground conditions and their physical properties. Most important, the ability to transmit radar energy to the depth necessary is often not known until one actually collects some reflection profiles. The best one can usually do prior to going to the field is to make some rough calculations from the best knowledge available, and then take antennas that will hopefully be necessary for the task. Depth of investigation and resolvability of objects and layers in the ground are both considerations. Antenna frequency choice can therefore be a difficult decision. As a rule, if the target features are within about 1 meter of the ground surface, antennas between 400 and 900 MHz will be adequate to transmit energy to that depth and to resolve most features and associated stratigraphy (Table 3.2). If the target features are quite small, and greater resolution is needed, the higher frequency antennas within this range should be used. If the target depth is between one and three meters, antennas with frequencies ranging from 500 to 200 MHz will be necessary, but there will be less resolution of buried materials. Antennas with a frequency higher than about 500 MHz will rarely transmit energy to greater than two meters in the ground, except in exceptionally dielectric media. Targets buried deeper than about three or four meters will usually require antennas with frequencies lower than 200 MHz, but it is important to remember that

**Table 3.3. Length (in meters) of radar waves in media of a given RDP and frequency**

RDP	Frequency (MHz)									
	100	200	300	400	500	600	700	800	900	1000
1	2.998	1.499	0.999	0.750	0.600	0.500	0.428	0.375	0.333	0.300
2	2.120	1.060	0.707	0.530	0.424	0.353	0.303	0.265	0.236	0.212
3	1.731	0.865	0.577	0.433	0.346	0.288	0.247	0.216	0.192	0.173
4	1.499	0.750	0.500	0.375	0.300	0.250	0.214	0.187	0.167	0.150
5	<b>1.341</b>	<b>0.670</b>	<b>0.447</b>	<b>0.335</b>	<b>0.268</b>	<b>0.223</b>	<b>0.192</b>	<b>0.168</b>	<b>0.149</b>	<b>0.134</b>
6	1.224	0.612	0.408	0.306	0.245	0.204	0.175	0.153	0.136	0.122
7	1.133	0.567	0.378	0.283	0.227	0.189	0.162	0.142	0.126	0.113
8	1.060	0.530	0.353	0.265	0.212	0.177	0.151	0.132	0.118	0.106
9	0.999	0.500	0.333	0.250	0.200	0.167	0.143	0.125	0.111	0.100
10	<b>0.948</b>	<b>0.474</b>	<b>0.316</b>	<b>0.237</b>	<b>0.190</b>	<b>0.158</b>	<b>0.135</b>	<b>0.119</b>	<b>0.105</b>	<b>0.095</b>
11	0.904	0.452	0.301	0.226	0.181	0.151	0.129	0.113	0.100	0.090
12	0.865	0.433	0.288	0.216	0.173	0.144	0.124	0.108	0.096	0.087
13	0.831	0.416	0.277	0.208	0.166	0.139	0.119	0.104	0.092	0.083
14	0.801	0.401	0.267	0.200	0.160	0.134	0.114	0.100	0.089	0.080
15	<b>0.774</b>	<b>0.387</b>	<b>0.258</b>	<b>0.194</b>	<b>0.155</b>	<b>0.129</b>	<b>0.111</b>	<b>0.097</b>	<b>0.086</b>	<b>0.077</b>
16	0.750	0.375	0.250	0.187	0.150	0.125	0.107	0.094	0.083	0.075
17	0.727	0.364	0.242	0.182	0.145	0.121	0.104	0.091	0.081	0.073
18	0.707	0.353	0.236	0.177	0.141	0.118	0.101	0.088	0.079	0.071
19	0.688	0.344	0.229	0.172	0.138	0.115	0.098	0.086	0.076	0.069
20	<b>0.670</b>	<b>0.335</b>	<b>0.223</b>	<b>0.168</b>	<b>0.134</b>	<b>0.112</b>	<b>0.096</b>	<b>0.084</b>	<b>0.074</b>	<b>0.067</b>
30	0.547	0.274	0.182	0.137	0.109	0.091	0.078	0.068	0.061	0.055
40	0.474	0.237	0.158	0.119	0.095	0.079	0.068	0.059	0.053	0.047
50	0.424	0.212	0.141	0.106	0.085	0.071	0.061	0.053	0.047	0.042
60	0.387	0.194	0.129	0.097	0.077	0.065	0.055	0.048	0.043	0.039
70	0.358	0.179	0.119	0.090	0.072	0.060	0.051	0.045	0.040	0.036
80	<b>0.335</b>	<b>0.168</b>	<b>0.112</b>	<b>0.084</b>	<b>0.067</b>	<b>0.056</b>	<b>0.048</b>	<b>0.042</b>	<b>0.037</b>	<b>0.034</b>

the wavelengths generated from these frequencies are only capable of resolving larger features. Also, the deeper in the ground the energy must penetrate, the more spreading of the transmission beam, and the more radar energy is attenuated, so it may not be possible to generate good reflections from deeper than three or four meters in most ground conditions, no matter what the antenna frequency. If targets are buried deeper than five meters or so, antennas with frequencies lower than about 100 MHz are usually necessary, and ground that is dielectric enough to allow radar penetration to that depth is uncommon. Usually, this ground must be dry and lacking in conductive clay or salts, be un-weathered quartz-rich volcanic ash, sand, or perhaps permafrost or ice.

Another way to determine if features of a certain size are resolvable in reflection profiles is to calculate how much of a propagating beam of radar energy will “illuminate” them. As a basic guideline, the cross-sectional area of the target to be detected should approximate the size of the energy “footprint” pattern at the target depth or a little smaller (Figure 3.25). Equation 3 in Figure 3.25 calculates the radius of a cross-section of the conical transmission of radar waves using different frequency antennas (Annan and Cosway 1992; Neal 2004; Yalciner 2009). If the target is much smaller than this footprint size, then only a fraction of the transmitted energy that intersects it within the cone of transmission will be reflected to the surface. The small number of reflections returned from a very small, buried feature in this case would probably be indistinguishable from other reflections generated elsewhere within the transmission cone and therefore be invisible in reflection profiles as all reflections would all be averaged together. Small features of this sort might still be detectable if they create very high-amplitude reflections.

An estimation of footprint size is also important when designing a survey and planning transect spacing within a grid so that all subsurface features of importance are illuminated by the transmitted radar waves and can therefore

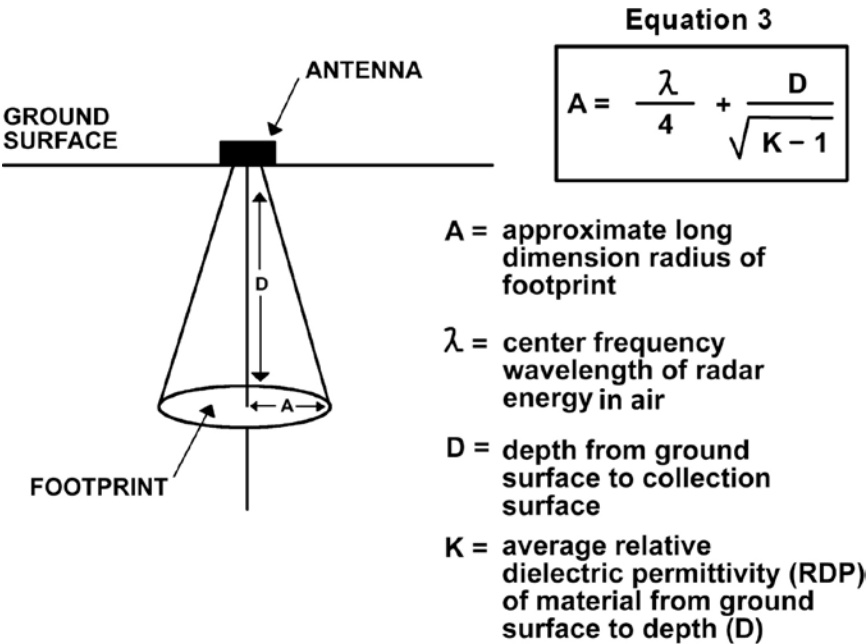


**Figure 3.25.** The radiation footprint (A) of an antenna with a given center-frequency can be calculated at estimated depths (D) if the relative dielectric permittivity (K) is known using Equation 3. *Source:* the author.



potentially generate reflections. In general, the angle of the transmission cone, and therefore the size of the footprint, varies as a function of the relative dielectric permittivity of the material through which the waves pass, and the frequency of the radar energy emitted from the antenna. Equation 3 in Figure 3.25 can only be used to estimate the width of the transmission beam at varying depths, but it can be helpful. For instance, if the radius of the cone was calculated to be 60 cm at a depth of one meter, then profiles separated by 50 cm would be sufficient to generate reflections from all potential materials in a grid (if a one-meter depth is about the depth of investigation needed). This equation can only be used as a rough approximation of real-world conditions because it assumes a consistent RDP of the medium through which the radar energy passes and one single frequency. In addition, sedimentary and soil layers within the ground almost always have variable chemical constituents, differences in retained moisture, compaction, and porosity that create other variables, so only be an estimate can be made and should be used accordingly.

Antennas, such as the 900 MHz or higher, have quite narrow cones of propagation, while the 200 and 300 MHz antennas spread energy outward a meter or more at depths of only about one or two meters below the ground surface (Figure 3.25). To complicate matters, cones of radar transmission in the ground are more elliptical than circular in cross-section because the electrical field produced by a dipole antenna is generated parallel to its long axis (Yalciner 2009), and it is propagating into the ground elongated in a dimension that is perpendicular to the dipole placements. If the antenna dipoles are positioned perpendicular to the direction of the antenna movement along a transect (the usual orientation), the cone of propagation will be more elongated parallel to the direction of transport. This will cause more waves to be propagated outward in front and behind the antennas, and less to the sides. I have also had antenna experts tell me they think there can be more waves propagated in front of an antenna than behind it. This is an interesting idea, but I can't find a reference to confirm it, and therefore I am a little skeptical of this claim.

Resolving a sequence of buried horizontal surfaces in the ground is even more complicated than determining whether individual objects might be visible in reflection profiles. To distinguish radar reflections generated from two parallel buried layers (for instance, the top and bottom of a layer of sediment), the two interfaces must be separated by at least one wavelength of the energy that is encountering them (Davis and Annan 1989). If the two reflections generated are not separated by that distance, then the resulting reflected waves can be destroyed or unrecognizable due to constructive and destructive interference, as illustrated in Figure 3.26. When two interfaces are separated by greater than one wavelength the waves moving in the ground, two distinct reflections will be generated from each interface, and both the top and bottom of the feature can potentially be resolved. But if the interface is within one wavelength, the bottom

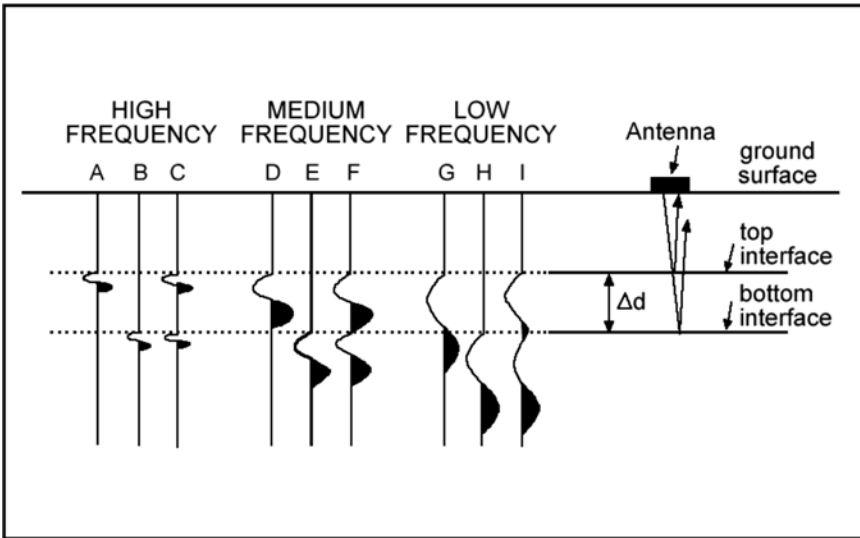


**Figure 3.26.** Resolution of two interfaces using different frequency antennas. With high-frequency waves, the top (A) interface is a reflection surface, as is the bottom (B), and the resulting trace (C) defines both interface. When the medium-frequency wavelength waves intersect the buried surfaces, the top (D) layer is defined, and the lower  $\epsilon$  may be visible, with the resulting trace (F) possibly defining both. With lower frequencies, the top interface produces a reflection (G), but the lower interface's reflection is distorted by the wave from the upper surface (H) and is effectively invisible in the resulting trace (I) due to constructive and destructive interference.  
Source: the author.

horizon reflection will interfere with the wave reflected from the upper surface and it will be distorted due to both constructive and destructive interference.

Any estimation of the orientation of transmitted energy is also complicated by the knowledge that radar energy propagated from most surface antennas is not one distinct frequency but can range many hundreds of megahertz around a center frequency. If one were to make a series of calculations on each layer in the ground (assuming all the soil and sediment physical and chemical variables could be quantified), and if one distinct antenna frequency was assumed, then the "cone" of transmission would be seen to widen in some layers, narrow in others, and create a very complex three-dimensional transmission pattern (Figure 3.27). The best one can usually do for most applications is to estimate the radar beam geometry and footprint size based on approximate field conditions and the center frequency of the antenna used. Some determination of the propagation beam dimensions is still important prior to conducting a survey so that grid lines can be spaced at distances smaller than the maximum footprint

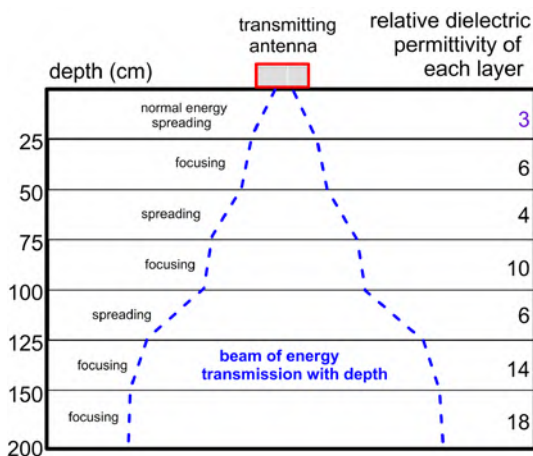


**Figure 3.27.** Model showing how the cone of illumination containing many propagating waves will refract with depth as waves cross, sometimes focusing and other times spreading out, depending on the RDP changes along the boundaries. *Source:* the author.

dimension at the depth necessary to delineate the features of interest (Equation 3 in Figure 3.25).

Field studies have shown that the amount of radar energy emitted from an antenna is greater directly beneath the antenna, and it tends to decrease in the more splayed portion of the cone of radiation (Leckebusch 2003; Neal 2004; Neubauer et al. 2002; Yalciner 2009). For this reason, survey line transects should be spaced as closely together as field conditions, equipment, and time allow (Jol and Bristow 2003; Neubauer et al. 2002). Comparisons of maps produced in grids containing variously spaced transects indicate that the highest-resolution images of buried features will always result from reflection data acquired in more closely spaced transects (Conyers 2015; Neubauer et al. 2002). For this reason, the multiple antenna arrays that space antennas as close as 10 cm or so produce much higher resolution images of buried features (Trinks et al. 2012).

Radar energy that is reflected off a buried interface that slopes away from a transmitting antenna will likely not travel back to a paired receiving antenna on the ground surface. In this case, all reflected energy would be effectively lost, and the sloping interface will go unnoticed in reflection profiles. A buried surface with this orientation would only be visible if additional antenna traverses were located in an orientation where that buried interface is sloping toward the receiving antenna. This is one reason why it is important to always

acquire transects of data within a closely spaced surface grid, and sometimes with profiles perpendicular to each other, so that all buried features, no matter what their orientation, will be visible. This scattering of radar waves due to the geometry of the reflective surface is the same concept exploited in the “stealth” technology for airplane construction. Wings and the fuselage of these stealthy aircraft are built in a geometry that reflects energy in any direction except back to the receiving antenna, making them essentially invisible to radar, especially when radar-absorbing material covers its surfaces.

In most geological and archaeological settings, the materials through which radar waves pass may contain many small point targets that generate good reflections that are very small in size (e.g., the small ceramic artifacts in Figure 3.23), which can only be described as clutter (if they are not the target of the survey). The amount of clutter visible in a reflection profile is dependent on the wavelength of the radar energy being propagated. Clutter can also be produced by large discontinuities, such as cobbles and boulders, but only when lower-frequency antennas that produces a long wavelength of propagating waves are used.

There will always be radar energy that propagates in many complex orientations depending on frequency changes and the complexities of materials in the ground. To minimize the amount of reflection data derived from the sides of a survey line (called side-scatter), the long axes of the antennas are usually aligned perpendicular to the survey transect. This allows the cone of transmission to be elongated in an in-line direction (Figure 3.25). If there are narrow elongated features in the subsurface that are parallel to the direction of antenna travel only a small portion of the radar waves will be reflected to the surface. In this case, if the antennas were not traversing almost directly on top of the buried linear feature, it might not be visible. Elongated buried features of this sort would usually have to be oriented perpendicular or at some angle to direction of antenna travel to be visible on GPR profiles. They would then be visible as distinct “point sources” reflection hyperbolas. Electrical engineers have developed a number of different antenna designs that produce other types of radiation patterns, most of which are not used in standard GPR surveys (Annan and Cosway 1992; Orlando and Slob 2009).

The amount of propagating wave refraction that occurs along interfaces that bound layers of different RDP can be determined by Snell’s Law (Sheriff 1984). This states that the amount of refraction that will occur at a boundary between two layers of this sort depends on the angle of incidence and the velocity change that occur at the interface. In general, the greater the increase in RDP in the layer below the intersected interface the greater the refraction angle.

The composition of surface materials within which the radar waves couple as it leaves the transmitting antenna will also affect the amplitude of the reflected waves below it. In Figure 3.28, good radar reflections were recorded to about 40 nanoseconds through a surface material composed of limestone

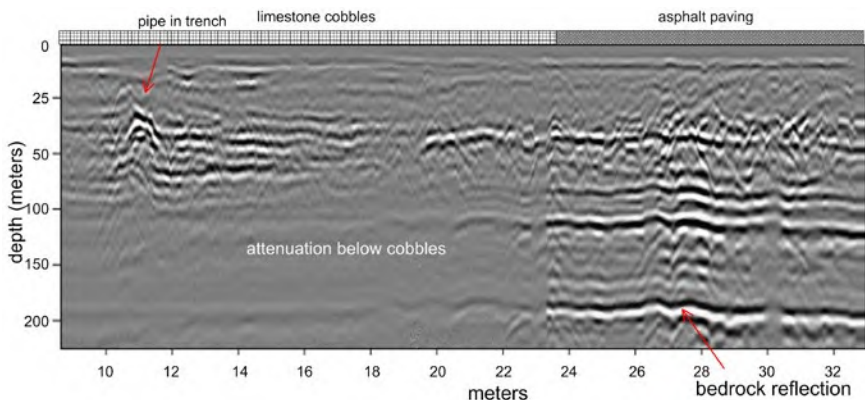


**Figure 3.28.** Reflection profile collected along a road in Portugal with differing resolution of bedding planes in the ground and coupling of energy depending on the roadbed composition. Very good coupling of propagating waves with the asphalt produces twice the depth of penetration compared to the limestone cobbles and corresponding resolution of buried surfaces. *Source:* the author.

cobbles. When the transmitting antenna crossed an asphalt paving surface, the amount of energy coupled with the ground greatly increased. Reflections along the same transect where the coupling materials was asphalt were recorded at 100 nanoseconds or more, presumably due to better coupling. Wave penetration depth in this case appears to be a function of the surface materials, and not the materials in the ground. It might also be a function of other factors, which are very difficult to quantify. The limestone cobbles might be scattering the propagating waves many directions, so they travel away from the surface recording antenna (Conyers 2012). It might also be possible that the asphalt is shedding rain away from the road surface, making the ground below it drier and perhaps less electrically conductive and therefore creating less radar wave attenuation. The cobbles would allow water to move in greater quantities downward producing more conductive ground below. I don't like that hypothesis much, as there are noticeable planar reflections visible below the asphalt paving that continue below the cobbles with no apparent velocity pull-up or push-down, which would have occurred with variations in water retention.

Frozen ground, especially with a thin layer of snow, can often be an excellent energy coupling surface producing little variation in transmitted waves. In fact, some of the highest-quality GPR data have been acquired in frozen ground conditions, with excellent depth penetration and the recording of high-amplitude waves. Data collected over the same ground after a thaw can often yield disappointing results, because of a drastic decrease in wave coupling. One survey I conducted in Colorado is notable because the ground was frozen when data collection started in the early morning, producing high-quality reflection data

with good depth penetration. As the day progressed, the sun slowly melted the ground surface with a noticeable decrease in the penetration depth of the waves and a corresponding decrease in their reflection amplitude. This change was totally the result of differences in energy coupling and not differing constituents of ground materials. A friend of mine tried to increase energy coupling by lashing a freezer-pack, used to keep drinks cold in his cooler, under his antenna during collection during the summer. This otherwise good idea proved to produce variable and unquantifiable changes in coupling because during the survey the ice pack melted, and the recorded waves became weaker and weaker as the day progressed. This produced a dataset of profiles, each of which had very different reflection amplitudes from the same buried interfaces.

Snow is an excellent medium for energy penetration and antenna coupling (Figure 3.29), but allowances must be made for how much energy spreads with depth, in those conditions. Snow has an RDP of about 5 (Table 3.1) and energy moving through it will spread out the propagating waves (Figure 3.25). As a result, reflections from the ground will be more “averaged” and less distinct, with smaller point-source hyperbolas effectively invisible (Figure 3.30). A comparison of profiles over the same transect collected with snow on the ground in winter and barren ground in the summer (Figure 3.30) illustrates this concept. During summer conditions the RDP of the ground was about 15, and the propagating cone was much narrower than in the winter with snow cover and frozen ground. This narrower propagation cone concentrated the



**Figure 3.29.** Collecting GPR data in snow in Alaska. *Source:* the author.

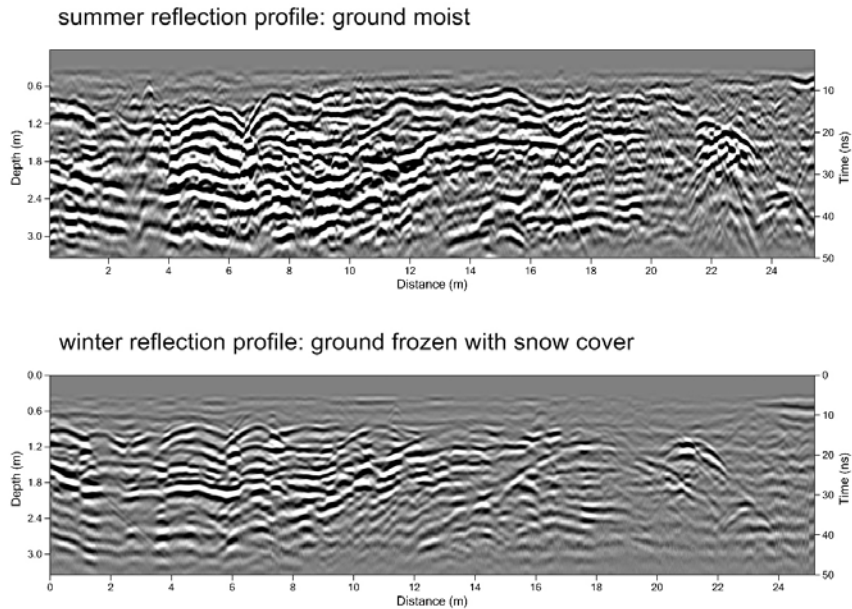


**Figure 3.30.** Comparison of two reflection profiles collected along the same transects in snow and during the summer with bare ground. The summer profile shows better bed definition as the waves are more focused in ground with a higher RDP. The winter profile where waves move through the snow illustrates less definition due to more energy spreading through the snow and underlying frozen ground, with much lower RDPs. *Source:* the author.

propagating waves on a smaller area on subsurface interfaces, and therefore produced a reflection profile with more detail (Figure 3.30). A calculation using wavelengths (Table 3.3) of antennas with RDP and Equation 3 in Figure 3.25 shows that a 400 MHz propagation cone at one-meter depth has a radius of about 27 cm. In winter with snow cover and frozen ground beneath, the RDP of the ground was about 5, and a calculation with the same antenna frequency had a cone radius of about 50 cm, or twice the size as during the summer. This doubling of the propagating cone radius in winter reduces the resolution of the subsurface features by about half, while in summer with an RDP of 15, the resolution is about double that in winter (Figure 3.30). This is apparent when comparing the two reflection profiles with the summer profile providing much more detail on small changes along the planar reflections. The question then becomes, is possible better wave coupling with snow and frozen ground worth the decrease in buried feature resolution? Or should a survey be put off until the snow melts, possibly leading to decreased wave penetration due to poorer coupling, but with higher resolution in interfaces of interest?

An additional complication that affects resolution of reflections in the ground is background radio wave noise, which is almost always recorded during GPR surveys. As the GPR antennas are within the frequency band of cell phones, analog television, FM radio, and other radio communication bands (Figure 3.2), there are almost always nearby radio wave transmitters of some kind (Figure 3.31). Even far away from the city, there will usually be background noise of some kind as radio waves are transmitted great distances in air. The background noise is often a more significant problem if a study site is near a military base, airport, or cell-phone transmission antenna. One survey I conducted near a U.S. military research site in New Mexico was occasionally disrupted by background noise from unknown sources that was visible during data collection as periodic very high-amplitude reflection traces that occurred in short bursts. Other times it was recorded at a lower frequency in long bursts,

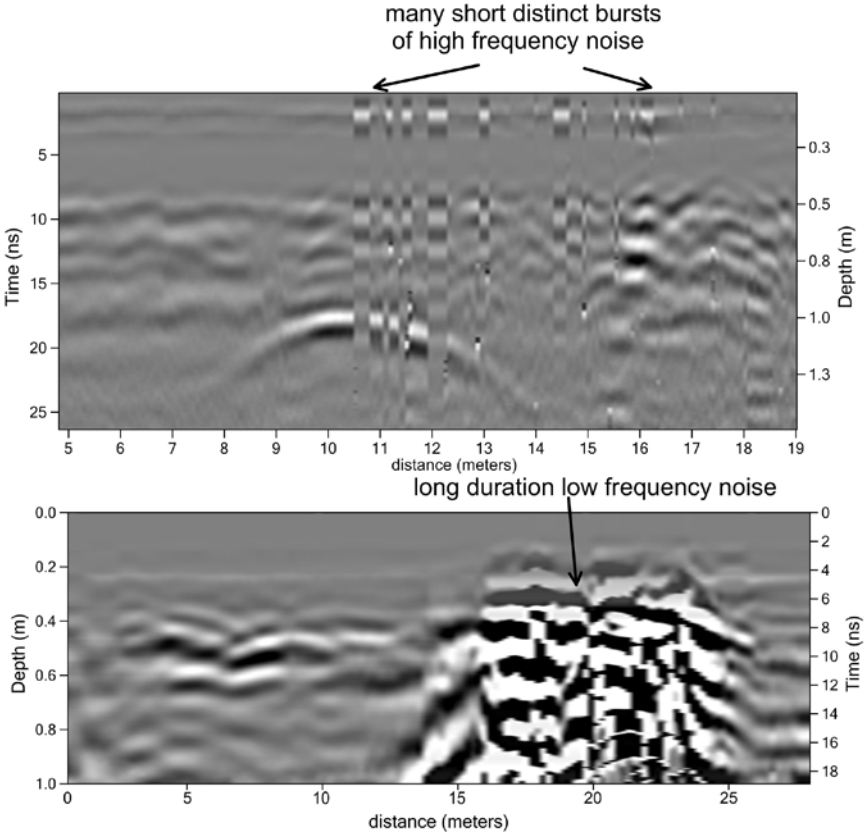


**Figure 3.31.** Different types of background noise from high-frequency bursts of energy and longer-duration, low-frequency radio waves. *Source:* the author.



which sometimes lasted many minutes. Those totally overwhelmed any reflections derived from within the ground (Figure 3.31). When this mystery transmitter or transmitters were active, I tried many different frequency-filtering schemes in the calibration settings, but all failed to remove this noise. In about an hour, all the recorded noise disappeared, and data collection could continue. The sources of the interfering electromagnetic waves were never discovered.

The recent proliferation of cellular (mobile) telephones that can be in use nearby during data acquisition has also become a problem, as they produce radio waves in the same frequencies as some of the higher frequency GPR antennas. Depending on 4G or 5G cell-phone technology different band widths are used, and these also vary with the service provider. Most of the noise from these transmissions is in the background and can be removed with processing steps. But if a cell phone is very near the receiving antenna and is actively transmitting, it can interfere with GPR-receiving antennas.

Reflection off a buried surface that is not horizontal and perhaps contains ridges or troughs, or other irregular features, can either focus or scatter radar energy, depending on the surface's orientation and the location of the antenna on the ground surface. If a reflective subsurface plane is slanted away from the surface antenna's location most waves that intersect it will be reflected away from the surface antenna, and none of those reflected waves will be recorded (Figure 3.32). This is termed "radar wave scatter." The opposite is true when

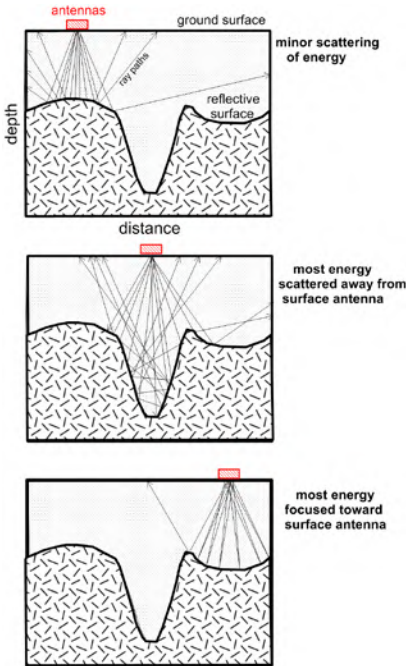


**Figure 3.32.** Radar waves are scattered from an upward bowing surface (top), are reflected in many complex ways. In a deep trench (middle), they are scattered away from the antenna and are focused, where a buried surface is concave upward. Source: the author.

the buried surface is tipping toward the antenna or is concave upward (Figure 3.32). Reflected waves in this case will be focused back to the surface, and a very high-amplitude reflections derived from a portion of the buried surface will be recorded.

This scattering effect would make a narrow channel's sides almost invisible in reflection profiles (Figure 3.32). When the antenna is located directly over the base of the channel there will be focusing of the radar energy, creating a higher-amplitude reflection from only this basal portion of the subsurface interface. Even a gently convex surface can scatter reflected waves, producing a planar reflection that varies greatly in its wave amplitude. These focusing, and scattering conditions are quite common and can occur repeatedly along one buried planar surface. It was noticed when mapping uneven floors of buried Roman buildings (Figure 3.33). The small areas of the floor that had sunken just a few centimeters created a concave upward surface that focused the radar energy, creating higher-amplitude reflections while the upward bowing portions of the floor scattered many waves, producing weaker reflections.

Energy radiated from a surface antenna generates a strong electromagnetic field around the antenna within a radius of about 1.5 wavelengths of the center frequency (Balanis 1989; Engheta et al. 1982; Kraus 1950; Sheriff 1984). Within this zone, waves are coupling with the ground, generating an advancing wave front of propagating waves in the conical transmission pattern. It can be said

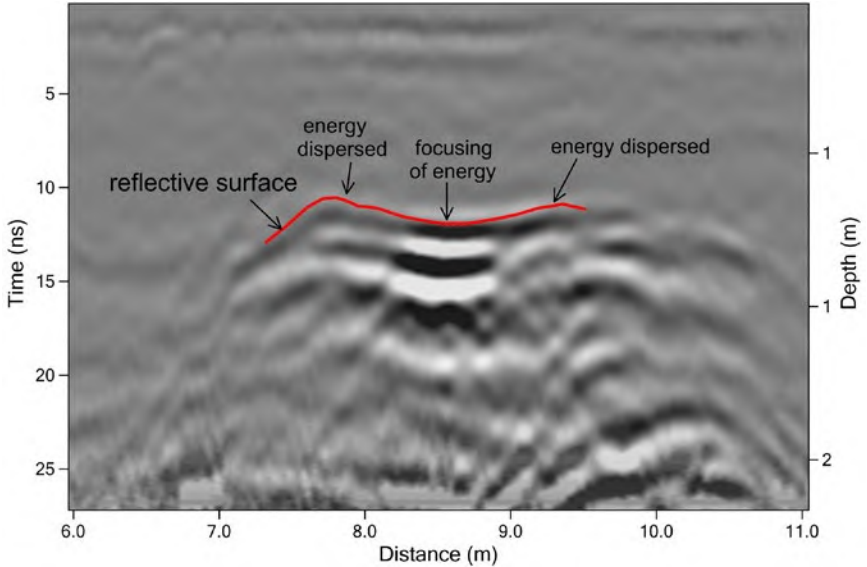


**Figure 3.33.** Example of a Roman floor that has subsided in the middle over the centuries, which focuses reflected waves where the surface is concave upward. *Source:* the author.

that the ground within about 1.5 wavelengths of a standard dipole antenna is technically “part of the antenna” in that no propagation is occurring. This is termed the “near-field” zone, which is visible in GPR profiles as a region of little or few reflections beginning at the ground surface to about 1.5 wavelengths. It is important to remember that during this coupling process the transmitted waves are also shortening their wavelengths, as the RDP of the ground increases. In the GPR literature, this near-field zone is sometimes incorrectly called the “near-surface zone of interference.” That is an old term and need not be used anymore as there is no interference happening, but only coupling. These first recorded waves in all traces are complicated because in this shallow part of the time-window there are some waves also moving in air (or along the ground-air interface) between the transmitting and receiving antennas and those are also being recorded. Even more complicated is that broad-band antennas are transmitting many frequencies of waves, and each frequency waves are coupling with the ground at different depths. While this complicated near-field zone is always recorded it can be removed by background removal software.

If lower-frequency antennas are used the near-field zone can be as much as 2.5 meters below the ground surface. If the target features are located within this zone, it is unlikely that they will be visible in GPR reflection profiles without post-acquisition filtering steps. Perhaps a higher-frequency antenna should be used. It is always important to consider that there may be some high frequency waves recorded within the near-field zone, even if they are not immediately visible on standard two-dimensional reflection profiles (Ernenwein 2006). They will couple with the ground at a much shallower depth, and some of their shallow reflections can still be visible in reflection profiles within what is broadly defined as the near-field zone. If these reflections are high enough in amplitude, they might still appear as weak reflections within the otherwise reflection-free near-surface layer. Some subtle reflections in the near field may never be noticeable in standard two-dimensional profiles but can potentially become visible after the data are computer processed to generate reflections of only a certain frequency (Ernenwein 2006). The usually weaker shorter wavelength reflections here may be difficult to see in standard reflection profiles but can be enhanced by applying gains.

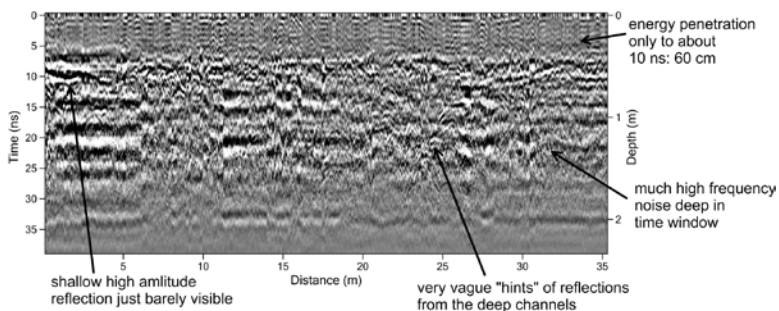
Resolution varies greatly depending on the frequency of the antenna used. Almost always the higher frequency antennas have greater resolution, both because of their wavelengths, but also due to the narrowing of the cone of transmission. This narrowing allows more propagating waves in these higher frequencies to reflect from a smaller area, and therefore more of the waves arrive back at the receiving antenna to be recorded. The lower frequency antennas with longer wavelengths spread waves out more as they propagate from the surface antenna and are capable of less resolution and produce more averaged when viewed in reflection profiles (Figure 3.34).

representative  
traces for each  
frequency

900 MHz

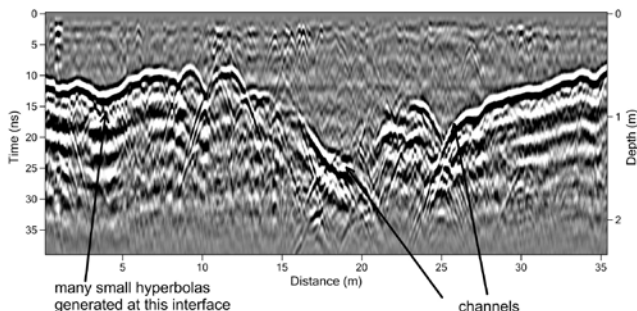


900 MHz antennas



400 MHz antennas

400 MHz



270 MHz antennas

270 MHz

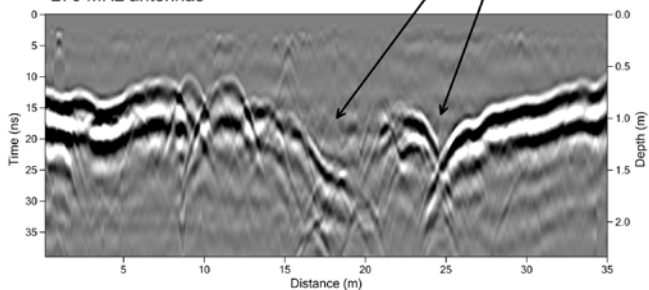
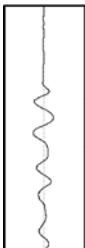


**Figure 3.34.** Three frequency antennas that collected profiles over the same transect show the variations in resolution and depth of propagation. The 900 MHz energy is attenuated at a shallow depth and only resolves thinly bedded near-surface layers. The 400 MHz waves are reflected from many small variations in a buried surface producing a very well-defined reflection profile. The 270 MHz waves spread out more during propagation and produce a more averaged profile of the same buried surface.  
*Source:* the author.

Air waves that are recorded from nearby objects on the surface can be a significant problem. In a deep excavation whose sides are bounded by exposed materials or even worse metal barriers (Carrozzo et al. 2003; Nuzzo 2005) produce high-amplitude air waves that can overwhelm and interfere with reflections produced from within the ground. These can be removed using a complex series of processing steps by first producing a mean profile of the air wave reflections generated from the metal walls, which creates a model from the known distance to the walls for each profile (Carrozzo et al. 2003; Nuzzo 2005). The location of the air waves in the model is known as the waves that produced them move at the speed of light and that velocity does not change. The mean reflection in the models is then subtracted from the recorded reflections to produce residual reflection profiles, which then can be re-gained to make the remaining reflections, presumably those generated from within the ground, more visible.

Very reflective buried materials often create multiple reflections that “ring down” through a reflection profile obstructing some or all features below them (Figure 3.35). This is very common when conducting GPR surveys on road surfaces or at any location where there are planar features that are highly reflective especially if they are near the surface. Multiples are produced as waves reflect many times from a buried surface, traveling back to the ground surface to be re-reflected into the ground and then reflected again to the surface from the same buried interface. This can happen over and over, especially when the material that is reflecting the energy is shallowly buried (Figure 3.35). Multiples are recognizable in reflection profiles as they are all evenly spaced in time, and mimic in general shape the surface from which they have been reflected.

Where metal reinforcing bars are used to stabilize concrete or where there is an abundance of buried pipes, there can be many closely spaced reflection hyperbolas generated (Figure 3.36). These are common in roadways and sidewalks and produce very distinct, often evenly spaced hyperbolas in reflection profiles (Figure 3.36). To test if energy can still be transmitted below the shallow metal bars to propagate deeper, be reflected and travel back to the surface between the metal bars, two frequency antennas were tested (Figure 3.36). It was known there was a road in this area before the paved surface was built with the metal bars in it. As the 500 MHz wave propagation cone is more focused these frequency waves travel between the metal, to be reflected from that deeper surface creating a coherent deeper planar reflection. The 200 MHz reflection profile shows that energy from its wider cone of propagation still makes it through the metal, but the buried surface reflection is less defined and more distorted.

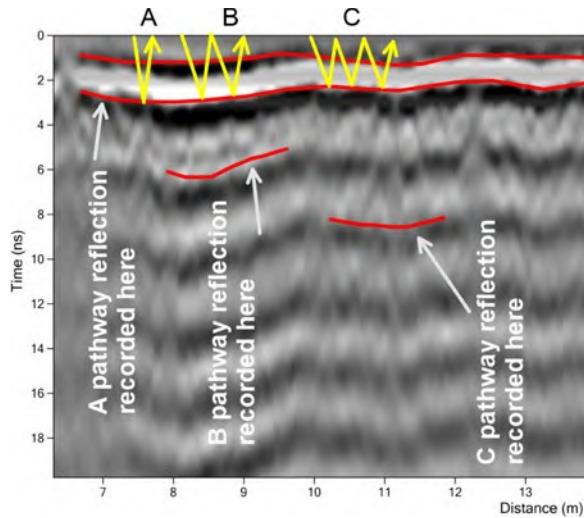


**Figure 3.35.** Multiple reflections produced from the very reflective upper and lower surface of a roadbed. The waves reflect multiple times between the upper and lower interface, creating a profile of equally spaced multiple reflections. *Source:* the author.

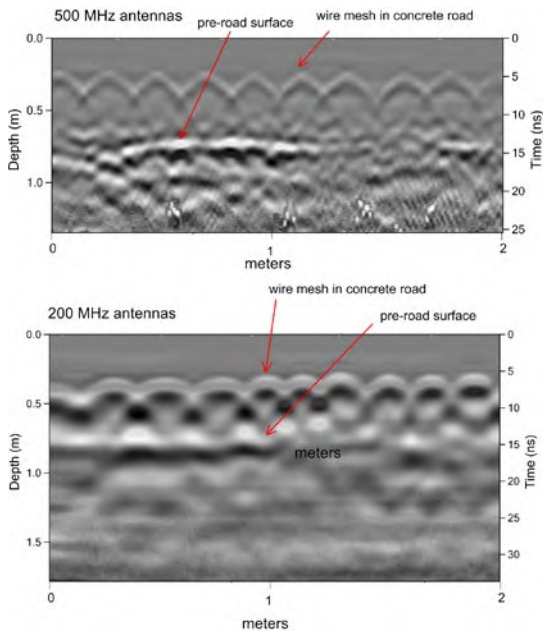


**Figure 3.36.** Metal reinforcing bars in the ground will generate equally spaced reflection hyperbolas, but both 500 and 200 MHz waves will still propagate below the metal to be reflected from the buried surface. The 500 MHz waves are more focused, and therefore more of those waves move between the metal to reflect from the lower interface, creating a more distinct planar reflection below the near-surface metal. *Source:* the author.



# 4

## *Ground-Penetrating Radar Equipment and Acquisition Software*

The most commonly used GPR units in North America are manufactured by Geophysical Survey Systems Incorporated (GSSI), located in North Salem, New Hampshire, and Sensors and Software Inc. of Mississauga, Ontario, Canada. There is a large presence in Europe of MALÅ in Sweden and IDS in Italy, with other manufacturers starting up elsewhere, all of which market multiuse GPR systems with excellent applications. Most of the systems produced for general-purpose GPR surveys employ antennas that transmit pulsed radar energy of one center frequency and most are also developing or have on the market multiple channel systems. Most of these collect and analyze data in the “time domain” meaning that reflections are collected within a programmed time-window and the amplitude and wavelengths of waves are recorded within that time. Some recent developments using “stepped-frequency” systems work in the “frequency domain” meaning that multiple programmed frequencies are propagated and recorded, and these data are converted to time-domain data through computer processing (Eide et al. 2014; Leckebusch 2011; Noon et al. 1994; Sala et al. 2012; Tronca et al. 2018).

All GPR systems on the market can collect data along transects using some kind of survey wheel or GPS unit that measures distance and spaces reflection traces equally along transects and placed precisely into space. Survey wheels roll along the ground surface, and their revolutions and the number of reflection traces collected are calibrated for distance.

There are many similarities and some differences between models and manufacturers of GPR units. Most new models are compact enough so that one person can theoretically collect large numbers of transects alone. These systems place the antennas, power source, and control system on a cart that can be rolled along the ground (Figure 2.3) or placed in a pack (Figure 3.6), relieving the antenna operator from having to be tethered to a base station, which was how GPR data used to be collected in the 1990s. Most systems can operate



for many hours on rechargeable lightweight batteries. All GPR systems contain one or more internal hard drives or flash drives that store data and this control system also contains the software and hardware to drive the system based on parameters input by the user. Systems typically have several different ports that allow acquired data to be transferred to a personal computer after a survey is complete. Some do this through blue-tooth wireless connections, and others using fiberoptic cables or in older versions of coaxial cables. The newer models save data on flash memory cards or chips that can hold many hundreds of megabytes of data with little power usage, making these systems very lightweight and allowing data to be quickly downloaded to other computers for processing.

The newer antenna array systems (Figure 3.8) join many antennas together and move all in unison across the ground. In these systems there are multiple sending and receiving antennas that fire in sequence at a very rapid rate, collecting a swath of reflections from within the ground. Distance and location data are collected simultaneously with the reflections in the ground, all programmed from a computer and control system, usually within the vehicle that pulls (or pushes) the array (Figure 4.1)

As an example of an array system, a row of nine transmitting antennas and a nearby row of eight receiving antennas can transmit sequentially, and

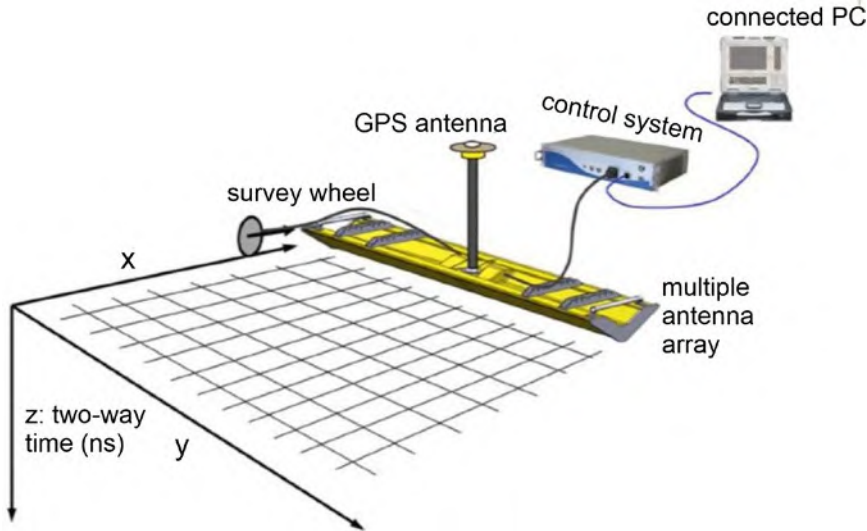


**Figure 4.1.** The components of an antenna array system with multiple antennas moved in the x direction and a desired distance in y, with many traces recorded in z as the array is pulled over the ground along the x dimension. GPS and survey wheels calibrate distance, and the GPS can record elevation changes, with all controlled in an attached system computer with reflection data visible on an external computer. *Modified from and courtesy of Arne Anderson-Stamnes and Kontur.*

the receiving antennas can record the reflections. With a 150 cm wide swath of antennas, this array can collect a reflection trace every 10 cm (Figure 4.2) in the “y” dimension and an even more closely spaced set of traces in the “x” dimension, depending on the programmed trace spacing along the direction the array is being moved.

All GPR systems employ a computer screen that is necessary for pre-survey calibration, which also allows reflection profiles to be viewed in real time during collection. Screens are sometimes built into the control box of the system or can be a peripheral laptop computer.

Manufacturers are continually introducing new GPR system models, striving for compactness, longer-life battery usage, transportability, and ease of data collection. There have been some recently developed systems that are “dumbed-down” versions of more standard GPR units, which are mostly used to find pipes or voids in the ground quickly for buried utility location where complex post-acquisition processing is not necessary. These simple systems have little ability to be calibrated to unusual field conditions or store complex datasets that can later be processed with GPR software and they should be avoided for most applications. There are also some unique GPR systems that can transmit and receive radar waves within or between bore holes (Akinci 2018; Wright and Lane 1998) by placing a transmitting antenna in a hole and

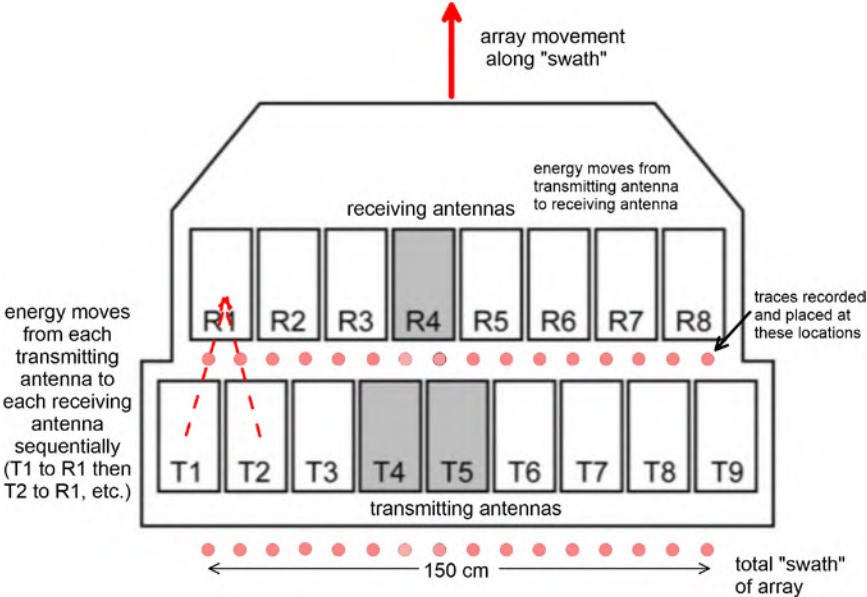


**Figure 4.2.** An array system with seventeen antennas, nine transmitters, and eight receivers that collect individual traces every 10 cm along a swath 150 cm wide. *Source:* the author.

collecting received waves in a second hole or with receiving antennas on the ground surface.

Standard GPR systems consist of three main elements, the control unit (pulse generator, computer, and associated software), the antennas (paired transmitting and receiving antennas), and the display unit (computer screen). The control unit can produce an electrical pulse or send commands to a pulse generator on the antennas. At the antennas the voltage is amplified, and the antenna shape and its components shape the electromagnetic pulse and emit it. The systems that produce the electrical pulse directly at the antenna use the fiber optic cables to only transmit a digital signal between the antennas and the control system, which greatly reduces some of the equipment-related noise that can affect the signal clarity. The recorded reflections are then digitized at the antenna and those data are transmitted by the fiber optic cables back to the control system for recording. Fiber optic connectors are not always “field durable,” and sometimes the smallest amount of dust on a connection, or any rough wear during data acquisition, can cause them to malfunction. When short fiber optic cables are needed to connect peripheral devices with the control unit, and these components are being transported on a cart or backpack, wear and tear of fiber optic cables can be minimized.

## **DATA ACQUISITION SOFTWARE: SETUP PARAMETERS**

Manual adjustments are always necessary prior to conducting any GPR survey (Conyers 2012; Kemerait 1994). In all modern GPR units, the collection parameters are visible in windows or tabs in the software and users can define the time-window, frequency filters, trace spacing and a variety of other settings. There are often preset acquisition settings in some systems that are presumably included for users who are not thinking about their surveys much and need to get directly to work locating pipes or do concrete scanning. In my experience these pre-setup calibration menus should be avoided, and settings should always be adjusted to meet the goals of a survey within the parameters of the ground conditions, equipment being used, depth of study, and many of the other variables commonly encountered at each new survey location. All GPR systems have a software interface to program all important collection parameters, which can be controlled from a keyboard or touch pad or using an attached laptop computer.

Most digital GPR control units also have a procedure where information can be input for each file or the grid, as a whole. This information typically includes the date of the fieldwork, antenna frequency, site name, grid name or number, and other pertinent information or comments. Some will also collect grid information and data that are saved include not only the reflections from the ground, but also locations within surface grids. I always neglect to fill in these fields, and instead I write this information in my field book. This is probably a mistake.

Recent control systems create what used to be called header files for each reflection profile that is recorded. This information is used by some software in data processing to place reflections into space and provide information about

the acquisition parameters. Some of the newer multi-channel systems save multiple sets of reflection data from each of the recording antennas in the array, producing very large datasets. I have heard that some of the array systems can collect one huge file that collects continuously as the antennas turn as they go back and forth across a grid, with location information also streaming from the GPS systems. These create huge reflection data files and specialized software is needed to place all reflections correctly into space.

With the more standard data collection individual profiles have their own location in a grid with file names and sequential numbers generated in a numerical sequence when saved. Some software also saves individual transect file locations in a predetermined grid. Files of this sort are usually recorded sequentially, with the first reflection profile in a grid saved as file1, file2, file3, and so on, as they are collected. To avoid confusion when more than one grid of data is being collected in a day, it is usually good to start each profile in a grid as file1 in a separate computer directory or with a different name, and always keep good notes of each grid's location and file orientations within the grids. But any names or numbering system works just as well, if good notes are made.

All GPR systems allow the user to select the time period over which reflection data are recorded. The time-window is defined as the amount of two-way travel time, measured in nanoseconds, that the receiving antenna will "listen" and record the reflected radar wave energy (Figure 1.1). This window will normally open just before the radar pulse is transmitted and is closed after all reflections of interest, from the depth desired in the ground, have been recorded. If the velocity of the material and the approximate depth of the features to be resolved are known, the amount of time necessary for radar energy to travel to and then be reflected from the zones of interest can be estimated in advance. The time-window can be adjusted at the outset of a survey so that it is open for at least this period so that all important reflections in all antenna transects within the survey grid are recorded. This window should be programmed so that more reflection data below a desired depth are recorded, even if it seems that is not necessary at the beginning of a survey. Often, due to unforeseen velocity changes, reflections from features of interest could possibly be received at times later than preliminary calculations estimate, and if the time-window is not open for long enough, those will not be recorded. It is also possible that buried horizons of interest might dip to deeper in the ground or be covered with a greater thickness of overburden, which may not be known in advance. This situation would necessitate a longer time-window to be set in advance to record them.

Often a time-window of 100 nanoseconds (two-way travel time) is usually sufficient to record reflections within two to four meters of the surface, depending on the velocity of radar wave propagation. In a material with a relative dielectric permittivity of 8, a 20-nanosecond window is capable of recording reflections to about one-meter depth (Table 4.1). These types of depth calculations are independent of antenna frequency.

**Table 4.1. Depth in meters to a reflector through a media of a given RDP**

	Relative Dielectric Permittivity																
2-way Time (ns)	1	2	3	4	5	6	7	8	9	10	15	20	30	40	50	60	80
10	1.50	1.06	0.87	0.75	0.67	0.61	0.57	0.53	0.50	0.47	0.39	0.34	0.27	0.24	0.21	0.19	0.17
20	3.00	2.12	1.73	1.50	1.34	1.22	1.13	1.06	1.00	0.95	0.77	0.67	0.55	0.47	0.42	0.39	0.34
30	4.50	3.18	2.60	2.25	2.01	1.84	1.70	1.59	1.50	1.42	1.16	1.01	0.82	0.71	0.64	0.58	0.50
40	6.00	4.24	3.46	3.00	2.68	2.45	2.27	2.12	2.00	1.90	1.55	1.34	1.09	0.95	0.85	0.77	0.67
<b>50</b>	<b>7.50</b>	<b>5.30</b>	<b>4.33</b>	<b>3.75</b>	<b>3.35</b>	<b>3.06</b>	<b>2.83</b>	<b>2.65</b>	<b>2.50</b>	<b>2.37</b>	<b>1.94</b>	<b>1.68</b>	<b>1.37</b>	<b>1.19</b>	<b>1.06</b>	<b>0.97</b>	<b>0.84</b>
60	8.99	6.36	5.19	4.50	4.02	3.67	3.40	3.18	3.00	2.84	2.32	2.01	1.64	1.42	1.27	1.16	1.01
70	10.49	7.42	6.06	5.25	4.69	4.28	3.97	3.71	3.50	3.32	2.71	2.35	1.92	1.66	1.48	1.35	1.17
80	11.99	8.48	6.92	6.00	5.36	4.90	4.53	4.24	4.00	3.79	3.10	2.68	2.19	1.90	1.70	1.55	1.34
90	13.49	9.54	7.79	6.75	6.03	5.51	5.10	4.77	4.50	4.27	3.48	3.02	2.46	2.13	1.91	1.74	1.51
<b>100</b>	<b>14.99</b>	<b>10.60</b>	<b>8.65</b>	<b>7.50</b>	<b>6.70</b>	<b>6.12</b>	<b>5.67</b>	<b>5.30</b>	<b>5.00</b>	<b>4.74</b>	<b>3.87</b>	<b>3.35</b>	<b>2.74</b>	<b>2.37</b>	<b>2.12</b>	<b>1.94</b>	<b>1.68</b>
110	16.49	11.66	9.52	8.24	7.37	6.73	6.23	5.83	5.50	5.21	4.26	3.69	3.01	2.61	2.33	2.13	1.84
120	17.99	12.72	10.39	8.99	8.04	7.34	6.80	6.36	6.00	5.69	4.64	4.02	3.28	2.84	2.54	2.32	2.01
130	19.49	13.78	11.25	9.74	8.71	7.96	7.37	6.89	6.50	6.16	5.03	4.36	3.56	3.08	2.76	2.52	2.18
140	20.99	14.84	12.12	10.49	9.39	8.57	7.93	7.42	7.00	6.64	5.42	4.69	3.83	3.32	2.97	2.71	2.35
<b>150</b>	<b>22.48</b>	<b>15.90</b>	<b>12.98</b>	<b>11.24</b>	<b>10.06</b>	<b>9.18</b>	<b>8.50</b>	<b>7.95</b>	<b>7.50</b>	<b>7.11</b>	<b>5.81</b>	<b>5.03</b>	<b>4.11</b>	<b>3.56</b>	<b>3.18</b>	<b>2.90</b>	<b>2.51</b>
160	23.98	16.96	13.85	11.99	10.73	9.79	9.07	8.48	7.99	7.58	6.19	5.36	4.38	3.79	3.39	3.10	2.68
170	25.48	18.02	14.71	12.74	11.40	10.40	9.63	9.01	8.49	8.06	6.58	5.70	4.65	4.03	3.60	3.29	2.85
180	26.98	19.08	15.58	13.49	12.07	11.02	10.20	9.54	8.99	8.53	6.97	6.03	4.93	4.27	3.82	3.48	3.02
190	28.48	20.14	16.44	14.24	12.74	11.63	10.76	10.07	9.49	9.01	7.35	6.37	5.20	4.50	4.03	3.68	3.18
<b>200</b>	<b>29.98</b>	<b>21.20</b>	<b>17.31</b>	<b>14.99</b>	<b>13.41</b>	<b>12.24</b>	<b>11.33</b>	<b>10.60</b>	<b>9.99</b>	<b>9.48</b>	<b>7.74</b>	<b>6.70</b>	<b>5.47</b>	<b>4.74</b>	<b>4.24</b>	<b>3.87</b>	<b>3.35</b>
210	31.48	22.26	18.17	15.74	14.08	12.85	11.90	11.13	10.49	9.95	8.13	7.04	5.75	4.98	4.45	4.06	3.52
220	32.98	23.32	19.04	16.49	14.75	13.46	12.46	11.66	10.99	10.43	8.51	7.37	6.02	5.21	4.66	4.26	3.69
230	34.48	24.38	19.91	17.24	15.42	14.08	13.03	12.19	11.49	10.90	8.90	7.71	6.29	5.45	4.88	4.45	3.85
240	35.98	25.44	20.77	17.99	16.09	14.69	13.60	12.72	11.99	11.38	9.29	8.04	6.57	5.69	5.09	4.64	4.02
<b>250</b>	<b>37.48</b>	<b>26.50</b>	<b>21.64</b>	<b>18.74</b>	<b>16.76</b>	<b>15.30</b>	<b>14.16</b>	<b>13.25</b>	<b>12.49</b>	<b>11.85</b>	<b>9.68</b>	<b>8.38</b>	<b>6.84</b>	<b>5.93</b>	<b>5.30</b>	<b>4.84</b>	<b>4.19</b>
260	38.97	27.56	22.50	19.49	17.43	15.91	14.73	13.78	12.99	12.32	10.06	8.71	7.12	6.16	5.51	5.03	4.36
270	40.47	28.62	23.37	20.24	18.10	16.52	15.30	14.31	13.49	12.80	10.45	9.05	7.39	6.40	5.72	5.23	4.53
280	41.97	29.68	24.23	20.99	18.77	17.13	15.86	14.84	13.99	13.27	10.84	9.39	7.66	6.64	5.94	5.42	4.69
290	43.47	30.74	25.10	21.74	19.44	17.75	16.43	15.37	14.49	13.75	11.22	9.72	7.94	6.87	6.15	5.61	4.86
<b>300</b>	<b>44.97</b>	<b>31.80</b>	<b>25.96</b>	<b>22.48</b>	<b>20.11</b>	<b>18.36</b>	<b>17.00</b>	<b>15.90</b>	<b>14.99</b>	<b>14.22</b>	<b>11.61</b>	<b>10.06</b>	<b>8.21</b>	<b>7.11</b>	<b>6.36</b>	<b>5.81</b>	<b>5.03</b>

I am always surprised that some GPR users seem to collect data within certain time-window, no matter what the depth of investigation necessary for a study, the velocity of the ground, or the depth of attenuation. Perhaps they are just creatures of habit? Surely with a little bit of thinking about acquisition variables and ground parameters in advance, there could be some prudent modifications of these acquisition settings so that the highest-quality data are collected at the depths needed. I often see results published where half or more of the time-window at the bottom of a reflection profile is only noise, showing that attenuation occurred at a much shallower depth than the operator had determined in advance. As silly as this critique of mine seems, it can be important because some GPR system have acquisition programs that will automatically determine how many samples are deemed necessary to define reflection traces within the time-window chosen. For instance, if a time-window of 100 ns is chosen, the software will determine that a certain number of digital samples are needed within that window to define the traces. But if half of the data are nothing but noise (say the lower half of the time-window) then the important upper 50 ns part of the recorded reflections will only be defined by half of the preset number of samples. This will lower the resolution of those reflections by half also. I have seen the opposite happen where some users have collected reflections over, say, a 30 ns time-window and programmed the acquisition software to use 1024 samples/trace to define the recorded waves. In this case, there are likely too many samples defining each trace and the files are twice the size as they should be, taking it longer to process and view images after returning to the field.

The method described here where an operator thinks through acquisition parameters before data are collected, is one I always recommend. Determining the optimum time-window in advance of data collection can be difficult but is important. Some materials with a high RDP allow radar energy to propagate at slow rates. If that material had a low electrical conductivity (water saturated peat or non-conductive soil) and did not attenuate radar wave propagation, energy could conceivably travel quite deep in the ground but at a very slow velocity. In that case, the time-window would need to be opened further than usual to collect received reflections over a longer time. If an operator were familiar with collecting GPR data in ground with an RDP of 9, a 30-nanosecond time-window would allow the collection of reflections to about 1.5 meters in the ground (Table 4.1), which might be suitable. But if it was later found that because of heavy rains or melting snow, the ground contained more water, and the RDP of the ground was closer to 20, then the radar propagation velocity would be slower, and that time-window would only have allowed collection to about one meter or less depth (Table 4.1). Perhaps the 30 ns time-window would still have been sufficient, but if it was later determined that the features of interest were located between 1 and 1.5 meters in the ground, the whole survey would have to be repeated as the pertinent reflections from the depth of

interest would not be within the programmed time-window. This sad scenario has happened more often than many GPR practitioners would like to admit. It can only be overcome by spending a good deal of attention to local conditions, doing velocity estimates in advance, and adjusting setup parameters for the correct time-window prior to data collection.

Once the time-window is set, the number of samples necessary to record a reflected waveform must be selected. Some systems have software that allows sample density to be individually chosen in set-up parameters, and others have default settings for samples per trace depending on the time-window set. I always prefer to manually set up the samples per trace and never counsel users to use default settings.

One sample is a digital value that record a small portion of the reflected waveform. The more digital samples there are to define a wave, the more accurately that wave is defined digitally. The longer the time-window is open, the larger number of samples that are necessary to adequately define the reflection traces. However, the more samples that are used to define each trace, the larger the digital files become, which can potentially affect speed of post-acquisition data processing and visualization.

Some systems allow for the operator to set any number of samples desired, or choose from standard sampling menus where 512, 1025, or 2048 samples/trace are the options. These become choices based on the resolution of the waves needed or desired. This resolution is a function of both the system sampling rate but also the wavelength of the reflected waves that are generated by the antenna, which is a function of the antenna frequency (Table 3.2). Higher-frequency antennas that generate shorter-wavelength waves may need more digital samples to define recorded waves within a given time-window. The waveform resolution employed with various sampling commands within a given time-window can be viewed on the system computer screen prior to starting collection, which is always appropriate. There are always estimates and assumptions necessary prior to determining these set-up parameters, so some experimentation may be prudent. Collecting some test profiles, moving the antennas to different areas of a grid and then analyzing the reflections collected in these pre-acquisition tests is always helpful.

There are setup commands in many systems that program acquisition parameters to stack or average traces prior to saving data files. Also, some frequencies can be filtered out at the same time, saving the "cleanest" and most representative traces. These are called horizontal filters, or spatial filters (sometimes termed horizontal smoothing). This procedure will stack sequentially recorded traces, or average traces sequentially as they are collected when collecting a profile. I am never in favor of this, as it is often difficult to determine what type or method of horizontal smoothing or stacking to use in the field. Once I made a mistake in Ethiopia on the first day of data collection, where very uneven ground produced by recent plowing was producing variations in en-

ergy coupling and large differences in the quality of reflections recorded along profiles. For some reason I thought it was a good idea to program collection with trace averaging along profiles as they were being collected and saved, which did produce a much more coherent and “nicer-looking” set of reflection profiles. What I had not considered (I blame it on jetlag) was that by doing this kind of horizontal smoothing all the smaller stones in the ground, which would have produced point-source hyperbolas, were filtered out of the saved data. The resulting profiles were certainly “pretty” and lacked many of the coupling change disturbances, but all the features I later determined were necessary to map had been effectively removed before any data were saved. Three days of data collection had to be redone after I discovered what a bad mistake in setups this was. Some of the newer GPR acquisition systems have a way to keep operators from making these kinds of mistakes by saving two or more sets of profiles, one that is raw data with no filtering or averaging, and a second set with whatever acquisition settings were applied prior to collection. This would have bailed me out of this big mistake that caused the total loss of three field days. I should have applied horizontal filters to the data later, if I desired “cleaner” reflection profiles.

Stacking takes a programmed number of sequentially recorded traces and averages them, saving a composite trace. This can be done during collection or afterward during data processing. If the stacking method chosen takes sequential traces (say seven traces are collected with one every three centimeters along a profile), this method will average them and produce one average trace every 21 cm. The result is a reflection profile that contains only the new averaged traces over some distance along a transect. This continues along for the whole profile, averaging traces. Some stacking methods place the new stacked trace in the middle of the trace array, and average those “in front of” and “behind” the new averaged trace. The final product with all these methods is an averaged reflection profile. This type of stacking should not be confused with some recent model GPR systems that employ what is called “hyper-stacking” which is the averaging of many traces all collected at one specific location along a transect very rapidly, and then saving that average trace for just that one location. This produces a much cleaner reflection profile as much background noise and other disturbances are filtered out of the received waves before one composite and averaged trace is recorded.

Trace averaging is much like stacking, but this method takes a “running average” of a programmed number of traces in a profile to smooth the reflections. There are two common types of averaging. Boxcar averaging moves a “box” of a certain width (defined by a number of traces or perhaps distance) through the profile, averaging the traces within that “boxcar” in front and behind each trace in the profile. This will create a smoother, more averaged profile and the number of traces in the profile will remain the same at the end of the operation. The trace averaging values applied for boxcar filtering are always odd numbers, as



this computation is taking a certain number of traces prior to and after the trace in the middle of the “box” to average, placing the resulting averaged trace in the middle. For instance, with a boxcar trace averaging of five, it will average two traces in front and two behind the middle trace and then replaces the middle trace with the averaged trace. This type of averaging then occurs for every trace along a profile and can be programmed to occur during collection, or more prudently, later during data processing. The risk of collecting only averaged data in the field (as I did in the plowed field in Ethiopia) is that reflections that might be of importance are effectively averaged “out” and not collected (Fisher et al. 1992; Grasmueck 1994; Majjala 1992). Other forms of trace averaging work the same way as boxcar but weight traces differently during averaging depending on their distance away from the traces that is recorded. These settings allow for greater weight to be given to the trace in the middle of an averaging “box,” and less for on the traces farther away from the middle.

Horizontal filtering can be a good idea when the ground surface is very uneven or there is highly variable stratigraphy in the subsurface (if that is not of importance to the questions at hand). What I thought was good in Ethiopia turned out to be a huge mistake. I now recommend that unless “real time” analysis is needed in the field it is usually best to collect all the reflection traces available and stack them later during data processing, if it is determined to be necessary. In this way raw and processed reflection profiles can be compared to study how this process changes the visualization products produced in post-acquisition data procedures.

Most of the older-vintage GPR systems generate radar pulses at a rate of more than 120,000 pulses per second (often measured in kilohertz [KHz]). These use incremental sampling methods that produce rapid sequential pulses of electricity on the antennas that generate very rapid sequential waves that propagate into the ground. Each incremental wave is reflected and as these are received back at the surface. The first wave in this sequence of propagating waves records digital sample #1 of the received waves, and the second pulse is used for sample #2 until all the necessary samples to define the waveform within the time-window have been recorded. For instance, if 512 samples are programmed to define recorded waves within a 30 ns time-window the first 512 pulses generated by the transmitting antenna will be used. As these types of systems can generate as many as 120,000 pulses per second, this is more than enough wave generation necessary for this type of collection procedure. If each trace was programmed to be defined by 512 samples and 120,000 sequential waves were being generated every second, then it is possible that 234 traces could be collected each second before the propagation rate is exceeded ( $234 * 512 = 120,000$ ). Without any stacking or averaging of traces along transects and with a programmed interval of one trace every 3 cm along a transect, an antenna could be moved as rapidly as about seven meters every second before the number of transmitted waves was insufficient to record the desired number of

traces. That is very fast data collection—just a little bit slower than Usain Bolt’s world record running speed in the 100 meters of 10.44 meters per second.

Many newer GPR systems avoid the incremental sampling method and instead of digitizing traces within the control system, received waves from the ground within a defined time-window are digitized directly at the antennas with some systems stacking multiple traces in real-time before the resulting average trace is digitized. This happens very rapidly and then the digital values that define the resulting reflection traces are saved. In this way the processing of the recorded traces is being done at the antenna, and only digital data moves along fiberoptic cables to the control system for saving (or in some systems saved in digital media directly at the antennas). Data can be collected faster using this system, and the real-time stacking of traces at every location programmed along a transect will produce reflections that are less cluttered by background noise.

Prior to acquiring reflection data from within the ground another important calibration must be made so that the first reflection recorded is that representing the ground surface (previously I have called this the first wave of the “near field” wave, or perhaps the first wave that moves from the transmitter to the receiver in air). There is some debate as to whether this first wave moves directly from the transmitting to receiving antenna in air, or along the ground-air interface. However it moves, this is recorded and termed the “direct wave.” For most users the top of this wave denotes the ground surface. It is often lagged in the time-window some number of samples or nanoseconds, so that the “straight line” portion of the trace (when no waves are being recorded) can be seen and there is a distinct deflection from that straight line, which is the arrival of the direct wave (Figure 1.1).

This calibration is done at the outset of any survey while the antenna is stable on the ground in the configuration that will be used for all subsequent data acquisition. Some systems do this automatically, and others need to be prompted to adjust for time-zero. This lag in time for the direct-wave within the time-window is then saved in the system so that all recorded traces have the direct wave arrival at the same value and all reflections are placed correctly in time (Yelf 2004).

I always want to make sure this is done correctly so that the ground surface can always be identified in reflection profiles after returning from the field, if there is any question. The time-lag of the first recorded sample in traces for the ground surface reflection is easily compensated for during data processing.

Gains (Figure 3.7) can also be applied prior to data acquisition. Usually this is done only so that reflection profiles of raw data can be viewed immediately as they are being collected, and all reflections of interest are visible immediately. Range gain settings are standard on most GPR equipment, and most systems have software that will automatically adjust waveform amplitudes, so they are “on scale.” The waves as they are recorded are then saved un-gained or with

some systems at a small percentage of the gains that were applied in the acquisition settings. This saving of files procedure is because users often made mistakes in gain settings at the outset of collection and “over gained” reflections, losing the higher amplitude values that were “off scale” and the waves are “clipped” (Figure 1.1). This newer saving procedure allows reflections to be visible on the system computer screen as they are being collected but keeps users out of trouble by saving un-gained files. Gains can be easily reapplied once data analysis begins.

What are termed by some manufacturers as vertical filters remove high- and low-frequency bands of radar waves from recorded reflection traces, which may be generated from system noise or external frequency interference. These can be set prior to collecting data. I am ambivalent about using these filters during acquisition as I am never sure where background noise is coming from and what its frequency might be. Others swear by setting these filters during calibration procedures, and they spend a good deal of time adjusting frequency filters in the field to collect the best data initially. I think that frequency filtering should mostly be applied during post-acquisition processing. In this way all reflections, whether “good” or “bad,” can be later filtered and improved upon.

As an example, a grid of 500 MHz data was collected in southern Arizona in a very “noisy” location near a US Air Force base and in the landing pattern of an international airport. There was radio wave interference that was so severe that I was sure the survey would amount to nothing. I was never able to determine what frequencies caused such noisy profiles. Many attempts to filter different frequencies in the field prior to data collection failed. A large grid of data was collected anyway. After doing data analysis a simple frequency filtering was applied, removing frequencies below 400 MHz and above 600 MHz. When this was done a variety of buried archaeological features became visible (Figure 4.3).

Vertical filters are also called band-pass filters (Bucker et al. 1996; Fisher et al. 1994; Urliksen 1992) and applied in various ways depending on the manufacturer. Old-fashioned terms are still used for these, which have been retained from the first days of radio in the early twentieth century. These filters are still called high-pass and low-pass filters. A high-pass filter allows all the frequencies higher than a desired value to “pass” the filter and therefore be recorded. If that high-pass filter value was set at 200 MHz, then all the frequencies above 200 MHz would be recorded. The opposite is the case for a low-pass filter, which, if set at 800 MHz, would allow frequencies lower than 800 MHz to be recorded.

With any filtering procedure (whether vertical or horizontal), care must be taken not to remove what may be important reflections from within the ground. This can happen if filters are applied only because a data-processing menu recommends that they be applied. Many times, I have been frustrated by not being able to identify the reflections I hope to see due to noisy data, and

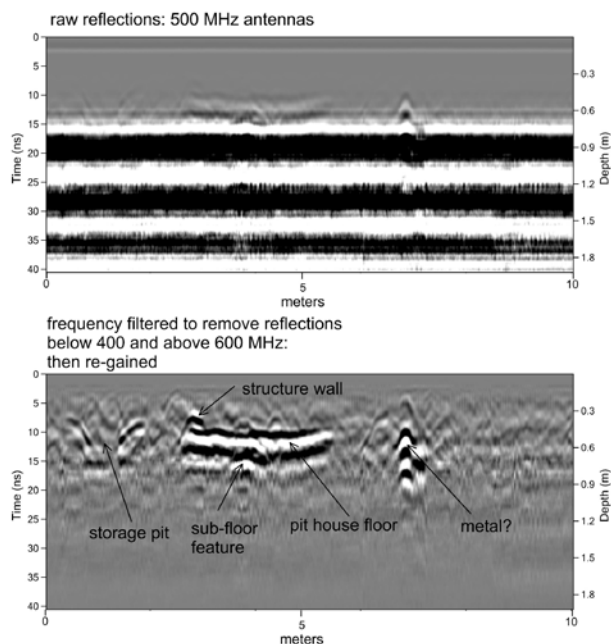


**Figure 4.3.** A 500 MHz reflection profile (top) with abundant background noise, which is removed (bottom) with frequency filtering and regaining the remaining waves.  
*Source:* the author.

then feel compelled to change filters in the field so that I can get immediate results. This has mostly been a mistake, and I often have to remind myself that prudent data processing can clean up data that appears to be worthless in the field (Figure 4.3).

It is important to note that when vertical and horizontal filters are applied in the field many other adjustments will then need to be made such as the time-window, sampling rate, transmit rate, and range gains. Each of these steps modifies the reflections being recorded, and if one is changed it is best to go back to all the other settings and modify those also. This becomes an iterative process and can be laborious at the outset of data collection, but it is time well spent. Once a good set of acquisition settings are obtained some experimental profiles should be collected and analyzed immediately, which may necessitate that different settings need to be applied. Once good reflection data are being acquired at the necessary depths, then these settings must remain the same for all reflection profiles acquired within a grid. The settings can also be saved on the system and recalled for the future—if they were successful. If conditions change, though, it will likely be necessary to modify these settings for later

days' collection, especially if it has rained overnight, making the previous settings inappropriate for the new conditions encountered.

The final pre-acquisition setting that needs to be done is to calibrate the survey wheel for distance, so that all collected traces can be placed into the proper space. This rudimentary procedure should always be done at the beginning of any survey as differences in ground conditions will cause wheels to slip or turn at differing rates. I have been told that some new GPR systems are "preset" for certain wheels or setups. Perhaps that is true, but I always feel good doing my own wheel calibrations just to make sure. It only takes a few minutes.

# 5

## *Velocity Analysis*

As GPR is used primarily to map buried features and related stratigraphy in three dimensions, the conversion of radar travel time to depth is a crucial step in data interpretation. The reflections of interest must be analyzed in depth and geometry as a first step to understanding the origins of those reflections (Conyers 2012). For this an accurate analysis of depth is especially pertinent, especially if the goal is to help define areas of features for future excavation, or to facilitate the avoidance of materials in the ground (Conyers 2010; Conyers and Leckebusch 2010).

Velocity, when estimated, is the crucial factor to convert the travel time of waves to depth. I often remember my grade school teacher lecturing us that distance equals rate times time ( $d=rt$ ). Little did I know how important that rudimentary equation would be for me later in life. For our purposes we can modify that equation just a little, as with GPR it is depth we care about, so instead we can modify this equation as  $\text{depth} = (\text{velocity} * \text{two-way travel time})$ . We measure two-way travel time directly, so all we need is velocity to convert those values to depth.

The initial dataset is always recorded waves whose arrivals are measured in two-way travel time (TWTT). Some systems allow for an initial input of velocity or RDP, so that recorded reflection data are saved in both time and depth. I have over the years adjusted my thinking to work both in both radar wave travel time and approximate depth, and mostly think in terms of TWTT until I can time later in the analysis phase of a project accurately convert those times to accurate depth. Often it is advisable to begin the time to depth conversion analysis as part of the pre-acquisition equipment calibration procedure, even though these estimates will likely need to be refined later so that accurate depths are obtained.

Different GPR people talk about velocity of waves in the ground differently, some using actual velocity measurements (cm/ns) and others use relative dielectric permittivity (RDP), so it can be confusing. Here I will only use RDP, as

it is a good proxy measurement for velocity and avoid any velocity misunderstandings between two-way or one-way time (Figure 3.18).

In the past, a variety of velocity determination methods have been developed. If it is possible, multiple velocity tests should be conducted at different locations in a study area because it is common for the velocity of waves to vary both laterally and with depth. Lateral velocity variations are most commonly caused by changes in water saturation as a function of the material changes. Those could be variations in surface soil types, compaction, vegetation and water-holding capacity near the surface. Or they may be variations in the sediments and soils deeper in the ground, or both of these factors. Water content is usually the single most significant variable that affects radar wave velocity (Conyers 2004; Conyers 2012). If there are only small variations in the retained water anywhere in the ground, wave velocities will decrease quite dramatically. In most settings, the water content of soil and sediment will naturally increase with depth, and therefore the average radar wave velocity of the material will correspondingly decrease if the average is for a thicker portion of the ground than a thinner one closer to the surface.

For instance, a simple calculation of how much variation in velocity there could be laterally between a water-saturated sand that varies in porosity from 30 percent (porosity is filled with water) to 20 percent (also water filled). That is a very subtle change, and one that would be difficult to see if this sand were exposed at the surface and visible to the human eye. The RDP would change from about 26 in the sand with 30 percent porosity to an RDP of about 18 in the 20 percent porosity sand. If there was something of interest in this sand that was perfectly horizontal, its depth would appear to vary in a reflection profile from 96 cm to 116 cm, respectively. That 20 cm difference in depth may not make a huge difference depending on the questions being asked, but it will make the planar reflection in a profile appear to “wiggle.”

An example of this minor variation in RDP, which can cause noticeable variations in the look of a planar reflection is a profile collected in an area where sheep were grazing (Figure 5.1). In this study a shell deposit, which was excavated and known to be almost perfectly horizontal, appears to vary in depth. While I would normally not take the trouble of noting where the grass was trampled in a location due to sheep sleeping there overnight, in this case there were pictures that showed this not-very-interesting phenomena for me to analyze later. It rained just before the GPR reflections were collected the next day. When viewing the profile, there are noticeable “wiggles” in this horizontal surface, which vary only about 8 cm or so, but produce a distorted planar reflection. No analysis was done of the amount of water change in this area, but it is likely that the compacted grass retained just a little more water where the sheep had slept and produced this distortion. That distortion, which produces this minor undulation in a reflection profile is the difference between an RDP of

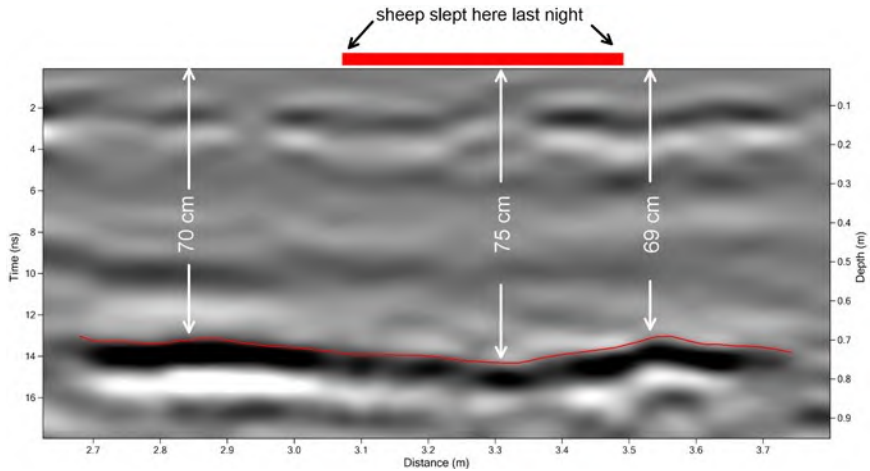


**Figure 5.1.** Very minor variations in the depth of a planar reflection surface due to a very minor change in the ground surface due to compaction where sheep slept the night before. That compaction increased the water retention in that area, increasing the average RDP of the ground from 8 to 8.1, which produced the very subtle change in the depth of a planar reflection. *Source:* the author.

8 and 8.1, a truly insignificant variation in velocity, but which produces a visible change in the reflection.

It can be difficult to explain to non-GPR people why perfectly horizontal features in the ground vary so much when viewed in reflection profiles (Figure 5.1). Everyone wants GPR images to look exactly like they want features to look like if excavated. This is never the case, and this minor change in water shown in Figure 5.1 can produce small variations in images. Often it is impossible to know what causes these “distortions,” as it is rare for anyone to spend the time necessary to calculate all velocity variations that occur in a grid of data both horizontally or with depth. It is best to answer queries about why GPR images are “distorted” with a general explanation, which is variations in water, and leave it at that. These distortions are even more apparent when displayed in a profile that is exaggerated in the vertical, which is common procedure with most software programs. When these “wiggles” in a horizontal layer are viewed in standard reflection profile software, the vertical exaggerations that are usually applied will accentuate them even more. Figure 5.1 was exaggerated about 2:1 in the vertical. At 10:1 exaggeration these types of velocity-difference distortions may look like mountains and valleys. For a report destined for an audience that doesn’t have the GPR knowledge or the interest to understand why these variations happen it might be better to produce profile images with no exaggeration (1:1) and hope for the best.



It is also important to recognize that velocity measurements at a site are often valid only for GPR data that are collected within a few days (or sometimes a few hours) of when the velocity tests were performed. Changes water saturation can vary dramatically over months with seasonal rainfall variations, or even daily with rainfall, snowmelt, or flooding. For example, velocity tests performed at a site in Central America, consisting of mostly volcanic ash, during the rainy season yielded an RDP of 12 (Doolittle and Miller 1992), while similar tests performed in the same area at the end of a six-month dry season measured an RDP of about five (Conyers 1995; Conyers and Lucius 1996). The same kind of dramatic changes have also been seen overnight. In the American Southwest, good radar reflections were obtained one day from depths approaching two meters with a 500 MHz antenna. Overnight, three inches of rain fell, and the next day, poor reflections from a maximum depth of only fifty centimeters were recorded, with a completely different calculated RDP (Conyers and Cameron 1998). In this case, the addition of water changed not only the velocity of radar propagation but also the depth of radar energy penetration in the ground due to changes in the attenuation of waves due to a larger electrical conductivity of the wet clay with the addition of water.

## **DIRECT VELOCITY MEASUREMENTS**

In the early days of GPR, before there was software for hyperbola-fitting, the most accurate way to determine velocity was with direct measurements in the field. Depth (or distance) to buried interfaces or features of interest was directly measured using a measuring tape in an open excavation or outcrop or by probing or coring. Layers in the ground that were visible were then measured and if reflections that “seemed to” have been generated from those layers could be identified and measured in time, then a velocity of wave propagation in the ground was calculated.

Many early GPR users used direct measurement of objects in the ground on objects as diverse as buried whale bones (Vaughan 1986), copper wire (Kenyon 1977), and empty paint cans (Doolittle and Miller 1992). Because metal is a near-perfect radar energy reflector, the reflections generated in a profile crossing a metal object are easily identifiable on most GPR profiles (Figure 3.4). Other tests of a similar sort can be performed when a buried wall or some other point source reflection feature is partially exposed in an excavation and can be identified in GPR profiles (Conyers and Lucius 1996). In a similar way, identifying a distinctive reflection generated from a noticeable material change in the ground, and then coring or excavating a test trench to expose it, or viewing it in a nearby outcrop will serve the same purpose if the exact reflection surface can be positively identified. This was done where a compact clay house floor and an associated charcoal-rich living surface was exposed by wave action along the Oregon coast (Figure 5.2). These archaeological and geological interfaces could be mapped laterally, and the reflections generated from both immediately

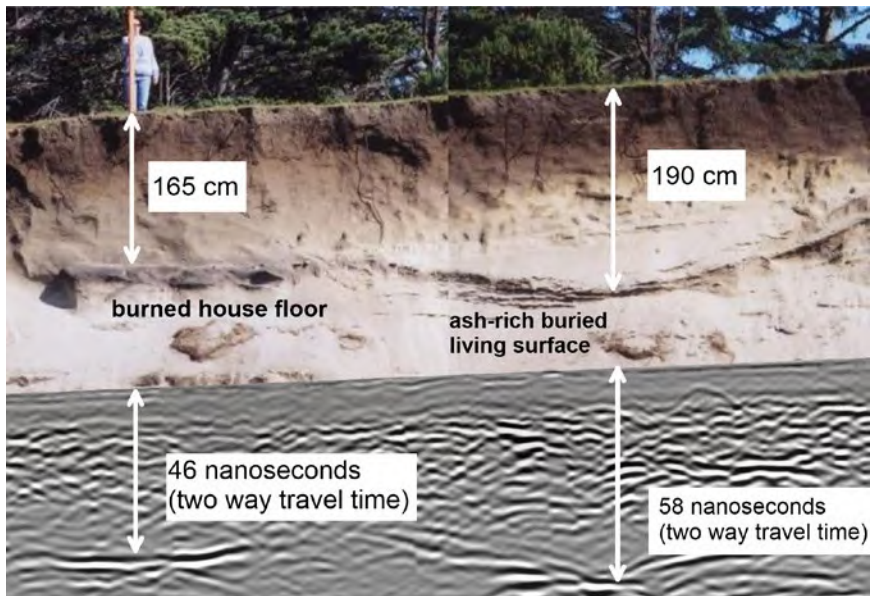


**Figure 5.2.** Direct comparisons of reflections visible in a reflection profile to visible units in an outcrop. These can be used to directly measure velocity and obtain average RDP values. *Source:* the author.

visible in a GPR profile collected on top of the preserved material. The depth of these interfaces was measured, and the elapsed time used to calculate velocity.

The easiest and most accurate method for determining velocity is to perform “direct tests” where an iron bar or some other reflective object is inserted horizontally in a vertical face. Antennas are then slowly pulled over the object while subsurface reflections are recorded in a profile. A metal bar will be apparent as a distinct reflection hyperbola, such as those displayed from buried reinforcing bars in Figure 3.35. To obtain the maximum amount of reflection from a thin metal bar, the long axis of the surface antennas (from side to side) must be oriented parallel to the length of the horizontal bar. This antenna orientation will create an electric field that is also oriented parallel to the bar, producing the maximum amount of reflection. Also, when doing these types of tests, the correct antenna frequency suitable for the depth and object size that needs to be illuminated must be used. If a low-frequency antenna is used, a large metal target may be necessary for it to be visible on standard two-dimensional profiles, because of this antenna’s lesser resolution. I often collect reflection traces in these types of tests that are 1 cm or so apart so that the relatively small reflections from the metal object will be more visible over more traces in a profile. When reflection profiles are visible on the computer screen during data collection, and if a time scale is superimposed on the profile,

the apex of the hyperbola can be measured in time and the depth of the metal can be directly measured. Time and depth will then yield velocity, which can be immediately used to calculate the time-window for the depth necessary to resolve features of interest. If the iron bar is not visible, the profile may have to be processed later to increase the visibility of the target, using data-filtering and enhancement methods. These types of tests are almost always successful, if there is enough time to perform them. However, I once collected velocity data of this sort in Texas in ground that was locally referred to as “gumbo clay.” This amazingly electrically conductive clay attenuated all radar waves as soon as they were transmitted, and I could not see a large piece of metal only 10 cm below the ground surface. This spot is in my “top five” worst places in the world for GPR.

Another type of mistake that is common with using direct methods for velocity tests can be choosing the wrong place to conduct direct tests (Conyers 2012). This occurred to me in a desert area in Jordan where wind-blown sand was the covering material at the site. We performed numerous direct-wave tests on an iron bar at different depths along that exposed exposure of this sand and velocities were found to be consistently very high throughout the section, with an RDP calculated at about 3. A large grid of reflection data was then acquired adjacent to this area and all reflections in the grid were corrected using that velocity value. Those depths were then used to place buried features and stratigraphic interfaces of interest into estimated depth. When these features were quickly excavated, it was found that all mapped features were almost twice as shallow than predicted in the GPR maps. After evaluating what could have gone wrong, it was concluded that the sand in the exposure where the velocity tests were performed had been allowed to dry out significantly along the excavation face, creating an anomalously dry material that allowed radar waves to travel at a very high velocity (RDP=3). The same material that remained buried (where the GPR data were collected) retained its natural moisture and had an RDP closer to 10. This erroneous velocity collected in the dried-out exposure was applied to all the reflection data. A later analysis of correct depths of the excavated features (and more robust velocity calculations from many hyperbolas) showed that the RDP of 3 in the dry exposure that was used to calculate depth indicated features of interest were 2.8 meters deep. The more accurate RDP of 10, if it has been used, would have shown these features to be only 1.4 meters deep, which was what they were found to be when excavated.

This simple, but potentially disastrous, mistake immediately called into question the capability of us conducting the survey, as the features were uncovered while we were still present in the field (Conyers et al. 2002). Fortunately, excavations were carried out immediately and we could explain what happened, and with a little bit of re-analysis all who were involved understood (or were made to understand) the potential velocity pitfalls. All maps and profiles were quickly adjusted, and this little mistake was forgotten by all concerned,

except me. I shudder to think what might have happened if the excavations had occurred weeks later when I was not there to recalculate these simple time-depth conversions. If that had happened the impression of the participants might have called GPR into question. These direct velocity tests on the iron bar should have been conducted in newly excavated trenches, not the older exposures where the sediment had been allowed to dry out. There were also plenty of point-source reflections visible in the reflection profiles and hyperbola-fitting tests could have easily been done to find the mistakes with the metal bar tests.

## **CMP AND WARR TESTS**

In the early days of GPR, with systems that could separate the transmitting and receiving antennas, tests were performed that transmitted energy one-way between antennas placed at various separations on the ground surface. In this method, one antenna transmits to the other at measured separation distances, and the one-way transmit time between the two is measured (Conyers and Lucius 1996). One type of this velocity test is called common midpoint (CMP) (Fisher et al. 1994; Leckebusch 2003; Malagodi et al. 1994; Neal 2004; Perroud and Tygel 2005; Tillard and Dubois 1995), and a similar one is termed wide-angle refraction and reflection (WARR) (Imai et al. 1987; Milligan and Atkin 1993; Reynolds 2011). A third variation on this method is called transillumination, based on the same general method where radar waves are transmitted in a one-way direction between two antennas that are separated by the material to be tested.

In all these types of tests, a GPR system that allows two antennas to be separated is necessary, or a system with more than one channel, where one channel controls the transmission of energy by one antenna, and a second channel controls its reception at a second antenna (Figure 5.3). As many GPR systems use antennas that are permanently attached in a housing, this method can be more complicated, and two channels are needed, or a cable splitter, with one antenna used to transmit and one to receive. A few GPR manufacturers produce dual antennas that are clipped together and can be easily separated but even here two cables for the two antennas must be used to separate them (Figure 5.3). I have used the cable splitter method with two different frequency antennas (500 and 900 MHz), but I no longer perform these tests as there are other methods that are easier to perform and have fewer equipment constraints.

Antenna array systems that have multiple antennas next to each other and will always transmit and receive waves at known separation distances can be programmed to collect CMP data rapidly. When employed in this way, variations in velocity across a large grid of data can also be quickly determined, and spatial maps of velocity variations produced.

In both WARR and CMP tests, radar waves are sent from one antenna to the other as they are moved an increasing distance apart in steps. Individual reflection traces are usually collected every interval (and traces often stacked



**Figure 5.3.** Collecting CMP data where the transmitting and receiving antenna are moved apart in steps, with one trace collected every distance of separation. *Source: the author.*

to improve their quality). The radar waves moving between the antennas as they are separated will propagate in the air, along the ground and reflected (or refracted) in layers in the ground, with all these waves received and recorded at the other antenna (Figure 5.4). It is also possible that many other waves will travel into the ground and travel in other pathways to be recorded. The distance of antenna separation is known for each trace collected and the arriving waves can be measured in time, allowing for velocity calculations. The greatest problem with these types of tests is that the pathways that waves take in the ground are unknowable. Are the waves going deeply into the ground to be reflected and refracted in complex ways, or are they traveling a more direct route? This inability to know wave travel paths in the ground makes these types of tests prone to errors and their velocity results must be assumed to be average near-surface velocities.

Reflection traces are collected in the same way in the WARR method, except only one antenna is moved while the other remains stable. Sometimes WARR tests must be performed instead of CMP tests if there are not enough people in the field at the time of the test to move both the antennas simultaneously. In both CMP and WARR tests there could be subsurface layers that reflect and transmit energy which are not horizontal (Reynolds 2011). When this is the case radar waves move in unpredictable ways between the two antennas.

Common midpoint and WARR results are typically displayed as a standard GPR reflection profile, with the antenna separation distance on the horizontal axis and time on the vertical axis (Figure 5.5). As the antennas are moved apart, the first wave received is the air wave. Ideally it is recorded at time zero when the distance of antenna separation is zero, or the zero offset (due to the distance in air between the transmitting and receiving antenna) can be later

considered during data processing. The second-wave arrival is usually the ground wave that travels along the ground-air interface and is recorded soon after the air wave. The third, and all subsequent arrivals, are usually reflected or refracted waves generated at subsurface interfaces.

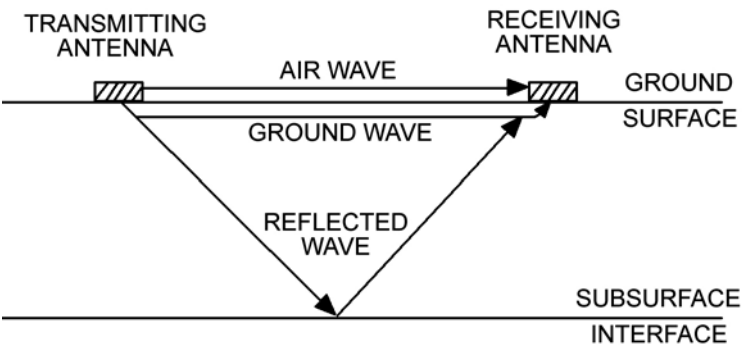


**Figure 5.4.** Various ray pathways in a CMP test with the first arrival waves transmitted in air from the transmitting to the receiving antenna. The second arrival is usually a ground wave, and all subsequent waves are reflections or refractions or a combination of both from buried interfaces. *Source: the author.*

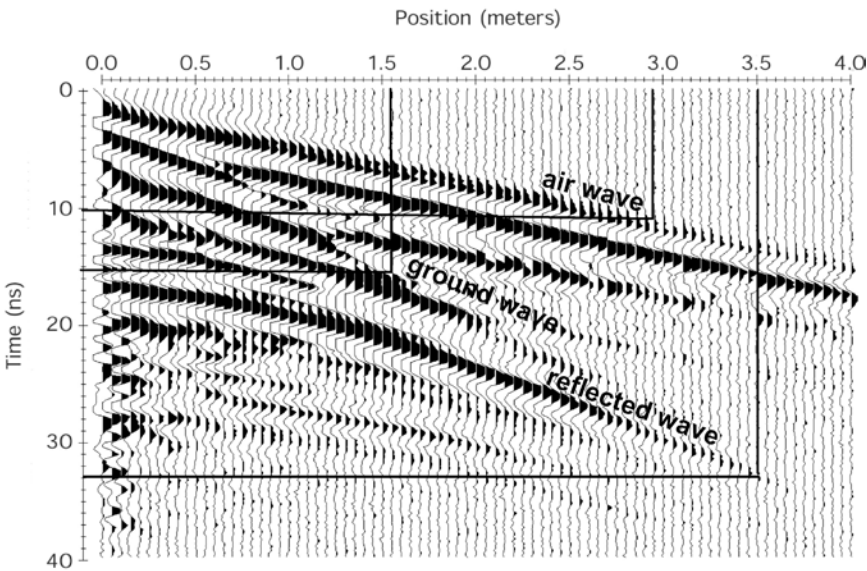


**Figure 5.5.** Results of a CMP test showing distance and travel times of traces, which denote the air wave, ground wave, and one reflected wave. *Source: the author.*

In areas with shallow water tables, it may be possible to distinguish between what are referred to as “dry” ground waves and those that are “wet” and that may be traveling within saturated ground near the surface (Fisher et al. 1994). The ground wave should also intersect the air wave at time zero on the portion of the radar profile where the two antennas were touching (Figure 5.4). Other radar waves that traveled deeper within the ground can be refracted within soil and stratigraphic units and sometimes reflected between subsurface layers before arriving at the receiving antenna, creating what can potentially be a confusing series of recorded wave arrivals. These subsequent arrivals can be differentiated from ground or air waves because they do not intersect at time zero when the two antennas were touching.

Many modifications of CMP tests can be made with multiple antennas in arrays, or perhaps just two antennas moved apart in steps within a small area. These calculations produce accurate volumes of reflection data that show lateral changes in velocity (Perroud and Tygel 2005; Pipan et al. 2001; Pipan et al. 1999). Thousands of traces can be collected in this way at multiple antenna spacings and excellent near-surface velocity variations can be mapped.

## **TRANSILLUMINATION TESTS**

The transillumination method is another direct-wave velocity test that is applicable to a few settings where there are nearby excavations separated by material that is to be tested. This type of test was originally developed as a method for evaluating the integrity of intact structures for both engineering and archaeological applications and is still used in the construction and building industries (Cardno 2019; Conyers and Lucius 1996; Bernabini et al. 1994). The two faces of material must not be too far apart, or transmitted waves will attenuate as they travel between them. It is also best if tests are performed soon after the material is exposed in the excavations so that any evaporation or seepage of water along the faces does not significantly change the water saturation characteristics of the material to be tested.

Two antennas, one to send and the other to receive, are then placed on the walls of the two excavations, pointing toward one another (Figure 5.6). It is important that the two excavations be separated by at least one wavelength or so of the center frequency of the antenna being used to transmit so the receiving antenna is beyond the near-field zone of the transmitting antenna.

Care must be taken to keep the antennas separated a known distance and a known height from the base of the excavation as they are move so that distance can be calculated (in this kind of test the distance is horizontal distance separating the antennas). If the walls of the excavation are sloping, then a series of distance measurements could be made to arrive at the antenna separations for each of the steps where data are collected.



**Figure 5.6.** Collecting transillumination data with one receiving on a vertical face of volcanic ash at Ceren, El Salvador. The transmitting antenna is on a parallel exposure off camera to the left. *Source:* the author.

When the material to be tested in this way is highly stratified, it is important that the electric field generated by the dipole antenna be oriented parallel to the bedding planes. To do this, the long axes (from side to side) of the antennas must be placed parallel to the bedding planes. In this way most of the electrical portion of the electromagnetic field will vibrate parallel to the bedding layers and there will be maximum isolation of the radar beam within each stratigraphic unit (Conyers and Lucius 1996). The cone of illumination of the radar antenna may, however, still transmit radar energy into adjacent layers regardless of the orientation of the antennas, and, as always with these types of tests, wave pathways are difficult to predict or define.

In one transillumination test of this sort, two excavations exposed a thick section of volcanic ash (Conyers and Lucius 1996). Eight different ash units were identified on the faces of the excavations, and reflection traces were collected at each bed in seven steps, from the base of the excavation upward. A 300 MHz antenna was put on one side of the exposure to transmit and a 500 MHz on the other to receive using a multi-channel control system. An analysis of the travel times at each step showed that velocity increased from about 6 centimeters per nanosecond at the base (RDP of 23.2) to 28 centimeters per



nanosecond (an RDP of 1.1) at the top (Figure 5.7). The two velocity measurements at the top of the exposure were probably not measuring radar wave travel in the ground, as those recorded waves probably traveled in air over the top of the excavation between the two antennas, producing the RDP calculation of 1.1, which is almost that of the velocity of radar waves in air.

The identification of the “leaked” air waves that traveled between the two excavations illustrates the importance of using fairly deep excavations when conducting transillumination tests. If tests are conducted too close to a pathway in air, radar waves will travel over the top or around the material to be tested, and the first arrivals may be only air waves. It is also critical that accurate distances between antennas at all positions be obtained so that air wave calculations can be made, and their arrival times calculated in advance and then identified.

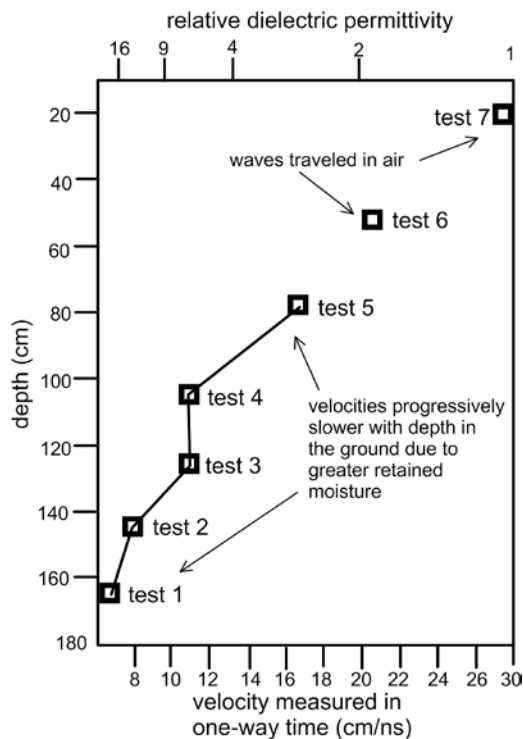


**Figure 5.7.** Results of a transillumination test displaying depth compared to the velocity and RDP of various units of volcanic ash that vary with depth due to increased water retention. *Source:* the author.

Knowing the horizontal separation of the antennas and the one-way travel time of the radar energy between the two antennas at each step, velocities can be calculated, and RDP determined, using Equation 3.1. When the velocity measurements at each of the seven steps as shown in Figure 5.7 were plotted against the depth of the antennas, a velocity gradient graph was constructed. Velocity information derived from transillumination tests can be of importance because it identifies velocity variations as a function of depth and sediment layer, which is not usually possible in other methods. In the graph in Figure 5.7, the velocity increases at a constant rate with depth, probably indicating gradually increasing residual water saturation, which was also visible as minor color changes in the exposed section of materials tested. The minor change in the velocity gradient at 100 centimeters depth may indicate a change in velocity between layers of different composition or porosity and therefore differing water saturations.

In all these types of tests, radar waves will tend to travel preferentially within the highest-velocity material, and the time of the first arrival being used to calculate the velocity may be from the waves that traveled in the “fastest” material, not necessarily those waves that moved within the material from the depth at which the antennas are placed. Any wave arrivals that traveled through the lower-velocity layer would then be overwhelmed, obscured, or otherwise unrecognizable in the recorded traces.

## **LABORATORY MEASUREMENTS OF RDP**

At most sites, samples of subsurface units can be collected for later processing in the laboratory to determine relative dielectric permittivity, electrical conductivity, and magnetic permeability (Shamir et al. 2018; Van Dam et al. 2013). This is almost never done outside of academic settings by practitioners with plenty of time on their hands. These measurements can then be used to estimate velocity and energy attenuation for materials at a site. They are also valuable when constructing two-dimensional computer models. If soil and sediment samples are collected and immediately stored in watertight containers, they can be considered as approximating field conditions. In reality, however, samples that are stored and transported in plastic bags or bottles will never replicate field conditions as their porosity, grain packing, and water saturation will all change somewhat in the process of gathering and transporting them (Comegna et al. 2019; Kargas and Soulis 2019).

Unfortunately, only a few devices can make these types of laboratory measurements, none of which are readily available to most GPR researchers. They are usually used by soil scientists or for people measuring the water content of spoil or agricultural products. One way of determining the magnetic and electrical properties in the lab is by using techniques described by Olhoef and Capron (1993) and Saarenketo (1998). In these tests, samples are first dried and crushed and then subjected to differing frequencies of electromagnetic

energy in a device called a network analyzer (Conyers 2004). Measurements of RDP, conductivity, and magnetic permeability can be made when the samples are totally dry and at differing water saturations. Water saturation changes that might be found in the field can be simulated by progressively wetting the samples with water from a dropper between tests, allowing time for the water to adequately penetrate the material.

A laboratory test of this sort was conducted on a clay soil from central Illinois (Conyers 2004). The sample was first desiccated in an oven to remove all residual water. Its RDP was then measured at many frequencies ranging from 10 to 1,200 MHz (Figure 5.8). The frequency-dependence of these measurements was accounted for somewhat as only the RDP values that were within the frequency range of most GPR antennas (200 to 1,000 MHz were used). At high frequencies, some electromagnetic energy is lost in the atomic structure of the materials due to displacement currents, caused by small perturbations within the orbits of electrons. At low frequencies, ions in the material cannot respond fast enough to the imposed electromagnetic field, and there is greater ionic conductivity, and therefore higher RDP values are measured.

Frequency variations aside, what is most remarkable about the test shown in Figure 5.8 is how sensitive the samples were to the addition of water. When only 0.5 cubic centimeters of distilled water was added to the total sediment

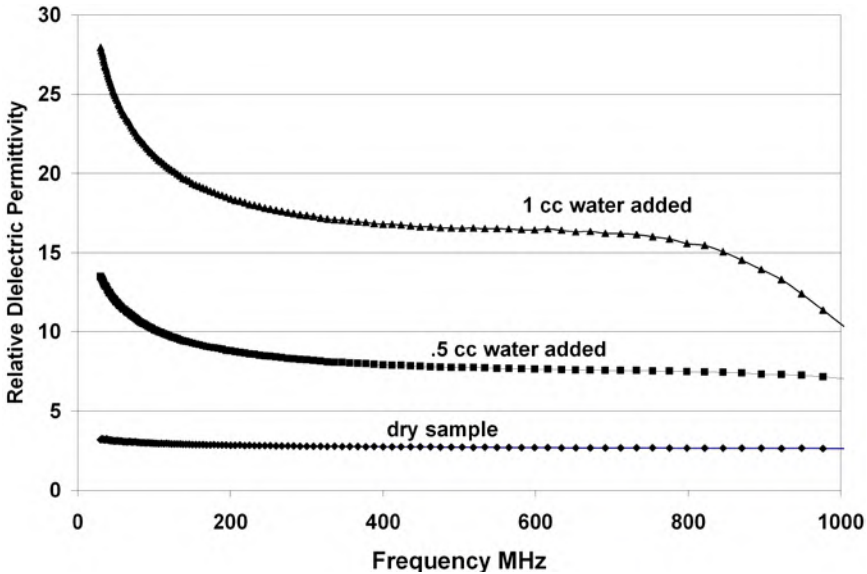


**Figure 5.8.** Laboratory tests of a soil sample showing some variations in RDP at high and low frequencies, but mostly uniform over the usual GPR antenna frequencies. A small addition of water to the sample raises the RDP dramatically. *Source:* the author.

sample of 13 cubic centimeters, the RDP increased from 3 to about 8. And with an additional 0.5 cubic centimeters of water added it increased to about 17. This test once again dramatically illustrates how important the addition of a small amount of water is to the velocity of radar travel, and therefore RDP of the material in the ground (Conyers 2012).

This is one of many tests that were made this way of soils and sediments from many different areas of the world. It was interesting that almost all these ground materials, when desiccated and tested, had RDP ranging from about 3 to 4.

An interesting approach to laboratory measurements was taken by Sternberg and McGill (1995) in Arizona. At their sites, samples were taken of subsurface sediment units, which were analyzed for their particle size, mineralogical constituents, and water saturation. Without having to rely on laboratory measurements of RDP and electrical conductivity, they compared their mixtures consisting of sand, clay, and water to published tables of RDP and other measurements for those materials (Olhoeft 1986) in a simplistic and marginally effective way. Relative dielectric permittivity and velocity were then estimated for their unique field conditions, and radar times were converted to approximate depth, with what were good results for the day (1995). When these tests were performed there were few good ways to measure velocity in the field, so this approach was adequate. Occasionally, I see a paper submitted to a journal with GPR results that claim to arrive at radar wave velocities using published RDP values for similar materials to their own. Surely, we have moved beyond those methods for determining velocity.

## **ANALYSIS OF POINT-SOURCE REFLECTION HYPERBOLAS**

Almost all GPR users now use the geometric displays of hyperbolic reflections generated from point-sources in the ground such as pipes, walls, rocks, or small void spaces (Figure 3.24). How steeply the axes of hyperbolas dip from their apex is a function of the average velocity of the material through which the radar energy passes moving to and from the surface antennas to the reflection source (Leckebusch 2000; Lucius and Powers 2002; Martinaud et al. 2004; Pannigau et al. 2004; Tillard and Dubois 1995). As most acquisition systems place reflections accurately in distance along transects, that measurement becomes the distance used for velocity calculations, and the travel times to and from the point source in the ground becomes the time. The geometry of the resulting hyperbola will then measure velocity at multiple locations as many radar waves move at many angles to and from the surface antenna within a conical envelope of energy transmission. Some systems have the ability to identify hyperbolas immediately during collection and acquire velocity data from them while still collecting data (Mertens et al. 2015).

Reflection profiles that contain hyperbolas are then displayed in profile and a computer-generated hyperbola is “fit” to the hyperbolas generated in the

ground, and its dimensions are calculated (Figure 5.9). As time and distance are measured the average velocity from the ground surface to the point source can be calculated using simple trigonometric functions.

When doing hyperbola fitting to arrive at RDP it is important to make a note of what depth within the time-window individual velocities were calculated. For instance, if many hyperbolas were analyzed in the top 10 ns of the time-window and their RDPs averaged this would be an accurate value for converting depths of features but only those that are within that depth from the surface. If hyperbolas are chosen for testing that are in the 20 to 30 ns part of the time-window, they will likely have RDP values that are on average higher. Those values need to be used to convert time to depth for buried features within that depth range. All RDPs are measuring velocity that is an average velocity from the surface to the point-source used.

A GPR survey that generates many hyperbolas in reflection profiles can be readily used to evaluate velocity with both depth and throughout a grid without having to resort to any of the other more complicated methods discussed above. Some software will take multiple velocity measurements in a grid and

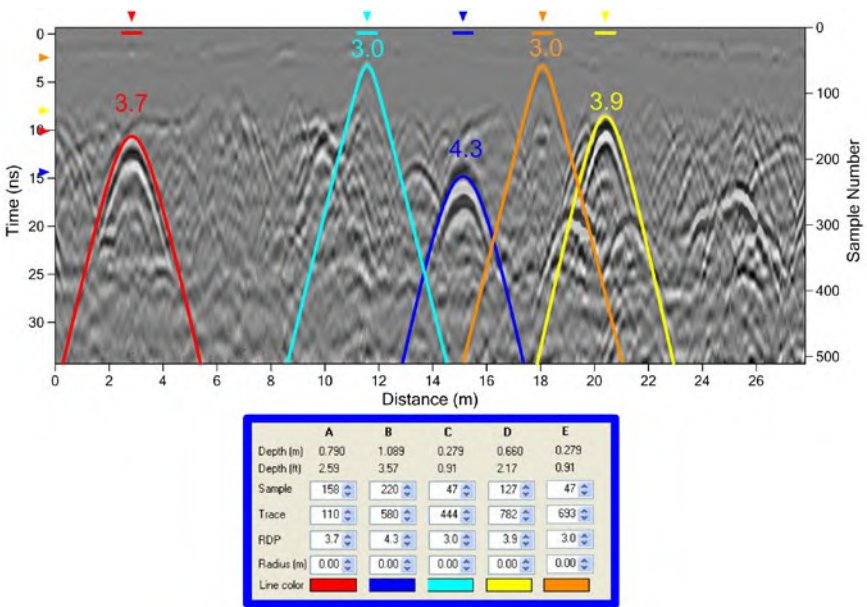


**Figure 5.9.** Hyperbolas used to determine velocities in one profile. RDP increases with depth, as is expected in most ground, and the shapes of the hyperbolas also change. *Source:* the author.

produce three-dimensional velocity distribution data. In this way all reflections measured in time and with spatial locations can be converted to depth for very accurate 3-D images. Without this kind of a detailed analysis, which I have only rarely performed, most of the rest of us will use some average RDP values from shallow, medium and deeper depths, and perhaps some general velocity trends laterally. We then convert TWTT to depth when it is necessary, depending on the images that are being interpreted at the time.



# 6

## *Post-Acquisition Data Processing*

Many software programs and other instructions that are common with GPR users have a list of recommended data processing steps that should be followed to produce “the best” images from recorded reflections. In some GPR circles these steps are considered mandatory, and sometimes little thought is given as to why certain steps are being done, or any consideration of variations on these recommended procedures that might be appropriate or not for a certain dataset, ground conditions or research questions.

I once hosted a visiting scholar who wanted to spend some time with my graduate students and me working with GPR. On our very first day together, this visitor told all of us that we were moving too slowly by thinking through processing steps we were considering. When I asked why we needed to bypass individual processing methods and think them through, the answer was, “Because my group has been told we must follow these steps to produce the best images.” No reason for why these steps were being done or for what they were doing was given. This relationship was a little fraught from then on.

I always recommend that analysis after returning from the field begin with reflection profiles, which can be viewed and analyzed for what reflections are most visible, and then for performing velocity tests on hyperbolas. These raw profiles on initial assessment will usually display reflections that are obscured by what interpreters sometimes refer to as “noise,” “reverberations,” “interference,” “multiples,” “clutter,” “spikes,” and “snow.” All those visual features of raw reflection data will make them difficult to initially interpret. One of the first tasks is to view reflection profiles on the computer screen and adjust depth or horizontal scales while re-gaining so that all reflections within the time-window can be seen (Figure 6.1). Time zero can be set so that depth can be corrected, and the vertical exaggeration adjusted so that profiles are more realistically representing the ground. This can be followed by another quick task to remove background noise. The depth of attenuation can be determined, and if there is a maximum depth of coherent recorded reflections, all reflection data below that depth can be cropped out or ignored in initial interpretation steps. Those initial



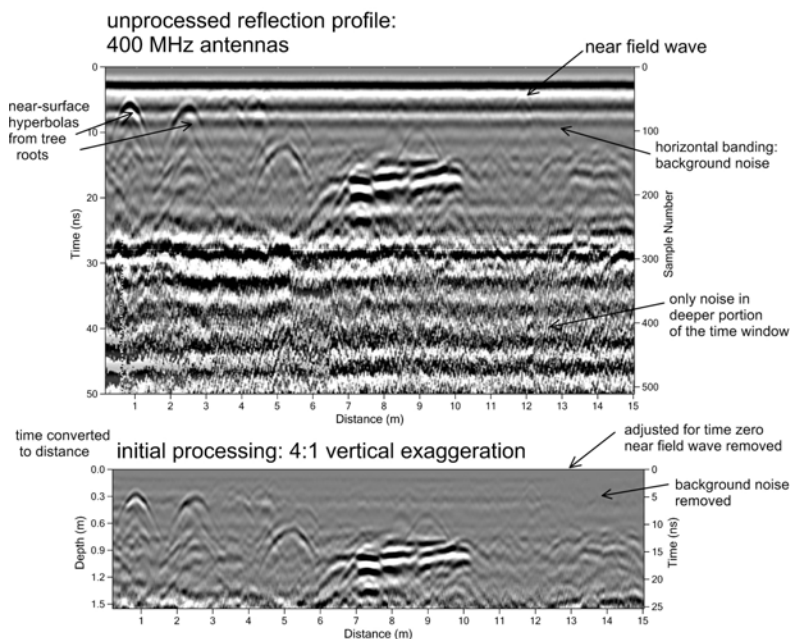


**Figure 6.1.** Basic processing steps on one profile. The background is removed, the scales are adjusted to view the profile in a more realistic display, and radar wave travel times are converted to depth. *Source:* the author.

processes will go a long way to allowing for some initial analyses of results and will not alter the raw data files whatsoever as these processes can take place just on the computer screen. I often make many notes of what is visible in profiles and start to develop some hypotheses about what a grid of profiles holds, so that these ideas can be elaborated on for the next steps in processing.

There are many commercial, proprietary, and a few free GPR processing programs available for all types of data processing. Many of the GPR processing techniques included in these programs were originally borrowed and then modified from software used in the petroleum industry, which processes seismic reflection data, or other remote sensing applications that deal with complex image processing (Hatton et al. 1986; Jeng 2009; Leucci et al. 2012; Malagodi et al. 1996; Milligan and Atkin 1993; Sheriff and Geldart 1985; Udphuay et al. 2010; Ulriksen 1992; Yilmaz 2001). To perform all the steps listed in this chapter, the original data must either have been recorded digitally or be analog data that have been digitized.

My advice is to never use the processing steps that follow “off the shelf” tasks and then perform them in some recommended order without understanding the implications of each technique. The basics shown in Figure 6.1 are

mostly harmless, but all steps that follow can alter the original data in ways that need to be understood. All more advanced processing techniques were constructed for very specific objectives, and some or even all, may not be applicable to ground conditions or a survey's objectives. There is nothing worse than trying some techniques in the software in the hope that a final product will "look better" (Conyers 2012).

A list of the common data processing techniques that can potentially be used for GPR data and their objectives is found in Table 6.1. There are many other published recommendations for processing steps, many of them taken from seismic procedures (Goodman and Piro 2013; Neal 200; Ovenden 1994).

I have read a good deal of literature on various GPR-processing steps that are possible in some software packages and have concluded that there are a few that are very useful for basic interpretation procedures, but there are many I just don't understand. I have asked very smart GPR people who work with software for a living to explain some of the more advanced steps to me, and the conversation usually degenerates quickly to "this seems to work for me" or "this can clean up the data." I am therefore hesitant to experiment with complex waveform processing procedures, especially when they were transferred to GPR from seismic wave processing software. This is especially true when I am unsure exactly what I am doing, or how to interpret the final product, especially when presumably smart people can't tell me exactly what some step is doing to the data.

**Table 6.1. Post acquisition processing objectives and methods**

<i>Processing objective</i>	<i>Methods to be used</i>
Correct vertical and horizontal scales in reflection profiles; average or smooth reflections along transects	Standard "rubber sheeting"; distance normalization and vertical exaggeration commands; trace stacking
Remove horizontal banding system noise and frequency interference	Background removal; vertical high pass filters
Remove high frequency noise ("snow")	Low pass frequency filters; F-k filters
Remove multiple reflections	Deconvolution
Remove and compress point source hyperbolas to their sources; correct the orientation of steeply dipping layers	Migration
Change resolution of reflections of different size and depth	Frequency filtering
Increase the visibility of subtle or low amplitude reflections	Range gaining; Hilbert Transform

## MORE ON INITIAL PROCESSING STEPS

The background removal method varies depending on software. The basic concept is that reflections that are recorded at the same time within a time-window and appear throughout a profile are likely to have been generated from an external source. Those reflections may vary in amplitude, but they vary little in their recorded time. A simple procedure is to digitally produce a composite trace that includes all the waves that occur at the same time through the profile, or in some programs, a given number of consecutive traces. This constructed composite trace (the background trace) of waves are then removed digitally from the waves recorded in every trace in the profile. This will produce a reflection profile that contains only the reflections recorded hopefully from within the ground, which usually vary somewhat in the TWTT they were recorded. The risk with this step is if there is a horizon that just happens to have generated a perfectly horizontal planar reflection, it will become part of the composite trace that is removed, and the “real” reflection feature will be removed also. I have heard several people warn of this possibility but have yet to see a good example. Even subtly undulating planar reflections that are the product of extremely small velocity changes would not be removed in this process (Figure 5.1). That doesn’t mean we shouldn’t be wary of this possibility and watch out for it. I don’t worry about it and always remove background when viewing profiles during the initial stages of processing (Figure 6.1). The background waves can always be quickly restored later if something “real” has been removed.

Many software manuals commonly suggest that background be removed before producing horizontal amplitude slice-maps. I have also found this to be unnecessary, as by definition, background waves will all be recorded at about same amplitudes and occur at the same recorded time, so in the process of producing amplitude slice-maps the background waves will be effectively filtered out as these types of maps are producing images of what is “different” in the slices programmed and assigning different colors to different amplitudes. Only the differences in amplitudes are being plotted in this way so the similar background waves that are included in the reflection profiles will not be included in these maps. This would not be the case if more complicated amplitude images are produced during data processing, for instance with images that cutting through many different horizontal layers recorded at varying times in a three-dimensional package of waves. So, with that said, it does little harm to remove background as an initial step in data processing in preparation for amplitude slice-map production to produce a “cleaner” set of reflection data.

A few interpreters of GPR profiles prefer “wiggle trace” format, which displays the individual traces and their amplitudes (Figure 6.2 upper image). Those who favor these kinds of displays have usually migrated to GPR from the seismic world, where this display is common. I prefer the amplitudes of reflections to be merged horizontally and averaged a little to generate continuous

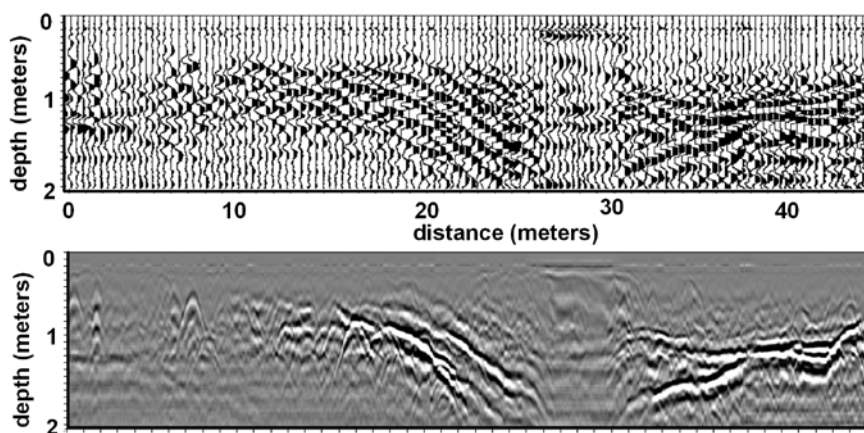


**Figure 6.2.** Two different displays of recorded reflections in a profile. The upper “wiggly trace” display shows all traces and the waves and amplitudes while the lower profile has merged the reflections and performed a minor amount of averaging along the profile to produce a more coherent display of reflections instead of the individual waves. *Source:* the author.

reflections. This produces an easier to interpret reflection profile (Figure 6.2 lower image). I also have grown accustomed to reflection profiles displayed with a gray scale where the amplitudes vary in shades of gray (Figure 6.2). This will produce individual wave deflections that are both white and black (and shades of gray between these end points) with the white being an initial part of the sine-wave deflection in one phase from the mean and black the other deflection. Those two phases of the wave, which produce a sine-wave of one wavelength, make up one wavelet produced from a reflection from one interface in the ground. Whether the initial deflection is in a positive or negative direction depends on the way antennas are constructed and whether the velocity change that created the reflection was from high to low velocity, or vice versa.

Besides adjusting for time-zero, perhaps axes for depth after velocities have been calculated, removing background and re-gaining, most interpreters do not venture to more complicated steps. These first minor processing steps are adequate for interpreting reflections in two-dimensions and the reflection profiles can be readily re-sampled to produce amplitude slice-maps at this point in the standard processing procedure.

## AMPLITUDE SLICE-MAP PRODUCTION

The next step in processing and image production is usually slicing the reflection data collected in many profiles in a grid to make amplitude maps. The re-sampling procedures used to produce these images in most software packages sample the relative amplitudes of reflections in all profiles at programmed

depths using certain input parameters. Those wave amplitude values are then plotted into maps that display a spatial variation in the variations in amplitude of the received waves, usually in a horizontal view. If the slicing thickness is defined in nanoseconds it can easily be adjusted to depth or these slices can be defined in two-way travel time. In some programs many amplitude maps are automatically generated and displayed in sequence, which can produce a dizzying array of images from the ground surface going deeper in the ground (Figure 6.3). This can be a very efficient way to display variations in wave reflection differences over a large area and with depth. While this can often display interesting patterns, they are not always understandable.

I prefer to think through my slice-map production and instead use my preliminary analysis of the two-dimensional profiles to generate slices in thickness that make sense using what I have seen in the initial processing steps (Figure 6.4). If the reflections that were generated from features can be identified, a logical method of slicing reflections in a grid would be to make sure one or perhaps multiple slicing envelopes contains these features. Slicing too thinly will cut through features, and they may be visible in one or more of the produced slices, making for confusing images (Figure 6.3). The wavelength of the reflections that were generated from the reflection features of interest needs to be considered also, as slice thicknesses should be at least this thick (in nanoseconds or actual depth). This can be determined by measuring the wavelets within a few traces. Slices can be programmed to slice in packages of time (time-slices) or depth, if velocities are known and times are converted to depth (depth-slices).

Thickness of the slices is very important, for if they are too thinly sliced packages of sampled reflections will cut across waves, sometimes sampling them at their mean, and therefore seeming to show no amplitude at all. A

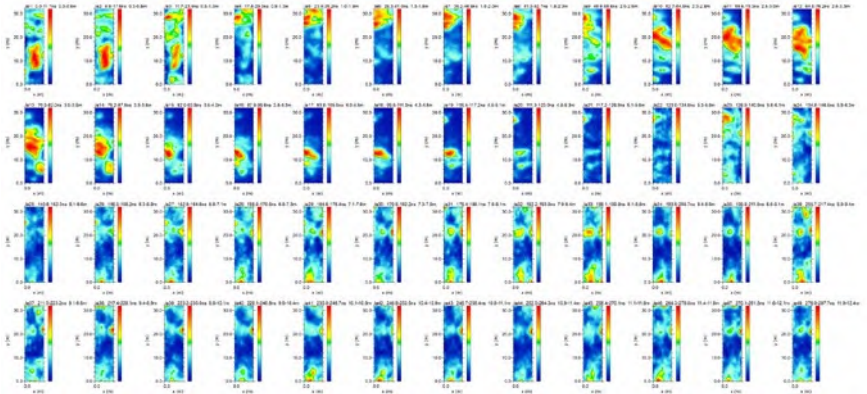


**Figure 6.3.** Display of automatically created amplitude slice-maps of a grid producing “visual overload” of images. *Source:* the author.

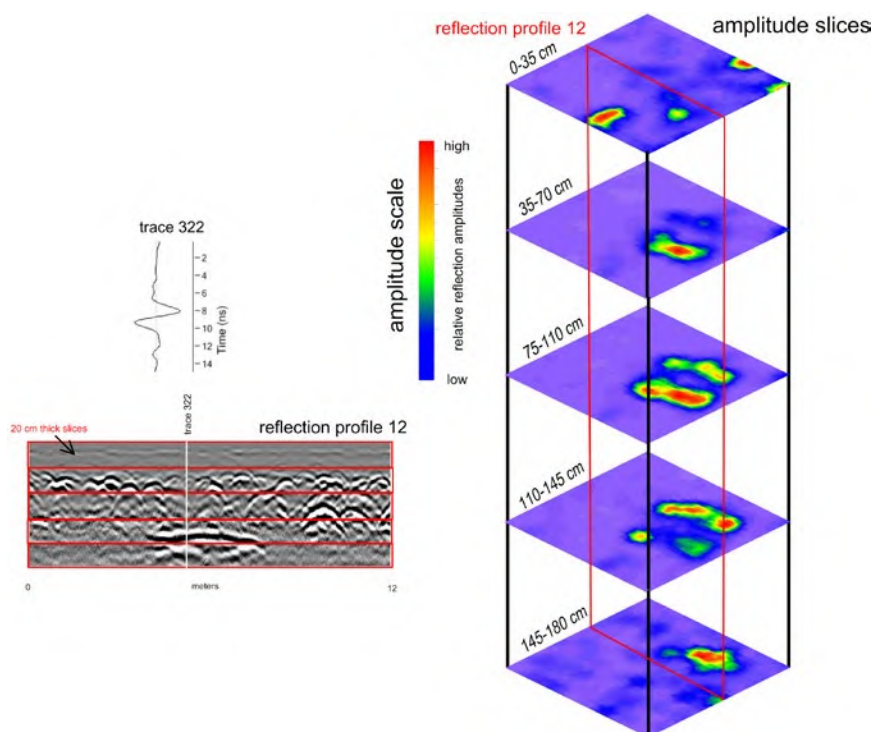


**Figure 6.4.** Construction of an amplitude slice-map from reflection profiles consisting of thousands of traces, which are re-sampled in programmed slice thickness. Sampled wave amplitude values are then gridded, mapped, and displayed in horizontal maps of relative wave strengths of programmed thicknesses. *Source:* the author.

friend of mine thought it would be a good idea to avoid this potential error of cross-cutting slices where one wavelength is sampled and then imaged in more than one slice. He instead chose to generate a slice for every digital sample in every recorded trace in the grid. So, for a grid collected with 512 samples defining each reflection trace, this created 512 amplitude maps. Those could not possibly be displayed in any functional way, so a video was created that started with the map generated from sample #1 and moving quickly down through the slices to map #512. Some of these very thin slices displayed were positive deflections of the wavelets and other times negative ones. All were displayed in gray scale and the videos were quite fun to watch, and there were some possibly interesting features visible, but I am mostly perplexed as to its usefulness. A perhaps more definitive slicing thickness procedure would be to determine what the wavelength of recorded waves are within the grid of data to be sliced. If these waves had about a 2 ns wavelength, then it is likely that a

slice-map thickness of about 4 ns for each slice would not cut across waves too much and features visible in one slice would be mostly representative of what is really in the ground from that depth.

Most software produces slices by taking an average of the wave amplitudes found in each trace within the programmed package and squaring those values to generate all positive numbers. This removes the positive and negative deflections of waves in the recorded wavelets. Some software allows for a similar process called a Hilbert Transform (Hilbert 1912) that uses very complex wave-processing algorithms that will also produce only positive values in a more complex way.

There are a variety of other programming parameters necessary to produce amplitude slice-maps. A crucial input is how many amplitude data points to generate along the profiles and between the profiles. Along the length of profiles there are usually many hundreds or thousands of traces, so collecting one amplitude point in that dimension every trace is not difficult. If there are traces that were collected every 2 cm along profiles a fifty-meter-long line will contain 1,000 traces. So, even though it might take the software some time to sample the amplitudes this densely, it would produce a very high-resolution map. However, if there is a 50 cm separation between profiles in a grid, a fifty-meter-wide grid will only have 101 individual two-dimensional profiles, so in that dimension to produce amplitude maps there can only be 101 total data points sampled. To overcome lack of data points between profiles data-gridding must be employed, which uses a variety of possible algorithms to interpolate between the values that were sampled directly from the reflection traces. This produces new points that are averages of amplitude in the areas between profiles through interpolation. In any gridding algorithm there must be interpolation and averaging employed, which can produce either precise images but more or less “busy” maps. A variety of gridding algorithms are available in most software packages and various search radii and other parameters can be employed to produce a dense grid of data for the final images. The search radius in some gridding methods to interpolate between profiles is very important, as too great a search radius will make buried features all but invisible (Figure 6.5)

Once having produced a first set of amplitude maps, I always return to profile viewing software to interpret individual profiles to make sure I know what features visible in profile are producing the amplitude areas visible in map form. If a grid is sliced too thickly or too thinly, or the interpolation parameters were wrong, this can usually be determined by studying both two and three-dimensional images, and then new more realistic maps can be generated. These are iterative steps so it is always important to think about what has been produced the amplitudes in the slice-maps by studying the reflections in the individual profiles they were produced from.

Many software programs allow for moving through slices visually and quickly choose reflection profiles to be viewed immediately on the computer

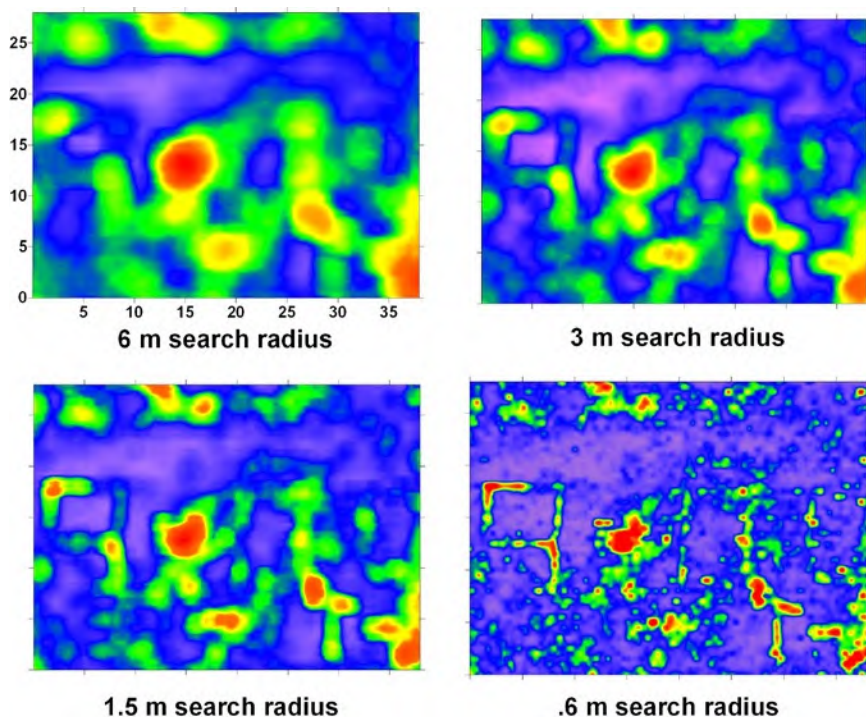


**Figure 6.5.** Differences in maps using different search radii in gridding and interpolation of amplitude data. The larger the search radius, the less visible the buried walls of this historic fort in Colorado. *Source:* the author.

screen (Figure 6.6). This makes for fast and efficient correlations between what is visible in the horizontal slice-maps and what can be seen in the 2-D profiles.

A few new and amazing software programs can process antenna array data that display reflection profiles anywhere within a grid desired, choosing traces from within a densely spaced array simply by moving a computer mouse on the screen. Two-dimensional reflection profiles can then be generated in any location and orientation and need not follow the straight lines of the originally collected data. Soon this very useful tool, which is common in seismic data processing, will be available to all of us in the GPR world. The new antenna array systems can collect traces that are as close as 10 cm apart in all dimensions, which will not only produce densely spaced grid of traces but very precise and “crisp” amplitude maps (Figure 6.7).

Once amplitude maps are generated, the display colors for the relative amplitudes can be modified so that amplitudes of certain values are assigned various colors, and colors can be changes with various palettes. Some of these are very difficult for me to interpret (especially a color palette that is called



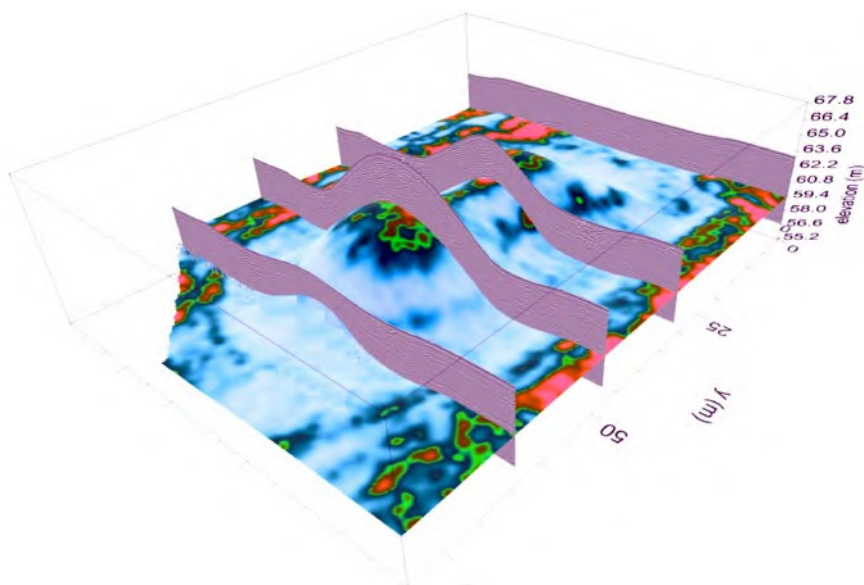


**Figure 6.6.** Display of software that can generate multiple images on the same screen from topographically adjusted amplitude slice-maps to user chosen reflection profiles at any desired location in the grid. *Courtesy of Dean Goodman.*

“bubblegum,” whatever that means). I use the Surfer program (Chen and Niu 2019) for my gridding and map creating, after sampling the GPR reflection profiles in other GPR software packages. This allows me to readily produce a variety of other images besides just horizontal slices, some of which are shown below. Most software has built-in map creating steps, but I have found these produce very “cookie-cutter” maps that may or may be suitable for the work at hand. I therefore prefer to export the sampled profiles as simple x,y,z data (text files), which can be readily imported into Surfer. Perhaps better, many software packages are very interactive so that processing steps are first done to all profiles in a grid and there is a production of slice-maps in “real time.” That is a huge advancement in data processing as each processing step can generate a new series of slice-maps.

With reflections collected in antenna arrays, there can be data saved into a gigantic database that may have been collected initially with traces spaced 10 cm apart in one dimension and even smaller spacing in the other (Figure 4.3). This dataset is likely to produce even more precise amplitude maps as there is almost no interpolation needed between points, which is necessary for profiles that are spaced some distance apart. An example of the difference between the array collection and the more standard individual profile method demonstrates this advance (Figure 6.7). Here a 400 MHz array of antennas was used to map

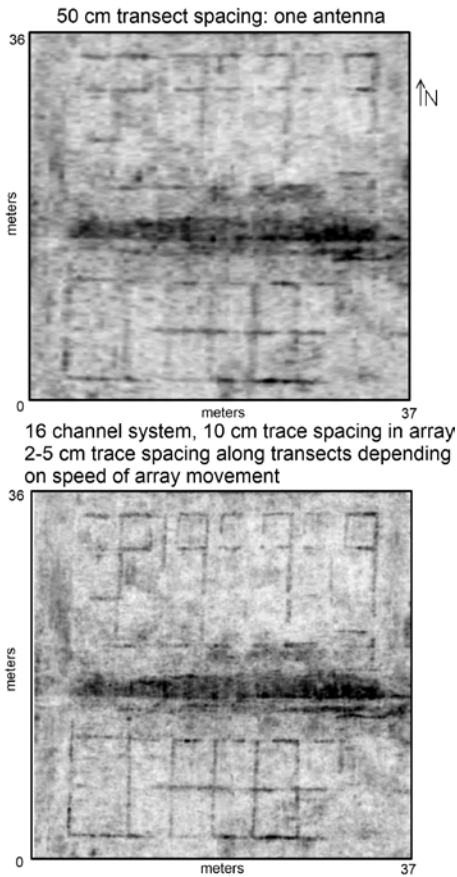


**Figure 6.7.** Comparison of resolution in amplitude slice-maps of a buried multi-room Roman building at Carnuntum, Austria, with 50 cm profile spacing on top, and reflection traces collected using an antenna array system with 10 cm trace spacing below. *Courtesy of Alois Hinterleitner, GeoSphere, Austria.*

a row of rooms in a Roman barracks at Carnuntum, Austria (Gugl et al. 2021). The array had sixteen antennas, with traces spaced 10 cm apart perpendicular to the transect lines, and between 2 and 5 cm along the transects, depending on the speed of the array movement.

Other types of amplitude slice-maps will also soon be available, produced from antenna arrays where each antenna sequentially transmits while all others receive. Those antennas may be spaced as closely as 10 cm or so in both x and y and in an array of 100 antennas there would be ninety-nine antennas recording while one transmits (transmitting antenna #1), then repeating this for antenna #2 that transmits and the other ninety-nine record, etc., until all one hundred antennas have transmitted. In this type of a system there would be 9,900 traces recorded for every 1x1 meter area of ground. That huge amount of data would need to be processed using software that is not yet publicly available for GPR. Our colleagues in the seismic reflection business have been doing this routinely

for many years, and perhaps one day this will be available for GPR arrays. I have heard of experimental prototypes of these systems. Reflection seismic grids of this sort can produce a variety of three-dimensional images and routinely generate any reflection profile from anywhere in a grid to display reflections in two dimensions.

Once suitable amplitude slice-maps have been generated and interpreted with the help of reflection profile interpretation it may be appropriate to generate other types of images of the ground. If the ground is not flat topography will need to be integrated into both profiles and amplitude maps. The reflection profiles will need to be adjusted for elevation (Figure 3.10) and then re-sliced horizontal to sea level instead of parallel to a variable ground surface. It might be appropriate to choose one extensive planar reflection that was created from one horizon of interest and prepare a “horizon slice.” This method samples amplitudes and depth from one defined package of reflections no matter what depth in the ground it was generated from. All these potentially useful amplitude maps might produce the final results, and any additional data processing would be superfluous.

### ISOSURFACES AND VIDEOS

Depending on the audience for an interpretation, it might be appropriate to produce an isosurface image or two of specific features discovered in a grid (Figure 6.8). These can sometimes help others visualize what a GPR study has focused on, but I rarely find them to be helpful for my basic interpretation. These types of images can be rotated, they can be shaded, and videos can be made of the buried features, and they are always a “crowd-pleaser” in public talks. Otherwise, I find them mostly “show and tell” types of images.

Videos can also be produced moving through amplitude slices from the ground surface to some depth. These are easy to produce once the reflection

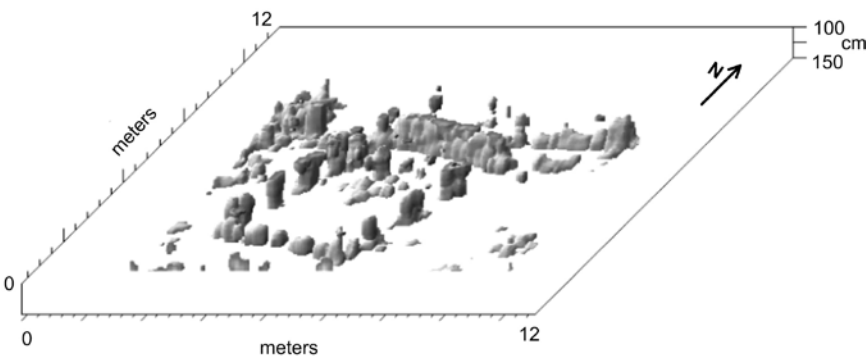


**Figure 6.8.** An isosurface rendering of the buried Roman temple at Petra, Jordan, shown in Figure 1.3. *Source:* the author.

data have been sampled and displayed in slices. They can often be illuminating, and I often play the videos many times on the computer screen looking for features that are not visible in the static displays of slices. I have read the human brain is selected for evaluating moving images more readily than static ones (Grossman and Blake 2013). That hypothesis comes from an understanding of our ancient past where finding prey or predators that move across a complex landscape meant either food to hunt or scary animals to flee from. Whatever the visual selection process, moving images often allow us to see and process features better than static ones.

## **MORE ADVANCED PROCESSING STEPS**

Once some understanding has been made with a dataset, it might be beneficial to employ more advanced processing steps, if specific needs are known. These are available in most software packages and some of their instruction menus suggest they be applied during a “first-try” processing on the way to basic image creation. I disagree, as I think it is best to understand a dataset initially in raw form, followed by some simple processing steps such as background removal, axis adjustments, vertical or horizontal exaggeration, re-gaining, and if necessary topographic adjustments. Only after this is done, and interpretations are made can a determination of the origins of reflections and how they can be modified for specific needs be made.

Horizontal banding is often present in raw reflection profiles. The background noise from radio transmissions is usually in the higher frequencies and can be quickly removed using the basic background removal filters. There is also low-frequency noise that produces horizontal banding termed “wow” by some (Neal 2004). This is slang that comes directly from seismic processing. There are procedures in software that are termed “de-wow,” which remove these bands using horizontal filters. There may also be horizontal bands visible in profiles that can also be the product of reflections from surface objects that were the same distance away from the antenna during acquisition, such as the person pulling the antennas or a towing vehicle. However they are produced, banding of whatever sort often obscures important subsurface reflections that would otherwise be visible on profiles and should be removed.

## **MIGRATION**

An important second-phase data-processing step that is commonly used prior to the production of amplitude maps is migration, which removes the axes of point-source hyperbolas and sometimes enhances the amplitudes of their apexes. This is particularly beneficial prior to creating amplitude slice-maps as hyperbola axes are adjacent to and lower in the time-window than the point-sources that generated them. When the splayed-out axes are sampled and integrated into a series of slice-maps they will produce reflection “signatures” for some point sources that are both broader and deeper than they should be.

Migration will remove these hyperbola axes and the resulting images produced from these processed profiles will be “crisper” as reflections from only the actual point-sources are precisely placed in space.

The geometry of the hyperbolas is a function of the velocity of the waves that moved in the ground to record a point-source (Figure 3.24), so if the velocity is known, these hyperbola axes can be “migrated back to their sources,” which gives this processing step its name. To perform migration, velocity estimates of the ground must be determined first. That velocity (or in some software a velocity model that shows variations in velocity across a grid and with depth) is then used to migrate all hyperbolas. All profiles in a grid are then processed in this way and the resulting new profiles (Figure 6.9) re-sliced to produce new amplitude slice-maps or other images (Figure 6.10).

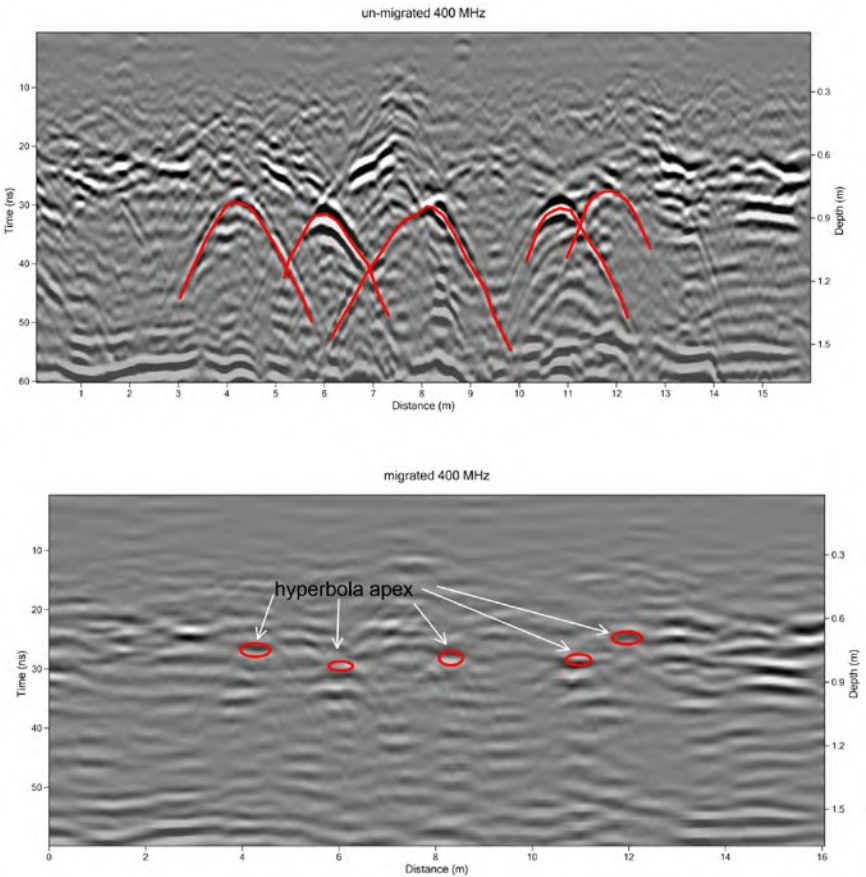


**Figure 6.9.** Raw reflection profile displaying many reflection hyperbolas (top) and the same profile after the hyperbola axes have been removed, leaving on their apexes.  
*Source:* the author.

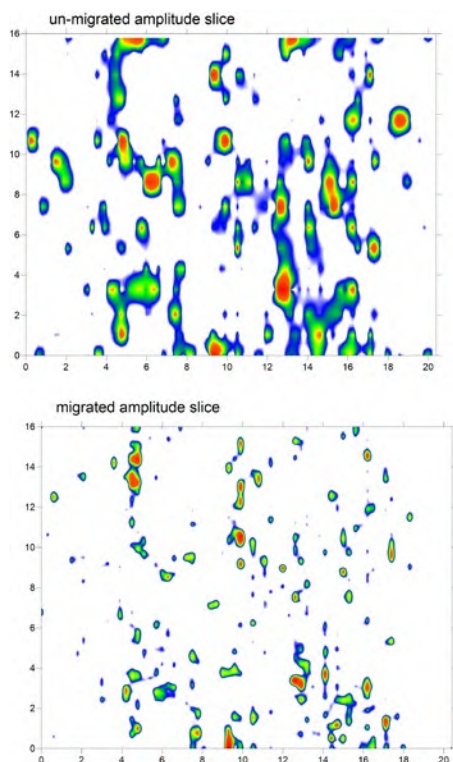


**Figure 6.10.** The difference in amplitude slice-maps with un-migrated profiles on top, and the same slice after the axes of hyperbolas have been removed during migration (bottom). *Source:* the author.

The resulting migrated profiles can be more difficult to interpret because the hyperbolas denote individual objects and features, and without their axes become more difficult to identify. I therefore always return to the un-migrated profiles for other interpretations even after producing a new set of amplitude images from the migrated data.

There are a variety of computations that software programs employ for migration. These are termed “Kirchhoff wave-equation migration,” “phase-shift migration,” and “frequency-wave number” (F-K) migration (Smith et al. 2016). To display the differences and similarities of these methods without having to discuss the complex equations for each, one profile is used that contains many hyperbolas and portions of hyperbolas to migrate (Figure 6.11). This is a complex reflection profile that contains many axes of hyperbolas from New York where a buried seventeenth-century living surface contains historical features and architecture buried by windblown sand. This surface is readily visible as a distinct planar reflection, and on it, or directly above it, are many objects, all of which generate reflection hyperbolas. One of these features used to test different migration methods is two individual stones, separated a short distance, which produces two “half hyperbolas from their edges in a profile” (Figure 6.11).

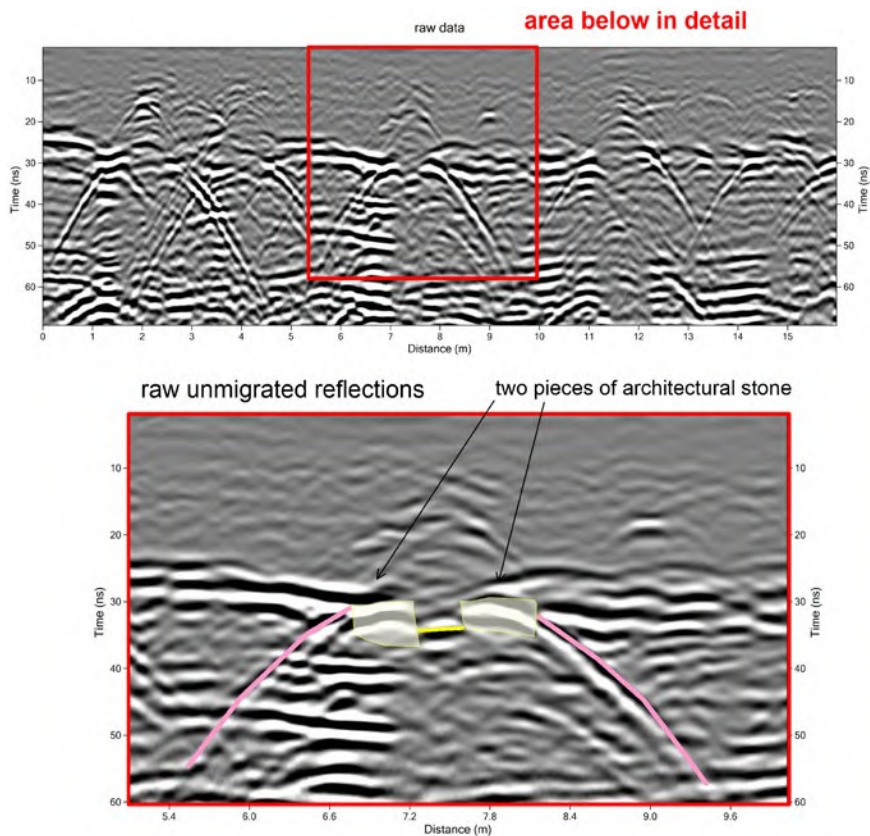


**Figure 6.11.** The hyperbola axes used to test migration methods. There are two “half-hyperbolas” generated from two closely spaced objects in the ground. Results of these migrations tests are below in Figure 6.12. *Source:* the author.

The stones are very close to each other and the propagating radar waves that encountered their interior edges were reflected away from the surface antenna so only the outer edges of these stones produce distinct reflection hyperbolas.

Three software programs were used to migrate these reflections: GPR-Slice, Kirchhoff method in RADAN, and GPR Process. Other software was also used in the tests including ReflexW and Ekko-mapper, which produced comparable results, and are not shown here.

The Kirchhoff method in RADAN nicely removed the hyperbola axes but produced a reflection feature above the stones shallower in the time-window, which is not real (Figure 6.12). It appears that the software was assuming that the two half-hyperbolas generated from two separate objects were generated from one point-source and therefore migrated the axes to a false point higher

in the time window. GPR Process used standard migration but did not generate the false apex (Figure 6.12). The GPR-Slice software was almost the same as that produced by RADAN. An extreme example of false reflection generated with migration was done in RADAN where an RDP of 10 was used incorrectly, where the real RDP was 23 (Figure 6.12). In this last example the hyperbola axes were migrated far above the point-source up and produced a “smiley face” above the point-source where they were generated.

These varied results from migration programs may not be that important as they vary only a little, and what is most important is the removal of the hyperbola axes. Amplitude maps generated from all these examples of correct migration would produce good results. The “smiley-face over migration,” however, would produce amplitude slice-maps that could be very misleading, placing a large object that does not exist into one of the shallower slices. If the goal is “crisper” and more distinct amplitude slice-maps, all these results would have been acceptable.

Steeply dipping reflection surfaces in the ground will also diffract radar energy during its transmission to and from a planar reflecting surface (Jol and Bristow 2003; Neal 2004). Longer travel times that result from this diffraction will then place reflections at incorrect depths or locations in the subsurface, distorting the size and geometry of some subsurface beds or features. Some migration processes can spatially adjust for these kinds of distorted or hyperbolic reflections and “collapse” them back to the point of origin.

With the advent of antenna array systems, very closely spaced antennas will receive waves that were generated from point-sources both from front and back but also from the sides (and actually any direction). The same can happen with closely spaced standard two-dimensional profile acquisition. While I have showed two-dimensional migration examples here, it is possible to migrate in three-dimensions (Liu et al. 2016; Radzevicius 2008) using techniques that have been adapted from seismic data analysis (Liner 2016).

## **FREQUENCY FILTERING**

Another useful processing step, which can be applied to data prior to producing amplitude maps, is frequency filtering (Grealy 2006; Szymczyk and Szymczyk 2013). As most GPR antennas are “wide band” transmitters and receivers, they are always producing and recording a range of wave frequencies around a mean. Most of the energy produced is near the center frequency but other waves in a range of frequencies also propagate to be recorded from various interfaces. At any location, there will be variations in what frequency waves are reflected from what interfaces, and each frequency will attenuate at different depths. When individual traces are viewed in most software both the longer and shorter wavelengths on either side of the center-frequency are averaged and therefore not usually visible. Software included with most packages can produce displays of all frequencies in a histogram (Figure 3.15).



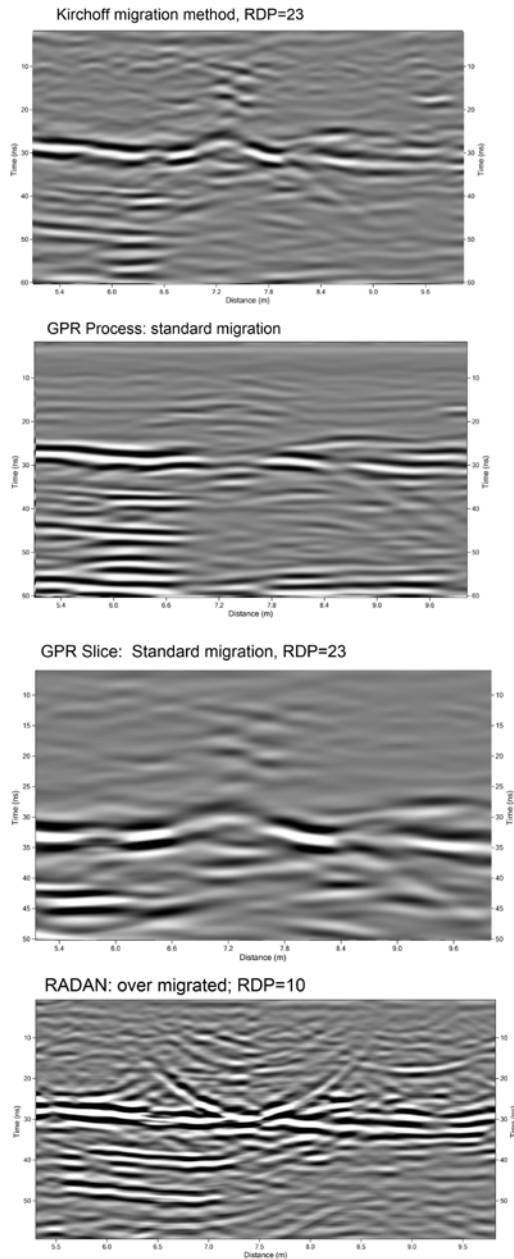


**Figure 6.12.** Results of some migration software of the reflections in Figure 6.11. Both Kirchhoff and standard migration methods produce a “bump” between the two reflection features. An “over-migration” using a very low RDP migrated these axes upward into the time-window to create a “smiley face”—a sure sign of poorly migrated reflections. *Source:* the author.

To frequency-filter data all traces in a reflection profile must be re-sampled using data processing software to remove whatever frequency is desired, producing a whole new set of profiles. Amplitude maps can then be generated from those processed profiles, displaying only the desired frequency waves. As higher frequency energy is shorter in wavelength, it will likely be reflected from smaller buried features, and some that are very near the ground surface, often within the near field. Those higher-frequency waves will attenuate at shallower depths than the lower frequency waves. The lower frequency longer wavelength waves will couple with the ground more deeply and will theoretically travel deeper in the ground, only to be reflected from the larger objects or thicker layers (Conyers 2004). Knowing these basic concepts certain frequencies can be filtered out and others retained to create new profiles that display reflections from desired features of different sizes.

Several filters employed in some processing programs attempt to remove frequencies can be either infinite impulse response (IIR) or finite impulse response (FIR) filters. Both filtering processes remove desired frequencies with the difference being the number of reflection traces used in averaging and the type of averaging and interpolation algorithms used in the filtering process. In all cases, what is being done is a sophisticated method to remove specific high (and sometimes low) frequencies.

A second or third version of the same set of reflection profiles can be produced and compared to the first in a way that can help define buried features of interest using some of these steps. Interpretations of this sort take time, as all these steps must be performed in a knowledgeable and deliberate way, and the outcomes can often be quite surprising and informative.

It is also important to follow processing steps in a sequential order that makes sense. For instance, it would not be appropriate to frequency filter reflections that include many hyperbolas that have not yet been migrated, or this step would end up with more hyperbolas of various frequencies. It is best to first migrate reflections with all the frequencies still present, remove the hyperbola axes, and then frequency filter what remains.

An example of how some of these processing steps used, reflection data to produce a series of amplitude maps of a buried Roman temple at Petra, Jordan (Figure 1.3) (Conyers et al. 2002). The unprocessed 400 MHz profiles, when horizontally sliced in 4 nanosecond thicknesses produces a good image of the back wall and the bases of what appears to be pillars of this structure (Figure 6.13). This “raw data” amplitude slice-map is quite good and displays all the buried features that might be necessary for a general-purpose interpretation. The back wall of the temple is visible as a mostly continuous reflection feature.

All the profiles in this grid were first migrated removing hyperbola axes (Figure 6.13) and the resulting profiles were then re-sampled, and an amplitude map was produced using the same slicing parameters (Figure 6.13, migrated data). In the resulting amplitude slice-map the back wall is better defined,

with individual stones becoming apparent. The migrated profiles were then frequency filtered, so that only the 500–800 MHz reflections remained (Figure 6.14). The new high frequency reflection profiles were re-sampled and sliced again using the same parameters as the previous maps. This frequency filtering process further defined the individual stones in the amplitude slice-map (Figure 6.13: migrated reflections, filtered 500–800 MHz).

The last final, highly processed image shows what had been originally interpreted as a continuous back wall of the temple is composed of small stones, which do not make up a contiguous wall but only the foundations of what was once a wall. The conclusion is that only a little remains of the structure but a few individual stones outlining what had been a substantial building. This feature was excavated, and these small stones were uncovered much to our surprise, as our initial interpretations were based on the un-processed reflection data. Our hopes of finding carved marble columns and other architectural elements were dashed and only building materials that were not considered important enough to recycle were left in place when this structure was dismantled.

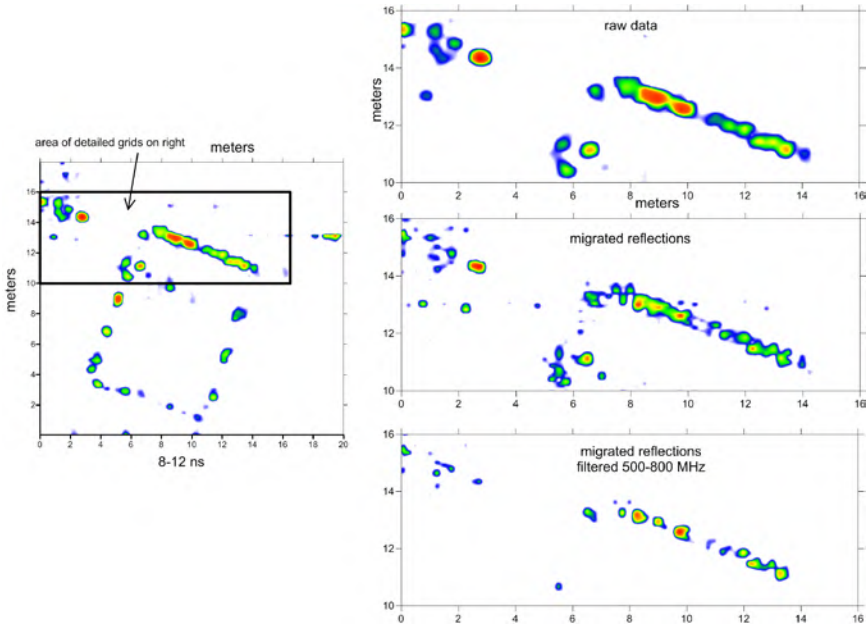


**Figure 6.13.** Amplitude maps displaying processing procedures of reflections from the north wall of the Roman temple at Petra seen in Figure 1.3. Raw data when sliced display a continuous wall. Migrated reflection profiles define individual stones in that wall, and frequency filtering of the migrated profiles display each individual stone in that wall. *Source:* the author.

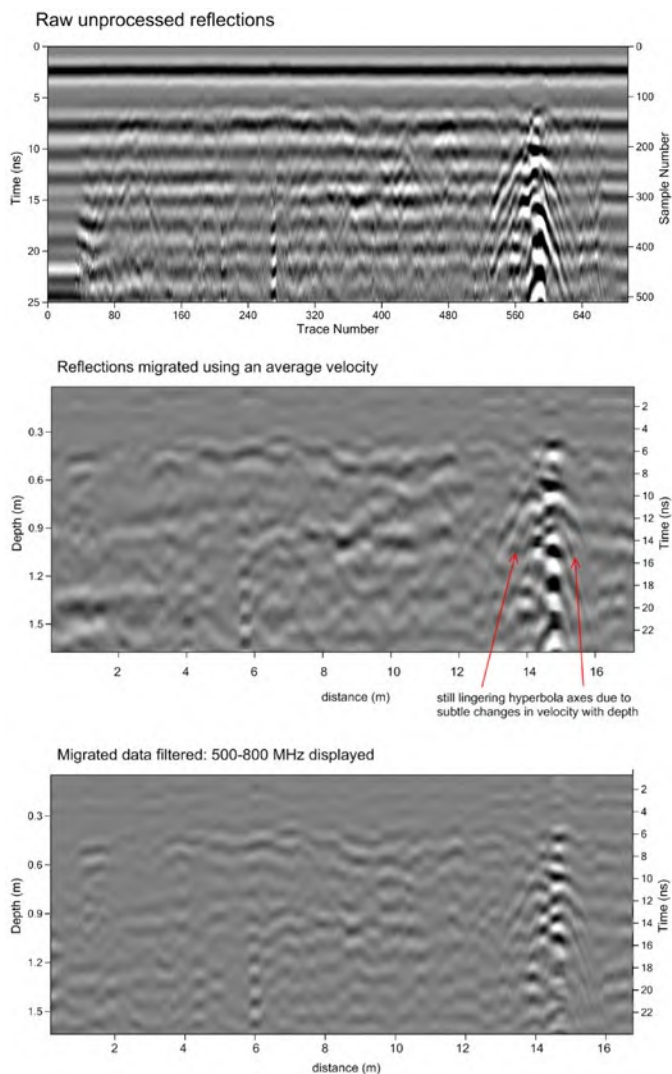


**Figure 6.14.** Reflection profiles displaying reflections in each of the individual processing steps used to create the amplitude slice-maps in Figure 6.13. *Source:* the author.

An important conclusion in this small study of just one wall of a building is that there were three separate data processing steps necessary to reach the conclusion. Time was expended after each step to understand and interpret what each data processing function was doing to the previous data. The raw data maps produced first were suitable for basic interpretations, and those were used to plan excavations. The migrated profiles were used to produce images of distinctly different stones that made up the wall, which indicated that the initial continuous wall interpretation was perhaps hasty. Frequency filtering of the migrated profiles showed that the stones in this wall were small and therefore likely unimportant to the people who removed the building's superstructure, and they were left in place for us to discover. Each of these steps was important and the processing procedure was conducted in an intuitive step-by-step process.

A variety of frequency filters can be applied and tested with reflection profiles to determine if various frequencies might have penetrated to a depth necessary to image features of interest. In Italy a Roman-age underground aqueduct was known to exist at Hadrian's Villa, as it has been entered and followed near a GPR test area (Ghezzi et al. 2019). Its extent was not known, but it projected into a GPR grid. The 200 MHz antennas were used, and the time-window was opened to 275 nanoseconds in the hope that energy with that frequency would penetrate to 10 meter or so (Figure 6.15).

One of many reflection profiles initially indicated that all energy had been attenuated about 40 ns, which is just a little less than two meters deep. This was disappointing as the aqueduct was known to be about three meters deep. To determine if some of the longer-wavelength lower frequency energy may have penetrated to a greater depth before it was attenuated, the reflection profiles were filtered so that only the 50 to 100 MHz waves remained. The resulting profile was interesting, as it displayed coherent reflections to about 150 ns, or about five meters depth. When zooming in on the location where the aqueduct projected into the GPR grid, an arched reflection from the ceiling-void interface of the tunnel was discovered in exactly the location and depth where it was expected to be found. If only the raw 207 MHz reflections had been used, this feature would not have remained invisible, but in this limestone ground the longer wavelengths propagated much deeper than the 200 MHz waves. The 50 to 100 MHz waves make up only a very small proportion of the energy that had been received and were overwhelmed by the rest of the broad-band frequency waves in the raw data reflection profiles.

## **DECONVOLUTION**

Multiple reflections (often just called multiples) are caused when radar energy reflects back and forth between a buried surface and the ground, or between subsurface layers multiple times before traveling back to the surface (Figure 6.16). When each of these reflections are received at the surface antenna and

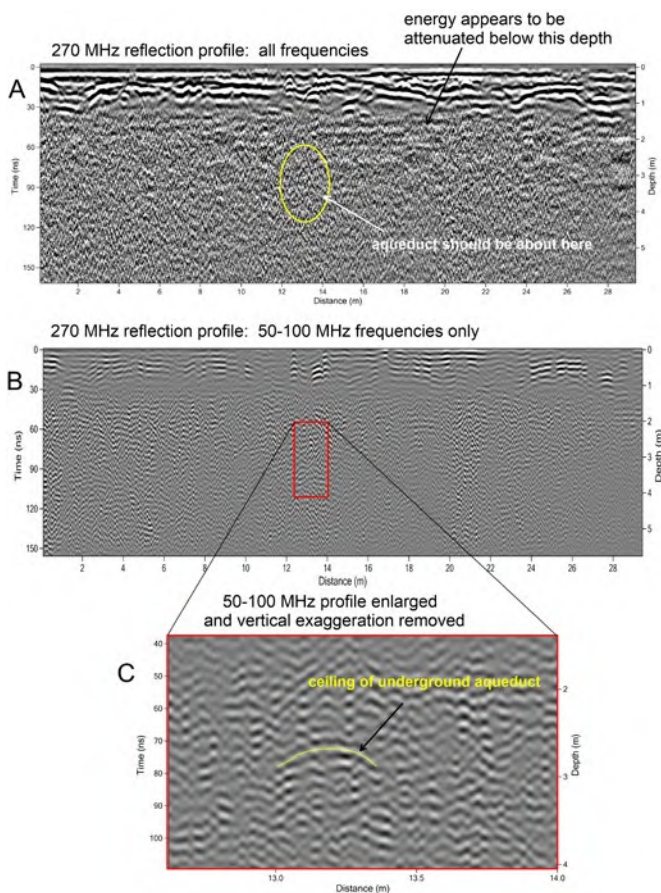


**Figure 6.15.** Filtering of a 200 MHz reflection profile to display only the 50-100 MHz frequency reflections. The arch of a subterranean aqueduct becomes visible, where it was obscured by the higher frequency waves when only the raw data were used to produce the profile. *Source:* the author.

recorded, they are displayed in a profile as repetitive reflections (Figure 6.17), all of which are an equal distance apart (as measured in time). Often multiples of this sort can be confused with “real” reflections that might have been created from stacked layers of materials in the ground. Usually, they can be determined to be multiples as they are spaced at an equal time interval apart (Figure 3.34). Sometimes other waves that appear to be multiples can be created by “ringing antennas” where a transmitter and receiver are located within each other’s near-field, and reverberate, creating the same effect. This was common in some early models of low-frequency antennas, but these flaws have been

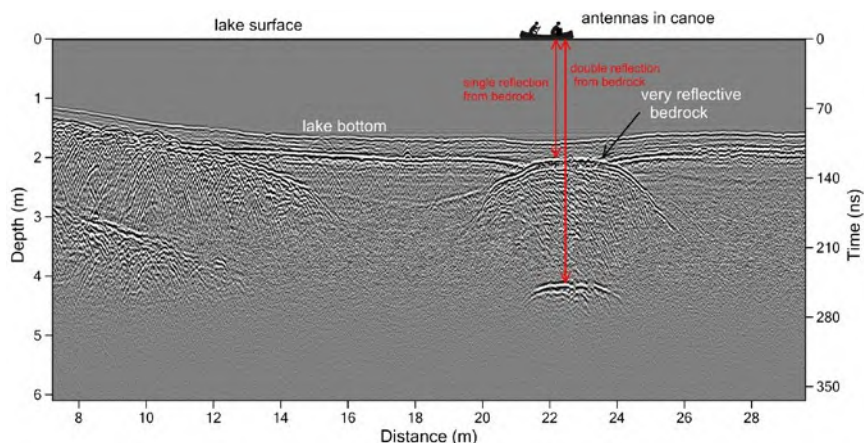


**Figure 6.16.** Multiple reflections produced from a very reflective bedrock unit in a lake bottom. *Source:* the author.

re-engineered in a different way recently, so this is no longer a problem with newer antennas.

Unwanted multiple reflections often obscure important reflections that might have been recorded at the same time in the reflection traces, and if so, they can be removed (Neal 2004; Schmelzbach and Huber 2015). This process is called deconvolution, or more precisely “predictive deconvolution,” because the method attempts to predict the shape of the transmitted radar pulse from the surface antenna and how its wavelength and dominant frequency will change as it moves in the ground. Changes of the amplitude and wavelength of propagating radar waves occur due to variations in coupling along surface changes, the imposition of background noise, water variations and many other variables that are often not known (Neal 2004). Deconvolution is a wave processing technique that has been modified for GPR from seismic studies (Belina et al. 2009; Fisher et al. 1994; LaFleche et al. 1991; Majjala 1992; Malagodi et al. 1996; Neal 2004; Neves et al. 1996; Rees and Glover 1992; Todoeschuck et al. 1992; Xia et al. 2004). It is based on the theory that as a radar wave is transmitted into the ground portions of the electromagnetic wave will change form or “convolve.” The purpose of this filter is to remove the portion of the recorded waves that have convolved during transmission in the ground, theoretically restoring the reflected waves in a profile to their original pattern.

An example of predictive deconvolution is an attempt to image layers below a highly reflective near-surface road surface. The 400 MHz antennas produced reflection profiles that show where the buried road is located, but the surface is so reflective that only multiples were recorded below it (Figure 6.17). A variety of steps that would mimic how the 400 MHz waves convolved in this ground to produce the multiples were attempted until a good match was made. The



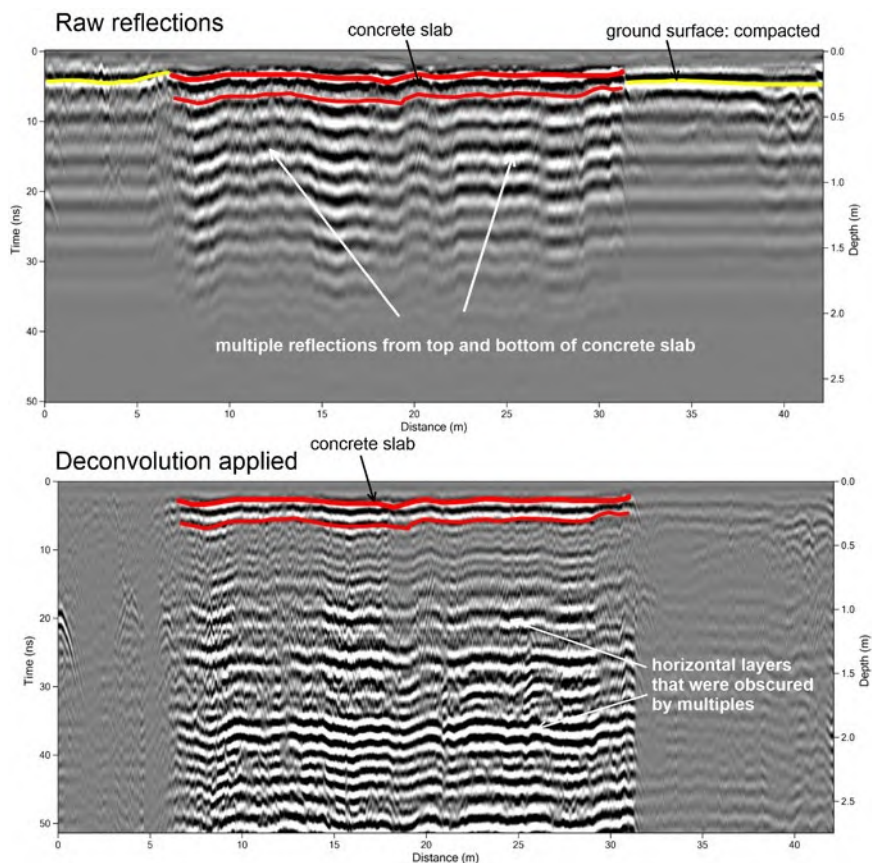


**Figure 6.17.** Deconvolution processing used to remove multiple reflections from a buried road bed in New Hampshire. *Courtesy of Peter Leach, GSSI.*

raw waves were then deconvolved to produce a reflection profile that displays the layers underlying the highly reflective roadway.

One of the problems with deconvolution processing is that restoring reflected waves to their original forms is mostly educated guesswork and many steps must be undertaken to arrive at a method that works. It is usually difficult to determine how the original transmitted waves were shaped and any deconvolution process may be modifying the data in unreal ways. Although many GPR experts claim to understand what radar waves do in the ground, much about this processing technique remains obscure. If deconvolution processing of radar data can be improved, it may yield important clues to understanding how the physical properties of the ground modify transmitted electromagnetic waves and help in all types of GPR data interpretation. It might be used to



determine components of various layers in the ground when little is known about the geology in an area of study (Conyers 2016).

### **HILBERT TRANSFORM**

Reflections generated from very subtle changes in the ground can also be enhanced with a processing step called a Hilbert transform (Todeschuck et al. 1992; Turner 1992; Yilmaz 2001). This step transforms the reflection amplitudes of waves and their geometry in the ground into spatially distinct frequency and phase information. The phase of reflections (whether they are positive or negative deflections in the waveform from the mean) is often indicative of important changes in relative dielectric permittivity of materials at a reflecting interface. For instance, the phase of a reflected wave will often change if generated at an interface where velocity increases instead of decreases. While this is not common in most field conditions, it can be apparent where there are void spaces in the ground, as is common with caskets in cemeteries (Conyers 2012; Damiata et al. 2012). In other cases, a phase change might be subtler, for instance a reflection that is generated at the interface of a moist clay that sits on a drier sand. In this case, the clay would allow only relatively slow transmission of radar waves, which would then speed up when moving into the underlying sand. The resulting first recorded deflection of the reflected wave would have a change in phase, and if the general nature of the beds in the ground was known, this subtle change in phase could potentially tell the interpreter what type of materials are generating the reflections.

### **MULTIPLE-OFFSET PROCESSING**

A processing method that has seen a good deal of research is multiple-offset acquisition (Berard and Maillol 2007, 2008; Booth et al. 2008, 2010; Brown et al. 2009; Forte and Pipan 2017; Perroud and Tygel 2005; Pipan et al. 1999, 2001). The collection process must use a system employing a transmitting and receiving antenna that can be separated or an antenna array system. To collect multiple-offset reflection profiles the transmitting antenna is kept stationary while the receiving antenna is moved away from it along a linear transect, in steps. At each step, which might be 10 or 20 cm, or more, one individual reflection trace is collected. Maximum antenna separation can be five meters or more in this process. In array systems, this can be done with collection procedures on the control system. After all traces are collected at the receiving antenna in multiple-offset distances away from a stationary transmitting antenna, the transmitting antenna is then moved forward along the transect and the procedure is repeated. Collected traces are usually a composite of many stacked traces at each step location to minimize background noise. This procedure using just one transmitting and one receiving antenna is both labor and time intensive but the resulting reflection profiles can have an improved “signal to noise” ratio, better depth penetration, and more accurate migration

of reflections (Berard and Maillol 2008; Booth et al. 2010). Air waves produced from nearby surface objects can also be removed in this process (Sun and Young 1995). The resulting reflection profiles produce reflections that are more accurately placed into space, as migration is accomplished by calculating velocity changes both with depth and laterally to generate the final product.

This type of analysis has not been commonly applied with GPR, but this is changing (Forte and Pipan 2017) with the advent of multiple antenna array systems can collect very rapidly offset reflections from many stationary antennas. Very soon there will be automatic data processing commands in software that can perform offset analysis from this type of data collection.

An example of multiple-offset processing was used along a Medieval wall in eastern England, which was built in 1390. The wall was constructed of small pieces of flint, brick, and chalk, cemented with local mud (Booth et al. 2010). Collection and processing of GPR at the site was particularly challenging as it was in an urban environment adjacent to a church, with numerous cars and other objects that produced air wave reflections. Two reflection profiles were collected along a line perpendicular to the buried remains of the wall. Its presence was confirmed by core holes after the GPR data were processed. A typical reflection profile, with one transmission and one collection antenna that stay the same distance apart is compared with a multiple offset profile, both of which were collected with 200 MHz antennas (Figure 6.18).

The single-offset reflection profile contains high frequency noise, an air wave produced from a parked car and the near-surface direct wave. The wall, which is composed of many small pieces of material in a clay and chalky mud matrix is non-reflective with the 200 MHz waves, and therefore not visible in the single-offset reflection profile. In addition, the water table defined by coring, does not produce a distinct reflection. The twenty-two-meter multiple-offset profile was collected in steps of 20 cm with a maximum antenna separation of 5.1 meters. The reflection traces were processed into the multiple-offset reflection profile with a seismic software program. Velocity information provided from the multiple-offset data allowed all reflections to be migrated to their correct location in the ground and low frequency noise was removed. The air wave generated from the parked car was also removed in this process. In the resulting processed and spatially corrected reflection profile the water table was readily visible, and the non-reflective wall can be discerned as the area of no reflection. In addition, all very high frequency reflections were removed and only those received from deeper in the ground are displayed.

There are many other experimental filtering techniques of this sort, originally developed for seismic data processing by the petroleum exploration industry, that have been applied to GPR reflection data (Lehmann et al. 1996; Majjala 1992; Milligan and Atkin 1993; Neal 2004; Yilmaz 2001; Yu et al. 1996). Care must be taken when using these processing steps because there are some important differences between radar and seismic reflection data. The wide

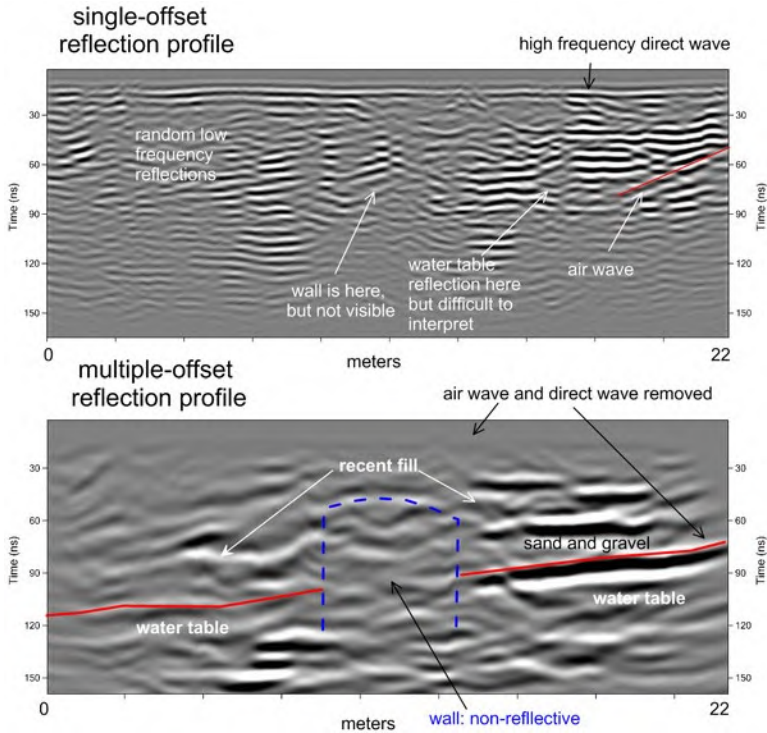


**Figure 6.18.** Multiple-offset processing displaying how this data collection and processing method can make it very difficult to see buried features that are obscured by high-frequency reflections. *Courtesy of Adam Booth.*

aperture of radar antennas, which transmit and receive reflections from a large subsurface area in a cone of transmission, make any automatic application of seismic techniques sometimes difficult as their wave transmission properties are much different (Neal 2004). Another difference is that radar waves almost always slow down during propagation in the ground, while seismic waves increase their velocity with depth (Leckebusch 2003).

## OTHER EXPERIMENTAL ANALYSES

Coherence analysis is a data processing technique that has been shown to work well with reflections collected in sandy ground (Trinks et al. 2020). This method is directly inherited from the seismic world (Li et al. 2021) but can be applied to GPR also. It is a method that measures the similarity between recorded waves both in individual reflection profiles and in three-dimensional volumes of reflections. Measurements about how “coherent” reflections are over some distance can be used to note the location of discontinuous reflections that might have

been produced from incisions in the ground or other geological phenomena such as river channels, slump blocks, or vertical faults.

Texture attribute analysis is another technique that comes from seismic data processing (Ball and O'Connor 2021; Mertes et al. 2017; Zhao et al. 2013, Zhao et al. 2018) and biological imaging (Depeursinge et al. 2014). This method uses models and statistical analysis to search for patterns in recorded waves. If several models can be constructed for various features in the ground that reflect radar waves, the software will go through profiles to compare the actual reflections to those models that are sometimes termed templates (Verdonck 2016). Statistical analysis can then determine the degree of “fit” to the models to locate modeled features in very large datasets (Verdonck et al. 2019). This type of analysis seems to be totally dependent on how well models (templates) represent the reflection features in the ground. Perhaps in an area where much is known already about buried materials, and a variety of features have already been excavated and compared to the radar wave reflections, this might be of some value. But I would hesitate to apply it to a large dataset at the outset of a research project when little is understood about the ground.

All these more sophisticated processing methods lend themselves to automatic data-processing techniques and artificial intelligence (Küçükdemirci and Sarris 2022). Sometimes called “machine learning” or “deep learning.” It is well recognized that large complex GPR datasets can be obstacles to more traditional data analysis and interpretation, especially when results are needed quickly, or there are limited people with GPR interpretive training to commit to the work necessary. These new computer methods provide multivariate analysis of millions of reflections in high-volume datasets that can potentially provide results that are sufficient for a research project. I have heard that there are new business models implemented by large firms that rely on these types of tools for customers who may not have processing and interpretation skills or the time to learn them. I can readily see the value of these applications when using GPR to find a few important targets, such as buried landmines (Núñez-Nieto et al. 2016) but am fearful about applying them to geologically complex environments where the complexity may be too great to be modeled and interpreted (Travassos et al. 2020).

## **DATA PROCESSING CONCLUSIONS**

As a matter of course, all GPR reflection profiles should be processed to normalize distance both horizontally and vertically. Background removal is a very simple and important technique that should always be performed to remove extraneous noise to allow visibility of important subsurface reflections. All these simplest GPR data-processing steps are very useful as a first step.

While reflection data containing many hyperbolas can often be corrected with migration to enhance the resolution of important reflections, there is always a risk in “over-processing.” The same is true with frequency filtering,

which produces very different datasets from the raw data. A critical study of a dataset is needed to determine what is being removed and what retained when this type of filtering is used. Too much data processing done in the hope of obtaining useful results from what might be considered a marginal survey can often produce results that are even more difficult to understand (Conyers 2012). Migration, deconvolution, and frequency filtering might be very useful in some situations, but arbitrarily applying them to all datasets in the hope of just obtaining “different” or “better” results is not recommended. There are very specific reasons for applying each of these types of processing procedures, and if the data manipulation methods are not understood, the results will be even less so.

In the seismic data-processing business, some people have devoted their lives to post-acquisition processing and these experts can often work wonders with poor-quality data. They also make jokes among themselves about their ability to modify data to such a degree that they can produce almost any result desired by a client. The standard joke in some seismic data-processing laboratories is that if the reflection data do not produce the desired outcomes, just send the data back to the data-processing experts, as they can produce whatever results one would like. Although it is hoped that one would never become this intellectually confused within the data-processing web, the potential exists with the abundance of processing steps discussed here, few of which are really understood in their complexity by many professionals, let alone the typical GPR user.

# 7

## *Interpretation of GPR Data*

How GPR is processed and interpreted has changed very much in the last twenty years. When GPR data were first used in the 1970s, most interpretations were made by viewing raw reflection profiles that were not processed in any way and consisted of only searching for “anomalies” that might have been produced from something interesting in the ground (Bevan 1977; Conyers 1995; Sheets et al. 1985). These early efforts were made with reflection profiles that were printed out and analyzed on paper, sometimes done immediately in the field, or viewed and interpreted on a video monitor. Those interpretation methods were at best crude and inaccurate, but they were all that could be done with analog reflection data that were not stored on digital medium for later processing and the production of more intuitive images.

There were some attempts at categorizing anomalies based on their shape, orientation, amplitude, or distribution that were marginally interesting, but usually these efforts were general of basic use, and interpretations were rudimentary. With the advent of digital data, filtering, and sophisticated data processing, in the late 1980s, profiles could finally be interpreted in a more refined and scientific manner than was previously possible (Conyers 1995; Conyers and Goodman 1997; Goodman 1994). The production of amplitude slice-maps led to a significant increase in interpretation power, but unless features defined in these maps were readily recognized, many of the images produced in this way were only larger maps of anomalies, often of unknown origin. Most users continued to analyze reflections in profiles to identify high amplitude reflections that “look like” buried features of interest. This procedure was adequate when correlating reflections to others in adjoining profiles. This laborious and often inaccurate technique identified buried features and estimated their depth and spatial placement within a grid. It is no wonder that the development of amplitude slice-mapping, which could process many profiles automatically and produce images with no manual interpretation was heralded by the community as a huge breakthrough. The slice-map method of data processing and interpretation then took hold, and newcomers to GPR had no good reason to go back to

individual profile analysis, if results could be obtained so readily using software for analysis and image creation.

Today we have a large variety of images that can be generated with our powerful software, many of which use a variety of data filtering and processing techniques that users can choose from and that produce some spectacular results. There are some teams of GPR users that closely guard their software, as its proprietary nature produces great esteem and often monetary rewards to their groups. It is said that even the members of those teams do not fully understand what is happening in their software, as it is controlled by a “guru” of the “black box.” As anyone who has read this book up to this chapter can tell, this is a method to which I am opposed, as I believe that all GPR users should understand all methods from the basics through all the data-processing steps to the production of images ready for interpretation. Only by appreciating all these aspects of their data and then choosing what to do in an intuitive and functional way can any dataset be interpreted in a complete and informed manner.

In this penultimate chapter of the book, I will therefore begin with some examples of the historical interpretive method of synthetic modeling, which many of us employed long ago to understand our complicated reflections. Few people use this method anymore, perhaps because everyone understands what radar waves do in the ground in ways that many of us were clueless about long ago? Or maybe his method may not be readily available to some users, or it is bypassed in the leap toward three-dimensional images? I continue to use it in a modified way in workshops I hold by projecting a reflection profile or two up on a white board and requiring participants to draw out in markers what they see. Even more important in this process we work as a group, delineating reflections that were produced from features in the ground that have been modified or distorted in important ways due to all of the variables associated with wave propagation, reflection, and recording that have been discussed so far in this book. This can be an excruciating process, as many users want to move directly to 3-D results, and not deal with the “minutiae” of radar waves. I make them persevere as these exercises are very useful in interpreting the results that come later from more “batch” processing.

In this chapter, I will then move to some important ways that reflection profiles can be interpreted to produce datasets not commonly employed in most software, which produce images that can be just as spectacular as amplitude slice-maps. These images are not only readily interpretable to GPR professionals but can be used to explain results to others who are not versed in the complexities of the “wiggles” used to create them. This reminds me of a comment Dean Goodman made many years ago when his career had advanced to very successful software development for commercial purposes. He told me that his goal was as a “cosmetician” for GPR reflections that would take the less attractive aspects of the method (the wiggles in raw data?) and “beautify” them for new GPR users. This he did, very successfully, and there are now many thou-

sands of GPR people all over the world who use his software. When I review papers for publication, I can immediately tell who has used Dean's software, as the images used are quite beautiful. I never went the "beautification" route and stayed with the less attractive raw data processed in steps, to address certain objectives in my GPR career.

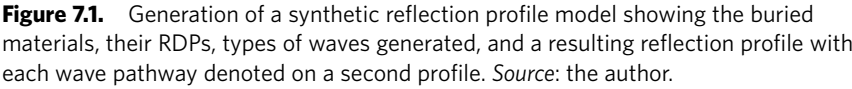
This chapter will then move to the amplitude slice-maps, as they are the "king" of the GPR images and used by almost all adherents to the method. Instead of showing examples of readily interpretable results, in this chapter I will instead show a few examples of how amplitude slice-maps can be used in different ways, concentrating on aspects of their results that may not be immediately recognized by casual observation.

## **SYNTHETIC GPR MODELS**

In the early days of GPR, Dean Goodman wrote a program that did synthetic modeling of two-dimensional reflection profiles in an attempt to model buried objects, stratigraphy, and important reflection surfaces (Conyers and Goodman 1997; Goodman 1994). This procedure comes directly from seismic data analysis also, where it is termed "forward-modeling." In the early days of GPR, many of us were confused about how reflections that were recorded over known buried features "looked different" in GPR reflection profiles than the features we knew were in the ground. Modeling therefore provided us with the ability to compare models of what is known to exist to the reflection profiles, to make direct comparisons. They provide the interpreter with an idea of what real-world GPR reflection data "should look like" and will allow more accurate interpretation of GPR reflection profiles once they are processed (Conyers and Goodman 1997; Goodman 1994; Goodman and Nishimura 1993). These can also be effectively used by interpreters to construct a model of known (or hoped for) stratigraphy and buried features prior to going to the field to determine if a GPR survey will be capable of delineating the materials of interest (Figure 7.1). Once models are constructed on the computer, they can also be quickly modified for different frequency antennas to determine the optimum equipment to take to the field for the depth necessary to resolve the features of interest.

After GPR data have been acquired and are processed into reflection profiles, models can then be readjusted to more accurately represent known field conditions as a guide in interpretation. When used in this way, they are a great benefit in making interpretations, especially in determining the origins of reflections visible in GPR profiles. Unfortunately, many GPR practitioners have tended to proceed directly in their data analysis to three-dimensional amplitude mapping as their first step in data interpretation, which often precludes an understanding of what is producing the reflections in the ground (Conyers 2012). Recently I have also neglected to use models, as I am perhaps a little overconfident in my ability to understand what radar waves do in the ground.





Computer-simulated radar profiles are generated by tracing the theoretical paths of radar waves during transmission through various media with specific RDP values for units, their electrical conductivities, and magnetic permeabilities (Figure 7.1). All possible reflections from modeled interfaces in the ground are considered (Goodman 1994), including multiple reflections and those that may refract from an interface to be later reflected to the surface. The two-dimensional geometry of the subsurface stratigraphy and archaeological features are programmed into the model to generate as close to a real-life case as possible. One helpful aspect of these models is that one can view all the radar travel paths, many of which never make it back the receiving antenna to be recorded, which may not be immediately important for an interpretation but useful in learning the complexity of radar wave travel paths.

As is often the case, two-dimensional reflection profiles can look significantly different from how the buried structures would appear in cross section if viewed in the wall of a trench. Most important, they are not at all like those most of us are used to seeing from other more common computer-enhanced images that use other wavelengths such as X-rays or computer tomography (CT) scans in medical imaging. This is because GPR profiles tend to be blurrier than medical images, and they contain many reflections that are produced in complicated ways as they are reflected and attenuated in the ground.

In most studies, the electrical and magnetic characteristics of sediment and soils must often be estimated and usually there is only a very basic geometry known of overburden units and the composition of any buried features of interest. These data, as can be best estimated, are then put into the computer

in a two-dimensional model that is a simplification of a vertical slice through the ground. The computer will use this information to predict reflectivity coefficients (Equation 3.2) encountered at various interfaces, energy attenuation with depth and within each unit, the velocity of radar energy in different layers, and the amplitude of reflections produced and received back at the surface (Goodman 1994). Various ray paths can be simulated depending on the cone of radiation being modeled for an antenna and the generation of multiple reflections. Refraction and transmission along modeled interfaces can also be simulated. Different frequency antennas and their generated waveforms and cones of propagation can be modeled.

When a model is produced, resulting reflections are plotted in two dimensions in the same fashion as standard GPR reflection profiles, and horizontal and vertical scales can be adjusted, just as with real reflection profiles. After analysis of any model, input parameters can be changed, and the simulation rerun until a reasonable match between the real and synthetic reflection profiles is obtained. This iterative process of parameter input and comparison to “real world” data is referred to as forward modeling in geophysical prospecting (Arixona et al. 2017; Powers and Olhoeft 1994, 1995; Zeng et al. 1995) and is a powerful interpretation tool.

Some possible wave paths that must be considered when creating a synthetic computer reflection profile shown for the example in Figure 7.1. These, and many other possible ray paths like them, must be programmed into the computer to generate an accurate model of what radar energy will do in the ground. In this example, there are four different media in which radar waves can travel through and be reflected from: air (not shown, but a small layer directly below the antenna), sandy soil near the surface, sandy silt below the sand, and a clay layer filling a trench. A synthetic reflection profile that would be produced for this simple model would therefore need to take into account waves that are reflected off each subsurface interface, but also ray paths that are partially reflected off some interfaces and partially transmitted and refracted across others.

Simulated waves will reflect off the interface between the sand and the sandy silt unit (Figure 7.1). Others will be transmitted through this interface and lost while in the clay in the bottom of the trench. That unit also reflects a good deal of energy. Most of the waves that are reflected from the clay unit are recorded but some reflect away from the surface antenna and are lost. In the real world, only a portion of the energy from each propagating wave would be reflected and refracted at each boundary, but for simplicity the model is set so that each radar ray has one distinct travel path. For instance, one wave will be reflected off the interface between the sand and the silty sand. Other waves travel at an angle from the surface antenna and is reflected from the edge of the trench at the clay interface. The waves of multiple reflections will then travel back into the ground to be re-reflected to the surface at the same interface.

There are many other paths within the transmission cone of the antenna, and all are simulated on the computer many thousands of times to arrive at a composite for all the reflected waves that arrive back at the surface antenna. The computer then moves the antenna along the modeled ground surface, and the process is repeated for many surface antenna locations along the programmed transect. Software predicts the time at which the modeled waves return to the receiving antenna on the surface and records their resulting amplitudes. The final model (Figure 7.2), shows the resulting “synthetic reflection profile” using these parameters. A comparison can then be made to a reflection profile from a similar feature in the real world. In this model the opposite side of the canal is producing the highest amplitude reflections and reflections, which are recorded directly below the antenna and some distance from where they were generated on the far side of the canal. The edges of the canal are barely visible in the modeled profile as they are a surface that either does not reflect because waves pass by it on a parallel trajectory or reflect away from the surface antenna and are not recorded.

Details about the electromagnetic theory involved and the mathematical description of all steps in the model is given in Goodman (1994). In real field conditions, numerous out-of-plane reflections should also be taken into account (Carcione 1996; Grasmueck 1996; Leckebusch 2003), which is not done with most synthetic modeling. Much more complicated three-dimensional modeling techniques have recently been developed for seismic reflection data used in petroleum exploration, which may someday be applied to GPR studies.

## **SYNTHETIC MODELING APPLICATIONS**

In the canal/trench model case (Figure 7.2), if the synthetic model were not constructed and analyzed, the reflections beneath a feature of this sort might be mistaken for a point source hyperbola derived from something buried in the bottom of the trench, or perhaps some other type of buried feature below the trench. An actual reflection profile from a prehistoric irrigation canal in southern Arizona (Figure 7.2) is exactly like the modeled feature and illustrates how important models are for understanding complex features in the ground (Conyers 2012b). Without the model, the ancient canal from southern Arizona might have been interpreted differently.

Another model that illustrates how layered materials of varying thickness, with differing RDP, produce reflections is shown in Figure 7.3. In this model, the flat interface between Layers 2 and 3 represents a buried living surface and is the interface of interest. The complexity in this model arises from the differences in RDP and thickness changes in the two overlying units. The thick section of material with a high RDP in Layer 2 will slow the radar energy as it travels vertically, from the ground surface to the interface of interest, and back to the ground surface. The thinner section of this high-RDP material in the middle of the model illustrates how radar energy will travel from the ground surface

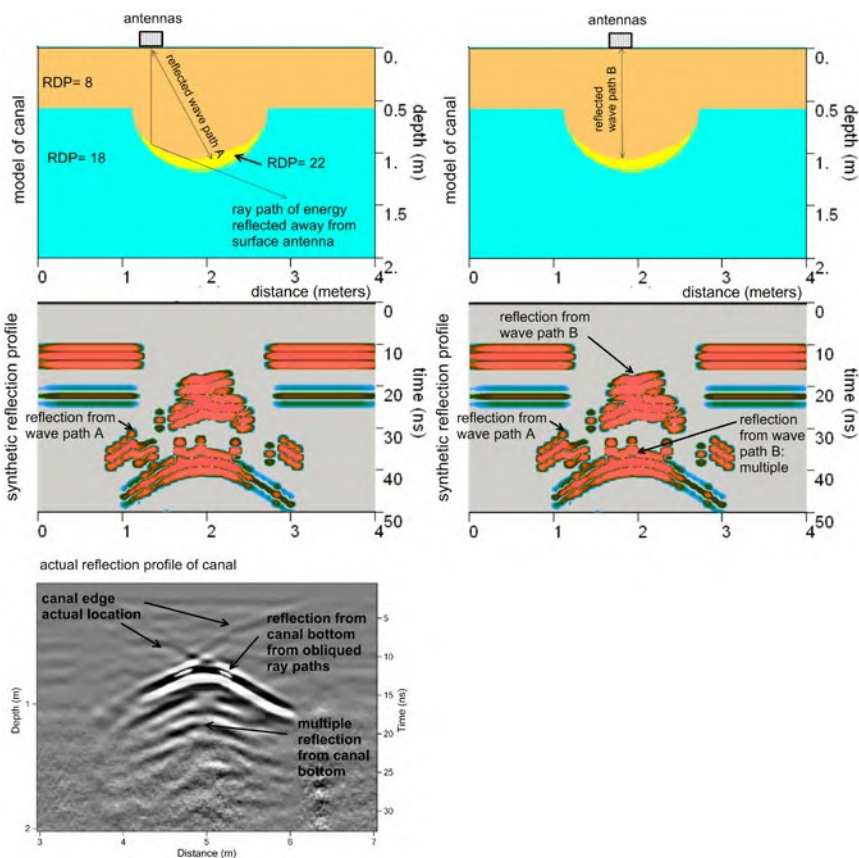


**Figure 7.2.** Synthetic reflection profile of a buried canal, with a reflection profile of a real canal from southern Arizona at bottom for comparison. *Source:* the author.

to the interface of interest, and then back to the ground surface in a shorter amount of time than at the edges because it is traveling for less distance in lower-velocity material. The resulting reflections generated from the interface of interest at the top of Layer 3, when plotted in two-way travel time, will therefore be distorted due to these velocity and thickness differences in the overlying unit. Under the area where a thinner section of low-velocity material (higher RDP) is modeled, the lower interface will appear to bow upward. This upward and downward bowing of the lower interface is caused only by differences in the velocity and thickness of the overlying material, creating the illusion of an undulating surface of the interface between units 2 and 3. This is referred to as a “velocity pull-up” in one area and “pull-down” in the other (Figure 7.3). This is exactly what is visible in a reflection profile from a known horizontal feature that has materials overlying it of different velocity (Figure 7.4). In this case, the

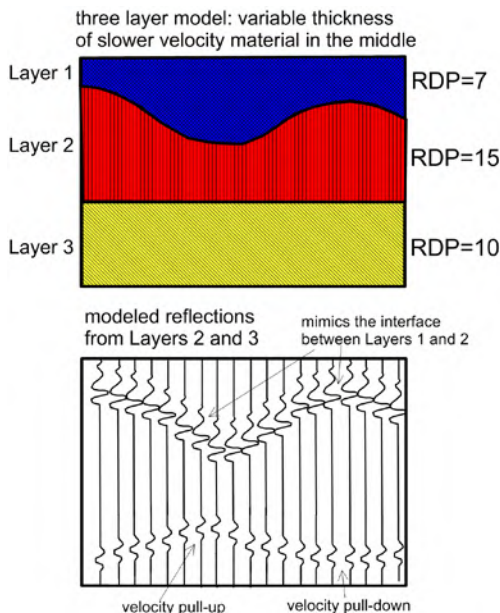


**Figure 7.3.** Synthetic reflection model of a three-layer system where velocity pull-ups and pull-downs can be seen due to the variations in thickness of a unit overlying a flat horizon. Source: the author.

velocity changes in the overlying material are caused by water saturation variations. The reflection recorded in the field was generated in a profile that was located directly above a known perfectly horizontal pipe. The material overlying the pipe is windblown sand that has a very consistent composition and therefore velocity differences are only caused by water saturation variations.

A velocity pull-up like the model in Figure 7.4 would also be noticeable in the field below a large, buried void space. A cave floor reflection that is known to be horizontal is “pulled-up” due to the increased velocity of the waves traveling in the void space. A pull-down could also occur where localized conditions create a decrease in radar wave velocity, possibly due to abrupt stratigraphic or archaeological change laterally along a feature or a possible change in overlying soil conditions. A fluctuating water table, or changes in the water saturation of buried units located above the water table, can also slow radar waves and distort underlying reflections due to localized variations in velocity.

The model in Figure 7.3 and the undulating pipe, which is horizontal (Figure 7.4), demonstrate one of many pitfalls that interpreters of GPR data can encounter when there are changes in velocity within the ground overlying buried materials of interest. These velocity variations that affect the geometry of reflections are found in almost all field conditions but are much more pronounced when mapping caves or tunnels with large openings that contain nothing but air, where radar waves travel at the speed of light, creating very distinct pull-ups (Conyers 2012).

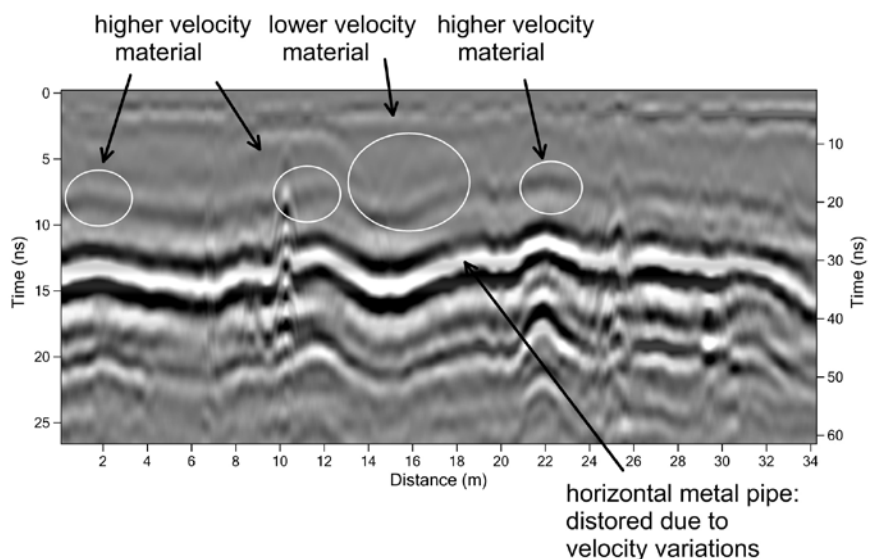


**Figure 7.4.** Example of planar reflections from a perfectly flat pipe, which varies in recorded depth due to subtle variations in the velocity of overlying sand beds. *Source:* the author.

In addition to these problems, because of complex refraction and transmission within subsurface layers, radar energy may not be transmitted at all through some types of materials because of total energy attenuation or complete reflection. These “un-illuminated” regions that occur below these types of materials are referred to by some as “shadow zones” (Goodman 1994). They are areas where no reflections occur even though features that could potentially reflect energy are present. Often these and many other “non-intuitive” reflection and transmission scenarios would not be recognized without first generating synthetic models of real-world conditions and studying their outcomes.

A relatively simple reflection profile of a buried pit house shown in Figure 3.22 was modeled with a clay floor, a hearth incised in that floor and storage cistern with a hard bottom (Figure 7.5). The model shows that the structure’s walls would not be visible as they are vertical and don’t provide a reflection surface, or if any waves encountered them, it would be reflected away from the surface antenna (like the canal edges discussed above). The floor and the hearth in the floor provided distinct reflections, but storage cistern reflections (if generated) would be obscured by the distinct reflection hyperbola generated from the hearth and floor (Figure 7.5). An actual pit-house in the American Southwest much like this model (Figure 3.22) was cored to confirm its presence and to evaluate the properties of its compacted and partially baked floor and the sediment covering (Conyers and Cameron 1998). It is not known if a storage

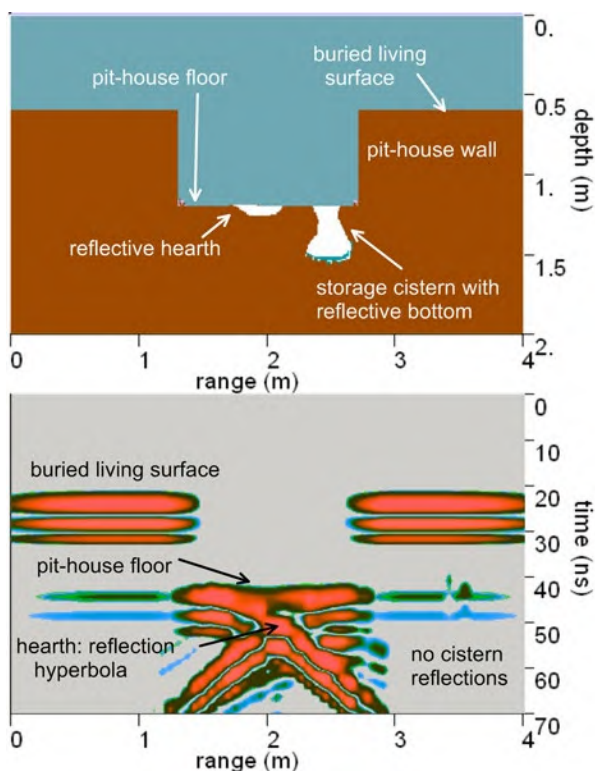


**Figure 7.5.** Synthetic reflection profile of a buried pit house with a floor, hearth, and sub-floor cistern. The house walls are invisible as they do not provide a surface to reflect waves. The hearth produces a very strong reflection hyperbola. The cistern is invisible and likely overwhelmed by the very high amplitude reflection of the floor. Source: the author.

cistern exists at this house, as the model shows it would be not visible in a GPR profile. Many similar floors have been discovered with GPR in the American Southwest, and many display these types of reflection features (Conyers 1998, 2021; Conyers and Cameron 1998; Conyers and Osburn 2006).

A more complex reflection profile was collected along what appeared to be a buried floor, but this reflection feature was quite complex and there were a number of other reflection features, whose origin was unknown (Figure 7.6). This site in the Middle East was known to contain buried floor features with architectural rubble overlying them. A model was generated and modified several times in an attempt to replicate the actual reflection profile. The best fit between the model and the actual reflection profile was a reflective floor (known to exist in this area from nearby excavations), with architectural materials overlying it, and a near-surface clay layer (also known from other excavations).

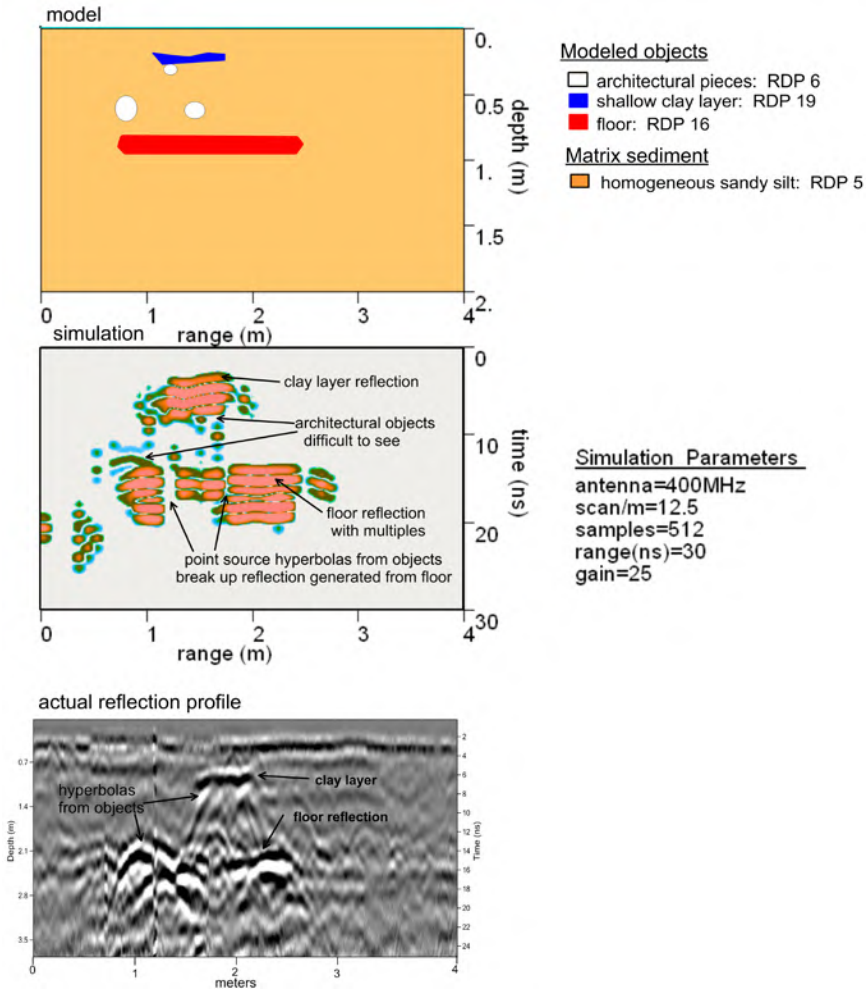


**Figure 7.6.** Example of a synthetic model that was adjusted to mimic a reflection profile collected at a Roman site at Ashkelon, Israel. The various materials in the model were adjusted until an approximate view corresponded to the actual reflection profile to determine the best fit for what is visible. *Source:* the author.

The distortions in the floor could be explained by the interference of hyperbolic reflections from the overlying objects, and the shallow low-velocity clay layer. The use of modeling in this fashion, to interpret features after returning from the field, provides a useful method for gaining confidence in interpretations after data are collected. In this case some limited excavations were crucial in providing information about what kind of features would be expected in this



area, so that the model could provide images of the most probable features in the ground visible in reflection profiles.

## **HORIZON PICKING**

An important software development that can help with reflection profile analysis and three-dimensional mapping is “automatic picking,” which allows the software to follow reflections in profiles and save important information for later mapping. This system assumes that an interpreter knows the origin of one or more reflections visible in profiles, and that there is a good reason to study the orientation and other factors of this unit in the ground. This method can take some of the drudgery out of the manual interpretation of profiles, with the final product being computer images and models that are very useful. Most of these automatic-picking programs first allow an interpreter to choose horizons in the ground that are important. They are displayed on the computer screen, and a mouse is used to identify a horizon at one end of the profile. The software will then “follow” that horizon across a profile, usually by choosing a particular peak or trough of the recorded wave. In this automatic picking, the generated horizon often gets off track, as very few layers are continuous along a profile. When this happens, the interpreter must recognize this and place the pick back to the correct wave to be followed farther along the profile. That correcting then allows the software to proceed, until all the pertinent points (usually one for every reflection trace) are saved for each profile in a grid. Those recorded values can be defined in advance as two-way travel time or wave amplitude, or both. Recorded values can also be programmed to be an average of amplitude in a package that included reflection above and below the “pick” as defined by digital samples or nanoseconds. These large datasets are then saved in a spreadsheet with multiple columns that contain x and y locations for each data point, and multiple z columns that are the chosen parameters of the reflections.

When velocity from the surface to the “picked” reflection is known, the picked radar travel times can be converted to depth and a detailed dataset from which a variety of images can be constructed (Conyers 1995; Conyers and Goodman 1997: 137; Conyers et al. 2013; Imai et al. 1987; Milligan and Atkin 1993; Nunez-Nieto et al. 2014; Rees-Hughes et al. 2021; Schneidhofer et al. 2017). This method, which is common in seismic data analysis, but rarely performed with GPR, can provide very important three-dimensional images of the ground. Those images are unlike the usual amplitude slice-maps and an important addition to any study that has complicated layers in the ground that vary in depth across a grid.

An example of this kind of mapping was performed along the west coast of Portugal where a buried living surface (Figure 7.7) was studied (Conyers et al. 2013). At this site, a few stone artifacts of the Magdalenian Age (the late Ice Age) were found on the surface, near where some heavy machinery had scraped off overburden to a geological unit that could be identified. That visible



**Figure 7.7.** Outcrop of the Jurassic bedrock and the overlying sand just to the west of where artifacts were found on the bedrock. These sediments were then “picked” to produce a buried surface map on that sediment layer. *Source:* the author.

layer had a unique color and texture that was the same as bedrock visible in exposures a few hundred meters away (Figure 7.7). There it was identified as a Jurassic-age unit. At the time our crew was considering doing this survey, a long lunch and work elsewhere in the morning had passed, which gave us only a few hours to collect the data. We therefore were only capable of collecting a grid 30x40 meters in size, with reflection profiles separated five meters. That large transect spacing is much too “course” a grid for any amplitude mapping or the production of other typical images, so we were left with only being able to do a manual interpretation of the reflections. Both 400 and 270 MHz antennas were used (Figure 7.8), as resolution of the Jurassic horizon was unknown (Figure 7.9). The horizon of interest is the Jurassic bedrock surface as we had studied it to just to the west, and there it is known to have been the ground surface (perhaps capped with a thin soil) toward the end of the Ice Age, when Magdalenian hunting and gathering people occupied this area. The landscape was then covered by windblown sand and buried by many meters of sediment during the Holocene period.

Reflection profiles clearly showed an incised bedrock with channels cut into the Jurassic bedrock (Figure 7.8). Both 400 and 270 MHz profiles accurately portrayed this horizon as a very high-amplitude reflection. Both were used in the interpretation, as it was not known which would produce the best results. In the

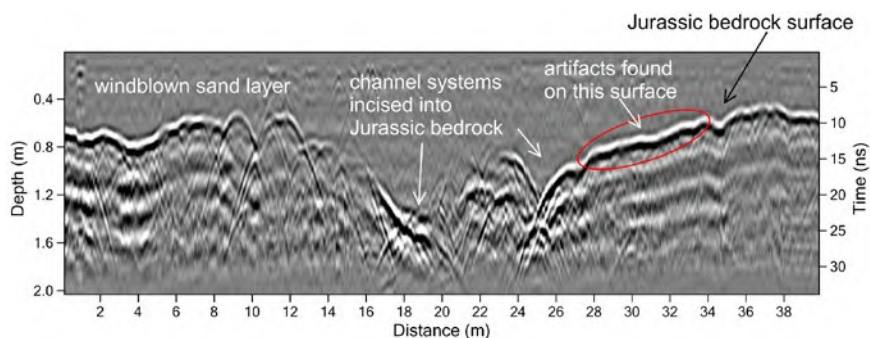


**Figure 7.8.** Reflection profile a few meters adjacent to where artifacts were found on the Jurassic bedrock surface. The buried living surface is visible as a high-amplitude planar reflection and fluvial channels are just to the west, visible in this 270 MHz reflection profile. *Source: the author.*

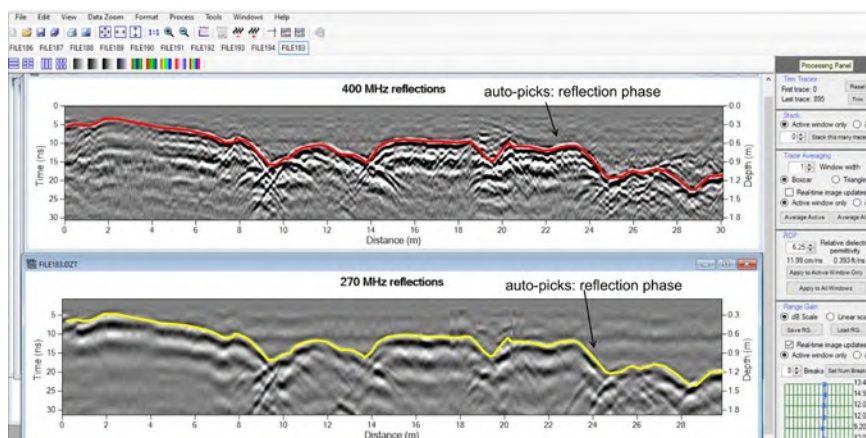


**Figure 7.9.** Automatic picking of the Jurassic reflection using both the 400 and 270 MHz reflection profiles. *Source: the author.*

reflection profiles the 270 MHz images were “less busy” than those recorded with the 400 MHz antenna, and it was thought initially those profiles would produce more generalized and averaged image of this buried surface. Interestingly, it was later found that both frequency reflections, when auto-picked, produced almost exactly the same resolution of this buried surface. At the time, I always thought that the 270 MHz waves, which are known to spread out more in their propagation cone, would average reflections that returned to the surface antenna from a broader area and therefore produce a less accurate surface to map the buried landscape. After the picking from both frequencies, however, it was found they were almost identical in recording the depth of that reflection. This needs to be studied more, but my preliminary thought is that while both antennas spread out energy in a conical pattern, most of the reflections that return to the ground surface to be recorded must be coming from directly below the antenna. Those that spread out more to travel along more complicated trajectories lose energy, are attenuated, or reflected in ways that generate hyperbolas or other unusual reflections. These types of reflections are quite visible in the 400 MHz profile (Figure 7.7) as reflections on either side of the base of channels. This is exactly what the model in Figure 7.2 shows with the canal. The important conclusion is that by picking just the surface of the Jurassic layer, and ignoring all the other reflections, both frequencies have almost the same accuracy when recording the reflection from the surface of interest. Easier to interpret reflection profiles for using this auto-picking method might have been created by migrating the data. That was not done here.

Profiles were imported into a software program for “auto-picking” (Herron 2000) (Figure 7.9). All were visually analyzed first, and the Jurassic bedrock reflection at the beginning of each profile was picked (on the left when viewed on the computer monitor). A wave peak was chosen for the auto-picking procedure (Figure 7.9). This was done for both 400 and 270 MHz reflection profiles. Each profile’s “picks” were exported and included in a very large spreadsheet that had unique x, y, and z coordinates and the picked data for the grid as a whole. The depth (as measured in two-way travel time) was the primary pick for this study.

Once these values are available, a variety of images can be produced. These were all done in the Surfer software program. A simple contour map shows a readily understood image of the buried Jurassic ground surface below the present-day ground surface, much like a topographic map (Figure 7.10). That image could also be visualized as an image map where the elevations can be assigned colors, which can sometimes be helpful. Most interesting was a three-dimensional surface creation colored with high areas as brown and green, and lower areas in blue (Figure 7.10). The program can shade this surface differently, and various angles of artificial sunlight are applied while the image is moved around and tilted. All provide different looks of the landscape of this buried late-Ice age land surface. All these images are quite good, and when the

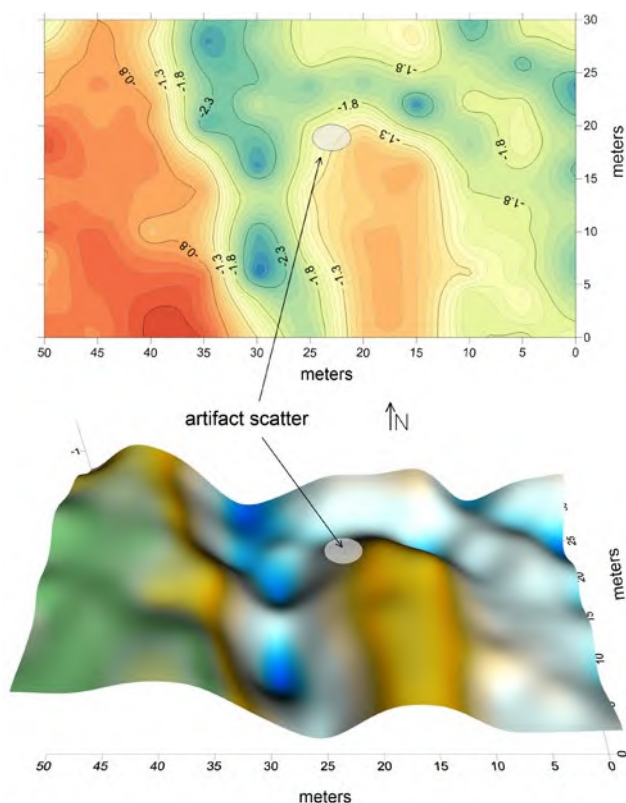


**Figure 7.10.** Contour map (top) of the Jurassic surface auto-picked (Figure 7.9) and a three-dimensional image of this surface (bottom). The artifact scatter is placed on this surface to help in interpreting late Ice Age human behavior in this area of western Portugal. *Source:* the author.

artifact scatter that led us to this area in the first place is placed on this buried landscape a variety of hypotheses about human behavior can be created.

It was known that this area was on the western flank of a river valley during the late Ice Age, with lakes and a broad floodplain just a few hundred meters to the east. My favorite hypothesis is that this was a good place for hunting people to stop and rest when pursuing animals on the floodplain, which was easily visible to them from this location. These people were hidden by the small hummock from those grazing animals, and they could perhaps wait here for their prey to come closer. At the same time, they sharpened their tools (therein the artifact scatter), and perhaps they had water nearby in the small creek to the north and west. Others have come up with different hypotheses, and we will never know for sure. But only a short afternoon of GPR collection and some auto-picking of an important horizon and then mapping that surface in three

dimensions tells us much more about this site than was known from just a few artifacts scattered on the ground surface. It also shows the utility of specific horizon-mapping that can be done either manually or automatically (with some manual adjustments along the way) to create important images of the ancient, buried landscape.

A similar project was done in Idaho, United States, where a very ancient site was discovered, which may be one of the oldest in North America (Davis et al. 2019). One horizon, termed LU-6, is visible in the excavations (Figure 7.11). This was a living surface on which people camped and performed other activities. It was high in organic materials, compacted, and contained artifacts. This buried soil horizon was of interest, and it could be correlated with a high-amplitude reflection visible in 270 MHz reflection profiles just to the east of the excavations (Figure 7.12). That horizon was picked in a large grid of data consisting



**Figure 7.11.** Top of a compacted, organic-rich horizon called the LU-6, which was a living surface in the last Ice Age in Idaho. *Source:* the author.

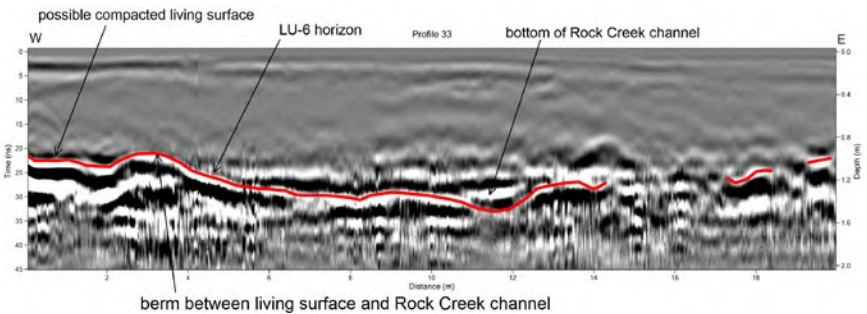


**Figure 7.12.** Reflection profile of the LU-6 horizon visible in Figure 7.11 east of the excavations where it was uncovered. *Source:* the author.



of profiles spaced one meter apart. The three-dimensional contour map of its depth below the present ground shows the site was on a high area to the west of a small river system, which flowed out of the highlands into the larger Salmon River to the south. When this buried landscape was viewed in three dimensions, it shows what an ideal camping place was chosen by these early American inhabitants, on the high spot adjacent to a river, and facing south and east for maximum sunlight exposure (7.13).

Another example that shows how the individual profile analysis is far superior to producing standard amplitude maps comes from southern Arizona, where it was known there were irrigation canals in the vicinity. A model constructed for a canal (Figure 7.14) indicates that the reflection likely to be recorded from a feature of this type if sliced and displayed in traditional amplitude slice-maps would be very complex and unlikely to produce an image of the canal.

A grid of profiles was collected north of where a canal had been excavated on the east bank of the Santa Cruz River, near Tucson, Arizona. Reflection profiles displayed reflections much like had been predicted from the model (Figures 7.15). A series of amplitude maps were created anyway every 10 cm in horizontal slices going through where the canal was visible in the profiles (Figure 7.16). This displays a linear high-amplitude feature on the south, which suggests a canal. But to the north, the canal is invisible in any of the depth slices. Later, with some study, it was found that the high-amplitude feature to the south was generated from sandy sediment that filled in the canal, but only in that portion of the linear trough.

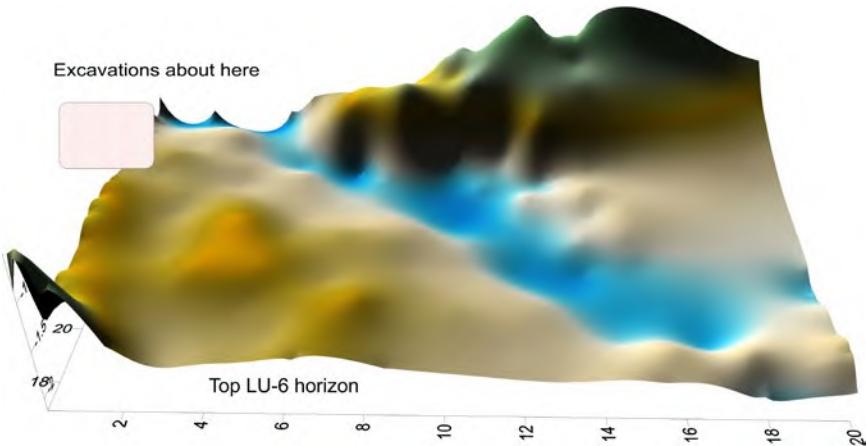


**Figure 7.13.** Three-dimensional surface of the LU-6 picked horizon to the east of the excavations showing a small river system, now buried, which existed here in the late Ice Age. Source: the author.

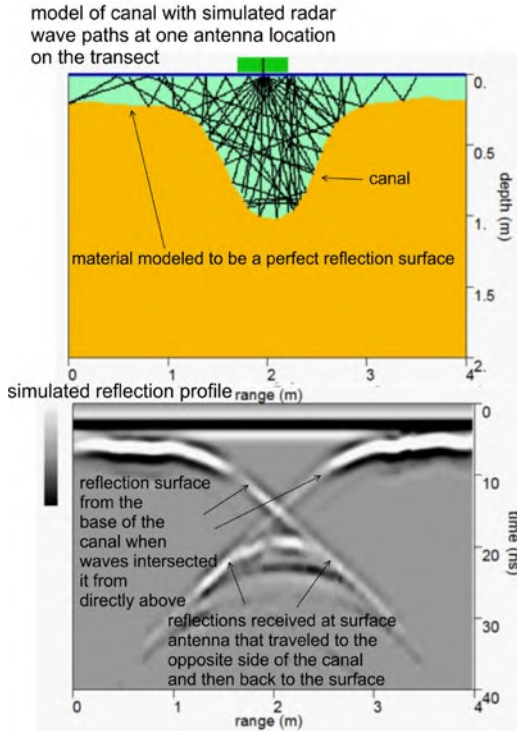


**Figure 7.14.** Synthetic reflection profile of a buried Hohokam canal in southern Arizona. The opposite edges of the canal are visible as hyperbola-like reflections lower in the time-window. The edges of the canal are very low in amplitude. *Source: the author.*

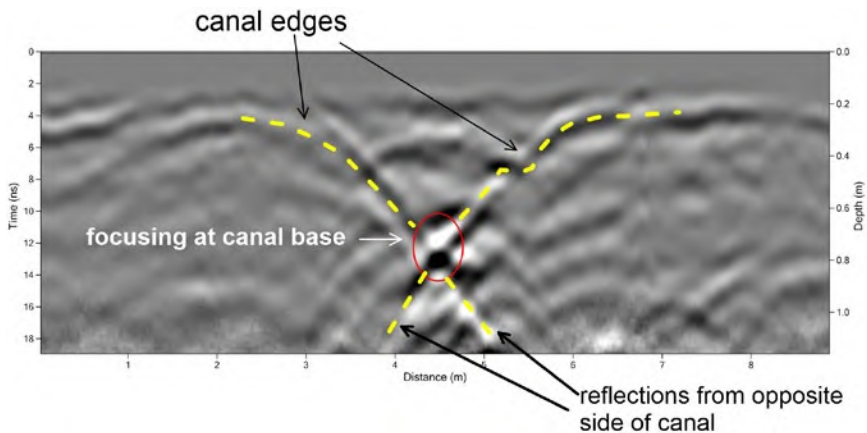


**Figure 7.15.** Reflection profile that mimics the synthetic model in Figure 7.14. This was used as a basis for hand-picking the canal in all profiles in the grid. *Source: the author.*



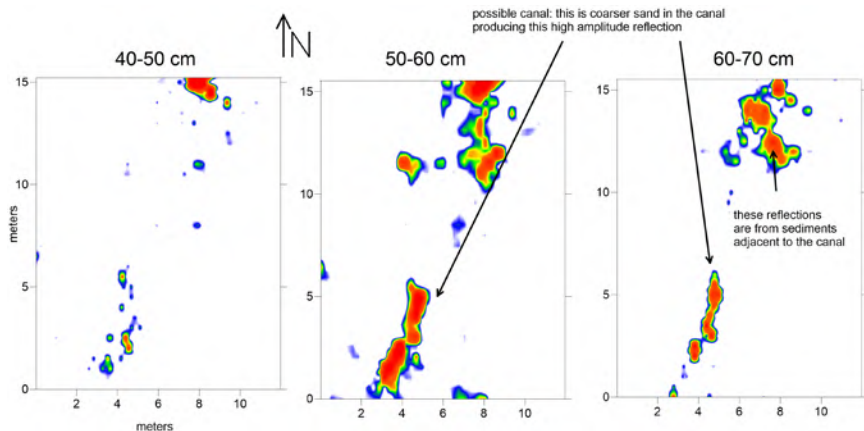


**Figure 7.16.** Amplitude slice-maps were of little use in this grid, as the canal edges are very low in amplitude and do not show up as higher-amplitude reflections. Only the southern part of the canal, filled with sand, is visible in this display. *Source:* the author.

All reflection profiles were analyzed individually, and the edges of the canal were hand-picked. In these profiles the auto-picking method will not work, as the reflections generated from the actual canal edges are too low in amplitude to be “followed” automatically. This took some time to produce a three-dimensional dataset of the canal sides and its banks. That large spreadsheet of the canal depths was imported into Surfer, and an image of the canal displayed (Figure 7.17). It turned out to be much more complicated than we imagined from only viewing the profiles. The detailed mapping of its edges showed places where the sides of the canal had slumped into the main channel and displayed how it is more sinuous than we had initially thought.

A more complicated three-dimensional mapping project was to image a cave, containing hominid and perhaps modern human remains at Atapuerca, Spain (Bermejo et al. 2020; Qawasmeh et al. 2021). A grid of 270 MHz reflections was collected over the top of the cave. It is accessible and could be entered and studied (Figure 7.18). The cave has a relatively flat floor, which consists of cemented rubble from a ceiling fall, while the intact ceiling is broad and arched, sloping down into more restricted areas on two sides.

This grid of data was used for a workshop I lead a few years ago, and all participants were required to figure out various ways to map the void, with the final product to use GPR to estimate the volume of the void space. A variety of the standard amplitude maps that most programs use was employed by some of the participants, with some using complicated procedures yielding a variety of three-dimensional images of the cave (Figure 7.18). None of these standard amplitude images were successful, as it is not a visualization of the amplitudes

**Figure 7.17.** A three-dimensional surface of the canal produced from the hand-picked canal edges in individual profiles. Source: the author.

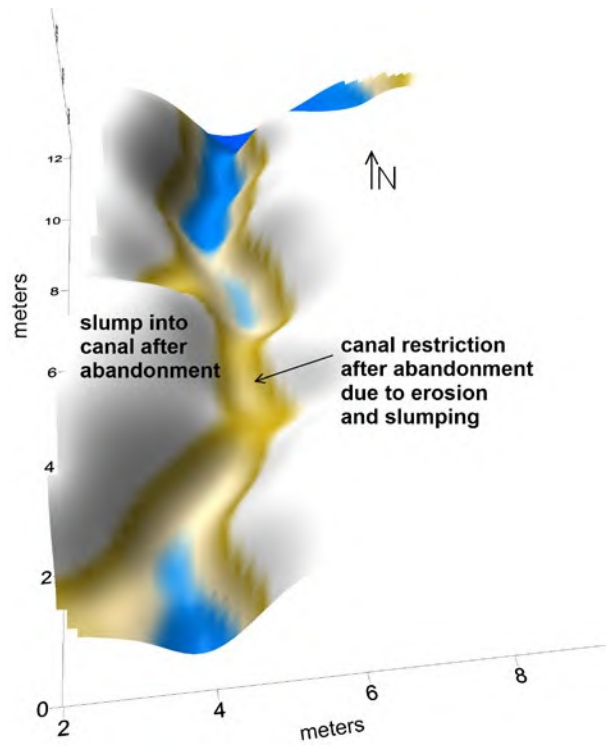


**Figure 7.18.** Inside the Cueva Peluda at Atapuerca, Spain. The GPR grid was collected directly overhead. Source: the author.

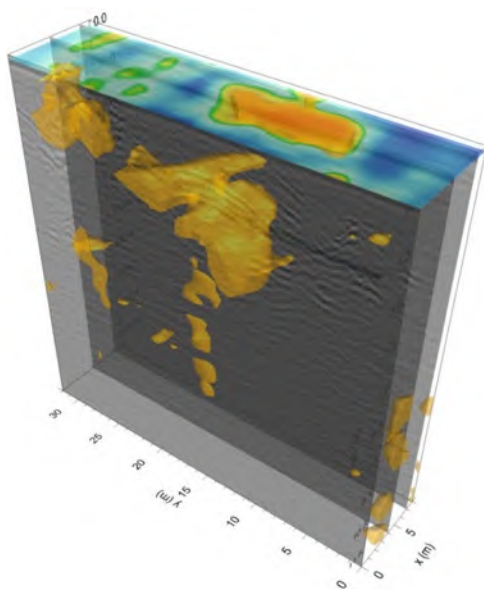


**Figure 7.19.** Three-dimensional images produced by GPR-Slice software of the cave. *Courtesy of Dean Goodman.*

that is necessary, but a “picking” of the individual reflections corresponding to only the ceiling and the floor.

The ceiling reflection was first identified as the wave generated from the stone-air interface that generated a reverse polarity reflection (Figure 7.20). This happens whenever propagating radar waves speed up at an interface, and the first deflection of the reflected sine-wave that moves back to the receiving antenna deviates in an opposite direction from the wave that is propagating in the ground.

Once the ceiling-air reflection was identified, it was picked in all profiles (Figure 7.20) in the grid, and depth was tabulated. The same was done for the floor reflection. This reflection generated from what was known to be an almost flat floor appears bowed-upward in the reflection profiles (Figure 7.20). This is a standard velocity pull-up caused by the radar waves moving through air from when they exited the rock ceiling and then reflected off the floor, traveling back again in the void at the speed of light. Those waves then moved back into the ceiling rock back to the surface to be recorded. For the void space volume to be correctly accounted for, the floor reflection must be placed back into its correct depth, and all the picks for the floor needed to be adjusted for the distance that each trace traveled in the void. This is easily adjusted once all the picks are put into a spreadsheet in two-way travel time. The times for the ceiling can

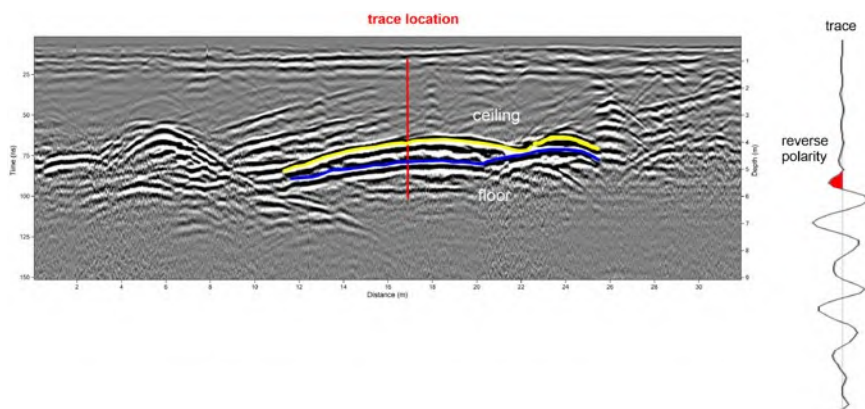


**Figure 7.20.** A reflection profile of the cave, showing both the ceiling and floor reflections. The ceiling is visible in individual traces by a reverse polarity reflected wave. The floor is distorted by a velocity pull-up. *Source:* the author

be corrected to depth in the ground when the velocity is used for wave travel in the bedrock. But the times for the floor picks must be corrected using the speed of light for the waves traveling in the cave void. Once these corrections are made, an image of the cave can be created, showing both the ceiling and the floor (Figure 7.21). This was done in Surfer, which has a mathematical ability to determine the void space between two distinct horizons. For the area mapped, this volume was calculated at 396 cubic meters.

## AMPLITUDE ANALYSIS IN SLICE-MAPS

As the primary goal of many GPR projects is to identify the size, shape, depth, and location of buried features within a geological matrix, it is no wonder that many users move from the more time-consuming horizon picking and move to amplitude slice-maps first.

In the early days of GPR, when all we had was two-dimensional reflection profiles as our basic data, the concept of doing a “batch processing” of many profiles all at once was a dream. Many of us knew it was possible, as the seismic geophysicists had been doing it, but no software was available to do this kind of image production until the early 1990s (Conyers and Goodman 1997; Goodman 1996; Goodman et al. 1998). As this technique became available, we all naturally migrated to create slice-maps to view the ground displaying reflected wave amplitude differences both spatially and with depth in a grid (Conyers 2012; Conyers et al. 2019). In this process, what is being imaged are the amplitudes of reflected waves (and their recorded depth in the ground), which are proxy measurements of the differences in materials at buried interfaces that reflect the radar energy (Neal 2004; Neubauer et al. 2002; Novo et al. 2012).

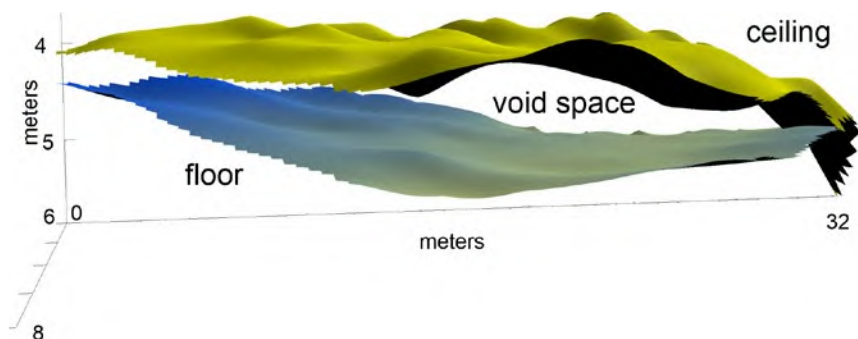


**Figure 7.21.** Three-dimensional analysis of the cave showing the floor placed back into its correct position after being adjusted for wave velocities within the void space. Source: the author.

With multi-channel systems, there can be millions of reflections in a study area, which is analyzed in this same way (Gaffney et al. 2012; Trinks et al. 2010). This slicing method can produce three-dimensional packages of relative amplitudes analyzed in bulk, quickly producing maps and images of important high (or sometimes low) amplitudes that were generated from buried features or related geological features of interest (Figure 7.22). The colors or shades of gray can be adjusted to highlight the amplitudes that are important, in much the same way that gains of reflected waves are adjusted in profile analysis. Some systems even allow for amplitude slice-maps to be created while data are still being acquired in the field, producing maps of the ground that expand as data are being saved and processed (Linford 2014).

An analysis of the spatial distribution of the amplitudes of reflected waves is important because it is an indicator of subsurface changes in lithology or other physical properties of buried materials. The greater the amplitude of a reflected wave, the greater difference in physical and chemical properties of materials at a buried interface reflecting that radar energy. Areas of low-amplitude reflections usually indicate a uniform matrix material or soils, while those of higher amplitude denote areas of high subsurface contrast such as contacts between the matrix and buried archaeological features, voids, or important stratigraphic changes. To be readily interpreted, amplitude differences are usually analyzed in horizontal slices that examine only changes within specific layers in the ground (Figure 7.22).

Each amplitude slice of a certain thickness is comparable to an arbitrary excavation level, except using GPR, data on each level consists of a spatial representation of reflected wave amplitudes instead of sediment, soil, or feature changes and associated artifacts. Software is now available that can display many slices at once, and the pertinent reflection profiles in any desired area of

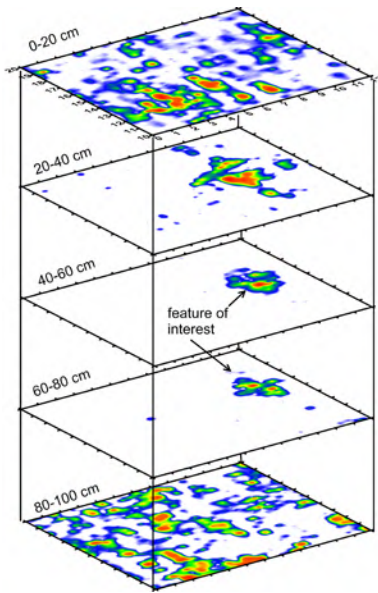


**Figure 7.22.** Creating amplitude slice-maps of a grid in Tennessee. Source: the author.

a grid can be also displayed, producing both three- and two-dimensional views of the ground.

A simple analysis is from a layer of shells in a midden, which contrast well with the surrounding sand and silt (Figure 7.23). The shell layer produces a velocity contrast in the propagating radar waves, generating higher amplitude reflected waves, which are readily visible in amplitude slice-maps. In this example from Tennessee, the feature was excavated, and the GPR-mapped surface corresponded very well to the shell layer.

Distinct amplitude maps, such as those shown in Figure 7.22, are used as an example of what GPR can do, and there is always the hope that similar data processing and image production at less-definitive sites will produce similar results. Often this is not the case. Although amplitude slicing can be definitive, if the buried materials of interest are within a package of ground with complex stratigraphic layers, they will often be obscured or so busy that nothing is immediately visible. I have found that in most cases, it is a mistake to produce only generic slice-maps, which all software programs can now produce very quickly, in the hope that what one is searching for will immediately appear in the resulting images. Even in the distinctly successful images, there are many still hidden features that are effectively filtered out. For instance, in the temple example (Figure 1.3), differences in floor-construction materials, and the location of trenches that were used to dig out the cut-stone to recycle, were visible only during profile analysis. So, while the production of amplitude slice-maps can be made automatically (like having photographs developed from film like





**Figure 7.23.** The distinctive feature in the amplitude slice-maps in Figure 7.22, when excavated. It is a large shell deposit. *Source:* the author.

in the old days of photography), there can be many important features that remain invisible if only this method is used. Data always needs to be studied also in individual reflection profiles that were used to produce the maps. Depending on what this reveals, reflections can be processed and filtered in informed ways to improve the resolution of the raw data and produce more exact images.

It is important that slices programmed to sample a large three-dimensional area of ground do not cross over buried interfaces (if possible), as the resulting amplitude maps will generate amplitude features of this interface in different depth slices as the buried surface crosses through different slices (Figure 7.24). When a high-amplitude layer or other buried feature is found at different depths and then sliced horizontally, reflection features can be produced that are almost meaningless, as they are one reflection from one horizon found in different depth levels (Figure 7.25). In the same way, if a smaller feature of interest is in different slices chosen for mapping, it will be found in different maps of different depths (Figure 7.22). There is nothing wrong with viewing features this way in different depth slices, as it is how materials are exposed in different levels in standard excavations. The GPR amplitude maps only need to be annotated so that one feature visible in different slices is identified.

Amplitude slice-maps are usually made in equal time intervals, with each slice representing an approximate thickness of buried material in the ground. These maps always first constructed in radar travel times (and are therefore termed time-slices), which can later be converted to depth to become depth-

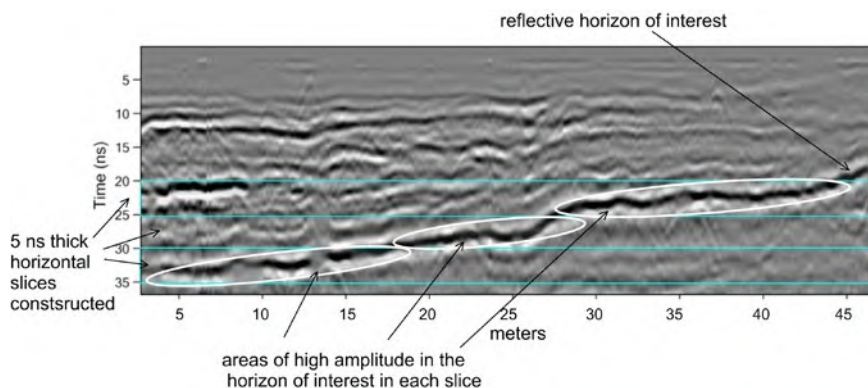


**Figure 7.24.** The possible errors that occur when horizontal slices cut across a surface of interest. This is a buried living surface at Ceren, El Salvador. *Source:* the author.

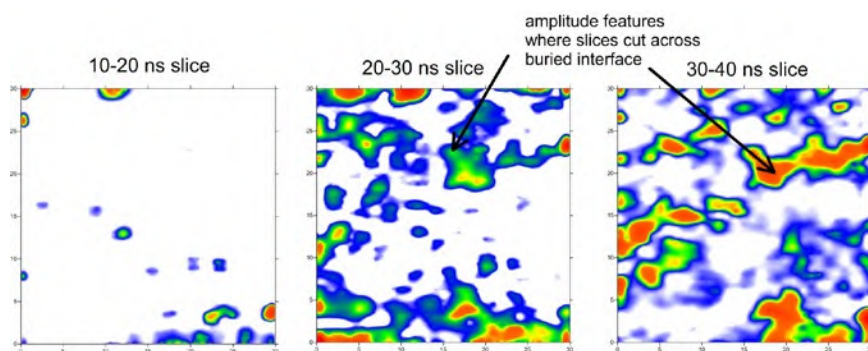


**Figure 7.25.** When the amplitudes from the buried living surface in Figure 7.24 are displayed in amplitude slice-maps, the visible features display that one surface was located in different depth-slices. This results in features that cannot be readily understood unless the slice geometry is recognized and understood. *Source:* the author.

slices, if velocity analysis has been performed. Viewing amplitude changes in a series of horizontal time slices in the ground is therefore analogous to studying geological and archaeological changes of equal depth layers (Conyers et al. 2002; Goodman et al. 1995; Malagodi et al. 1996; Milligan and Atkin 1993). When amplitude features in each slice are correlated to known buried features and stratigraphic changes that might be available for study in nearby excavations, extremely accurate three-dimensional maps of a site, broken down into levels, can be constructed.

A grid of GPR-reflection data may be sliced very thinly and viewed as a video, with slices projected sequentially on a computer screen, as layers are



“uncovered” from the ground surface to some depth in the ground (Conyers et al. 2002; Grasmueck et al. 2004). The precise location of all reflections in the ground, if processed into many sequential slices, can also be analyzed as a three-dimensional “cube” of data (Goodman and Piro 2013). Certain amplitudes can then be rendered to produce realistic images of the subsurface as three-dimensional objects called “isosurfaces” (Bornik and Neubauer 2022; Conyers et al. 2002; Goodman et al. 1998; Heinz and Aigner 2003; Leckebusch 2003; Leckebusch and Peikert 2001).

Amplitude slice-maps need not be constructed horizontally, or even in equal time intervals. They can vary in thickness and orientation, depending on the archaeological and geological questions being posed (Conyers 2010). Surface topography and the subsurface orientation of features and stratigraphy of a site may sometimes necessitate the construction of slices that are neither uniform in thickness nor horizontal. They can also be constructed to follow one distinct horizon (Conyers and Goodman 1997).

When many grids are collected adjacent to one another, there can be problems with “edge matching” to produce large-scale amplitude maps. The variations in reflected wave amplitudes between grids can be caused by different collection procedures and changes in equipment or perhaps due to battery power changes, producing striping and edge discontinuities (Ernenwein and Kvamme 2008). There are several statistical and grid merging procedures possible to overcome this problem.

A method has also been suggested that will synthesize the amplitudes of reflections at in sequential slices and merge them into a single composite map (Goodman et al. 2006; Goodman and Piro 2013). In this process, the slicing software can be programmed to add only the highest amplitude reflections from various depths and then overlay only those programmed amplitudes throughout a three-dimensional grid. In some areas where there are many complex reflections that produce very “busy” amplitude maps, this process can potentially highlight only some features while filtering out others (Goodman 2009).

Distorted reflection features in amplitude slice-maps can be produced when the ground surface varies a good deal. If the layers in the ground were mostly flat (as measured in distance above sea level, for instance), but the reflection data were collected on complex terrain that varied across a grid, a standard slice-map would cross those layers several times as the distance between the surface antennas and the layers in the ground, as measured in time, would also vary a good deal. This situation would also produce a few unusual-looking features that are only the product of the varying terrain.

Topographic and cross-cutting complications can often be adjusted for if the orientation and thickness of the subsurface layers are known, which can be determined by interpreting processed reflection profiles before slicing. The slicing problem illustrated in Figures 7.24 and 7.25, where amplitude slices cross stratigraphic boundaries, demonstrates how multiple interpretation

techniques, including slice-mapping and profile interpretation, should always be employed in an iterative fashion.

To test the various images produced from amplitude slice-map construction in topographically complicated ground, two series of amplitude time slices were constructed at a test site in Illinois (Isaacson et al. 1999). At this site, two burial crypts were constructed to simulate human burials (even including pig carcasses to simulate human remains). A mound was then constructed of roughly horizontal layers of soil over the crypt. Reflection profiles were collected using 400 MHz antennas in twenty-five-centimeter spaced transects over the mound (Hildebrand et al. 2002). The easiest way to produce amplitude slice-maps of this feature, which most of us routinely produce as a first try, is to construct each slice parallel to the ground surface. By doing so, the slices cross-cut many of the boundaries between horizontal soil layers in the mound as shown in Figure 7.26. The resulting twenty-five-centimeter-thick amplitude slices constructed in this way produced a series of concentric high amplitude areas in many of the slices, with each high-amplitude ring in the maps denoting the location where those slices crossed the horizontal bedding boundaries. Those slices, which were not corrected for topography, are therefore illustrating amplitudes of horizontal layers that are displayed in various depth-slices, which have no validity to what is buried below the surface. They are only a function of incorrect slicing geometry.

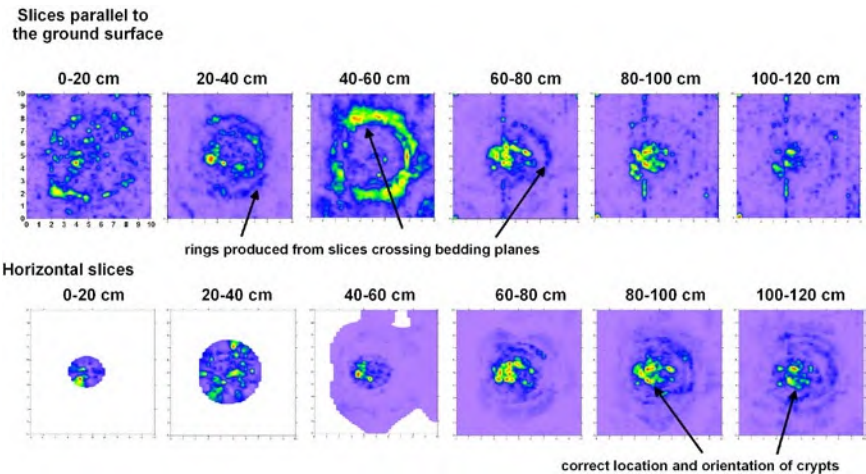


**Figure 7.26.** Two different sets of slices of the same grid. The top slices are uncorrected for surface elevations, and the slices cross bedding planes to produce false circular features. When elevations are adjusted and then the ground is sliced horizontally, these figments are removed, and the burial features within this mound are visible. *Source:* the author.

When all reflection profiles are instead corrected for the ground-surface elevation and then the grid is sliced horizontally, each amplitude slice-map is parallel to the bedding surfaces created by the mounding up of soil over the crypts. The slices do not cross horizontal layers and no spurious amplitude readings are created (Figure 7.26). The deeper slices cross the crypts themselves, and high-amplitude anomalies are produced in the exact location of the void spaces and crypt edges within the mound.

## **SUBTLE FEATURE DISCOVERY WITH AMPLITUDE MAPPING**

Often reflection profiles can be difficult to interpret, even after filtering, post-acquisition processing, and the production of many profiles with differing vertical and horizontal exaggeration are produced. But don't give up, as there may be important information contained in them, which can be teased out with amplitude slice-mapping. I have been tempted to give up and call the survey a failure when confronted with profiles such as these as there are no amplitude changes readily visible. The profile in Figure 7.27 was collected with 900 MHz antennas in a boggy area in the California Sierra Nevada Mountains. The goal was to map recently deposited sedimentary units in the hope of defining fluvial, marsh, and floodplain sediments that might have been present in the mid-nineteenth century. Historic records indicated that the ill-fated Donner party, a wagon train that was immigrating to California and attempting to cross the mountains in November 1846, camped near a creek in the study area and were stranded there all winter (Dixon et al. 2010). Many eyewitness accounts reported that the survivors found themselves in a bog in the spring of 1847, when the snow melted. Finding the remains of that camp today is complicated because the environment has changed, and it is now on the edge of a reservoir that was flooded in the 1960s. It was hoped that an analysis of the historic environment as it existed during the time of the Donner party encampment might yield clues to where the winter campsite was located, as it was known there was a small creek nearby in the early winter, and the area became a bog in the spring. The GPR method was considered because even though almost all the prospective area is today wet and boggy, similar environments with an abundance of peat beds had proven excellent areas for GPR mapping in elsewhere (Conyers 2016; Clarke et al. 1999; Leopold and Volkel 2003; Utsi 2004).

All the reflection profiles collected in this present-day bog appear to be noisy, and there are no continuous reflections that can be readily interpreted (Figure 7.27). With a little imagination, one can see some "character" variations in the reflections, with some areas containing many concentrated small hyperbolic reflections, especially within the upper twenty centimeters of the reflection profiles.

The amplitude slice-maps from this site display one sinuous area of higher-amplitude reflections in the ten- to twenty-centimeter slice (Figure 7.28). After further study of the reflection profiles (Figure 7.27), it was hypothesized that

the anomalously high-amplitude area corresponded to the presence of many small gravel clasts deposited in a creek that flowed through the boggy area. Each pebble would have generated a small reflection hyperbola, and many thousands of them were recorded, all interfering and distorting the recorded reflections from each. This produced the very “noisy” reflections visible in the profile, but these amplitudes were sampled and displayed in the amplitude slice-maps. Auger holes were then dug on either side of the high-amplitude feature and within it (Figure 7.28), and these results showed that holes one and three consisted of silt and peat, with abundant charcoal, while the sediment in hole two was mostly sand and small gravel clasts, which contained very

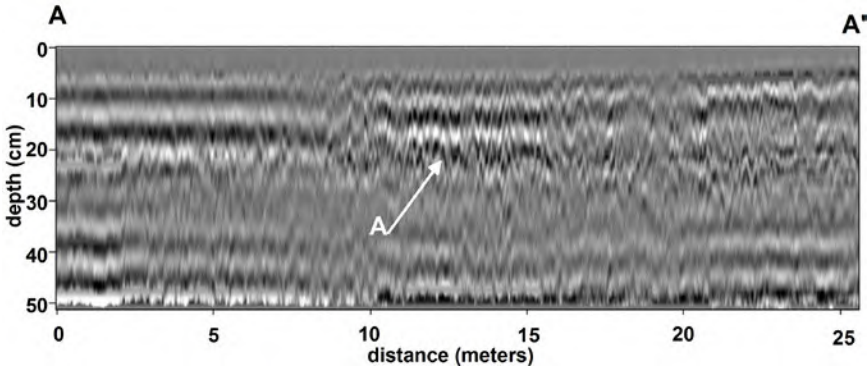


**Figure 7.27.** Reflection profile showing very subtle reflection differences where the channel is composed of gravel. This profile location is shown in Figure 7.28. *Source:* the author.

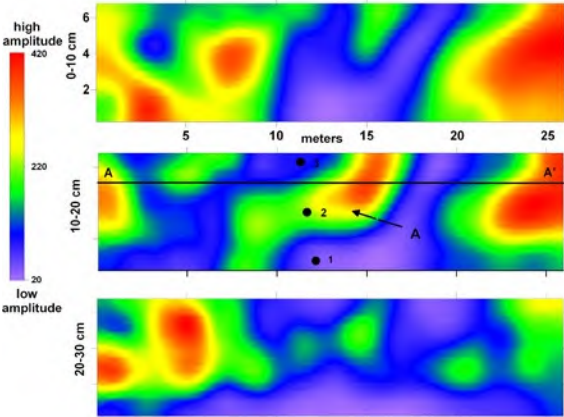


**Figure 7.28.** Amplitude slice-maps of a wetland area in the Sierra Nevada Mountains, California. A sinuous reflection feature in the ten- to twenty-centimeter slice is a small river channel. This area was cored north and south of the channel (1 and 3), and within it (2), to confirm it is filled with very fine gravel. *Source:* the author.

little peat. This subsurface information confirms that the sinuous feature in the ten- to twenty-centimeter (Figure 7.28) slice represents a small sand- and gravel-filled creek channel. The areas adjacent to it are marsh and floodplain sediments.

Although remains of the Donner party camp were not found in this immediate area, the GPR study was successful in defining the shallow creek with adjacent marshy floodplain deposits, which can be used as a guide for further subsurface testing in a search for artifacts. Most important, this study illustrates how even reflection data that are difficult to interpret in two-dimensional profiles can produce useful data when studied in amplitude slice-maps. When data of this type are then incorporated with standard archaeological and historical information, large areas of ground can be studied quickly, and excavation efforts can be concentrated in the most prospective locations.

There is a bias with most GPR interpreters to concentrate on the high amplitudes, which are usually generated from interfaces of interest. But sometimes buried materials of interest are those that have little or no reflectivity of radar waves (Conyers 2011). In southern Arizona, thick adobe walls were the target of GPR mapping. They were made by mixing clay, sand, and organic binding materials and then puddled up into walls. These architectural features have few if any interfaces within them to reflect energy (Figure 7.29).



**Figure 7.29.** Photo of a puddled adobe wall in southern Arizona. It was crossed by the reflection profile in Figure 7.30. *Source:* the author.

During GPR interpretation, our eyes are always drawn to the high amplitudes in both reflection profiles and amplitude slice-maps. We tend to ignore areas that have no reflection, almost as if we are concluding “there is nothing there.” I was fooled in this way for many years working in southern Arizona, where adobe architecture is common. After collecting many grids of data, which were interpreted and excavated by University of Arizona field school students, the results always came up as “nothing but clay and windblown sand here.” I had been guiding them to excavate areas that were most apparent to me during GPR interpretation, and I finally figured out I had been directing them to dig the “melt” layers that were adjacent to the buried walls. Those layers were interbedded aeolian sand and layers of clay, which had been eroded from the standing walls of buildings after abandonment, and then deposited on the wall flanks.

As the walls are a mixture of clay and sand that were well homogenized, the wall, when completed, contained no layers that were “different” enough in composition (and therefore water retention) to produce reflections of transmitted radar waves. The high concentration of clay and calcium carbonate in these walls was desirable to the builders as they cemented the structure to make it sturdier and more resistant to erosion and weathering. This type of material is also electrically conductive, and therefore attenuates radar waves moving through it. A reflection profile across one of these large walls clearly shows this phenomenon (Figure 7.30), and it is a good representation of an adobe wall of this sort (Figure 7.29).

Slicing up a grid of profiles (Figure 7.30) that contains complicated layers from the adobe melt, and a few areas where the non-reflective adobe walls still remain, produces a very difficult to interpret image (Figure 7.31). There are some places where the walls remain intact and are visible as areas of no

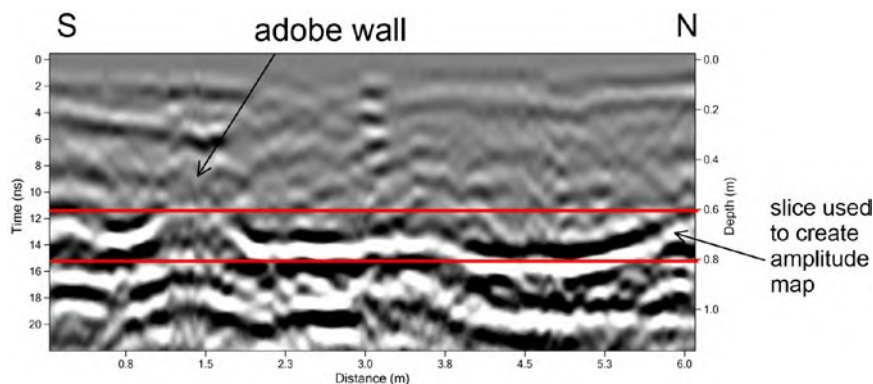


**Figure 7.30.** Reflection profile showing the adobe wall in Figure 7.29 as an area of low or no reflection. When all the profiles in this grid were sliced to produce amplitude maps (Figure 7.31), these walls were areas of no reflection. *Source:* the author.

reflection. Elsewhere, adobe melt layers sometimes overlap just the bases of walls, and in other areas, the walls have completely disintegrated. A carefully constructed slice (Figure 7.30) that includes only the wall segments where they are still standing, and many areas where adobe melt layers were deposited, yielded an image, which, with some thought, shows the areas of the walls. While complicated by some higher-amplitude adobe melt layers, it still can illustrate the three rooms in this building, and the walls can be sketched out with fair precision. This building was excavated, and exactly this was found (Figure 7.29), where walls and sometimes, to our surprise, reconstructed and additional walls, were preserved at the depth indicated by the GPR mapping.

This exercise in an analysis of the non-reflective units was important, as it is a lesson on how to train an interpreter's eye to look at GPR images in a different way than most people do. The non-reflective areas in a GPR dataset can be just as important as the reflective areas. It is disconcerting to look back on my own experience with this and admit that I spent a few years (off and on) mapping the unimportant adobe melt layers, when all the while the areas of non-reflection were there for me to see.

## **PRODUCTION OF RENDERED IMAGES**

The unique ability of GPR systems to collect reflection data in a three-dimensional package lends itself to the production of a number of other three-dimensional images not possible using other methods (Conyers et al. 2002; Goodman et al. 1998, 2004; Heinz and Aigner 2003; Leckebusch 2000, 2003). If reflection data are collected in a grid of closely spaced transects, and if there are many reflection traces gathered along each transect, reflection amplitudes can be accurately placed in three dimensions and then rendered using several visual display programs. In this way, GPR data from study sites become analogous to many other imaging techniques used in other disciplines, which rely on energy sources, such as sonic waves and magnetic resonance. In medical imaging complex, three-dimensional techniques can produce images of certain amplitudes derived from these energy sources to display internal body parts, or even electrical impulses in the brain as a function of different stimuli (Grossman and Blake 2013). Radar wave reflections can be used in the same way, but instead they produce images of a variety of buried features.

Using GPR data, buried features or interfaces can be rendered into iso-surfaces, meaning the interfaces producing the reflections are placed in three dimensions, and a pattern or color is assigned to specific amplitudes in order for them to be visible (Gacidepeursah 2019; Heinz and Aigner 2003; Leckebusch 2003 Peña and Teixidó 2013; Piro and Goodman 2013). In programs that produce these types of images, certain amplitudes (usually the highest ones) can be patterned or colored, while others are made transparent. Computer-generated light sources, to simulate rays of the sun, can then be used to shade



and shadow the rendered features in order to enhance them, and the features can be rotated and shaded until a desired product is produced.

These types of images have been denigrated by some as “too flashy,” “without any practical value,” or more like high-tech video games than real geophysical interpretation. The three-dimensional images are much easier to see than interpreting reflections in profiles or standard amplitude slice-maps. One of the goals of archaeological geophysics should be to “see into the ground,” and what better way than to make an image of the ground that is representative of what a site would look like if totally excavated? Three-dimensional renderings can often be the most readily comprehensible of all GPR images for this purpose, especially for the non-geophysically initiated.

To produce rendered images with GPR profiles, all reflection profiles in a grid must first be processed and filtered to produce the “cleanest” final product possible. Background noise and interfering frequencies should be removed and important amplitudes from features range gained to enhance their visibility. Hyperbolic reflections may need to be migrated if there are many in the data. Many slice maps must then be produced in very thin time intervals, to produce layers of digital data in closely spaced parallel planes. If these slices are constructed too thinly, reflection waveforms can sometimes be dissected into many small meaningless packages, and the resulting amplitude values may contain only a part of each wave reflected, not the wave as a whole. For instance, if there is a twenty-nanosecond window over which reflection data were collected, and each reflected wave in the ground has a wavelength of about two nanoseconds (about average for a 400 MHz antenna), then the most slices that should be generated (and not dissect the waves into many pieces to obtain amplitudes)

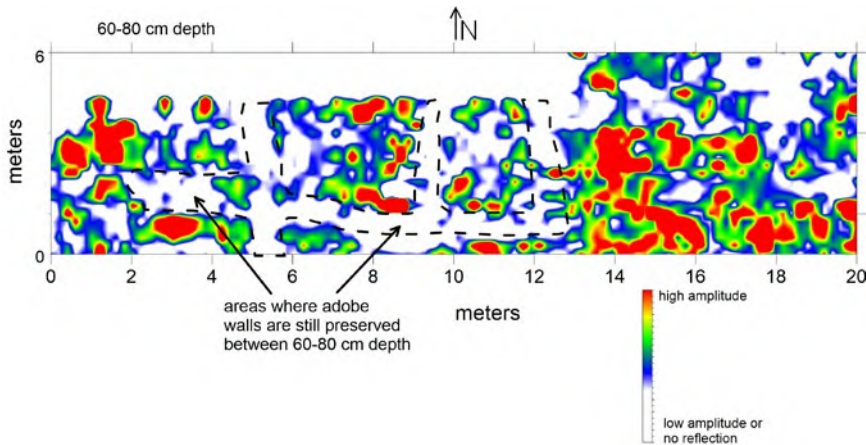


**Figure 7.31.** Amplitude map of the area where the adobe walls were uncovered. The walls are areas of no reflection amplitude. *Source:* the author



would be ten. For this reason, a running average may be preferable for creating a large three-dimensional database for rendering, where a twenty-nanosecond window of reflections is dissected into forty horizontal slices, each three nanoseconds in thickness, but overlapping the adjoining slices by a nanosecond or two. There would be some averaging of the amplitude data in this method, but a greater likelihood that complete waveforms will be averaged in each slice, and then made visible by rendering. Grasmueck et al. (2004), however, have shown that in some contexts very thin slices with no overlap can still produce good images.

Other aspects of reflected waves can also be mapped besides amplitude. There are aspects of waves that are data attributes such as their coherency and similarity across a grid (Boniger and Tronicke 2010; Piro and Goodman 2013). These properties are somewhat subjective and are usually applied to a three-dimensional package of re-sampled digital data using seismic processing programs.

When the buried structure from Petra in Figure 6.7 was sliced very thinly and only the highest amplitudes were rendered into an isosurface, a very distinct image of a buried building was constructed. In this rendering, the shallowest reflections were not included, as they contained many small point-source reflections from shallow rock rubble. The very deepest slices were also not included, as the data from that depth tended to be noisy and resulted in high-amplitude streaking in the rendered images (Conyers et al. 2002). These reflection data were ideal for rendering because most of the reflections collected in the grid were generated from buried architecture, and the surrounding wind-blown sand matrix generated almost no reflections of any amplitude. Once the rendering was constructed on the computer, it could also be rotated or tilted in several different orientations in a video display (Conyers et al. 2002).

## **VERY HIGH-FREQUENCY GPR**

Recently there has been some interest in using very high-frequency GPR antennas for mostly geological and construction applications (Johnston et al. 2018; Okazaki et al. 2013). An interesting application is to test very small and subtle features, such as the famous footprints in volcanic ash at Laetoli, Tanzania (McNutt et al. 2012). Elsewhere, GPR has been used for imaging footprints, such as those of humans and mammoths in New Mexico (Urban et al. 2019). In preparation for going to Tanzania, a model of human footprints was prepared that mimics those in Africa (Wiewel et al. 2021). This model was constructed in moist volcanic soil in Oregon, and two sets of prints were made in the ground, making sure each penetrated to about 4 cm or so, to mimic the depth that the hominid prints were emplaced along the edge of a lake in a volcanic sediment about 3.8 million years ago (Figure 7.32). A set of six male prints was produced, with seven female prints just to the south. Neither were correct in terms of stride, but both sets created between 3 and 4.5 cm deep prints. They



**Figure 7.32.** Human footprints placed in mud to simulate the Laetoli prints in Tanzania. This model was left to dry in the sun and then covered with sand for testing with very high-frequency antennas. Source: the author.

were dried in the sun for two days and gently covered with 6 cm of basalt sand, which was dried an additional two days. A variety of collection procedures were attempted, starting with placing a piece of plywood on the sand and collecting reflection data through it. Three antennas were used—the 900 MHz, 2 GHz, and 2.6 GHz—with reflection profiles collected at 10 cm intervals oriented both north-south and east-west. The plywood collection method was quickly rejected, as small air pockets between the base of the plywood and the sand produced many air waves and velocity changes, which distorted and obscured the resulting reflections. It was replaced with a flexible yoga mat, which could be gently pushed down into the sand to remove air pockets. The 900 MHz reflection data were rejected, as resolution was too low to image the subtle prints. An analysis of Table 3.3 shows that the wavelength of a 900 MHz wave in materials with an RDP of about 10 is about 10.5 cm. Using the rule of thumb for resolution, one half wavelength is about the best resolution that can be expected, which in this ground is about 5 cm, not nearly suitable to resolve footprints that were emplaced at between 3 and 4.5 cm deep.

Both the 2 GHz and 2.6 GHz reflection profiles were capable of resolving these subtle prints. The 2.6 GHz profiles were first sliced using standard amplitude maps, which proved wholly unsatisfactory. There was almost no correlation between the prints and amplitudes that were generated. Each reflection profile was instead “picked” and the horizon that is the contact between the

mud layer that the prints were constructed on, and the overlying basalt sand was sampled for its depth below the top of the yoga mat (Figure 7.33). Along with the depth of that horizon (in nanoseconds), the amplitude of the waves reflected from this interface were also recorded. In a standard reflection profile, the two prints in this example are visible as depressions (Figure 7.33). There are also very subtle reflections below the print depressions, much like what was visible in the canal model (Figure 7.2), but on a much smaller scale. The edges of the prints are lower in amplitude, as they reflected waves away from the antenna, and the base of the prints is higher in amplitude due to focusing (Figure 7.33). All picks of depth below the ground were then contoured to produce a map of this unit (Figure 7.34). That image shows a few features that are distorted, such as the depression in the middle of the map, caused by retained moisture in that part of the test bed, which had not dried out as much as its edges of the grid. This caused a velocity pull-down, with a corresponding pull-up on the edges. Some closed contours that are showing the location of the prints are visible, but some are very indistinct. To overcome some of these

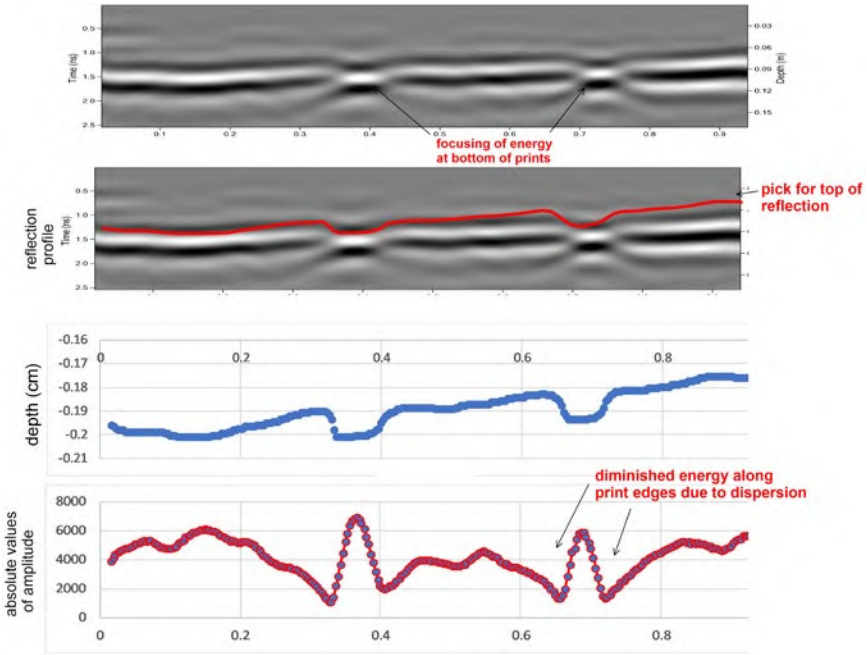


**Figure 7.33.** Reflections from the top of the clay surface where the footprints were made. They are very subtle indentations and exhibit lower-amplitude waves on their edges, where energy was reflected away from the surface and not recorded. The depth of this horizon and its amplitude was auto-picked for further analysis. Source: the author.

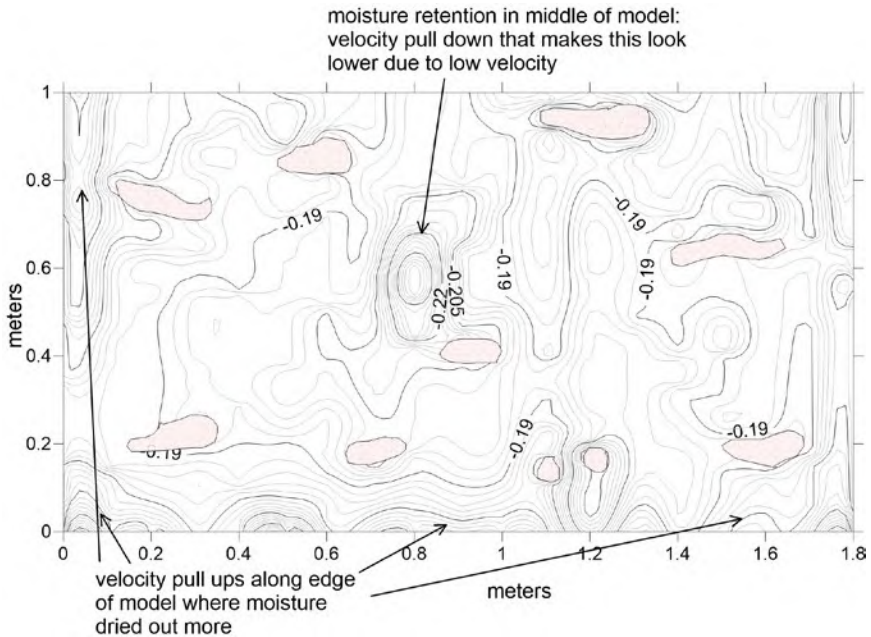


**Figure 7.34.** Depth of the prints contour map produced from the auto-picked points. The prints are partially visible as closed contours, but this is not a good representation. Source: the author.

distortions, a trend map was produced on this horizon using GPR Slice (Wiewel et al. 2021), and that trend surface was then subtracted from the picked horizon to produce a residual map that shows almost all the prints very well (Figure 7.35). That three-dimensional surface was then shaded with artificial light to display the prints satisfactorily.

This model was constructed to test different collection and data processing methods in preparation for going to Tanzania and collecting the data over the real prints. These tests show that for the depth of investigation necessary and the resolution needed to resolve these subtle prints, the 2 GHz and 2.6 GHz antennas are the best solution. The yoga mat collection surface was also the best, as air pockets due to the variation in the ground surface could be removed. How this may work on a possibly more varying ground surface in Africa is a variable that I worry about. Also, it is unknown how attenuating the ground there might be, so it remains to be seen if the 2-GHz or 2.6-GHz antennas are capable of propagating waves to the depth necessary in the rocks that are present. The amount of time it took to process all thirty reflection profiles in this small grid of 1×1.8 meters with picking, and then processing all picks into the three-dimensional images, also may preclude those methods if a large amount of ground needs to be evaluated. The prints were quite visible in individual profiles as

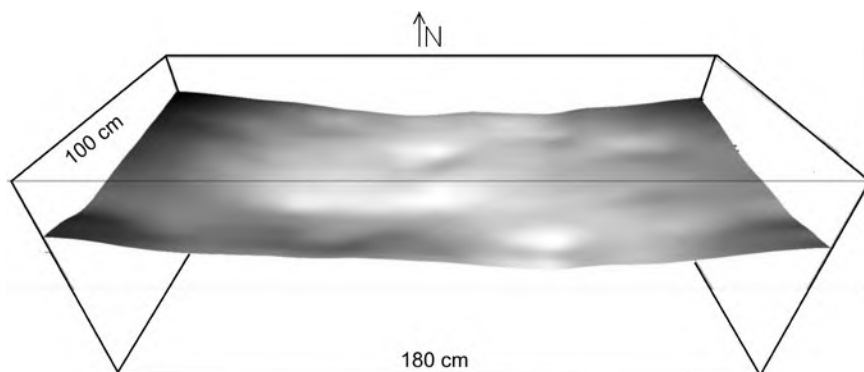


**Figure 7.35.** The data points used to produce the contour map in Figure 7.34 were used to create an averaged depth surface, and a residual image that is the difference between this modeled surface and the picked depths displays the picks. *Source: the author.*

depressions with corresponding high amplitudes of waves that were focused on the bottom of the prints and lower amplitudes on their edges. Perhaps the best way to process many profiles over a larger area would be to view each profile to find the depressions and amplitude changes, and then compile many “x marks the spot” locations on a base map to see if a trend of a hominid pathway can be found. Later, when there is more time available, a generation of some of the more visually appealing images can be constructed.

### **GPR AND MAGNETICS USED TOGETHER**

The three-dimensional aspects of GPR are a very good complement to other geophysical methods, which can yield important information about the composition of materials in the ground. The most conducive for this is magnetics, which produces two-dimensional maps of the magnetic characteristics of the ground, usually within the upper 1.5 meters or so (Conyers 2018). I have been disconcerted in the last ten years or so to see the plethora of published works that compare and contrast GPR amplitude slice-maps and magnetic maps (Conyers 2016; Hansen et al. 2014; Matera et al. 2015; Morelli et al. 2013; Trinks et al. 2014). At first glance, these maps appear similar, as they often show the same trends and general pattern similarities. Authors who have published results showing these types of comparisons point out the similarities, but they are often a little confused when they are not directly comparable. There have been spatial statistics attempts to determine how similar or different they are. Even innovative color composite techniques (Kvamme et al. 2019) produce interesting new colors when there is a direct overlay between, for instance, some high-amplitude radar wave reflections in a certain slice and some positive magnetic features. For many years, I never knew what to think about these

methods, and so I avoided them, sticking to GPR. However, starting in 2015, my graduate students began to collect both GPR and magnetics, and they were confronted with the same problems that others had encountered. I tried to do this myself, and I published a paper showing “moderately correlative” maps (Conyers 2015). I am now embarrassed to say those results were partially indicative of good comparisons between the two methods, but when studied in detail, it became clear they are not really very good.

With a growing dataset that I had available, mostly from my students and other collaborators, I felt that it was time I tried to understand what GPR and magnetics are showing about the ground and try to understand the comparisons and contrasts between the two (Conyers 2017; Conyers et al. 2020; Welc et al. 2019). In an area where we knew a good deal about the geology, maps of GPR and magnetic results showed general comparisons that were interesting (Figure 7.36), with some high-amplitude radar reflections being generally correlative with high-magnetic readings. Other areas of the grid showed high amplitudes in a deeper GPR slice, but in this case, those deeper high amplitude areas overlaid well with negative magnetic areas. This suggests there are certain aspects of the ground in this grid that are showing up in either deeper or shallower slice-maps, which the magnetic readings indicate are materials with either higher or lower magnetic readings.

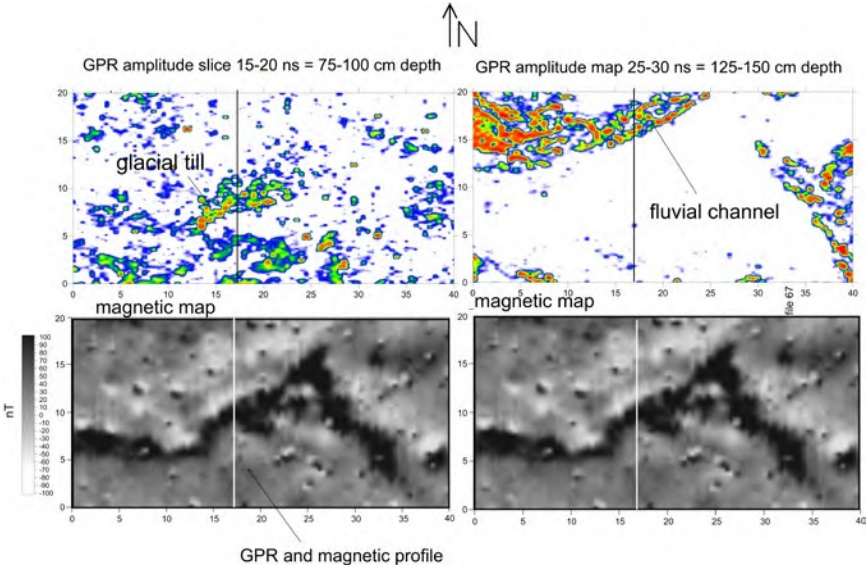


**Figure 7.36.** GPR-amplitude maps on top and corresponding magnetic maps below display similar trends, but they do not overlay in any meaningful way. *Source:* the author.

The obvious way to confront this situation is to analyze GPR reflection profiles across the grid, then compare what can be seen in those profiles to the magnetic readings. This is a simple procedure, as GPR reflection profiles are readily visible in profile. The magnetic maps also are constructed from individual data points can be extracted from those data and displayed in comparison to the GPR profiles (Figure 7.37). Fortunately, we knew much about the ground in this location of New England, and we knew that there were fluvial channels that had cut into glacial till units, at the end of the last Ice Age. Higher-elevation till deposits are found at about 1.2 meters depth, while the channels, which were glacial outwash units deposited after the glaciers had receded about fifteen thousand years ago, cut down through the till to about two meters or more. The till units are composed of granite and other metamorphic clasts, which are high in magnetite, and they have remained relatively un-weathered. The fluvial channels are filled with mostly sand, which washed in from a different source and contains much fewer constituents that are magnetic.

A comparison of the GPR reflection profile to the magnetic readings shows exactly why this is the case (Figure 7.37). Magnetic readings, in this case collected with a gradiometer system, usually average readings in the upper 1.5 meters or so of the ground. That is exactly the area where the higher glacial till deposits are located, and where the magnetic readings show high positive values. Where the channel cut through the till, the less magnetic channel sand has negative readings. It must be remembered that magnetics collected in this way are showing “relatively” high and low readings compared to where the system was calibrated. So absolute readings of magnetics are not usually understood, and instead are relative readings.

In this grid, many GPR reflection profiles were collected and compared to the magnetic readings, and all showed these important comparisons. While the GPR amplitude slice-maps were, with some interpretation, showing where the channels are, and where the glacial till deposits are close to the surface, it is only when the two data are specifically analyzed in profile that these two methods’ results can be understood. In this case, it is no wonder that the general “patterns” in the maps of results are alike, but the details are very different.

To test this idea more, a small grid of magnetic data and GPR-reflection profiles were collected over a small Roman house in Croatia (Welc et al. 2020). The magnetic map shows a two-room building, with the southern room containing a partial wall (Figure 7.38). A GPR-amplitude slice-map from 10 to 14 ns appears to show only one square room (Figure 7.38), which roughly fits within the southwestern part of the building, as indicated by the magnetic readings. A few other interesting areas can be seen with the magnetic image, the most distinctive being the highly magnetic area within the room on the southwest part of the building. A few questions remain: Why are no walls visible with the GPR that can be seen in the magnetic map on the north side of that southwest-



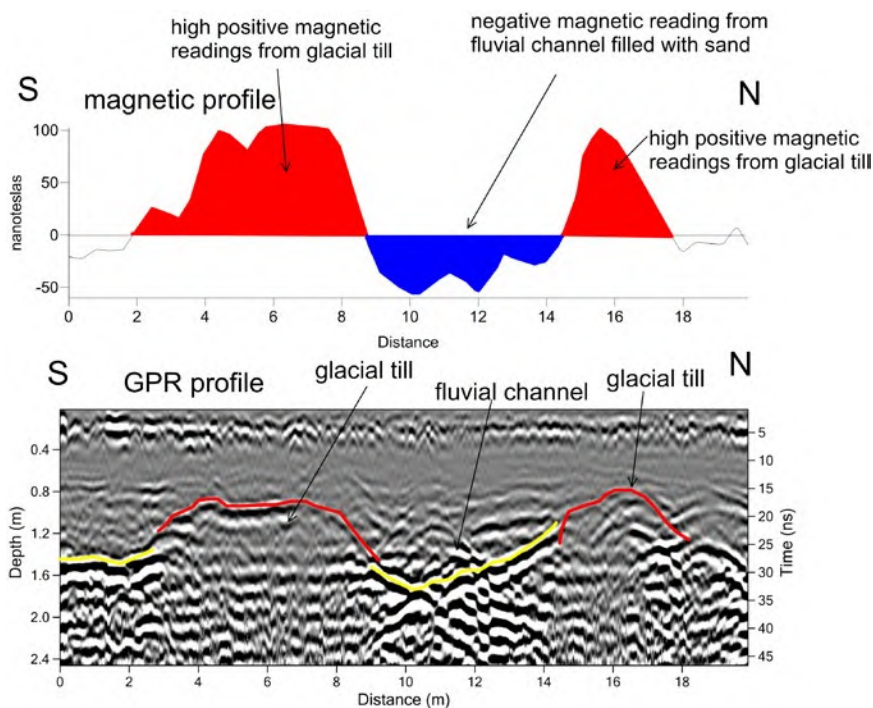


**Figure 7.37.** When the reflection profiles are viewed, with the corresponding magnetic values for the grid shown in Figure 7.36, it is apparent that the high amplitudes in the upper slice-map were generated from where the bedrock glacial till was near the surface. Those sediments produced a high magnetic reading. The channels that incised the till units are not visible as high-amplitude reflections in the deeper GPR slice-map, and they are low in magnetic readings as they are composed of less-magnetic materials. *Source: the author.*

ern part of the building? What has created the highly magnetic area inside the room in the southwest? And is there a floor in this building?

These questions can be readily answered by looking at both datasets in profiles. The walls visible in the amplitude slice-map (Figure 7.38) are visible as short "stumps" with subtle reflection hyperbolas on the planar reflections from floors (Figure 7.39). The architecture of this building is limestone, which is very low in remnant magnetism, and this is displayed as negative values in the profile and in the map. Inside the room on the southeast is a distinct hole that cuts through the floor. Part of the floor was removed in that room, and the hole was filled with something with remnant magnetism or high magnetic susceptibility. That material might be organic material (Fassbinder 2015) or perhaps burned materials. Elsewhere, the floor is intact and visible as a continuous planar reflection. It has negative magnetic values, much like the wall stumps, indicating



it was probably made of limestone plaster. In much of this building, the floor is intact, which can be seen in both GPR and magnetic images.

In this archaeological example, the three-dimensional aspects of the architecture, and the post-abandonment holes in the floor, are visible. The composition of the walls and floors can be readily determined using the magnetic values. The GPR slice-map that shows only one room that retains small stumps of the walls that remain sticking up above the floors and can be seen

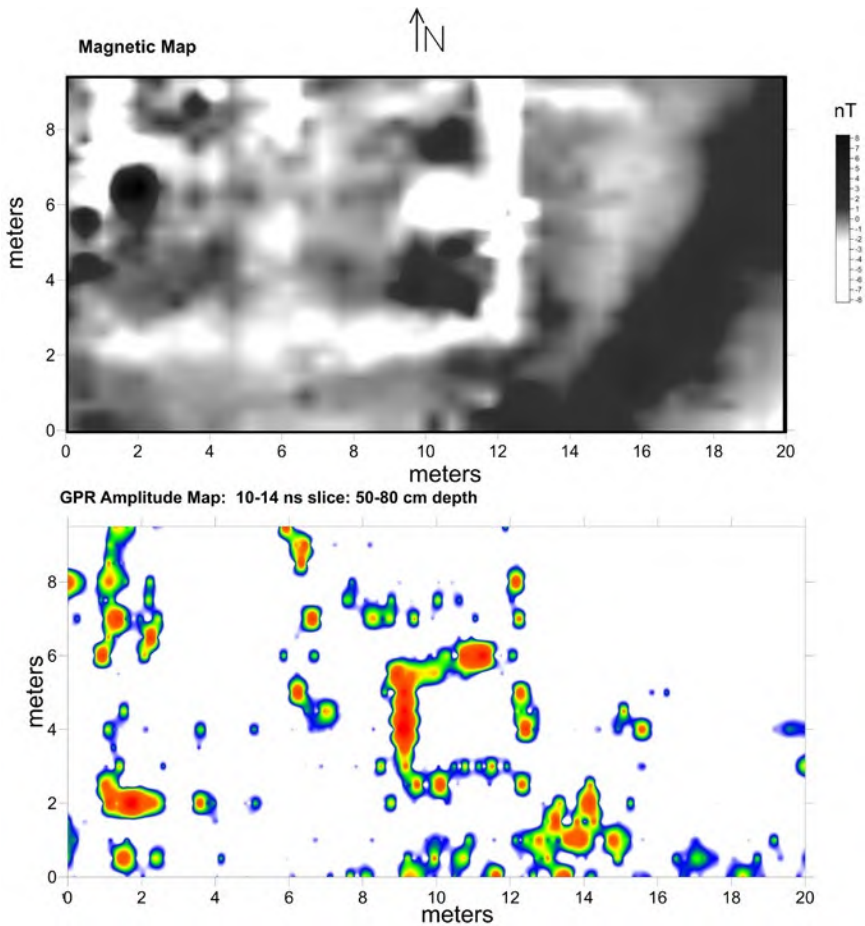


**Figure 7.38.** Magnetic map (upper) and an amplitude slice-map below, of a small Roman house in Croatia. Source: the author.

in the GPR-amplitude slice-map (Figure 7.38). The building materials used to construct the other walls in this house must have been removed, leaving only the foundations that are low-magnetic limestone. A moderately interesting question remains about the deep incision in the southeastern room. What were the people thinking who dug through the floor in that part of the house? Were they looking for buried treasure? We will never know, but the two geophysical methods working together at least allows us to ask this intriguing question.

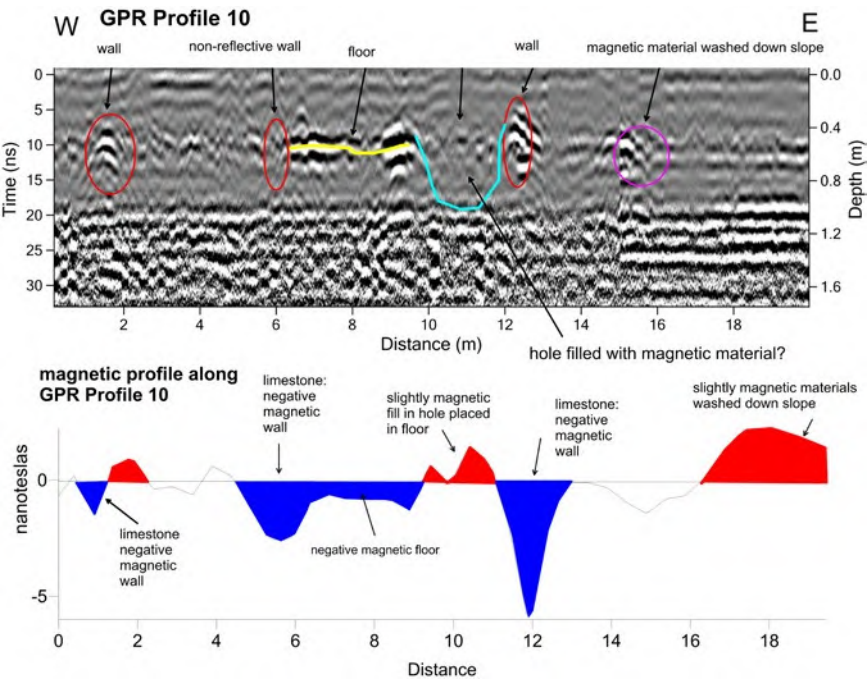


**Figure 7.39.** Reflection profile over the house shown in Figure 7.38, showing that the walls are low magnetically, while the incised area where the floor was cut out is higher in remnant magnetism. *Source: the author.*



# 8

## *Conclusions*

Ground-penetrating radar's power comes from its ability to create accurate maps, profiles, and other images in three-dimensions. The numerous variables that must be accounted for in the method need not be intimidating, as they can be understood and accounted for. One of the most important considerations is how radar waves spread out when they travel in the ground, and reflected, refracted, and attenuated due to complexities with layering and associated other features. This will always produce complex radar wave pathways. With some thought about how radar waves were reflected, refracted and lost the recorded reflections can be understood, and if necessary, placed correctly in space. While much of the radar energy is transmitted directly below the transmitting antennas raw data can usually produce understandable profiles and slice-maps without having to be processed a great deal. There will always be reflections in every dataset that have been recorded after having traveled in ways other than directly to and from an overlying antenna. Those need to be understood and used in data interpretation, and then removed if necessary.

We often talk about our GPR images in slice-maps or isosurfaces as being three-dimensional, but that is not technically the case. They are more "pseudo-3-D" or "2½-D," as they are usually created from two-dimensional data collection procedures, whose products are resampled and then transformed into three-dimensional images using interpolation algorithms that create a cloud of data, much of which has been mathematically created. If the GPR field ever reaches true 3-D, where arrays of simultaneously recording receiving antennas record from an equal number of transmitters that are closely spaced, then we will have arrived at true 3-D. Our friends in the seismic reflection field arrived here about twenty years ago, but their budgets for both hardware and software are gigantic compared to most GPR users. This will come someday to our smaller (and less well-funded) GPR community.

The last twenty years have not been a static time for advancements in GPR. We now have very fast digitization, which has led to "real time" trace stacking and improved reflection resolution. With hardware, there is now wireless

connectivity in some new systems, allowing antennas to transmit to the recording systems without cables, relieving us of cable snags and other connection failures. The ability to synchronize GPS with GPR has become less “buggy” than it used to be, which, when combined with very fast digitization of recorded reflections, can also be incorporated with very accurate spatial placement.

There are still many skeptics of the artificial intelligence methods for data processing and interpretation. Put me in the camp of believers in the human brain, who still think that simultaneously viewing multiple images created in a variety of ways can be integrated intelligently. I will wait to be convinced that machine-learning can take the place of human intelligence.

I remain critical of software that tries to do anything imaginable for any possible GPR user. These software programs have row after row of icons that perform some amazing procedures, many of which may not be necessary or important for the standard GPR user. Surely versions of these robust programs can be simplified and made easier to use for many of us. Even more important, a software manual that is written by a user of the software instead of the code-writer would go a long way toward helping those who need to perform certain tasks.

Every site where GPR is employed is a new adventure. It is always a good idea to spend some time looking around for exposures in road-cuts, erosional escarpments, wells, or even in nearby construction sites to get a feel for what is in the ground. Here some background in geology, soils, and landform analysis can help. Often hypotheses can be arrived at with this kind of site analysis long before a grid is set up and equipment is readied for a survey. Even better, some basic research in the library to obtain soil survey results or other information about the ground can go a long way to providing knowledge on how a survey should be conducted and a system calibrated for data gathering.

I require my graduate students to spend two years doing GPR, with weekly projects where data are collected or used from previous work to process complex grids of data into images and make interpretations. That undertaking gives them confidence about both collection and processing methods, and the ability to modify these under different conditions. This is perhaps too much time spent doing this for my students, but it has produced some very adept and experienced GPR users, and they have benefited in their careers. I led two workshops for GPR users who were located on four different continents during the COVID-19 lockdown days, and we did the same thing, but virtually using Zoom. These participants were in seventeen different time zones around the world, and they spoke many different languages as first languages besides English. Soon we were all speaking the same “GPR language,” and while they came to the workshop using eight different software programs, we all were soon using our individual tools in a collaborative way. This was an enlightening experience for us all, and once we understood each other’s outlooks with geophysics and software capabilities, we quickly learned what methods worked best in what

situations. It was not apparent to me before this international collaboration that this might work. Each week there was a new dataset to be struggled within the group, and many varieties of software were employed for certain tasks. All participants were soon employing not just their own GPR software, but also various other general mapping programs, GIS analysis, and basic spreadsheets for various tasks. In this way, the GPR workshops became much like a home workshop for woodworking, where all the tools were available, and we had to think through what could or should be used in each for what task. Instead of saws and drills, we used GPR processing and image production software. In this book, I have only done a little of that, but using my own GPR software to perform the bulk of the tasks has presented “horizon picking” from other programs and Surfer for producing specialty maps and images. All GPR users should be thinking of what tools they might have at their disposal and use them all when appropriate.

With tools in mind, it is always important to be thinking about procedures to accomplish certain tasks. In this mental procedure to think about waves and how they travel and reflect, and then how they are recorded, which becomes crucial. At each stage in data acquisition and processing, those software tools can be programmed to complete a task, with those results studied and conclusions made. This type of iterative experimentation is a very good way to work through complexity, stopping along the way after certain steps and evaluating what has been done and interpreting those results. Rarely is GPR a “one and done” method, especially with data processing and analysis.

It is very rare to collect totally worthless data. I have done it a few times, to my chagrin, but even those rare times when radar energy will not propagate more than a few centimeters in the ground, it is telling us something about the ground. A GPR friend of mine always told me that “GPR data do not lie,” as if data were a living creature. What he meant to say in a less dramatic way is that all GPR reflections are providing interpreters with a database from which we can conclude something about the ground. Our jobs are to determine what that is, even if what is concluded was not necessarily what the proposed goals were at the outset. Just because wonderful images do not appear in amplitude slice-maps is no reason to conclude that the survey was a failure. When results lead to disappointment and confusion, more work needs to be done with toolkits and a GPR understanding to determine why this is the case.

Workflow patterns are a new concept in many technical professions, and they are applicable to GPR, even if there is just one person performing all the tasks. Sometimes tasks can be performed in “orchestration,” where certain procedures need to be done first, and others are done later based on the results of those first results. Even if only one person makes up the “orchestra” of these tasks, this is still a valid concept. But to optimize how procedures are done, a sequential model of workflow need not be used. While with GPR there is a basic sequence, from collection to processing to other possible processing

methods to image generation and interpretation, these need not be done in a linear way. Instead, there can be a “modified parallel workflow” of procedures that can often be performed simultaneously, such as profile analysis and slice-map construction and modification. Both types of images can be constructed at the same general time, and the results of one or the other, when interpreted in unison, can perhaps determine if a next step should be taken, or perhaps a minor regression to begin a task again differently with modified input parameters. These methods are anything but linear, and they can provide breakthroughs as various methods of data processing and analysis are used. When this method is used, be careful to document everything, as images and attempts will soon become overwhelming. Only careful documentation of each step will allow one to reconstruct and explain results when the project is finished.

Many of us publish the results of our GPR work, and as a reviewer of many submitted papers for publication on the subject, I often conclude that quantity of GPR images is not equal to quality. Some software programs, especially those that are semi-automated, produce a wealth of images of many sorts. There is no good reason to do an “image dump” in a paper just to document how many images were generated. It is much better instead to provide a few easy to visualize images that are annotated to point out aspects of the conclusions that are necessary. If these are included with a short description in the text or figure caption, the reader will understand readily what is being interpreted.

I have been remiss to not spend more time discussing how geophysics can be used to tell us more about the ground beyond pointing out what is there. We can use this powerful tool to arrive at conclusions that no other discipline can. This can be a powerful tool in any research project, and we all must spend more time using our results to conclude important things about whatever it was that motivated us to do the work in the first place. If the goal was just to find things and report on those findings, then that is fine. But even a few sentences in a conclusion about how those findings could be used in conjunction with other information to arrive at important conclusions would be warranted and appreciated.

# *Glossary of Common GPR Terms Used in This Book*

**air waves:** recorded radar waves visible in reflection profiles, which moved in air from the transmitting antenna to a reflection surface and then back to the receiving antenna. These waves are often straight but can be various shapes depending on the how antennas are moved during recording in relation to the reflective surface. The reflection surfaces that produce these waves can be walls, trees, stones, vehicles, above-ground utility lines, and any other object that can reflect radar waves. They are more common with lower-frequency antennas where radar energy spreads out from the transmitting antenna.

**amplitude:** a measure of the “strength” of radar waves recorded by GPR systems. These values are recorded in a dynamic range of digital values that define each sine wave that is recorded. Variations in wave amplitudes are a function of differences in velocity of traveling waves as they cross bounding surfaces that reflect energy, with the greater the velocity contrast, the higher the reflected wave amplitude.

**amplitude slice-maps:** common maps produced by resampling the digital values of amplitudes recorded from interfaces in the ground. They are often referred to as “time-slice” maps or “depth-slice” maps, as they are produced from slices of ground defined by wave recording times or depth. Most often they are generated over a “thickness” of material in the ground, such as 5 to 10 nanoseconds or 20 to 40 centimeters. They can also be constructed from one distinct plane. These maps can also be produced to follow specific horizons that vary in their depth in the ground.

**antennas:** in GPR antennas these electronic devices transmit radio waves. They can be various shapes and sizes to generate different frequency and record waves, with larger antennas usually producing lower-frequency (longer wavelength) waves. Electrical pulses are applied to an electrically conductive material, which, depending on their shape, size, and other electronic components, generate electromagnetic waves that propagate outward. They are often used in pairs, with one antenna transmitting with the other receiving and recording waves produced from reflections generated from interfaces in the ground, or other surfaces.



**attenuation:** the weakening and general reduction in the strength of radar waves as they move through a medium. In the ground, this occurs when waves propagate through electrically conductive or magnetically permeable materials. Weakening also occurs as propagating waves, moving in a conical transmission pattern and spread over a greater volume of ground creating additional weakening.

**background removal:** a processing method that can remove an average waveform from all reflection traces recorded from within the ground. The method generates an average wave by sampling all waves within a given number of sequential traces in a profile, which occur at the same recorded times. That average wave can be the “background noise,” which was recorded from external radio transmissions or system noise or both. This composite trace is then subtracted digitally from each trace in a profile, hopefully leaving only those waves that were recorded from within the ground. The number of sequential waves used to compute the background average trace can be programmed, or all traces in a profile used as a default.

**band-pass filters:** the removal of programmed frequencies from recorded radar waves. Low-pass filters remove all frequencies below a certain value in MHz. High-pass allow values above a programmed frequency to remain, removing lower values.

**bi-static antenna:** two antennas placed together, one of which transmits, and the other receives.

**bowtie:** slang term for a reflection feature that looks in reflection profiles like a vertical necktie, knotted in the middle. They are usually product of reflections generated from steep-sided trenches, canals, or channels where the conical shaped radar transmissions produce waves that are reflected off features in front of and behind moving surface antennas.

**broad-band:** referring to a range of frequencies transmitted and received from bowtie antennas.

**calibration, of GPR systems:** pre-collection settings applied to the digital controls that determine the number of traces recorded within certain time windows and with a programmed wave resolution. A variety of settings are necessary for optimum data collection that are dependent on the depth and resolution desired, the amount of ground to cover, frequency of antennas used, and the physical and chemical composition of the ground.

**cation exchange capacity (CEC):** a measurement of the number of exchangeable positive ions that are attracted to and retained by materials in the ground. Ground that is electrically conductive has a high CEC, which attenuates propagating radar waves.

**cell phone, frequency:** important as generators of background noise recorded with GPR. They generally range from 800 MHz to 3500 MHz, with some lower frequencies in some parts of the world. The newer 5G frequencies are in the higher frequency range. When using GPR antennas in the 500- to 1,200-MHz range, interference from these devices can be a problem. That cell phone noise must be removed from data using post-acquisition filtering programs common in most software programs. All cell phone and personal communication devices will produce extraneous electromagnetic interference when transmitting, but usually not when only in receiving mode.

**center frequency:** the nominal frequency of antennas common in GPR. Most GPR antennas are defined by these center frequencies but are really transmitters and receivers from a “broad band” of frequencies, often within one “octave” of the center (one-half to two times). For instance, a 400-MHz center frequency antenna is really transmitting waves from the one octave on either side of 400, which is about 200 to 800 MHz.

**clipping:** when the highest amplitude portions of recorded waves in traces are “off scale” and therefore not completely recorded. Usually produced by over-gaining.

**coefficient of reflection:** a parameter that describes how much energy of a propagating radar wave is reflected at an interface. The greater the velocity change, the higher the coefficient of reflection and the higher the wave amplitudes that are generated.

**conductivity, electrical:** an intrinsic property of a material that quantifies how it allows the flow of an electrical current. The inverse is resistivity. High electrically conductive materials in the ground have a high cation exchange capacity, and absorb radar energy, creating radar wave attenuation.

**coupling, of radar energy with the ground:** a relative measurement of how well transmitted radar waves move across the ground-air interface to propagate into the ground. Variations in coupling can be caused by the constituents of surface materials, the placement of the antenna on the ground, the amount of tilt of antennas, the distance of the antenna off the ground, and other factors. Good coupling means radar waves have moved into the ground and are being transmitted to depth. Coupling variations along an antenna transect create anomalous reflections in GPR reflection profiles and can distort the resulting GPR images.

**data processing, post-acquisition:** digital software methods that modify GPR reflection data after they have been acquired to adjust the reflections in some ways prior to display and interpretation. These methods can be vertical and horizontal axes adjustments, filtering of frequencies, gaining of reflection amplitudes, and

many other methods used to overcome noise, distortion, and other common GPR variations.

**deflections, of waves positive and negative:** the amplitudes of recorded sine waves collected in traces with GPR. All recorded waves have positive and negative deflections, as when paired they produce a complete wave, the product of one sine-wave reflection generated from one interface.

**dielectric:** when referring to a property of the ground. Ground that is dielectric means that it has a lower electrical conductivity, and therefore allows radar waves to propagate through it more readily.

**dynamic range:** a term taken from audio and visual technology, which in GPR is a ratio of the highest amplitude to the lowest in recorded waves.

**electromagnetic energy:** energy propagated through space or a material that are the co-joined waves of electrical and magnetic waves. GPR waves are electromagnetic, classified as radio waves (defined only by their frequency). Other electromagnetic energy types, not applicable to this book, are infrared radiation, visible light, ultraviolet radiation, X-rays, and gamma rays.

**filtering:** any digital process that modifies the radar waves collected, removing some portions of the data, and enhancing others in some fashion.

**frequencies, of antennas:** the rate at which a wave vibrates, measured per second in values of hertz. The higher the frequency, the shorter the wavelength generated. Most GPR antennas produce an electromagnetic field that creates propagating waves that vibrated in in the 500- to 1,200-MHz range. One unit of megahertz is 1,000,000 oscillations per second.

**gains, applied to radar waves:** a parameter, or series of parameters that change the intensity, or amplitude of waves recorded by an antenna. These are numerical values often applied to wave amplitudes during collection, or during post-acquisition processing to enhance the amplitude of waves generated from deeper in ground, which have undergone attenuation, and are therefore weaker than shallower generated waves.

**hyperbola fitting:** a method where a computer-generated hyperbola is “fit” to one visible in a profile to estimate velocity. The shape of the axes of hyperbolas is a function of the velocity that waves move to and from buried “point source” reflection surfaces.

**hyperbola, as in describing a reflection:** shape of reflections generated from “point sources” in the ground, caused by the spreading of transmitting radar energy as it moves deeper in the ground from a surface antenna.

**interval sampling:** a method of recording received waves where the first radar wave transmitted into the ground and then reflected is received and its time and amplitude become the first sample of a wave. The second wave is used for the second sample and so on, until all the waves in the time-window have been recorded by digital samples. For instance, if 512 samples are set to record all the waves in a trace, the same number of sequential pulses would need to be also transmitted sequentially.

**isosurfaces:** a computer-rendered three-dimensional surface that in GPR studies can be used to visualize on the computer a reflection surface from a buried feature in the ground.

**megahertz:** unit of measurement of frequency common in with GPR antennas, which are units of the oscillation of waves. Equal to one million hertz. One hertz is one oscillation per second.

**migration:** a post-acquisition processing method that adjusts reflections recorded in the ground for velocity distortions and the spherical spreading of transmitted energy. Usually in GPR it is used to “migrate” the axes of point-source reflection hyperbolas back to their source, which is the apex of the hyperbolas. Can also, less commonly, used to adjust the geometry of steeply dipping planar reflections.

**modeling:** a method used in GPR to create a visualization of what reflection profiles would be generated by buried materials and objects. Produced by inputting known or inferred electrical and magnetic parameters and shape of buried materials in the computer and then generating simulated wave paths to produce artificial two-dimensional reflection profiles.

**mono-static antenna:** where one antenna is used both as a transmitting and receiving antenna, oscillating between both modes very quickly to record a trace.

**multiple array systems:** using multiple transmission and recording antennas placed together to record a variety of reflected waves in the ground from a three-dimensional unit of ground. Usually, each antenna transmits and then records its own reflections from below. Other arrays record the reflected, and refracted waves from one transmitting at multiple receiving antennas. More complex arrays transmit and record from all antennas joined together. All reflections recorded in array-systems need specialized software to place reflection traces into a three-dimensional package of ground for processing and visualization.

**nanoseconds (ns):** the time used to record the two-way travel times of radar waves. These are units of one billionth of a second.

**noise:** any unwanted waves recorded during GPR collection. Most commonly they are background radio transmissions but could be internal system-generated waves or air waves, to name a few.

**pattern analysis:** a method of GPR analysis where amplitude slice-maps are visually analyzed to find patterns that represent what it is hoped features in the ground will look like.

**point-source:** a discrete object in the ground that produces a hyperbolic-shaped reflection. These are often rocks, pipes, objects, or any aerially limited reflection surface.

**pulse:** an electrical charge placed on a transmitting antenna that creates a propagating electromagnetic wave.

**radar:** an acronym, which has now become a word, which began to be used in 1942 for reflected radio waves used for detecting objects in the air. It stands for “radio detection and ranging.” This acronym replaced the British acronym RDF that originally stood for “radio direction finding.”

**radio interference:** any background noise within the frequency of GPR antennas.

**ray paths:** pathways that individual radar waves move in the ground or in air.

**reflections:** other than the obvious definition of a wave being reflected from a surface, it is also commonly used as slang in GPR and seismic wave interpretation for a visually continuous planar surface visible in a reflection profile.

**relative dielectric permittivity (RDP):** a complex equation, that produces a quantifiable value for different materials through which radar waves move, referred to as a dielectric constant by some GPR practitioners. It calculates variations in the propagation of an electromagnetic field, depending on changes in the properties of various materials in the ground. It is used here as a proxy measurement for the velocity of radar waves moving in the ground. RDP is defined as the value of one for radar energy moving in a vacuum, with greater values of RDP calculated for slower velocities. The highest RDP for GPR is 80, for radar waves moving in fresh water.

**resistivity, electrical:** an intrinsic property of a material that quantifies how well it allows the flow of an electrical current. The inverse is conductivity. High electrically

resistive ground materials have a low cation exchange capacity (CEC), and readily allow the passage propagating radar waves.

**shields, used in antennas:** any material that impedes or destroys propagating radar waves. These can be as simple as a copper plate with attached resistors, which has a high electrical conductivity and absorbs all radar waves, which are then destroyed before they can propagate. Other materials (such as “stealth” compounds) can also be used to stop the propagating waves moving in certain directions. In GPR antennas, they are usually placed to stop energy propagation upward and to the sides, so that energy will move only downward. They have less effectiveness in lower frequency antennas and are not used at all in very low (50 MHz or lower) antennas because of their size.

**spreading of radar waves:** movement of waves from a surface antenna in a generally conical shape, with the apex of the cone at the surface antenna. The conical radiation pattern produced by most GPR antennas is elongated in the direction of antennas movement, if the paired transmission and recording antennas are placed perpendicular to the transect (the usual way antennas are moved for most applications).

**stacking:** word that can be used to describe how multiple reflections generated from layered buried interfaces are placed vertically to generate a reflection trace. Also, commonly used in a somewhat different way to describe a method used to average traces during collection, or in post-acquisition processing to generate a less noisy or distorted reflection profile. Stacking during trace averaging usually takes one or more traces in front and behind one trace to average, storing the averaged trace in place of the trace in the middle. For instance, a “stack” of seven traces would average the amplitudes of three traces in front and three behind one trace to be recorded. The stacking values in this type of data processing must be odd numbers of traces and the process is then continued for all traces in a profile, in a moving average.

**survey transects:** any line along the ground surface that an antenna moves. Often, they are linear if collected within a grid, using a Cartesian coordinate system to define their location. But they can be placed in any orientation or geometry if antennas are moved around obstacles or placed in a way to optimize how reflections are recorded from buried interfaces.

**time-window:** the period of time, measured in nanoseconds, which a GPR system is programmed to record waves that were generated from the receiving antenna.

**trace:** a digital recording of waves recorded at one spot on the ground. Usually composed of multiple reflections recorded within a “time window,” where all waves

are “stacked” into one composite waveform. Traces can be analyzed individually to help define reflection at one location but are most commonly “stacked” together sequentially along a survey transect, to generate a reflection profile.

**travel time:** usually the “two-way” time that is measured from when a radar wave leaves the transmitting antenna, moves through a medium, and is then received and recorded at a paired receiving antenna. Can sometimes be “one-way” if antennas are separated and certain types of velocity tests are being performed.

**velocity analysis:** any method that estimates the travel speed of radar waves in a medium. Important so that travel times can be converted to depth, or distance, in GPR studies.

**waveform:** the shape of a received wave in a trace that displays amplitude and wavelength over a time-window.

**wavelet:** Once oscillation of a radar wave that begins with an amplitude of zero, increases or decreases, and then returns to zero one or more times. Usually in GPR it is one positive and one negative deflection of amplitude from zero.

**wide-band:** term to describe most GPR antennas that transmit and receive from more than one frequency. For most GPR antennas this is usually one octave around the “center frequency.”

# References

- Akinci, M. N. "An efficient sampling method for cross-borehole GPR imaging." *IEEE Geoscience and Remote Sensing Letters* 15, no. 12 (2018): 1857–61.
- Al-Qadi, Imad L., and S. Lahouar. "Measuring layer thicknesses with GPR—Theory to practice." *Construction and building materials* 19, no. 10 (2005): 763–72.
- Alani, Amir M., Morteza Aboutaleb, and Gokhan Kilic. "Applications of ground penetrating radar (GPR) in bridge deck monitoring and assessment." *Journal of applied geophysics* 97 (2013): 45–54.
- Alsharahi, G., Driouach, A., and Faize, A. "Performance of GPR influenced by electrical conductivity and dielectric constant." *Procedia Technology* 22 (2016): 570–75.
- Annan, A. Peter. "GPR methods for hydrogeological studies." *Hydrogeophysics*, Springer, Dordrecht. (2005): 185–213.
- Annan, A. P., and L. T. Chua. "Ground penetrating radar performance predictions." In *Ground Penetrating Radar*, J. A. Pilon (editor). 1992 Geological Survey of Canada, Paper 90-4: 5–13.
- Annan, A. P., and S. W. Cosway. "Ground penetrating radar survey design." In *5th EEGS Symposium on the Application of Geophysics to Engineering and Environmental Problems*, pp. cp-210. European Association of Geoscientists & Engineers, 1992.
- Annan, A. P., and S. W. Cosway. "GPR frequency selection." In *Fifth International Conference on Ground Penetrating Radar*, European Association of Geoscientists & Engineers, 1994.
- Annan, A. P., J. L. Davis, and J. Pilon. "Design and development of a digital ground penetrating radar system." *Ground Penetrating Radar, Geological Survey of Canada Special Paper* 90, no. 4 (1992): 15–23.



- Annan, A. P., and J. L. Davis. "Impulse radar applied to ice thickness measurements and freshwater bathymetry." *Geological Survey of Canada, Report of Activities Paper 77* (1977): 117-24.
- Annan, A. P., W. M. Waller, D. W. J. Strangway, J. R. J. Rossiter, J. D. Redman, and R. D. Watts. "The electromagnetic response of a low-loss, 2-layer, dielectric earth for horizontal electric dipole excitation." *Geophysics* 40, no. 2 (1975): 285-98.
- Arcone, Steven A. "Numerical studies of the radiation patterns of resistively loaded dipoles." *Journal of Applied Geophysics* 33, no. 1-3 (1995): 39-52.
- Arcone, Steven A. "High resolution of glacial ice stratigraphy: a ground-penetrating radar study of Pegasus Runway, McMurdo Station, Antarctica." *Geophysics* 61, no. 6 (1996): 1653-63.
- Arcone, Steven A., and Karl Kreutz. "GPR reflection profiles of Clark and Commonwealth Glaciers, Dry Valleys, Antarctica." *Annals of Glaciology* 50, no. 51 (2009): 121-29.
- Arisona, A., Nawawi, M., Ishola, K. S., & Safiuddin, L.O. "Forward modeling of ground penetrating radar for the reconstruction of models response profiles using synthetic data." *Journal of Geology & Geophysics* 6, no. 3 (2007): 1-6.
- Baker, P. L. "Response of ground-penetrating radar to bounding surfaces and lithofacies variations in sand barrier sequences." *Exploration Geophysics* 22, no. 1 (1991): 19-22.
- Balanis, Constantine A. *Advanced Engineering Electromagnetics*. John Wiley & Sons, 2012.
- Ball, A., and L. O'Connor, "Geologist in the loop: A hybrid intelligence model for identifying geological boundaries from augmented Ground Penetrating Radar." *Geosciences*, 11, no. 7 (2021): 1-15.
- Barone, P. M., T. Bellomo, E. Mattei, S. E. Lauro, and E. Pettinelli. "Ground-penetrating radar in the Regio III (Pompeii, Italy): Archaeological Evidence." *Archaeological Prospection* 18, no. 3 (2011): 187-94.
- Barone, P. M. "Roman Archaeology: The benefit of using GPR investigations." In *2018 17th International Conference on Ground Penetrating Radar (GPR)* (2018): 1-4.

- Barone, P. M., and L. Desibio. "Landscape archaeology of southern Umbria (Italy) using the GPR technique." In *8th International Workshop on Advanced Ground Penetrating Radar (IWAGPR)*, 1–4. IEEE, 2015.
- Barone, P. M., R. M. Di Maggio, and C. Ferrara. "Not necessarily buried bodies: forensic GPR investigations from criminal to civil justice." In *2015 8th International Workshop on Advanced Ground Penetrating Radar (IWAGPR)*, 1–4. IEEE, 2015.
- Barone, Pier Matteo, and Rosa Maria Di Maggio. "Forensic geophysics: ground penetrating radar (GPR) techniques and missing persons investigations." *Forensic Sciences Research* 4, no. 4 (2019): 337–40.
- Basson, Uri, Yehouda Enzel, Rivka Amit, and Zvi Ben-Avraham. "Detecting and mapping recent faults with a ground penetrating radar in the alluvial fans of the Arava Valley, Israel." In *Fifth International Conferention on Ground Penetrating Radar*, European Association of Geoscientists & Engineers, 1994.
- Belina, F. A., B. Dafflon, J. Tronicke, and K. Holliger. "Enhancing the vertical resolution of surface georadar data." *Journal of Applied Geophysics* 68, no. 1 (2009): 26–35.
- Benech, Christophe. "New approach to the study of city planning and domestic dwellings in the ancient Near East." *Archaeological Prospection* 14, no. 2 (2007): 87–103.
- Berard, Brooke A., and Jean-Michel Maillol. "Multi-offset ground penetrating radar data for improved imaging in areas of lateral complexity—application at a Native American site." *Journal of Applied Geophysics* 62, no. 2 (2007): 167–77.
- Berard, Brooke A., and J. M. Maillol. "Common- and multi-offset ground-penetrating radar study of a Roman villa, Tourega, Portugal." *Archaeological Prospection* 15, no. 1 (2008): 32–46.
- Beres, Milan and F. P. Haeni. "Application of ground-penetrating-radar methods in Hydrogeological Studies." *Groundwater* 29, no. 3 (1991): 375–86.
- Beres, Milan, Peter Huggenberger, Alan G. Green, and Heinrich Horstmeyer. "Using two- and three-dimensional georadar methods to characterize glaciofluvial architecture." *Sedimentary Geology* 129, no. 1–2 (1999): 1–24.

- Bernabini, M., E. Brizzolari, L. Orlando, and G. Santellani. "Application of ground-penetrating radar on Colloseum pillars." In *Fifth International Conference on Ground Penetrating Radar*, European Association of Geoscientists & Engineers, 1994.
- Bermejo, Lucía, Ana Isabel Ortega, Josep M. Parés, Isidoro Campaña, José María Bermúdez de Castro, Eudald Carbonell, and Lawrence B. Conyers. "Karst features interpretation using ground-penetrating radar: A case study from the Sierra de Atapuerca, Spain." *Geomorphology* 367 (2020): 107311.
- Bevan, B. W. "Ground-penetrating radar at Valley Forge." *Geophysical Survey System, North Salem, New Hampshire* (1977).
- Bevan, Bruce W. "Geophysical exploration for archaeology: An introduction to geophysical exploration." (1998).
- Bevan, Bruce W. "An early geophysical survey at Williamsburg, USA." *Archaeological Prospection* 7, no. 1 (2000): 51-58.
- Bevan, Bruce. "Ground-penetrating radar for historical archaeology." *MASCA Newsletter* 11, no. 2 (1975): 2-7.
- Bianchini Ciampoli, Luca, Fabio Tosti, Nikos Economou, and Francesco Benedetto. "Signal processing of GPR data for road surveys." *Geosciences* 9, no. 2 (2019): 96.
- Birkeland, Peter W. *Soils and Geomorphology*. Oxford University Press, 1984.
- Bjelm, L. "Geologic interpretation of SIR data from a peat deposit in northern Sweden." *Professional Paper Lund Institute of Technology* (1980).
- Bogorodsky, Vitalii Vasil'evich, Vitaliĭ Vasil'evich Bogorodskii, Charles R. Bentley, and P. E. Gudmandsen. *Radioglaciology*. Vol. 1. Springer Science & Business Media, 1985.
- Bornik, Alexander, and Wolfgang Neubauer. "3D visualization techniques for analysis and archaeological interpretation of GPR data." *Remote Sensing* 14, no. 7 (2022): 1709.
- Bongiovanni, María Victoria, Matías de la Vega, and Néstor Bonomo. "Contribution of the resistivity method to characterize mud walls in a very dry region and comparison with GPR." *Journal of Archaeological Science* 38, no. 9 (2011): 2243-50.

- Böniger, Urs, and Jens Tronicke. "Integrated data analysis at an archaeological site: A case study using 3D GPR, magnetic, and high-resolution topographic data." *Geophysics* 75, no. 4 (2010): B169–B176.
- Booth, Adam D., Roger A. Clark, Ken Hamilton, and Tavi Murray. "Multi-offset ground penetrating radar methods to image buried foundations of a medieval town wall, Great Yarmouth, UK." *Archaeological Prospection* 17, no. 2 (2010): 103–16.
- Bradford, John H., Cody R. Johnson, Troy Brosten, James P. McNamara, and Michael N. Gooseff. "Imaging thermal stratigraphy in freshwater lakes using georadar." *Geophysical Research Letters* 34, no. 24 (2007).
- Bridge, John S., J. A. N. Alexander, Richard E. LI Collier, Rob L. Gawthorpe, and Jack Jarvis. "Ground-penetrating radar and coring used to study the large-scale structure of point-bar deposits in three dimensions." *Sedimentology* 42, no. 6 (1995): 839–52.
- Bristow, Charlie S., and Harry M. Jol, eds. *Ground Penetrating Radar in Sediments*. Geological Society of London, 2003.
- Bristow, Charlie, Jonathan Pugh, and T. I. M. Goodall. "Internal structure of aeolian dunes in Abu Dhabi determined using ground-penetrating radar." *Sedimentology* 43, no. 6 (1996): 995–1003.
- Brown, Joel, Josh Nichols, Leah Steinbronn, and John Bradford. "Improved GPR interpretation through resolution of lateral velocity heterogeneity: example from an archaeological site investigation." *Journal of Applied Geophysics* 68, no. 1 (2009): 3–8.
- Bruschini, Claudio, Bertrand Gros, Frédéric Guerne, Pierre-Yves Pièce, and Olivier Carmona. "Ground penetrating radar and imaging metal detector for antipersonnel mine detection." *Journal of Applied Geophysics* 40, no. 1–3 (1998): 59–71.
- Buderi, Robert. *The Invention That Changed the World: The Story of Radar from War to Peace*. New York: Little Brown, 1996.
- Butler, Dwain K., Janet E. Simms, and Daryl S. Cook. "Archaeological geophysics investigation of the Wright Brothers 1910 hangar site." *Geoarchaeology* 9, no. 6 (1994): 437–66.

- Cai, Jun, and George A. McMechan. "Ray-based synthesis of bistatic ground-penetrating radar profiles." *Geophysics* 60, no. 1 (1995): 87–96.
- Calia, Angela, Giovanni Leucci, Nicola Masini, Loredana Matera, Raffaele Persico, and Maria Sileo. "Integrated prospecting in the crypt of the Basilica of Saint Nicholas in Bari, Italy." *Journal of Geophysics and Engineering* 9, no. 3 (2012): 271–81.
- Campana, S., Salvatore Piro. "Putting everything together: GIS-based data integration and interpretation." In S. Campana, S. Piro (eds.), *Seeing the Unseen. Geophysics and Landscape Archaeology* (325–30). 923 CRC Press, 2008.
- Carcione, José M. "Radiation patterns for 2-D GPR forward modeling." *Geophysics* 63, no. 2 (1998): 424–30.
- Cardno, Catherine A. "Ground-penetrating radar redefines archaeology site's methodology." *Civil Engineering Magazine Archive* 89, no. 6 (2019): 40–41.
- Carrozzo, Maria Teresa, Giovanni Leucci, Sergio Negri, and Luigia Nuzzo. "GPR survey to understand the stratigraphy of the Roman ships archaeological site (Pisa, Italy)." *Archaeological Prospection* 10, no. 1 (2003): 57–72.
- Chandra, M., and Tanzi, T. J. "Drone-borne GPR design: Propagation issues." *Comptes Rendus Physique* 19, 1–2 (2018): 72–84.
- Chen, Lianwu, and Fei Niu. "Processing Method of Geological Data in Contour Map based on Surfer." *World Scientific Research Journal* 5, no. 11 (2019): 102–8.
- Chignell, Richard J. "The radio licensing of GPR systems in Europe." In *Proceedings of the Tenth International Conference on Grounds Penetrating Radar, 2004. GPR 2004.*, vol. 1, IEEE (2004): 3–6.
- Clark, Oliver Anthony, and Anthony Clark. *Seeing Beneath the Soil: Prospecting Methods in Archaeology*. Routledge, 2003.
- Clarke, Ciara M., Erica Utsi, and Vincent Utsi. "Ground penetrating radar investigations at north Ballachulish Moss, Highland, Scotland." *Archaeological Prospection* 6, no. 2 (1999): 107–21.
- Collins, Mary E. "Soil taxonomy: A useful guide for the application of ground penetrating radar." In *Fourth International Conference on Ground Penetrating Radar*, European Association of Geoscientists & Engineers, 1992.

- Comegna, Alessandro, Antonio Coppola, Giovanna Dragonetti, and Angelo Sommella. "A soil non-aqueous phase liquid (NAPL) flushing laboratory experiment based on measuring the dielectric properties of soil-organic mixtures via time domain reflectometry (TDR)." *Hydrology and Earth System Sciences* 23, no. 9 (2019): 3593-602.
- Conyers, Lawrence B. "The use of ground-penetrating radar to map the buried structures and landscape of the Ceren site, El Salvador." *Geoarchaeology* 10, no. 4 (1995): 275-99.
- Conyers, Lawrence B. "Acquisition, processing and interpretation techniques for ground—penetrating radar mapping of buried pit-structures." In *Proceedings: GPR'98, Seventh International Conference on Ground-Penetrating Radar: May 27-30, 1998, University of Kansas, Lawrence, Kansas, USA*, Radar Systems and Remote Sensing Laboratory, University of Kansas (1998): 53-58.
- Conyers, Lawrence B. "Ground-penetrating radar." In *Remote Sensing in Archaeology: An Explicitly North American Perspective* (2006): 131-60.
- Conyers, Lawrence B. "Moisture and soil differences as related to the spatial accuracy of GPR amplitude maps at two archaeological test sites." In *Proceedings of the Tenth International Conference on Grounds Penetrating Radar, 2004. GPR 2004.*, IEEE (2004): 535-38.
- Conyers, Lawrence B. "Ground-penetrating radar for landscape archaeology: method and applications." In *Seeing the Unseen. Geophysics and Landscape Archaeology*, CRC Press (2008): 271-82.
- Conyers, Lawrence B. "Ground-penetrating radar for anthropological research." *Antiquity* 84, no. 323 (2010): 175-84.
- Conyers, Lawrence B. "Ground-penetrating radar mapping of non-reflective archaeological features." In *Proceedings of the 9th International Conference on Archaeological Prospection, September 19-24, Izmir* (2011): 238-42.
- Conyers, Lawrence B. "Discovery, mapping and interpretation of buried cultural resources non-invasively with ground-penetrating radar." *Journal of Geophysics and Engineering* 8, no. 3 (2011): S13-S22.
- Conyers, Lawrence B. *Interpreting Ground-penetrating Radar for Archaeology*. Routledge, 2012.

- Conyers, Lawrence B. "Advances in ground-penetrating radar exploration in southern Arizona." *Journal of Arizona Archaeology* 2, no. 1 (2012): 80–91.
- Conyers, Lawrence B. *Ground-penetrating Radar for Archaeology*, 3rd Edition. Routledge, 2013.
- Conyers, Lawrence B. "Analysis and interpretation of GPR datasets for integrated archaeological mapping." *Near Surface Geophysics* 13, no. 6 (2015): 645–51.
- Conyers, Lawrence B. "Ground-penetrating radar data analysis for more complete archaeological interpretations." *Archaeologia Polona* 53 (2015): 272–75.
- Conyers, Lawrence B. "Analysis and interpretation of GPR datasets for integrated archaeological mapping." *Near Surface Geophysics* 13, no. 6 (2015): 645–51.
- Conyers, Lawrence B. "Ground-penetrating radar mapping using multiple processing and interpretation methods." *Remote Sensing* 8, no. 7 (2016): 562–70.
- Conyers, Lawrence B. *Ground-Penetrating Radar for Geoarchaeology*. John Wiley & Sons, 2016.
- Conyers, Lawrence B. *Ground-penetrating Radar and Magnetometry for Buried Landscape Analysis*. Springer, 2017.
- Conyers, Lawrence B. "Integration of GPR with and magnetics to understand the composition and origin of units to study the interior features and history of earthen mounds, Mapoon, Queensland, Australia." In *18th International Conference on Ground Penetrating Radar*, Society of Exploration Geophysicists (2020): 10–13.
- Conyers, Lawrence B. "Using ground-penetrating radar to analyze interior details of a Hohokam Dwelling to test ideas about cultural change and community dynamics in 10th century southern Arizona, USA." *Revue d'Archéométrie* 45 (2021): a219.
- Conyers, Lawrence B. "GPR mapping for more than just finding buried materials: A case study in testing ideas about cultural change and community dynamics in 10th century southern Arizona, USA." In *19th International Conference on Ground Penetrating Radar*, Society of Exploration Geophysicists (2022): 9–11.

- Conyers, Lawrence B. and Catherine M. Cameron. "Finding buried archaeological features in the American Southwest: New ground-penetrating radar techniques and three-dimensional computer mapping." *Journal of Field Archaeology* 25, no. 4 (1998): 417-30.
- Conyers, Lawrence B., and Samuel Connell. "The applicability of using ground-penetrating radar to discover and map buried archaeological sites in Hawaii." *Hawaiian Archaeology Journal* 11 (2007): 62-77.
- Conyers, Lawrence B., J. Michael Daniels, Jonathan A. Haws, and Michael M. Benedetti. "An Upper Paleolithic landscape analysis of coastal Portugal using ground-penetrating radar." *Archaeological Prospection* 20, no. 1 (2013): 45-51.
- Conyers, Lawrence B., Eileen G. Ernenwein, and Leigh-Ann Bedal. "Ground-penetrating radar discovery at Petra, Jordan." *Antiquity* 76, no. 292 (2002): 339-40.
- Conyers, Lawrence B., and Dean Goodman. *Ground-penetrating Radar: An Introduction for Archaeologists*. AltaMira Press, 1997.
- Conyers, Lawrence B., and Juerg Leckebusch. "Geophysical archaeology research agendas for the future: Some ground-penetrating radar examples." *Archaeological Prospection* 17, no. 2 (2010): 117-23.
- Conyers, Lawrence B., and Jeffrey E. Lucius. "Velocity analysis in archaeological ground-penetrating radar studies." *Archaeological Prospection* 3, no. 1 (1996): 25-38.
- Conyers, Lawrence B., and Tiffany Osburn. "GPR mapping to test anthropological hypotheses: a study from Comb Wash, Utah, American Southwest." In *11th International Conference on Ground Penetrating Radar* (2006): 146-50.
- Conyers, Lawrence B., Emma J. St. Pierre, Mary-Jean Sutton, and Chet Walker. "Integration of GPR and magnetics to study the interior features and history of earth mounds, Mapoon, Queensland, Australia." *Archaeological Prospection* 26, no. 1 (2019): 3-12.
- Conyers, Lawrence B., Mary-Jean Sutton, and Emma St. Pierre. "Dissecting and interpreting a three-dimensional ground-penetrating radar dataset: an example from Northern Australia." *Sensors* 19, no. 5 (2019).
- Cook, John C. "Radar exploration through rock in advance of mining." *Trans. Soc. Min. Eng. AIME; (United States)* 254 (1976).



- Corradini, Erica, Daniel Groß, Tina Wunderlich, Harald Lübke, Dennis Wilken, Ercan Erkul, Ulrich Schmölcke, and Wolfgang Rabbel. "Finding Mesolithic sites: A multichannel ground-penetrating radar (GPR) investigation at the ancient Lake Duvensee." *Remote Sensing* 14, no. 3 (2022): 781.
- Damiata, Brian N., John M. Steinberg, Douglas J. Bolender, and Guðný Zoëga. "Imaging skeletal remains with ground-penetrating radar: comparative results over two graves from Viking Age and Medieval churchyards on the Stóra-Seyla farm, northern Iceland." *Journal of Archaeological Science* 40, no. 1 (2013): 268-78.
- Daniels, David J. "GPR for landmine detection, an invited review paper." In *Proceedings of the Tenth International Conference on Grounds Penetrating Radar, 2004. GPR 2004.*, vol. 1, IEEE (2004): 7-10.
- Davis, J. L., and A. Peter Annan. "Ground-penetrating radar for high-resolution mapping of soil and rock stratigraphy 1." *Geophysical Prospecting* 37, no. 5 (1989): 531-51.
- Delaney, Allan J., Steve A. Arcone, Allen O'Bannon, and John Wright. "Crevasse detection with GPR across the Ross Ice Shelf, Antarctica." In *Proceedings of the Tenth International Conference on Grounds Penetrating Radar, 2004. GPR 2004.*, IEEE (2004): 777-80.
- Deiana, R., Leucci, G., and Martorana, R. "New perspectives on geophysics for archaeology: A special issue." *Surveys in Geophysics*, 39 (2018): 1035-38.
- Depeursinge, A., Foncubierta-Rodriguez, A., Van De Ville, D., and Müller, H. "Three-dimensional solid texture analysis in biomedical imaging: review and opportunities." *Medical Image Analysis* 18, no. 1 (2014): 176-96.
- Dixon, Kelly J., Shannon A. Novak, Gwen Robbins, Julie M. Schablitsky, G. Richard Scott, and Guy L. Tasa. "'Men, women, and children starving': Archaeology of the Donner family camp." *American Antiquity* 75, no. 3 (2010): 627-56.
- Dobrin, M. B., and C. H. Sovit. *Introduction to Geophysical Prospecting*. McGraw-Hill Inc., USA, 1988.
- Dolphin, Jr., Lambert T., Robert L. Bollen, and George N. Oetzel. "An underground electromagnetic sounder experiment." *Geophysics* 39, no. 1 (1974): 49-55.

- Doolittle, James A. "Characterizing soil map units with the ground-penetrating radar." *Soil Survey Horizons* 23, no. 4 (1982): 3-10.
- Doolittle, James A., and Loris E. Asmussen. "The years of applications of ground penetrating radar by the United States department of Agriculture." In *Fourth International Conference on Ground Penetrating Radar*. European Association of Geoscientists & Engineers (1992): 303-7.
- Doolittle, James A., and Mary E. Collins. "Use of soil information to determine application of ground penetrating radar." *Journal of applied geophysics* 33, no. 1-3 (1995): 101-8.
- Doolittle, James A., and W. Frank Miller. "Use of ground-penetrating radar techniques in archaeological investigations." In *Applications of Space-Age Technology in Anthropology Conference Proceedings*, 2nd ed. NASA Science and Technology Laboratory, Stennis Space Center, Mississippi (1991): 1-13.
- Doolittle, James A., Fred E. Minzenmayer, Sharon W. Waltman, Ellis C. Benham, J. W. Tuttle, and S. D. Peaslee. "Ground-penetrating radar soil suitability map of the conterminous United States." *Geoderma* 141, no. 3-4 (2007): 416-21.
- Draganits, Erich, Michael Doneus, Terje Gansum, Lars Gustavsen, Erich Nau, Christer Tonning, Immo Trinks, and Wolfgang Neubauer. "The late Nordic Iron Age and Viking Age royal burial site of Borre in Norway: ALS-and GPR-based landscape reconstruction and harbour location at an uplifting coastal area." *Quaternary International* 367 (2015): 96-110.
- Economou, Nikos, Antonis Vafidis, Francesco Benedetto, and Amir M. Alani. "GPR data processing techniques." In *Civil Engineering Applications of Ground Penetrating Radar*. Springer, Cham (2015): 281-97.
- Eide, E., Linford, N., Persico, R. and Sala, J., "Advanced SFCW GPR systems." In *Innovation in Near-Surface Geophysics* (2019): 253-85.
- Eide, E., Våland, P. A., and Sala, J. "Ground-coupled antenna array for step-frequency GPR." In *Proceedings of the 15th International Conference on Ground Penetrating Radar*. (2014): 756-61.
- Engheta, N., C. H. Papas, and C. Elachi. "Radiation patterns of interfacial dipole antennas." *Radio Science* 17, no. 6 (1982): 1557-66.

- Ernenwein, Eileen G. "Imaging in the ground-penetrating radar near-field zone: a case study from New Mexico, USA." *Archaeological Prospection* 13, no. 2 (2006): 154–56.
- Ernenwein, E. G. "Integration of multidimensional archaeogeophysical data using supervised and unsupervised classification." *Near Surface Geophysics*, 7 (2009): 147–58.
- Ernenwein, Eileen G., and Kenneth L. Kvamme. "Data processing issues in large-area GPR surveys: correcting trace misalignments, edge discontinuities and striping." *Archaeological Prospection* 15, no. 2 (2008): 133–49.
- Fassbinder, Jörg WE. "Seeing beneath the farmland, steppe and desert soil: magnetic prospecting and soil magnetism." *Journal of Archaeological Science* 56 (2015): 85–95.
- Filzwieser, Roland, Lis Helles Olesen, Wolfgang Neubauer, Immo Trinks, Esben Schlosser Mauritsen, Petra Schneidhofer, Erich Nau, and Manuel Gabler. "Large-scale geophysical archaeological prospection pilot study at Viking Age and medieval sites in west Jutland, Denmark." *Archaeological Prospection* 24, no. 4 (2017): 373–93.
- Filzwieser, Roland, Lis Helles Olesen, Geert Verhoeven, Esben Schlosser Mauritsen, Wolfgang Neubauer, Immo Trinks, and Milena Nowak. "Integration of complementary archaeological prospection data from a Late Iron Age settlement at Vesterager—Denmark." *Journal of Archaeological Method and Theory* 25, no. 2 (2018): 313–33.
- Fischer, Peter M., Sven GW Follin, and Peter Ulriksen. "Subsurface interface radar survey at Hala Sultan Tekke, Cyprus." *Applications of Technical Devices in Archaeology* (1980): 48–51.
- Fisher, Elizabeth, George A. McMechan, and A. Peter Annan. "Acquisition and processing of wide-aperture ground-penetrating radar data." *Geophysics* 57, no. 3 (1992): 495–504.
- Fisher, Steven C., Robert R. Stewart, and Harry M. Jol. "Ground penetrating radar (GPR) data enhancement using seismic techniques." *Journal of Environmental and Engineering Geophysics* 1, no. 2 (1996): 89–96.
- Forte, Emanuele, and Michele Pipan. "Review of multi-offset GPR applications: Data acquisition, processing and analysis." *Signal Processing* 132 (2017): 210–20.

- Forte, Emanuele, Arianna Mocnik, Patrizia Basso, Giulia Casagrande, Davide Martinucci, Simone Pillon, Marco Possamai, and Roberta Zambrini. "Optimised extraction of archaeological features from full 3-D GPR data." *Applied Sciences* 11, no. 18 (2021): 8517.
- Fredengren, C. "Unexpected encounters with deep time enchantment. Bog bodies, crannogs and 'Other-worldly sites.' The materializing powers of disjunctures in time." *World Archaeology* 48, no. 4 (2016): 482-99.
- Freeland, Robert S., Ronald E. Yoder, and John T. Ammons. "Mapping shallow underground features that influence site-specific agricultural production." *Journal of Applied Geophysics* 40, no. 1-3 (1998): 19-27.
- Fuchs, Michaël, Milan Beres, and Flavio S. Anselmetti. "Sedimentological studies of western Swiss lakes with high-resolution reflection seismic and amphibious GPR profiling." In *Proceedings of the Tenth International Conference on Grounds Penetrating Radar, 2004. GPR 2004.*, IEEE (2004): 577-80.
- Fullagar, P. K., and D. Livelybrooks. "Trial of tunnel radar for cavity and ore detection in the Sudbury mining camp, Ontario." In *Fifth International Conference on Ground Penetrating Radar*, European Association of Geoscientists & Engineers (1994): cp-300.
- Gaballah, Mahmoud, Mark Grasmueck, and Motoyuki Sato. "Characterizing subsurface archaeological structures with full resolution 3D GPR at the early dynastic foundations of Saqqara Necropolis, Egypt." *Sensing and Imaging* 19, no. 1 (2018): 1-15.
- Gaballah, Mahmoud. "GPR measurements with advanced isosurface rendering technique for accurately characterizing subsurface archaeological structure at Al-Nadura roman temple in Egypt." *Sensing and Imaging* 20, no. 1 (2019): 1-16.
- Gabler, Manuel, Claes Olof Johan Uhnér, Nils Ole Sundet, Alois Hinterleitner, Pål Nymoen, Monica Kristiansen, and Immo Trinks. "Archaeological prospection in wetlands—Experiences and observations from ground-penetrating radar surveys in Norwegian bogs." *Remote Sensing* 13, no. 16 (2021): 3170.
- Gabryś, Marta, and Łukasz Ortyl. "Georeferencing of multi-channel GPR—Accuracy and efficiency of mapping of underground utility networks." *Remote Sensing* 12, no. 18 (2020): 2945.

- Gaffney, Chris, Vince Gaffney, Wolfgang Neubauer, Eamonn Baldwin, Henry Chapman, Paul Garwood, Helen Moulden et al. "The Stonehenge hidden landscapes project." *Archaeological Prospection* 19, no. 2 (2012): 147–55.
- Garrison, Ervan. "Geophysical techniques for archaeology." In *Techniques in Archaeological Geology*, Springer, Cham (2016): 115–43.
- Gerber, Rolf, Peter Felix-Henningsen, Christina Salat, and Andreas Junge. "Investigation of the GPR reflection pattern for shallow depths on a test site." In *Proceedings of the Tenth International Conference on Grounds Penetrating Radar, 2004. GPR 2004.*, vol. 1, IEEE (2004): 275–78.
- Ghezzi, Annalisa, Antonio Schettino, Pietro Paolo Pierantoni, Lawrence Conyers, Luca Tassi, Luigi Vigliotti, Erwin Schettino, Milena Melfi, Maria Elena Gorrini, and Paolo Boila. "Reconstruction of a segment of the UNESCO World Heritage Hadrian's Villa tunnel network by integrated GPR, magnetic-paleomagnetic, and electric resistivity prospections." *Remote Sensing* 11, no. 15 (2019): 1739.
- Gizzi, Fabrizio Terenzio, and Giovanni Leucci. "Global research patterns on ground penetrating radar (GPR)." *Surveys in Geophysics* 39.6 (2018): 1039–68.
- Goodman, Dean. "Ground-penetrating radar simulation in engineering and archaeology." *Geophysics* 59, no. 2 (1994): 224–32.
- Goodman, Dean. "Comparison of GPR time slices and archaeological excavations." In *Proceedings of the 6th International Conference on Ground Penetrating Radar (Sendai, Japan)*, (1996): 77–78.
- Goodman, Dean, Hongo Hiromichi, Noriaki Higashi, Yasushi Nishimura, and Masashi Tokuda. "The application of GPR overlay analysis in archaeological prospection: Discovery at the Japanese Imperial Family tombs in Miyazaki Prefecture." *ArcheoSciences. Revue d'Archéométrie* 33 (2009): 295–97.
- Goodman, Dean, and Salvatore Piro. *GPR Remote Sensing in Archaeology*. Vol. 9. New York: Springer, 2013.
- Goodman, Dean, and Yasushi Nishimura. "A ground-radar view of Japanese burial mounds." *Antiquity* 67, no. 255 (1993): 349–54.

- Goodman, Dean, Yasushi Nishimura, and J. Daniel Rogers. "GPR time slices in archaeological prospection." *Archaeological Prospection* 2, no. 2 (1995): 85–89.
- Goodman, Dean, Yashushi Nishimura, Hiromichi Hongo, and M. Okita. "GPR amplitude rendering in archaeology." In *Proceedings of the Seventh International Conference on Ground Penetrating Radar* (1998): 91–92.
- Goodman, Dean, Salvatore Piro, Yasushi Nishimura, Helen Patterson, and Vince Gaffney. "Discovery of a 1st century AD Roman amphitheater and other structures at the Forum Novum by GPR." *Journal of Environmental & Engineering Geophysics* 9, no. 1 (2004): 35–41.
- Goodman, Dean, John Steinberg, Brian Damiata, Y. Nishimure, Kent Schneider, Hongo Hiromichi, and N. Hisashi. "GPR overlay analysis for archaeological prospection." In *Proceedings of the 11th International Conference on Ground Penetrating Radar*, Columbus, Ohio: (2006): 19–22.
- Grab, Melchior, Andreas Bauder, Florian Ammann, Lisbeth Langhammer, Sebastian Hellmann, Gregory J. Church, Lino Schmid, Lasse Rabenstein, and H. R. Maurer. "Ice volume estimates of Swiss glaciers using helicopter-borne GPR—An example from the Glacier de la Plaine Morte." In *2018 17th International Conference on Ground Penetrating Radar (GPR)*, IEEE (2018): 1–4.
- Grandjean, G., J. C. Gourry, and A. Bitri. "Evaluation of GPR techniques for civil-engineering applications: study on a test site." *Journal of Applied Geophysics* 45, no. 3 (2000): 141–56.
- Grasmueck, Mark. "Application of seismic processing techniques to discontinuity mapping with ground-penetrating radar in crystalline rock of the Gotthard massif, Switzerland." In *Fifth International Conference on Ground Penetrating Radar*, European Association of Geoscientists & Engineers (1994): cp–300.
- Grasmueck, Mark. "3-D ground-penetrating radar applied to fracture imaging in gneiss." *Geophysics* 61, no. 4 (1996): 1050–64.
- Grasmueck, Mark, Ralf Weger, and Heinrich Horstmeyer. "Full-resolution 3D GPR imaging for geoscience and archeology." In *Proceedings of the Tenth International Conference on Grounds Penetrating Radar, 2004. GPR 2004.*, vol. 1, IEEE (2004): 329–32.
- Grealy, Michael. "Resolution of ground-penetrating radar reflections at differing frequencies." *Archaeological Prospection* 13, no. 2 (2006): 142–46.

- Grossman, Emily D., and Randolph Blake. "Brain areas active during visual perception of biological motion." In *Social Neuroscience*, Psychology Press (2013): 101-14.
- Gugl C., Wallner M., Hinterleitner A., and Neubauer W. "The seat of the Roman governor at Carnuntum (Pannonia Superior)." *Heritage*. (2021): 3009-31.
- Gustavsen, Lars, Arne Anderson Stamnes, Silje Elisabeth Fretheim, Lars Erik Gjerpe, and Erich Nau. "The effectiveness of large-scale, high-resolution ground-penetrating radar surveys and trial trenching for archaeological site evaluations—A comparative study from two sites in Norway." *Remote Sensing* 12, no. 9 (2020): 1408.
- Haeni, F. P., Marc L. Buursink, John E. Costa, Nick B. Melcher, Ralph T. Cheng, and William J. Plant. "Ground penetrating radar methods used in surface-water discharge measurements." In *Eighth International Conference on Ground Penetrating Radar*, vol. 4084, SPIE (2000): 494-500.
- Hamran, Svein-Erik, David A. Paige, Abigail Allwood, Hans EF Amundsen, Tor Berger, Sverre Brovoll, Lynn Carter et al. "Ground penetrating radar observations of subsurface structures in the floor of Jezero crater, Mars." *Science Advances* 8, no. 34 (2022): 8564.
- Hansen, James D., Jamie K. Pringle, and Jon Goodwin. "GPR and bulk ground resistivity surveys in graveyards: Locating unmarked burials in contrasting soil types." *Forensic Science International* 237 (2014): e14-e29.
- Hatton, Leslie, Michael H. Worthington, and John Makin. *Seismic Data Processing: Theory and Practice*. Merlin Profiles Ltd., 1986.
- Heinz, Jürgen, and Thomas Aigner. "Three-dimensional GPR analysis of various Quaternary gravel-bed braided river deposits (southwestern Germany)." *Geological Society, London, Special Publications* 211, no. 1 (2003): 99-110.
- Herrmann, Jason T., and Paola Sconzo. "Planning Punic cities: geophysical prospection and the built environment at Motya, Sicily." *Antiquity* 94, no. 376 (2020): 983-98.
- Herron D.A., "Horizon autopicking." *The Leading Edge* 19, no. 5 (2000): 491-92.
- Hilbert, David. *Grundzüge Einer Allgemeinen Theorie der Linearen Integralgleichungen* [Framework for a General Theory of Linear Integral Equations] (in German).

Leipzig & Berlin, DE (1912); New York, NY (1953): B.G. Teubner (1912); Chelsea Pub. Co. (1953).

Hildebrand, J. A., S. M. Wiggins, P. C. Henkart, and L. B. Conyers. "Comparison of seismic reflection and ground-penetrating radar imaging at the controlled archaeological test site, Champaign, Illinois." *Archaeological Prospection* 9, no. 1 (2002): 9–21.

Hong, W. T., Kang, S., Lee, S. J., & Lee, J. S. "Analyses of GPR signals for characterization of ground conditions in urban areas." *Journal of Applied Geophysics*, 152 (2018): 65–76.

Imai, Tsuneo, Toshihiko Sakayama, and Takashi Kanemori. "Use of ground-probing radar and resistivity surveys for archaeological investigations." *Geophysics* 52, no. 2 (1987): 137–50.

Irving, James, and Rosemary Knight. "Numerical modeling of ground-penetrating radar in 2-D using MATLAB." *Computers & Geosciences* 32, no. 9 (2006): 1247–58.

Isaacson, John, R. Eric Hollinger, Darrell Gundrum, and Joyce Baird. "A controlled archaeological test site facility in Illinois: Training and research in archaeogeophysics." *Journal of Field Archaeology* 26, no. 2 (1999): 227–36.

Jackson, John David. *Classical Electrodynamics*. John Wiley & Sons, 2021.

Jeng, Yih, Yi-Wei Li, Chih-Sung Chen, and Hsin-Yi Chien. "Adaptive filtering of random noise in near-surface seismic and ground-penetrating radar data." *Journal of Applied Geophysics* 68, no. 1 (2009): 36–46.

Johnson, Jay K. "A Comparative Guide to Applications." *Remote Sensing in Archaeology: An Explicitly North American Perspective* (2006): 305.

Johnson, R. W., R. Glasscum, and R. Wojtasinski. "Application of ground penetrating radar to soil survey." *Soil Survey Horizons* 23, no. 3 (1982): 17–25.

Johnston, Brian, Alastair Ruffell, Jennifer McKinley, and Patricia Warke. "Detecting voids within a historical building façade: A comparative study of three high frequency GPR antenna." *Journal of Cultural Heritage* 32 (2018): 117–23.

Jol, Harry M., ed. *Ground Penetrating Radar Theory and Applications*. Elsevier, 2008.



- Jol, Harry M., and Charlie S. Bristow. "GPR in sediments: advice on data collection, basic processing and interpretation, a good practice guide." *Geological Society, London, Special Publications* 211, no. 1 (2003): 9–27.
- Jol, Harry M., and Derald G. Smith. "Ground penetrating radar of northern lacustrine deltas." *Canadian Journal of Earth Sciences* 28, no. 12 (1991): 1939–47.
- Jol, Harry M., Derald G. Smith, and Richard A. Meyers. "Digital ground penetrating radar (GPR): a new geophysical tool for coastal barrier research (examples from the Atlantic, Gulf and Pacific Coasts, USA)." *Journal of Coastal Research* (1996): 960–68.
- Kargas, George, and Konstantinos X. Soulis. "Performance evaluation of a recently developed soil water content, dielectric permittivity, and bulk electrical conductivity electromagnetic sensor." *Agricultural Water Management* 213 (2019): 568–79.
- Kemerait, Robert C. "Ground penetrating radar considerations for optimizing the data collection scenario." In *Fifth International Conference on Ground Penetrating Radar*, European Association of Geoscientists & Engineers (1994): cp-300.
- Kenyon, Jeff L., and Bruce Bevan. "Ground-penetrating radar and its application to a historical archaeological site." *Historical Archaeology* 11, no. 1 (1977): 48–55.
- Kraus, J. D. *Antennas*. McGraw Hill Book Company Inc., New York, 1950.
- Küçükdemirci, M., & Sarris, A. "GPR Data Processing and Interpretation Based on Artificial Intelligence Approaches: Future Perspectives for Archaeological Prospection." *Remote Sensing* 14 (2022): 3377.
- Kvamme, Kenneth L. "Geophysical surveys as landscape archaeology." *American Antiquity* 68, no. 3 (2003): 435–57.
- Kvamme, Kenneth L. "Integrating multidimensional geophysical data." *Archaeological Prospection* 13, no. 1 (2006): 57–72.
- Kvamme, K. L., Ernenwein, E. G., Menzer, J. G., "Putting it all together: Geophysical data integration." In R. Persico, S. Piro, N. Linford (Eds.), *Innovation in Near-Surface Geophysics. 1035 Instrumentation, Application, and Data Processing Methods*. (2019): 287–339.

- LaFleche, P. T., J. P. Todoeschuck, O. G. Jensen, and A. S. Judge. "Analysis of ground-probing radar data: predictive deconvolution." *Canadian Geotechnical Journal* 28, no. 1 (1991): 134–39.
- Lai, W. W. L., Dérobert, X., & Annan, P. "A review of ground penetrating radar application in civil engineering: A 30-year journey from locating and testing to imaging and diagnosis." *Ndt & E International*, 96 (2018): 58–78.
- Leckebusch, Jürg. "Two- and three-dimensional ground-penetrating radar surveys across a medieval choir: a case study in archaeology." *Archaeological Prospection* 7, no. 3 (2000): 189–200.
- Leckebusch, Jürg. "Ground-penetrating radar: a modern three-dimensional prospection method." *Archaeological Prospection* 10, no. 4 (2003): 213–40.
- Leckebusch, Jürg. "Problems and solutions with GPR data interpretation: Depolarization and data continuity." *Archaeological Prospection* 18, no. 4 (2011): 303–08.
- Leckebusch, Jürg, and Ronald Peikert. "Investigating the true resolution and three-dimensional capabilities of ground-penetrating radar data in archaeological surveys: measurements in a sand box." *Archaeological Prospection* 8, no. 1 (2001): 29–40.
- Leckebusch, Jürg. "Comparison of a stepped-frequency continuous wave and a pulsed GPR system." *Archaeological Prospection* 18, no. 1 (2011): 15–25.
- Lehmann, Frank, and Alan G. Green. "Semi-automated georadar data acquisition in three dimensions." *Geophysics* 64, no. 3 (1999): 719–31.
- Lehmann, Frank, and Alan G. Green. "Topographic migration of georadar data: Implications for acquisition and processing topographic migration of georadar data." *Geophysics* 65, no. 3 (2000): 836–48.
- Leopold, Matthias, and Jörg Völkel. "GPR images of periglacial slope deposits beneath peat bogs in the Central European Highlands, Germany." *Geological Society, London, Special Publications* 211, no. 1 (2003): 181–89.
- Leucci, Giovanni, and Sergio Negri. "Use of ground penetrating radar to map subsurface archaeological features in an urban area." *Journal of Archaeological Science* 33, no. 4 (2006): 502–12.

- Leucci, Giovanni, Nicola Masini, and Raffaele Persico. "Time-frequency analysis of GPR data to investigate the damage of monumental buildings." *Journal of Geophysics and Engineering* 9, no. 4 (2012): S81-S91.
- Li, Fangyu, Bin Lyu, Jie Qi, Sumit Verma, and Bo Zhang. "Seismic coherence for discontinuity interpretation." *Surveys in Geophysics* 42, no. 6 (2021): 1229-80.
- Linford, N. T., and P. K. Linford. "Ground penetrating radar survey over a Roman building at Groundwell Ridge, Blunsdon St Andrew, Swindon, UK." *Archaeological Prospection* 11, no. 1 (2004): 49-55.
- Linford, N. "Rapid processing of GPR time slices for data visualisation during field acquisition." In *Proceedings of the 15th International Conference on Ground Penetrating Radar*, IEEE (2014): 702-6.
- Liner, Christopher L. *Elements of 3D Seismology*. Society of Exploration Geophysicists, 2016.
- Liu, H., Y. X. Zhang, Z. J. Long, F. Han, and Q. H. Liu. "Three-dimensional reverse-time migration applied to a MIMO GPR system for subsurface imaging." In *2016 16th International Conference on Ground Penetrating Radar (GPR)* IEEE (2016): 1-4.
- Lowry, Sarah, and Shawn Patch. "Using GPR in a cultural resource management context to map large-scale Mississippian village sites in the Tennessee River Valley, United States." In *18th International Conference on Ground Penetrating Radar*, Society of Exploration Geophysicists (2020): 18-21.
- Lucius, Jeffrey E., and Michael H. Powers. *GPR Data Processing Computer Software for the PC*. US Department of the Interior, US Geological Survey, 2002.
- Maijala, Pekka. "Application of some seismic data processing methods to ground penetrating radar data." In *Fourth International Conference on Ground Penetrating Radar*, European Association of Geoscientists & Engineers, 1992.
- Malagodi, S., L. Orlando, S. Piro, and F. Rosso. "Location of archaeological structures using GPR method: Three-dimensional data acquisition and radar signal processing." *Archaeological Prospection* 3, no. 1 (1996): 13-23.
- Matera, L., Noviello, M., Ciminale, M., Persico, R., "Integration of multisensor data: an experiment in the archaeological park of Egnazia (Apulia, Southern Italy)." *Near Surface Geophysics*, 13 (2015): 613-21.

- McNutt, Ellison J., Kevin G. Hatala, Catherine Miller, James Adams, Jesse Casana, Andrew S. Deane, Nathaniel J. Dominy et al. "Footprint evidence of early hominin locomotor diversity at Laetoli, Tanzania." *Nature* 600, no. 7889 (2021): 468-71.
- Mertens, Laurence, Raffaele Persico, Loredana Matera, and Sebastien Lambot. "Automated detection of reflection hyperbolas in complex GPR images with no a priori knowledge on the medium." *IEEE Transactions on Geoscience and Remote Sensing* 54, no. 1 (2015): 580-96.
- Merz, Kaspar, Hansruedi Maurer, Thomas Buchli, Heinrich Horstmeyer, Alan G. Green, and Sarah M. Springman. "Evaluation of ground-based and helicopter ground-penetrating radar data acquired across an Alpine rock glacier." *Permafrost and Periglacial Processes* 26, no. 1 (2015): 13-27.
- Miller, Jacquelynn F., Alice R. Kelley, Joseph T. Kelley, Daniel F. Belknap, and Arthur E. Spiess. "Ground-penetrating radar as a cultural resource management tool for assessment of eroding shell middens." *Conservation and Management of Archaeological Sites* 20, no. 4 (2018): 199-214.
- Milligan, Robert, Malcolm Atkin, and J. Andresen. "The use of ground-probing radar within a digital environment on archaeological sites." *Computing the Past: Computer Application and Quantitative methods in Archaeology* (1993): 285-91.
- Moffatt, David L., and R. J. Puskas. "A subsurface electromagnetic pulse radar." *Geophysics* 41, no. 3 (1976): 506-18.
- Morelli, G., G. Pagano, S. Floris, M. Pelorosso, Maria Di Nezza, G. A. Pichardo, Flavio Cecchini, Siro Margottini, and Michele Di Filippo. "A multi-methodological approach for archaeology." In *Second EAGE International Conference on Engineering Geophysics*, European Association of Geoscientists & Engineers (2013): cp-368.
- Neal, Adrian. "Ground-penetrating radar and its use in sedimentology: Principles, problems and progress." *Earth-Science Reviews* 66, no. 3-4 (2004): 261-330.
- Nelson, Peter A. "The role of GPR in community-driven compliance archaeology with tribal and non-tribal communities in central California." *Advances in Archaeological Practice* 9, no. 3 (2021): 215-25.

- Neubauer, Wolfgang, Alois Eder-Hinterleitner, Sirri Seren, and Peter Melichar. "Georadar in the Roman civil town Carnuntum, Austria: An approach for archaeological interpretation of GPR data." *Archaeological Prospection* 9, no. 3 (2002): 135-56.
- Noon, David A., Dennis Longstaff, and Richard J. Yelf. "Advances in the development of step frequency ground penetrating radar." In *Fifth International Conference on Ground Penetrating Radar*, European Association of Geoscientists & Engineers, 1994.
- Novo, Alexandre, Henrique Lorenzo, Fernando I. Rial, and Mercedes Solla. "Three-dimensional ground-penetrating radar strategies over an indoor archaeological site: Convent of Santo Domingo (Lugo, Spain)." *Archaeological Prospection* 17, no. 4 (2010): 213-22.
- Novo, Alexandre, Guido Manacorda, and Alessandro Simi. "Multichannel 3D GPR array systems: Recent results in engineering and archaeology." In *Symposium on the Application of Geophysics to Engineering and Environmental Problems 2013*, Society of Exploration Geophysicists and Environment and Engineering Geophysical Society (2013): 433-41.
- Núñez-Nieto, Xavier, Mercedes Solla, Paula Gómez-Pérez, and Henrique Lorenzo. "GPR signal characterization for automated landmine and UXO detection based on machine learning techniques." *Remote sensing* 6, no. 10 (2014): 9729-48.
- Nuzzo, Luigia. "Identification and removal of above-ground spurious signals in GPR archaeological prospecting." *Archaeological Prospection* 12, no. 2 (2005): 9-103.
- Okazaki, Hiroko, Hiroomi Nakazato, and Youngjoo Kwak. "Application of high-frequency ground penetrating radar to the reconstruction of 3D sedimentary architecture in a flume model of a fluvial system." *Sedimentary Geology* 293 (2013): 21-29.
- Olhoeft, G. R. Electrical properties of rocks. *Physical Properties of Rocks and Minerals*, 2 (1981): 257-97.
- Olhoeft, G. R. "Electrical properties from 10<sup>-3</sup> to 10<sup>+9</sup> HZ—Physics and chemistry." In *AIP Conference Proceedings*, vol. 154, no. 1, American Institute of Physics (1987): 281-98.

- Olhoeft, Gary R. "Modeling out-of-plane scattering effects." In *Fifth International Conference on Ground Penetrating Radar*, European Association of Geoscientists & Engineers (1994): cp-300.
- Olhoeft, Gary R. "Geophysical observations of geological, hydrological and geochemical heterogeneity." In *7th EEGS Symposium on the Application of Geophysics to Engineering and Environmental Problems*, European Association of Geoscientists & Engineers (1994): cp-208.
- Olhoeft, Gary R. "Electrical, magnetic and geometric properties that determine ground penetrating radar performance." In *Proceedings of GPR*, vol. 98 (1998): 177-82.
- Olhoeft, Gary R., and Dennis E. Capron. *Laboratory measurements of the radio frequency electrical and magnetic properties of soils from near Yuma, Arizona*. US Department of the Interior, US Geological Survey, 1993.
- Orlando, Luciana. "Georadar data collection, anomaly shape and archaeological interpretation—a case study from central Italy." *Archaeological Prospection* 14, no. 3 (2007): 213-25.
- Orlando, Luciana, and Evert Slob. "Using multicomponent GPR to monitor cracks in a historical building." *Journal of Applied Geophysics* 67, no. 4 (2009): 327-34.
- Ovenden, S. M. "Application of seismic refraction to archaeological prospecting." *Archaeological Prospection* 1, no. 1 (1994): 53-63.
- Ozkaya, Umut, Farid Melgani, Mesay Belete Bejiga, Levent Seyfi, and Massimo Donelli. "GPR B scan image analysis with deep learning methods." *Measurement* 165, 2020.
- Peña, José Antonio, and Teresa Teixidó. "Cover surfaces as a new technique for 3D GPR image enhancement. Archaeological applications." (2013). University of Granada, Spain. <https://digibug.ugr.es/handle/10481/22949>.
- Perroud, Hervé, and Martin Tygel. "Velocity estimation by the common-reflection-surface (CRS) method: Using ground-penetrating radar data." *Geophysics* 70, no. 6 (2005): B43-B52.
- Pipan, Michele, L. Baradello, Emanuele Forte, A. Prizzon, and Icilio Finetti. "2-D and 3-D processing and interpretation of multi-fold ground penetrating

- radar data: a case history from an archaeological site." *Journal of Applied Geophysics* 41, no. 2-3 (1999): 271-92.
- Pipan, Michele, L. Baradello, Emanuele Forte, and Icilio Finetti. "Ground penetrating radar study of iron age tombs in southeastern Kazakhstan." *Archaeological Prospection* 8, no. 3 (2001): 141-55.
- Piro, Salvatore, Dean Goodman, and Yasushi Nishimura. "The study and characterization of Emperor Traiano's Villa (Altopiani di Arcinazzo, Roma) using high-resolution integrated geophysical surveys." *Archaeological Prospection* 10, no. 1 (2003): 1-25.
- Piro, S., and D. Goodman. "Advances in imaging of archaeological structures using GPR." In *PIERS Proceedings*. 2013.
- Powers, Michael H., and Gary R. Olhoeft. *GPRMODV2; One-dimensional Full Waveform Forward Modeling of Dispersive Ground Penetrating Radar Data, Version 2.0*. No. 95-58. US Geological Survey, 1995.
- Qawasmeh, Huthaifa, Mohammed M. Al-Hameedawi, and Lawrence B. Conyers. "Three-dimension (3D) presentation of a hominid cave using ground-penetrating radar." *ArcheoSciences* 452, no. 2 (2021): 91-95.
- Radzevicius, Stanley. "Practical 3-D migration and visualization for accurate imaging of complex geometries with GPR." *Journal of Environmental & Engineering Geophysics* 13, no. 2 (2008): 99-112.
- Rafezi, Hamed, Alexandre Novo, and Ferri P. Hassani. "An investigation into application of ground penetrating radar (GPR) in surface mining." *Symposium on the Application of Geophysics to Engineering and Environmental Problems 2015*. Society of Exploration Geophysicists and Environment and Engineering Geophysical Society, 2015.
- Ranieri, G., Zucca, R., Trogu, A., Calcina, S. V., Piroddi, L., & Usai, A. "Multi-channel GPR prospection in the archaeological site of Monte Prama (Cabras, Italy)." In *20th Annual Meeting of European Association of Archaeologists* (2014): 187-88.
- Rees, Huw V., and Jonathan M. Glover. "Digital enhancement of ground probing radar data." *Ground penetrating radar: Geo. Survey Canada Paper* 90, no. 4 (1992): 187-92.

- Rees-Hughes, Luis, Natasha LM Barlow, Adam D. Booth, Landis J. West, George Tuckwell, and Tim Grosse. "Unveiling buried aeolian landscapes: reconstructing a late Holocene dune environment using 3D ground-penetrating radar." *Journal of Quaternary Science* 36, no. 3 (2021): 377-90.
- Reynolds, John M. *An Introduction to Applied and Environmental Geophysics*. John Wiley & Sons, 2011.
- Rhoades, J. D., P. A. C. Raats, and R. J. Prather. "Effects of liquid-phase electrical conductivity, water content, and surface conductivity on bulk soil electrical conductivity." *Soil Science Society of America Journal* 40, no. 5 (1976): 651-55.
- Rojansky, Vladimir Borisovich, and Vladimir Rojansky. *Electromagnetic Fields and Waves*. Courier Corporation, 1979.
- Saarenketo, Timo. "Electrical properties of water in clay and silty soils." *Journal of Applied Geophysics* 40, no. 1-3 (1998): 73-88.
- Sala, Jacopo, and Neil Linford. "Processing stepped frequency continuous wave GPR systems to obtain maximum value from archaeological data sets." *Near Surface Geophysics* 10, no. 1 (2012): 3-10.
- Schmelzbach, Cedric, and Emanuel Huber. "Efficient deconvolution of ground-penetrating radar data." *IEEE Transactions on Geoscience and Remote Sensing* 53, no. 9 (2015): 5209-17.
- Schneidhofer, Petra, Erich Nau, Alois Hinterleitner, Agata Lugmayr, Jan Bill, Terje Gansum, Knut Paasche et al. "Palaeoenvironmental analysis of large-scale, high-resolution GPR and magnetometry data sets: the Viking Age site of Gokstad in Norway." *Archaeological and Anthropological Sciences* 9, no. 6 (2017): 1187-213.
- Shamir, O., Goldshleger, N., Basson, U., & Reshef, M. "Laboratory measurements of subsurface spatial moisture content by ground-penetrating radar (GPR) diffraction and reflection imaging of agricultural soils." *Remote Sensing* 10, no. 10 (2018): 1667.
- Sheets, Payson D., William M. Loker, Hartmut AW Spetzler, and R. W. Ware. "Geophysical exploration for ancient Maya housing at Ceren, El Salvador." *National Geographic Research Reports* 20 (1985): 645-56.
- Sheriff, Robert E. *Encyclopedic Dictionary of Applied Geophysics*. Society of Exploration Geophysicists, 2002.



Sheriff, Robert E., and Lloyd P. Geldart. *Exploration Seismology*. Cambridge University Press, 1995.

Shragge, Jeff, James Irving, and Brad Artman. "Shot-profile migration of GPR data." In *Proceedings of the Tenth International Conference on Grounds Penetrating Radar, 2004. GPR 2004.*, vol. 1, IEEE (2004): 337-40.

Simmons, Gene, David Strangway, Peter Annan, and Richard Baker. "Surface Electrical Properties Experiment." *Apollo 17: Preliminary Science Report* 330, 1973.

Smith, Derald G., and Harry M. Jol. "Ground penetrating radar: antenna frequencies and maximum probable depths of penetration in Quaternary sediments." *Journal of Applied Geophysics* 33, no. 1-3 (1995): 93-100.

Smitha, N., D. R. Ullas Bharadwaj, S. Abilash, S. N. Sridhara, and Vipula Singh. "Kirchhoff and FK migration to focus ground penetrating radar images." *International Journal of Geo-Engineering* 7, no. 1 (2016): 1-12.

Solla, M., H. Lorenzo, A. Novo, and F. I. Rial. "Ground-penetrating radar assessment of the medieval arch bridge of San Antón, Galicia, Spain." *Archaeological Prospection* 17, no. 4 (2010): 223-32.

Srivastav, A., Nguyen, P., McConnell, M., Loparo, K. A., & Mandal, S. A highly digital multiantenna ground-penetrating radar (GPR) system. *IEEE Transactions on Instrumentation and Measurement* 69, no. 10 (2020): 7422-36.

Stern, Walter. "Versuch einer elektrodynamischen Dickenmessung von Gletschereis." *Gerlands Beitrage zur Geophysik* 27 (1929): 292-333.

Stern, Nicola. "Stratigraphy, depositional environments, and paleolandscape reconstruction in landscape archaeology." *Handbook of Landscape Archaeology* (2008): 365-78.

Sternberg, Ben K., and James W. McGill. "Archaeology studies in southern Arizona using ground penetrating radar." *Journal of Applied Geophysics* 33, no. 1-3 (1995): 209-25.

Stumpf, Tyler, Daniel P. Bigman, and Dominic J. Day. "Mapping complex land use histories and urban renewal using ground penetrating radar: A case study from Fort Stanwix." *Remote Sensing* 13, no. 13 (2021): 2478.

- Sturm, Jennie O. "Using GPR to map complex patterns and palimpsests of prehistoric land use." In *18th International Conference on Ground Penetrating Radar*, Society of Exploration Geophysicists, (2020): 33-36.
- Szymczyk, M., & Szymczyk, P. "Preprocessing of GPR data." *Image Processing & Communications* 18, no. 2-3 (2013): 83.
- Szymczyk, Magdalena, and Piotr Szymczyk. "Preprocessing of GPR data." *Image Processing & Communications* 18, no. 2-3 (2013): 83.
- Sun, Jingsheng, and Roger A. Young. "Recognizing surface scattering in ground-penetrating radar data." *Geophysics* 60, no. 5 (1995): 1378-85.
- Tamba, Robert. "Testing the use of geostatistics to improve data visualization. Case study on GPR survey of Tarragona's Cathedral." *Archaeological Prospection* 19, no. 3 (2012): 167-78.
- Tillard, Sylvie, and Jean-Claude Dubois. "Analysis of GPR data: Wave propagation velocity determination." *Journal of Applied Geophysics* 33, no. 1-3 (1995): 77-91.
- Tronca, G., I. Tsalicoalou, S. Lehner and G. Catanzariti, "Comparison of pulsed and stepped frequency continuous wave (SFCW) GPR systems," 2018 *17th International Conference on Ground Penetrating Radar (GPR)* (2018): 1-4.
- Todoeschuck, J. P., P. T. LaFleche, O. G. Jensen, A. S. Judge, J. A. Pilon, and J. Pilon. "Deconvolution of ground probing radar data." *Ground Penetrating Radar, Geological Survey of Canada* (1992): 227-30.
- Tomizawa, Y., I. Arai, M. Hirose, T. Suzuki, and T. Ohhashi. "Archaeological survey using pulse compression subsurface radar." *Archaeological Prospection* 7, no. 4 (2000): 241-47.
- Travassos, Xisto L., Sérgio L. Avila, and Nathan Ida. "Artificial neural networks and machine learning techniques applied to ground penetrating radar: A review." *Applied Computing and Informatics* 2020.
- Trinks, Immo, Bernth Johansson, Jaana Gustafsson, Jesper Emilsson, Johan Friberg, Christer Gustafsson, Johan Nissen, and Alois Hinterleitner. "Efficient, large-scale archaeological prospection using a true three-dimensional ground-penetrating radar array system." *Archaeological Prospection* 17, no. 3 (2010): 175-86.

- Trinks, I., M. Kucera, A. Hinterleitner, K. Löcker, E. Nau, W. Neubauer, and T. Zitz. "Large-scale, high-definition ground penetrating radar prospection in archaeology." In *EGU General Assembly Conference Abstracts*, 2012.
- Trinks, Immo, and Alois Hinterleitner. "Beyond amplitudes: Multi-trace coherence analysis for ground-penetrating radar data imaging." *Remote Sensing* 12, no. 10 (2020): 1583.
- Trinks, Immo, Wolfgang Neubauer, and Alois Hinterleitner. "First high-resolution GPR and magnetic archaeological prospection at the Viking Age settlement of Birka in Sweden." *Archaeological Prospection* 21, no. 3 (2014): 185–99.
- Trinks, Immo, Wolfgang Neubauer, and Michael Doneus. "Prospecting archaeological landscapes." In *Euro-Mediterranean Conference*, Springer (2012): 21–29.
- Turesson, Anita. "Water content and porosity estimated from ground-penetrating radar and resistivity." *Journal of Applied Geophysics* 58, no. 2 (2006): 99–111.
- Turner, Greg, and Commonwealth Scientific. "Propagation deconvolution." In *Fourth International Conference on Ground Penetrating Radar*, European Association of Geoscientists & Engineers (1992): cp303.
- Udphuay, Suwimon, Vivian L. Paul, Mark E. Everett, and Robert B. Warden. "Ground-penetrating radar imaging of twelfth century Romanesque foundations beneath the thirteenth century Gothic abbey church of Valmagne, France." *Archaeological Prospection* 17, no. 4 (2010): 199–212.
- Urban, Thomas M., Jeffrey T. Rasic, Claire Alix, Douglas D. Anderson, Sturt W. Manning, Owen K. Mason, Andrew H. Tremayne, and Christopher B. Wolff. "Frozen: the potential and pitfalls of ground-penetrating radar for archaeology in the Alaskan Arctic." *Remote Sensing* 8, no. 12 (2016): 1007.
- Urban, Thomas M., Matthew R. Bennett, David Bustos, Sturt W. Manning, Sally C. Reynolds, Matteo Belvedere, Daniel Odess, and Vincent L. Santucci. "3-D radar imaging unlocks the untapped behavioral and biomechanical archive of Pleistocene ghost tracks." *Scientific Reports* 9, no. 1 (2019): 1–10.
- Utsi, Erica. "Ground-penetrating radar time-slices from north Ballachulish Moss." *Archaeological Prospection* 11, no. 2 (2004): 65–75.

- Valle, S., Luigi Zanzi, H. Lentz, and H. M. Braun. "Very high-resolution radar imaging with a stepped frequency system." In *Eighth International Conference on Ground Penetrating Radar*, vol. 4084 (2000): 464–70.
- Van Dam, Remke L., and Wolfgang Schlager. "Identifying causes of ground-penetrating radar reflections using time-domain reflectometry and sedimentological analyses." *Sedimentology* 47, no. 2 (2000): 435–49.
- Van Dam, Remke L., Elmer H. van den Berg, Sytze van Heteren, C. Kasse, Jeeroen AM Kenter, and Koos Groen. "Influence of organic matter in soils on radar-wave reflection: Sedimentological implications." *Journal of Sedimentary Research* 72, no. 3 (2002): 341–52.
- Van Dam, R. L., Hendrickx, J. M., Cassidy, N. J., North, R. E., Dogan, M., & Borchers, B. (2013). "Effects of magnetite on high-frequency ground-penetrating radar effects of magnetite on high-frequency GPR." *Geophysics* 78, no. 5 (2013): H1–H11.
- Vaughan, C. J. "Ground-penetrating radar surveys used in archaeological investigations." *Geophysics* 51, no. 3 (1986): 595–604.
- Venkateswarlu, B., & Tewari, V. C. "Geotechnical applications of ground penetrating radar (GPR)." *Journal of Industrial Geology Congress* 6, no. 1 (2014): 35–46.
- Verdonck, L. "Detection of buried roman wall remains in ground-penetrating radar data using template matching." *Archaeological Prospection* 23 (2016): 257–72.
- Verdonck, L., De Smedt, P. and J. Verhegge, "Making sense of anomalies: Practices and challenges in the archaeological interpretation of geophysical data." In *Innovation in Near-Surface Geophysics. Instrumentation, Application, and Data Processing Methods*; Persico, R., Piro, S., Linford, N., Eds.; Elsevier (2019): 151–94.
- Vickers, Roger S., and Lambert T. Dolphin. "A communication on an archaeological radar experiment at Chaco Canyon, New Mexico." *MASCA Newsletter* 11, no. 1 (1975): 3.
- Vickers, Roger S., Lambert T. Dolphin, and David Johnson. "Archaeological investigations at Chaco Canyon using subsurface radar." *Remote Sensing Experiments in Cultural Resource Studies* (1976): 81–101.

Von Hippel, Arthur R. "Dielectrics and waves." *Polyatomic Molecules* (1966): 150-55.

Wadsworth, William TD, Kisha Supernant, and Ave Dersch. "Integrating remote sensing and indigenous archaeology to locate unmarked graves: A case study from northern Alberta, Canada." *Advances in Archaeological Practice* 9, no. 3 (2021): 202-14.

Wadsworth, William TD, Kisha Supernant, and Vadim A. Kravchinsky. "An integrated remote sensing approach to Métis archaeology in the Canadian Prairies." *Archaeological Prospection* 28, no. 3 (2021): 321-37.

Walden, A. T., and J. W. J. Hosken. "An investigation of the spectral properties of primary reflection coefficients." *Geophysical Prospecting* 33, no. 3 (1985): 400-35.

Walker, John W., William H. Hulse, and Donald W. Eckart. "Observations of the electrical conductivity of the tropical soils of Western Puerto Rico." *Geological Society of America Bulletin* 84, no. 5 (1973): 1743-52.

Welc, Fabian, Luis D. Nebelsick, and Dariusz Wach. "The first Neolithic roundel discovered in Poland reinterpreted with the application of the geophysical amplitude data comparison (ADC) method." *Archaeological Prospection* 26, no. 4 (2019): 283-97.

Welc, Fabian, Corinne Rousse, and Gaetano Bencic. "Results of geophysical scanning of a Roman senatorial villa in the Santa Marina Bay (Croatia, Istria) using the amplitude data comparison method (ADCM)." *Studia Quaternaria* 37 (2020): 101-41.

Wiewel, Adam, Lawrence B. Conyers, Luca Piroddi, and Nikos Papadopoulos. "An experimental use of ground-penetrating radar to identify human footprints." *ArcheoSciences* 451, no. 1 (2021): 143-46.

Wensink, W. A. "Dielectric properties of wet soils in the frequency range 1-300 MHz." *Geophysical Prospecting* 41, no. 6 (1993): 671-96.

Witten, A. J. *Handbook of Geophysics and Archaeology*. Routledge, 2017.

Wu, Yuxuan, Feng Shen, Yue Yuan, and Dingjie Xu. "An improved modified universal ultra-wideband antenna designed for step frequency continuous wave ground penetrating radar system." *Sensors* 19, no. 5 (2019): 1045.

- Xia, Jianghai, Evan K. Franseen, Richard D. Miller, and Thomas V. Weis. "Application of deterministic deconvolution of ground-penetrating radar data in a study of carbonate strata." *Journal of Applied Geophysics* 56, no. 3 (2004): 213–29.
- Yelf, Richard. "Where is true time zero?" In *Proceedings of the Tenth International Conference on Ground Penetrating Radar, 2004. GPR 2004.*, vol. 1, IEEE (2004): 279–82.
- Yilmaz, Öz. *Seismic Data Analysis: Processing, Inversion, and Interpretation of Seismic Data*. Society of Exploration Geophysicists, 2001.
- Zajícová, Katerina, and Tomas Chuman. "Application of ground penetrating radar methods in soil studies: A review." *Geoderma* 343 (2019): 116–29.
- Zhao W., Forte E., Fontolan G., and Pipan M., "Advanced GPR imaging of sedimentary features: integrated attribute analysis applied to sand dunes." *Geophysical Journal International* 213, no. 1 (2018): 147–56.
- Zhao, W., Forte, E., Pipan, M., & Tian, G. "Ground penetrating radar (GPR) attribute analysis for archaeological prospection." *Journal of Applied Geophysics* 97 (2013): 107–17.
- Zhao, Wenke, Emanuele Forte, and Michele Pipan. "Texture attribute analysis of GPR data for archaeological prospection." *Pure and Applied Geophysics* 173, no. 8 (2016): 2737–51.
- Zhao, Wenke, Gang Tian, Emanuele Forte, Michele Pipan, Yimin Wang, Xue-jing Li, Zhanjie Shi, and Haiyan Liu. "Advances in GPR data acquisition and analysis for archaeology." *Geophysical Journal International* 202, no. 1 (2015): 62–71.
- Zhao, Wenke, Gang Tian, Emanuele Forte, Michele Pipan, Yimin Wang, Xue-jing Li, Zhanjie Shi, and Haiyan Liu. "Advances in GPR data acquisition and analysis for archaeology." *Geophysical Journal International* 202, no. 1 (2015): 62–71.



# Index

- acquisition, continuous, 33, 49, 87
- adjustments, pre-acquisition, 35
- air waves, 43-45, 53, 82, 108-10, 143, 183
- amplitude:
  - analysis, 169-76;
  - non-reflective features, 12, 148, 188-89;
  - rendering, 23, 133, 190-91;
  - slice-maps, 3, 6-9, 21, 43, 61, 124-32;
  - subtle features, 7-8, 80, 100-101, 155, 176-77, 182-83, 189
- analog units, 20, 38
- anomalies, 18-19, 20, 22
- anomaly:
  - coupling, 75-76;
  - hunting, 20, 22, 49
- antennas:
  - arrays, 15, 15, 34, 41, 64, 86-87, 89, 93, 105, 125-27, 133, 142;
  - beam, 64, 68-70, 109;
  - bow tie, 29, 50;
  - center frequency, 29-30, 35, 51-53;
  - choice, 67;
  - dipole, 50, 70, 80, 109;
  - frequencies, 50-52, 62, 67-68, 71, 76, 82, 92, 103;
  - low-frequency, 52-53, 103, 140;
  - multiple, 15, 72, 108, 143;
  - orientation, 46, 103;
  - ringing, 139;
  - selection, 50-52;
  - shielded, 53;
  - unshielded, 53
- ash, volcanic, 56, 68, 102, 109-10, 182
- attenuation:
  - below different media, 57, 62, 74, 91, 102, 111, 117;
  - with depth, 62, 74, 91
- averaging:
  - boxcar, 93;
  - traces, 93-95;
  - weighted, 93
- background, removal, 80, 119, 120, 129, 145
- barber pole reflections, 32
- basalt:
  - clays in, 27;
  - energy penetration, 27
- batteries, 15, 86
- beach deposits, 18-19, 35
- beam, antenna, 64, 69-71, 109
- bedding planes, 17, 74, 109, 175-76, 189
- bedrock, 17, 60
- bentonite clay, 28
- bistatic mode, 36
- bore hole collection, 87
- boundaries, resolution, 33, 63, 73
- boxcar averaging, 96-97
- buried:
  - landscapes, 161-64;
  - soil horizons, 63, 163;
  - topography, 19
- cables, coaxial, 86
- calibration:
  - steps, 88, 95-99
- carbonate, affecting transmission, 31, 179
- cart, for collection, 15, 34, 38, 52, 85-88
- Cartesian coordinates, in grid collection, 34, 41-42
- cell phone energy, 25, 40, 77-79
- center frequency, antennas, 29, 36, 50-52, 66-69, 71, 79, 85, 108, 132
- clay:
  - bentonite, 28;
  - floor, 155;



- kaolinite, 28;
- minerals, 27-31;
- porosity, 56-59;
- saturated, 59;
- types, 28;
- wet, 31, 61
- clipping, of traces, 39
- clutter, 73, 95, 117
- CMP tests, 105
- coaxial cables, 38, 86
- cobbles, limestone, 74
- coefficient of reflectivity, 57
- concrete scanning, 82, 88
- cone:
  - of radiation, 69-73, 75-76, 80-82, 109, 144, 161;
  - of transmission, 25, 151-52
- conical projection of energy, 113, 161
- constant, dielectric, 54
- control system, 38, 85-88, 95, 142
- corrections, topographic, 43
- coupling:
  - anomaly, 46;
  - changes, 93
- data:
  - digital, 4, 95, 147, 181-82;
  - raw, 6, 12, 93, 95, 118, 135, 138, 146, 148, 172, 193;
  - recording, 34, 37
- data processing:
  - edge matching, 174;
  - frequency removal, 135;
  - post-acquisition, 15, 39, 43, 50, 62, 80, 92, 96, 117-31, 184
- deconvolution, 138-41, 146
- de-wow, 129
- dielectric constant, 54
- digital, samples, 91-92, 158
- digitizer, 20
- dipole antennas, 29, 50, 70, 80, 109
- direct wave, 2, 95, 104, 108, 143
- dispersion, of energy, 67
- distortion, vertical, 100-101, 157-58
- downloading energy, 67
- edge matching, 174
- electromagnetic:
  - air, 27;
  - conductivity, 31;
  - convolve, 140;
  - field, 54, 79, 109, 112;
  - loss, 114;
  - spectrum, 25-26;
  - velocity, 50;
  - waves, 13, 25, 27-29, 78, 141
- elliptical, transmission beam, 70
- energy:
  - dispersion, 62;
  - focusing, 72, 79, 184;
  - leakage, 110;
  - relaxation, 27
- exaggeration, scales, 101, 117-19, 129, 176
- fiber optic, cables, 38, 88
- filters:
  - band-pass, 96;
  - high-pass, 96;
  - horizontal, 92-93, 97, 129;
  - low-pass, 96;
  - vertical, 96
- focusing:
  - energy, 72, 79, 184;
  - as a function of RDP, 79
- footprint:
  - calculation of, 69-71;
  - beam, 64-68, 70-71, 109;
  - equation, 55;
  - as a function of RDP, 55;
  - radius of, 55-57;
  - size, 69
- frequency:
  - filtering, 78, 96, 132-38, 145;
  - dominant, 66, 140;
  - stepped, 85
- gains, 39, 39, 80, 95-97, 170
- geological materials, RDP, 56
- GIS, 195
- glacial ice, 17, 66
- GPS, 13, 15, 34, 37-38, 41-43, 85-86, 194
- grayscale display, 20, 65, 121, 123, 170
- grids:
  - collection in, 34;
  - complex, 194;
  - rectangular, 41, 43;

- rectilinear, 41, 43
- ground wave, 107–8
- header files, 88
- high-pass filters, 96
- Hilbert transform, 119, 124, 142
- hyperbola:
  - apex, 64–65, 104, 113, 133;
  - collapse of, 65, 133–35;
  - generation, 155;
  - point source, 32, 63–65, 75, 93;
  - removal, 129–30
- illumination of energy beam, 72, 105
- image processing, 118
- incremental sampling, 94–95
- interface:
  - buried, 14, 53–54, 75, 102, 107, 169, 172;
  - ground-air, 34, 53, 80, 95, 107;
  - resolution of, 71;
  - stratigraphic, 33, 104
- interference:
  - constructive, 70–71;
  - destructive, 70;
  - near-surface zone of, 80
- interpolation:
  - in amplitude slice-mapping, 124–26, 135, 193;
  - level ground, 176
- ions, movement, 28
- isosurface, production of, 22, 128, 174, 180–82, 193
- kaolinite clay, 28
- Kirchoff method, migration, 133–34
- laboratory measurements, RDP, 32, 49, 54, 111–13
- lakes, collection on, 7, 43, 48, 50, 162
- landscape reconstruction, 1, 9, 15, 129, 159–64
- lateral velocity change, 100, 108
- lava, 27
- low-pass filters, 96
- magnetic, component of EM waves:
  - permeability, 27, 53, 111–12;
  - susceptibility, 189
- magnetics, 189–92
- magnetite minerals, 27
- manufacturers of GPR systems, 4, 37–39, 50, 85, 87, 96, 105
- marshes, 6–7, 56, 176, 178
- metal bar velocity test, 82, 103–5
- midden, 64, 171
- migration, 65, 129–34, 142–46
- military base noise, 77
- moats, 43
- modeling, 148–52
- models:
  - applications, 148–52;
  - synthetic, 149–57, 165
- monostatic mode, 36
- multichannel systems, 36, 89, 109, 127, 170:
  - velocity tests, 109, 127
- multiple-offset collection, 142–43:
  - processing, 142
- multiple reflections, 32, 82, 119, 138–41, 150–51
- multiples, 82, 117, 138
- near-field zone, 80, 108
- noise, in data:
  - problems with, 2, 20, 28, 37, 39, 47, 51, 77, 79, 88;
  - removal, 96–97, 119, 129, 140;
  - system, 96, 119
- non-reflective features, 12, 143, 179–80
- normal polarity, 168–69
- obstacles, surface, 16, 41–46, 145
- octave, in frequency, 50
- organic matter, affecting transmission, 23, 55–56, 60, 163, 178, 189
- oscillation frequency, 30
- over-processing, 145
- patterns, analysis of, 3
- paving surfaces, 46, 74
- peat, radar transmission in, 18, 55, 91, 176–78
- penetration:
  - depth, 19, 27, 30, 37, 39, 74–75, 142;
  - function of frequency, 71, 75;

- vs. resolution, 67, 71, 75
- permeability:
  - of ground materials, 56, 66;
  - magnetic, 27, 53, 111;
  - relative dielectric, 54-57, 60, 69-70, 89, 99, 111, 113
- pipes, 17, 33, 47, 63, 82, 87-88, 113
- pit house, 6, 19, 60, 63, 155-56
- planar reflections, 44, 63, 74, 76, 79, 82-83, 100-101, 120, 128, 131, 133, 155, 160, 189
- plastic objects, 33, 48-49, 52, 58
- point-source hyperbolas, 32, 63-65, 75, 93:
  - removal of, 130
- polarity, 168-69
- post-acquisition processing, 15, 39, 43, 50, 62, 80, 92, 96, 117-31, 184
- pre-collection, parameters, 38
- predictive deconvolution, 119, 138-41, 146
- processing:
  - band-pass, 96;
  - de-wow, 129;
  - steps, 6, 78, 82, 117-21, 129, 135-37, 143, 145-48
- pull-down, velocity, 153-54, 184
- pull-up, velocity, 74, 153-54, 168-69, 184
- pulse, consecutive, 36
- radiation cone, 7, 69-76, 80, 109, 144, 151-52, 161
- radio waves, 16, 25, 28-30, 39-40, 77-78, 96, 129
- radius:
  - of cone of illumination, 72, 109;
  - search for interpolation, 124-26, 135, 193
- range gains, 95
- ray paths, 151
- RDP:
  - of materials, 56;
  - as a measurement of velocity, 55, 99-115
- RDP-velocity equation, 55
- reflected wave method, velocity, 102
- reflections:
  - barber pole, 32;
  - bowtie, 50;
  - coherent, 2, 29, 82, 93, 117, 121, 138, 144;
  - generation, 2, 63, 102, 133, 168;
  - multiples, 82, 117, 138-41;
  - point-source, 32, 63-65, 75, 93, 105, 113-14, 129-33;
  - planar, 44, 74, 76, 79, 82-83, 100-101, 120, 128, 131, 133, 155, 160, 189
- reflectivity, coefficient of, 57-58
- reinforcing bars, 82-83, 103
- relative dielectric permeability (RDP), 54
- rendered images, 174, 180-82
- resistive materials, 18
- resistivity, 32
- reverberations, of reflections, 117
- reverse polarity, 168-69
- ring down, 82
- ringing, in antennas, 83
- rubber sheeting, data processing, 119
- rubble, 156, 166, 182
- salt:
  - affecting energy transmission, 28, 30, 48-49, 55, 60;
  - in ground, 28, 30
- saltwater, 30, 55, 60
- samples:
  - to define amplitudes, 36, 92, 94;
  - digital, 36-37, 91-92, 158;
  - per trace, 92
- sampling, incremental, 94-95
- scale corrections and adjustments, 129, 199
- scattering, of energy, 73-74, 79
- search radius, in slice-mapping, 124-25
- settings:
  - acquisition, 38, 88, 91-93, 96-97;
  - calibration, 16, 78, 87-88, 95-96, 99;
  - default, 92;
  - range gain, 39, 95-97
- shielded antennas, 53
- slicing geometry, 173, 175
- smoothing:
  - horizontal, 92-93;
  - traces, 92
- snow:
  - affecting radar penetration, 74-76;
  - noise removal, 117, 119
- soil, buried, 1, 20, 64, 169
- sonic waves, 180
- spikes, in data, 117

- spreading, energy, 25, 33, 62, 68, 72, 76
- stacking:
  - hyper, 37, 93;
  - rate, 86;
  - real-time, 37
- stealth technology, 73
- stepped frequency systems, 85
- storage, cistern, 155-56
- surface:
  - dipping, 34, 119, 133;
  - concave, 78-80
- survey wheel, 35-37, 85, 98
- susceptibility, magnetic, 198
- synthetic models, 149-57, 165
- time:
  - elapsed, 1, 13-14, 38, 103;
  - two-way, 14, 38, 54, 64, 89, 99-100, 122, 153, 158, 161, 168;
  - window, 2, 20, 38-39, 44-45, 51, 80, 85, 88-89, 91-95, 97, 104, 114, 117, 120, 133-34, 138, 165;
  - zero, 14, 95, 106, 108, 117, 121
- trace:
  - averaging, 37, 93-94;
  - clipped, 96, 105;
  - generation, 25-38;
  - sequential, 93;
  - stacking, 37, 92-95
- transect:
  - linear, 63, 142;
  - offsets, 143;
  - spacing, 69, 159
- transillumination, 105, 108-11
- transmission, wireless, 15, 86, 193
- transmitter, antenna, 15, 36, 95, 139
- velocity:
  - analysis, 99-115, 173;
  - changes, 33, 53, 59, 73, 121;
  - measurements hyperbola fit, 102, 105, 114;
  - pull-down, 153-55, 184;
  - pull-up, 74, 153-54, 168-69, 184
- velocity tests:
  - CMP and WARR, 105-8;
  - direct wave methods, 104, 108;
  - metal bar, 103-5;
  - transillumination, 105, 108-11
- vertical filters, 96
- video imaging, 22, 123, 128-29
- virtual reality, 22
- void spaces, 12, 25, 33, 58-59, 113, 138, 142, 154, 166, 168-70
- voltage, differences in antennas, 20
- WARR tests, 105-6
- water:
  - content 33-34, 57-58, 100, 111;
  - fresh, 48-50, 55-60;
  - residual, 111-12;
  - salt, 30, 49, 55, 60;
  - saturation, 67, 100-102, 108, 111-13, 154;
  - table, 63, 143-44, 154
- weighted averaging of traces, 94
- wiggle trace display in profiles, 120
- window, time, 2, 20, 38-39, 44-45, 51, 80, 85, 88-89, 91-95, 97, 104, 114, 117, 120, 133-34, 138, 165
- wireless transmission, 15, 86, 193
- zero position, adjusting, 106-8, 117, 121



## *About the Author*

**Lawrence B. Conyers** received a bachelor of science degree in geology from Oregon State University and a master of science degree from Arizona State University. He was awarded M.A. and Ph.D. degrees from the University of Colorado, Boulder. Before turning his attention to ground-penetrating radar, he spent seventeen years in petroleum exploration and development, where he worked with seismic geophysical prospecting. His GPR research is conducted throughout the United States and at many sites throughout the world. Many videos and publications can be found on his website: <http://www.gpr-archaeology.com/>.

